Concessionaria per la progettazione, realizzazione e gestione del collegamento stabile tra la Sicilia e il Continente Organismo di Diritto Pubblico
(Legge n° 1158 del 17 dicembre 1971, modificata dal D.Lgs. n°114 del 24 aprile 2003)

PONTE SULLO STRETTO DI MESSINA

PROGETTO DEFINITIVO

EUROLINK S.C.p.A.

IMPREGILO S.p.A. (MANDATARIA)
SOCIETÀ ITALIANA PER CONDOTTE D'ACQUA S.p.A. (MANDANTE)
COOPERATIVA MURATORI E CEMENTISTI - C.M.C. DI RAVENNA SOC. COOP. A.R.L. (MANDANTE)
SACYR S.A.U. (MANDANTE)
ISHIKAWAJIMA - HARIMA HEAVY INDUSTRIES CO. LTD (MANDANTE)
A.C.I. S.C.P.A. - CONSORZIO STABILE (MANDANTE)

IL PROGETTISTA	IL CONTRAENTE GENERALE	STRETTO DI MESSINA	STRETTO DI MESSINA
COWI Ing. E.M. Veje Dott. Ing. E. Pagani Ordine Ingegneri Milano n° 15408	Project Manager (Ing. P.P. Marcheselli)	Direttore Generale e RUP Validazione (Ing. G. Fiammenghi)	Amministratore Delegato (Dott. P. Ciucci)

Unità Funzionale	OPERA DI ATTRAVERSAMENTO	PF0066_F0
Tipo di sistema	SOTTOSTRUTTURE	
Raggruppamento di opere/attività	BLOCCHI DI ANCORAGGIO	
Opera - tratto d'opera - parte d'opera	Geotechnical Design Reports	
Titolo del documento	Calabria Anchor Block – earthquake induced displacements and safety against ultimate limit states, Annex	

CODICE: G C 1 0 0 0 | P | C L | D | P | S T | B 4 | B C | 0 0 | 0 0 | 0 0 | 0 2 | F0

REV	DATA	DESCRIZIONE	REDATTO	VERIFICATO	APPROVATO
F0	20-06-2011	EMISSIONE FINALE	LM	LC	SR

NOME DEL FILE: PF0066_F0_ANX

INDEX

1 Executive summary

In this report the geotechnical safety of Calabria anchor block is evaluated against ultimate limit state using the pseudo-static approach, including safety against sliding and rotation and bearing capacity failure, and earthquake-induced block displacements are evaluated using the displacement-based approach. The most likely sliding mechanisms to be used for earthquake-induced displacements was estimated through plane strain FE analyses. Computations were carried out using the cable forces provided by the tender design that for the ULS load combination result slightly higher than the values obtained from the global IBDAS model (5% for the version 3.3b, 7% for the version 3.3f), this resulting in a conservative estimate of the behaviour of the Calabria Anchor Block.

The companion report "Calabria Anchor Block – evaluation of block behaviour via 3D FE analyses and of bearing capacity" describes results from static 3D FE analyses of Calabria Anchor Block.

Chapter 2 describes the soil profile on the Calabria shore (Figure 2.1).

Starting from ground level and moving downwards the following units are encountered: *Depositi Costieri* (Coastal Deposits); *Ghiaie di Messina* (Messina Gravel)/*Sedimenti dei terrazzi* (Terrace Deposits); *Depositi Continentali* (Continental Deposits)/*Calcarenite di Vinco* (Vinco Calcarenite); *Conglomerato di Pezzo* (Pezzo Conglomerate); *Cristallino* (Crystalline bedrock). A plan view at the site of the Calabria Anchor Block is shown in Figure 2.2. The two longitudinal sections and the cross section indicated in Figure 2.2 are shown in Figure 2.3 – 2.5. For the Calabria Anchor Block, the relevant geological unit is the Pezzo Conglomerate, with a weathered shallow layer (20 m < z < 40 m), overlain by the Coastal Deposits of small thickness. Table 2.1 summarises the main mechanical parameters obtained from the geotechnical characterisation for the three relevant layers.

Chapter 3 details the constitutive model adopted in the FE analyses discussed in the report.

This is an elastic-plastic rate independent model with isotropic hardening (Hardening Soil) available in the library of the code *Plaxis*. In the model, the elastic behaviour is defined by isotropic elasticity through a stress-dependent Young's modulus, E'. For plastic loading from isotropic stress states, the model predicts a non linear stress-strain relationship with tangent initial modulus equal to E'. Values of E' were related to the shear modulus at small-strain G_0 obtained from the cross-hole test carried out in the site. In particular, values of the parameters reported in Table 3.1 were obtained by best fitting the cross-hole test results in Figure 3.2. In the FE analyses discussed in the report, a simplified soil profile was assumed, characterised by lower values of the shear stiffness (Table 3.2).

Chapter 4 examines the governing equations for the safety of anchor blocks against sliding.

In static conditions (section 4.1) and following the global safety factor approach (section 4.1.1), safety against sliding can be expressed through the global safety factor given in eq.(1). For the meaning of the symbols in eq.(1) refer to Figure 4.1 of the report. Following the partial safety factors approach (section 4.1.2), the design values of the actions E_d and the resistance R_d are computed from the corresponding characteristic values applying partial safety factors to actions, resistances and strength parameters. Condition $R_d \geq E_d$ must then be satisfied (D.M. 14.01.2008). The characteristic actions and the characteristic resistance are defined in eq. (2). Following Approach 1, Combination 2 to study geotechnical (GEO) limit states (section 2.6.1 - D.M. 14.01.2008), the design actions and resistances can be computed from eq.(3) in which: γ_φ = 1.25 and γ_P = 1.1, the cable forces, T, are inclusive of partial load factors as provided by structural analyses of the tender design for each limit state and therefore are not factored, the weight of the anchor block (permanent load) is multiplied by the same load factor, γ_{G1} = 1, irrespective of its effect (D.M. 14.01.2008), and the components of S_a and R_p normal to the sliding surface are neglected. Safety against sliding under static loading conditions is not be evaluated in the report since the pseudo-static loading conditions are the most critical.

Analysis of the anchor blocks under seismic conditions (section 4.2) is carried out using the pseudo-static approach and the displacement-based sliding block approach. In the pseudo-static approach (section 4.2.1), the stability of the block is measured either by a global factor of safety F, that is the ratio of the total resisting force to the total driving force (section 4.2.1.1) or using partial safety factors (section 4.2.1.2). The global factor of safety against sliding is given in eq.(4). For the meaning of the symbols in eq.(4) refer to Figure 4.2 of the report. In the partial safety factors approach (section 4.2.1.2) the stability of the block is measured by a comparison of the design action with the design resistance. The design values of the actions E_d and the resistance R_d are computed from the corresponding characteristic values applying partial safety factors to actions, resistances and strength parameters. Condition $R_d \geq E_d$ must then be satisfied. Under seismic condition the load factors of the design actions are set equal to unity: $\gamma_G = \gamma_Q = 1$ (§ 7.11.1 - D.M. 14.01.2008) and are therefore omitted in the relevant equations. The characteristic actions and the characteristic resistance are defined in eq. (5). Following Approach 1, Combination 2, to study geotechnical (GEO) limit states, the design actions and resistances can be computed from eq.(6) in which: γ_φ = 1.25 and γ_P = 1.1, the cable forces, T, are inclusive of partial load factors, as provided by structural analyses of the tender design for each limit state, and the components of S_a and R_p normal to the sliding surface are neglected. In the displacement-based approach (section 4.2.2), the safety of the anchor block is evaluated comparing the permanent displacement developed during the earthquake with a threshold value. The critical acceleration is first determined using the pseudo-static approach and then the cumulative displacement of the potentially sliding mass is evaluated using the sliding block analysis. The sliding mass is treated as a rigid body with permanent displacements taking place whenever the ground acceleration exceeds the critical acceleration. The permanent displacement is calculated by integrating twice the relative acceleration time history over the time intervals in which the velocity of the sliding mass relative to the ground is positive. The critical acceleration is evaluated using the characteristic values of the strength parameters c'_k and φ'_k; under seismic conditions load factors are equal to one. The pseudo-static seismic action acts with an angle (α-θ) with respect to the sliding surface (Fig. 4.3). Assuming conditions of limit equilibrium (F = 1) and neglecting the contributions of passive and active earth thrusts, the expression of *K* given in eq.(8) is obtained. The minimum value of *K*, that is the critical seismic coefficient K_c, is obtained for $\theta = \alpha + \varphi_s' \Rightarrow \alpha - \theta = -\varphi'_s$ (Fig. 4.3) and has the expression given in eq.(9). During sliding ($K > K_c$), it can be assumed that the net earth thrust ΔR increases with increasing block displacements *u* as per eq.(10), in which k_d is a non linear spring stiffness, depending on relative displacement (Fig. 4.4). The effect of ΔR is explicitly included in the equation of relative motion used for computing the earthquake-induced displacement of the anchor block. Separating the horizontal and vertical components of the acceleration time histories, and for $\theta = \alpha + \varphi_s' \Rightarrow \alpha - \theta = -\varphi'_s$, the equation of relative motion can be written as in eq. (21).

Chapter 5 examines safety against sliding for the Calabria Anchor Block.

The self-weight of the anchor block (section 5.1) was calculated on the basis of the drawings the tender design (Fig. 5.2). At the location of Calabria anchor block the hydraulic head is H_w = 94.5 m a.s.l.. In order to reduce pore water pressure, the tender design requires the construction of a drainage tunnel, lowering the water head to H_w = 88.0 m a.s.l. In the analyses both the presence and the absence of the drainage tunnel are considered. Relevant data are listed in Tables 5.1 and 5.2.

Three possible sliding mechanisms (section 5.2) were considered in the analyses (Fig. 5.3), characterised by angles α = 33.7°, 25.3° and 0° on the horizontal; in each mechanism, the contribution of soil between the sliding surface and the anchor is considered as an added weight, as reported in Tables 5.3 and 5.4.

In order to estimate the most likely sliding mechanism (section 5.3), plane strain FE analyses were carried out using *Plaxis* 8 (Figure 5.4). Soil-anchor block contact was modelled through interface elements with reduced shear strength and stiffness. The anchor block was assumed to behave as an elastic non-porous material. The analyses were carried out in terms of effective stresses, assuming drained conditions. The presence of diaphragm walls in front and behind the anchor block were not accounted for in the analyses. Table 5.5 summarises the equivalent unit weight, γ_{eq}, of both the cable chambers and the filled chambers that were used in the plane strain FE analyses. ULS loading conditions were considered in the analyses, spreading the cable load T over the width B = 100 m of the anchor block, to account for plane strain conditions. Table 5.6 details the sequence of computation steps. To estimate the most likely sliding surface, the block displacement and its direction were evaluated as the average between the displacements of the centre of gravity and of four nodes of the block at the contact with the soil (Figures 5.9 -5.10). Table 5.7 and Table 5.8 show the results obtained with or without the drainage system. Under ULS loading condition, the average direction of the displacement is in the range of 6.1° to 8.4° on the horizontal. The most likely sliding mechanism is therefore between the second and the third mechanism and is only slightly affected by the drainage system.

The sliding resistance T_L developed on the sides of the anchor block (section 5.4) was computed under the conservative hypothesis that active limit equilibrium is achieved behind the diaphragm walls during the excavation stages, reducing $\tan\varphi'$ and $\tan\varphi'_s$ by factor γ_φ = 1.25 as prescribed by D.M. 14.01.2008. Table 5.10 and 5.11 list the characteristics and design values of lateral resistance T_L. The former are used to evaluate the critical seismic coefficient $K_{c(red)}$ given by eq.(9), while the latter is used in the pseudostatic approach. Appendix A gives computation details.

The passive resistance R_P developed in front of the block on sliding is dealt with section 5.5. In the pseudostatic approach (section 5.5.1) R_P was computed using the solution obtained by Chen and Liu (1990) reducing $\tan\varphi'$ by factor γ_φ = 1.25 (D.M. 14.01.2008). Table 5.13 reports the values of characteristic and design passive earth pressure coefficients, K_{Pk} and K_{Pd}, respectively. Values of K_h and K_v used in computation are also listed in Table 5.13. These were obtained assuming the values of a_g specified in document GCG.F.04.01. Site effects were accounted for assuming a topographic amplification factor S_T = 1.2 and a subsoil amplification factor S_S = 1.0; a coefficient β_m = 0.31 was used for computing K_h (D.M. 14.01.2008). Table 5.14 and Table 5.15 summarise the computed design values of passive resistance R_{Pd} developed in front of the block; for comparison the characteristic values of R_P are also given in the Tables. Appendix B gives computation details. In the displacement based approach (section 5.1.2), R_P is assumed to increase progressively with the relative displacement u induced by the earthquake loading. To obtain the analytical relationship between R_P and u, plane strain FE analyses were carried out with reference to mechanisms 2 (α = 25.3°) and 3 (α = 0°) in which an ideal perfectly smooth wall, located in the position corresponding to the front of the anchor block and extending to the depth of the sliding mechanism modelled in the analysis, was progressively displaced towards the soil. The analyses were carried out both with and without the drainage system. The assumption of smooth soil-wall interface and plane strain conditions are both conservative. For each value of the applied displacement, *u* (= 1 mm to 1 m), the earth resistance ΔR was calculated as the integral of the difference of the horizontal stresses acting on the wall for the given displacement and under geostatic conditions over the length of the wall. The relationship between ΔR and *u* and the ultimate value of ΔR were obtained by hyperbolic interpolation of the resulting data. The results obtained with and without the drainage system are summarised in Table 5.17 and Figure 5.13 and Table 5.18 and Figure 5.14, respectively.

In the pseudo-static approach (section 5.6), safety against sliding was evaluated using eq.(6) with the prescriptions of D.M. 14.01.2008. The design resistances were computed considering the contributions of sliding resistance at the base and at the block sides and the passive resistance in front of the block; the active earth trust behind the block was accounted for only along the vertical portion of the back wall. Design actions and resistances were computed using the pseudo-static seismic coefficients reported in Table 5.13. Table 5.19 gives the values of *T* provided by structural analyses of the tender design for each limit state. The characteristic value of φ'_s mobilised on the sliding surface was assumed to be φ'_{sk} = atan[(3/4)tanφ_k']=32°. Table 5.21 reports the pseudostatic seismic coefficients, the active earth pressure coefficients and the active earth thrust used for computations. Table 5.22 a-d report the comparison between design resistances and design actions for the three sliding mechanisms assumed in the analyses, for each hydraulic condition: in all cases $\Sigma R_d / \Sigma E_d > 1$ and safety against sliding is satisfied. Appendix C gives computation details.

The first step of the displacement based approach (section 5.7), is the selection of acceleration time histories (section 5.7.1). These were 22 real accelerograms from the PEER strong-motion database with magnitudes between 6.5 and 7.28, hypocentral distances between 12 and 82 km, and peak acceleration between 0.29 and 1.16 g, and 8 artificial strong motion accelerograms, fully compatible with the response spectrum of the preliminary design. Table 5.23 and 5.24 report the main parameters of their horizontal and vertical components, respectively. Each horizontal component was scaled to the design peak acceleration a_{max} = 0.58g and the corresponding vertical component was scaled by the same factor (Tables 5.25 and 5.26). The horizontal components of each event were independently considered and combined with the vertical component. The analyses were also repeated using the scaled horizontal component combined with the vertical component scaled to 0.58g (Table 5.27). Figures 5.27–5.31 show the elastic response spectra of the selected accelerograms, compared to the design response spectrum.

The values of critical seismic coefficients (section 5.7.2) were evaluated for each limit state, considering the contribution of the base and the lateral sides of the block and a passive earth resistance in front of the block gradually increasing with block displacement. The values of K_c, computed using eq.(9) with and without the drainage system are listed in Table 5.28 and 5.29, respectively. The lowest values of K_c were obtained for the ULS condition and therefore the displacements were computed only for this condition.

The earthquake-induced displacements (section 5.7.3) were computed by numerical integration of equation (21) for mechanisms 2 and 3 only, as the pseudo-static analyses showed that mechanism 1 is the less critical and the FE analyses showed that the most likely sliding surface is between mechanisms 2 and 3. Computations were carried out both with and without the drainage systems. Each scaled horizontal component was combined with the corresponding vertical component, first scaled by the same factor and then scaled to 0.58g and the analyses repeated considering both directions of applications of the horizontal components. The maximum computed displacements are summarised in Table 5.30 and 5.31. The highest displacements were obtained for mechanism 3 (α = 0), without the drainage system and when the vertical components are scaled by the same factor as the corresponding horizontal component. The results obtained for each accelerogram are summarised in Tables 5.32, 5.33 and 5.34. Appendix D reports time histories of acceleration, velocity and displacement obtained for each seismic input for sliding mechanism 3.

Chapter 6 examines safety against rotation for the Calabria Anchor Block.

Safety against rotation was evaluated by imposing momentum equilibrium around point O belonging to the plane of motion (Figure 6.1). The load factors of the design actions are set equal to unity (seismic conditions § 7.11.1 - D.M. 14.01.2008). Safety against rotation is treated as an equilibrium limit state of rigid body (EQU) using the partial safety factor of group M2 and is ensured when the resistant moments are equal or larger than driving moments, as per eq.(28), in which: e_i is the distance of the line of action of each force from point O, factored values of the cable force T are introduced as provided by structural analyses of the tender design; the passive earth resistance R_{Pd} refers to mechanism 3, and the contribution of slide resistance T_{Ld} developed along the sides of the anchor block is neglected. Calculations were carried out both with (section 6.1) or without (section 6.2) the drainage system. Table 6.2 and 6.3, and Tables 6.4 and 6.5 report the resistant and the driving actions, with or without the drainage system, respectively. The ratios of the resisting actions and the driving actions, with or without the drainage system, are equal to 1.5 and 1.4, respectively. In both cases the requirements of D.M. 14.01.2008 are fulfilled.

Chapter 7 examines safety against bearing capacity failure for the Calabria Anchor Block.

Safety against bearing capacity failure was evaluated using Approach 1, Combination 2 (D.M. 14.01.2008). The loads considered for the evaluation of bearing capacity are the cable force *T*, the weight of the anchor block *W* and the horizontal and vertical components of the pseudostatic inertial force, $K_h W$ and $K_v W$. The sliding resistance developed on the side walls of the anchor block the passive earth resistance were neglected. Both assumptions are conservative.

The bearing capacity was evaluated in terms of effective stress using appropriate correction factors to take into account the inclination of the applied load, the shape of the foundation, and the inclination of the foundation base, using Terzaghi's theory as from eq.(30). To account for the eccentricity of the load, the bearing capacity was computed for an equivalent rectangular foundation with reduced width *B′* and length *L′*. Design values of resistances and forces were obtained from the corresponding characteristic values and are those acting normally to the foundation plane. Safety against bearing capacity failure is ensured if $R_d \geq E_d$. The partial safety factors of the design actions are set equal to one: $\gamma_G = \gamma_Q = 1$ (seismic conditions: § 7.11.1 - D.M. 14.01.2008). However, the cable forces used to compute the design components of the loads acting normally and tangentially to the foundation plane in eqs. (31) and (32) are inclusive of partial load factors, as provided by structural analyses of the tender design. Calculations were carried out both with (section 7.1) or without (section 7.2) the drainage system, with reference to the ULS loading condition. Tables 7.2 and 7.3 and Tables 7.4 and 7.5 give the values of the design loads acting normally and tangentially to the foundation plane, with or without the drainage system, respectively. The ratio of the design bearing resistance and the normal design load, with or without the drainage system, are equal to 1.71 and 1.34, respectively. In both cases the requirements of D.M. 14.01.2008 are fulfilled.

Chapter 8 summarises the contents of the report.

The seismic performance of the Calabria anchor block was evaluated using the pseudo-static approach, in which the anchor block is assumed to be in a state of limit equilibrium under the action of inertial and static forces, and the displacement-based approach, in which the earthquake-induced displacements of the anchor block are evaluated for a number of input seismic motions. Safety verifications were carried out both considering and neglecting the effect of the drainage system. Three possible sliding mechanisms were examined, characterised by angles of inclination α= 33.7°, 25.3° and 0°. Companion plane strain FE analyses of the anchor block permitted to evaluate that the prevailing inclination of the displacement vectors is in the range 0°-25.3° so that the second and the third mechanisms were recognised to be the most likely to occur. The sliding mechanism is only slightly affected by the pore water pressure distribution. As far as the pseudo-static conditions are concerned, both design actions and design resistances were computed using the pseudo-static seismic coefficients given by the Italian building code (D.M. 14.01.2008). The obtained results showed that safety against sliding is adequately satisfied for each of the loading condition provided by structural analyses. Earthquake-induced displacements were computed using 30 input accelerograms. The horizontal component of the selected acceleration time histories was scaled to 0.58 g, while the vertical component was scaled either by the same factor used for the corresponding horizontal component, or to 0.58 g as well. The earthquake-induced displacements decrease with decreasing inclination of the sliding mechanism. If the effect of the drainage tunnel is accounted for, the maximum displacement is equal to 14 mm for mechanism 2 (α=25.3°) and equal to 69 mm for mechanism 3 (α=0°), while, if the effect of the drainage system is neglected, the maximum displacement is equal to 21 mm for mechanism 2 and to 72 mm for mechanism 3. Finally, bearing capacity and safety against rotation were estimated following the prescriptions of D.M. 14.01.2008, the results showing that both the requirements are satisfied for the considered loading conditions.

Appendix F and Appendix G. Updated cable forces obtained from global IBDAS model version 3.3b and version 3.3f

The forces transmitted by the main cables to the Calabria Anchor Block have been re-evaluated using the global IBDAS model version 3.3b and version 3.3f. The worst load combinations were selected for each limit state (SILS, SLS2 and ULS) for both static and seismic conditions, using 6 different criteria (Table F.1 – Table F.2 for version 3.3b, Table G.1 – Table G.2 for version 3.3f). For both IBDAS model versions, a low difference is observed between the Tender Design and the updated (IBDAS) cable forces, the ratio being in the range of 1.05 to 0.96 for IBDAS version 3.3b (Table F.3) and in the range of 1.07 to 0.93 for IBDAS version 3.3f (Table G.3); the higher value refers to the ULS load combination, while the lower is obtained for the SILS load combination. For the Ultimate Limit State (ULS) cable forces provided by the Tender Design are 5% higher than the corresponding IBDAS 3.3b values and 7% higher than the corresponding IBDAS 3.3f values, this resulting in a conservative estimate of the behaviour of the Calabria Anchor Block.

2 Soil profile and geotechnical characterisation

Figure 2.1 shows the soil profile on the Calabria shore. Starting from ground level and moving downwards the following units are encountered:

Depositi Costieri (Coastal Deposits). Sand and gravel with very little or no fine content, with a thickness varying between a minimum of 5 m towards inner land and a maximum of 45 m towards the sea shore. At this location, these deposits are generally coarser in the first 15 to 20 m b.g.l. and become sandier with depth; towards inner land these deposits are generally sandier. Occasionally, silty peaty layers appear in the lower part of the formation.

- *Ghiaie di Messina* (Messina Gravel)/*Sedimenti dei terrazzi* (Terrace Deposits). Gravel and sand, with very occasional silty layers; difficult to distinguish from the Coastal Deposits and of small thickness, at times totally absent, so that the Coastal Deposits rest directly above the underlying Continental Deposits/Vinco Calcarenite.
- *Depositi Continentali* (Continental Deposits)/*Calcarenite di Vinco* (Vinco Calcarenite). Clayey-sandy deposit, consisting of layers of silt or silt and sand, with significant gravel content/Bio-calcarenite and fossiliferous calcarenite, with thin silty layers.
- *Conglomerato di Pezzo* (Pezzo Conglomerate). Soft rock, consisting of clasts of different dimensions in a moderately cemented silty-sandy matrix and sandstone. The thickness of this formation is larger than 200 m.
- *Cristallino* (Crystalline bedrock). Tectonised granite.

A plan view at the site of the Calabria Anchor Block is shown in Figure 2.2 together with the location of the available site investigations. The actual level of the ground is in between 114 m a.s.l. and 127 a.s.l., and the groundwater level varies between 95 m a.s.l. and 107 m a.s.l. with an average value of 102.3 m a.s.l.

The two longitudinal sections and the cross section indicated in Figure 2.2 are shown in Figure 2.3 – 2.5. The sections in the figures show that in front of the anchor block the Coastal Deposits, about 20 m thick (~ 120 – 100 m a.s.l.), overlie the weathered Pezzo Conglomerate with a thickness of about 20 m (~ 100 – 80 m a.s.l.), while the Pezzo Conglomerate is found below an elevation of 80 m a.s.l., then extending over a thickness of about 130 m. For the Calabria Anchor Block, the relevant geological unit is the Pezzo Conglomerate, with a weathered shallow layer (20 m $<z<$ 40 m), overlain by the Coastal Deposits of small thickness.

The permeability of the Coastal Deposits was evaluated by pumping tests carried out from a well located in the area of the Calabria Tower and extending 33 m b.g.l., and by Lefranc permeability tests carried out in two boreholes at depths between about 5 m b.g.l. and 45 m b.g.l. The value of the horizontal permeability resulting from the more reliable well pumping tests is $k_h = 2.6 \cdot 10^{-3}$ m/s; the measured value of the ratio between vertical and horizontal permeability ranges between $k_v/k_h = 0.10$ and $k_v/k_h = 0.17$. The permeability of the Pezzo Conglomerate was evaluated by Lugeon tests carried out at the location of the Calabria Tower foundation in one of the boreholes used for Lefranc tests, at pressures of 1, 2, and 3 atm, between depths of 48 to 58 m b.g.l.. The results show values of permeability possibly decreasing with depth, with an average value of $2.3 \cdot 10^{-2}$ m/s.

Standard and large penetration tests provided high values of N_{SPT} and N_{LPT} in the Coastal Deposits, although a large scatter was observed (Figure 2.6); an estimate of the coefficient of earth pressure at rest is $K_0 = 0.43 – 0.47$.

The Pezzo Conglomerate is cemented and geologically relatively old (Miocene); it is likely that the geological history of the formation includes mechanical overconsolidation. An estimate of the values of the coefficient of earth pressure at rest is K_0 = 0.6-0.9

The relative density of the Coastal Deposits and Messina Gravel was estimated from the SPT and LPT results using the procedure proposed by Cubrinovski and Ishihara (1999): values of D_R = 40 % to 70 % were obtained as shown in Figure 2.7. The angle of shearing resistance φ' = 41° – 44° was then evaluated through the relationship proposed by Schmertmann (1975) (Figure 2.7).

The shear strength parameters of the Pezzo Conglomerate were obtained from the results of large diameter (865 mm) plate loading tests carried out in the area of the Calabria Anchor Block. These were carried out at three different depths of 5, 11.85, and 16 m b.g.l. within a 2.5 m diameter shaft.

The results were interpreted adopting the available solutions for the limiting pressure, q_u, of a circular shallow foundations (Berezantzev, 1964):

$$q_u = C_K c' + B_K \gamma D + A_K \gamma \frac{B}{2}$$

In which γ (= 20 kN/m^3) and c' are the unit weight and the cohesion of the soil, B (= 0.865 m) is the diameter of the plate, D (= 0) is the depth of the plate and A_K, B_K and C_k are capacity factors depending on the friction angle φ'.

The values of q_u were obtained directly for the test carried out at 5 m b.g.l. which was taken to failure, and extrapolated with a hyperbolic law for the other two tests. In this manner, for any given value of φ' it is possible to calculate the corresponding value of c'. Figure 2.8 shows the values of c' obtained at depths between 5 and 16 m b.g.l. assuming that the friction angle is in the range φ' = 38°÷42°. For depths larger than 16 m b.g.l. it is conservative to assume that c' is constant and equal to its value at 16 m b.g.l.; this assumption is consistent with the existence at the top of the Pezzo conglomerate unit of a layer of weathered conglomerate, also shown by the shear wave velocity profiles of the following section. In this type of materials, an increase of cohesion with depth does not affect the friction angle (see *e.g.:* Jamiolkowski *et al*., 1991)

The stiffness characteristics of the deposits were obtained from one cross-hole test carried out in the vicinity of the Calabria Anchor Block (AC-BH1), using three boreholes reaching a maximum depth of 100 m b.g.l., at a distance of 5 m from one another. The results of the cross-hole test in terms of shear wave velocity, V_s, versus depth are given in Figure 4.3.60 of Report PP-2R-A24. In Figure 2.9 the same results are shown as profiles of small strain shear modulus, G_0. This has been obtained from the shear wave velocity as:

$$G_0 = \rho V_S^2$$

The three data sets refer to the values obtained in each of the three boreholes, while the continuous line is the average of the three data at each depth.

The G_0 profile with depth shows three different trends: for 0 m<z<20 m G_0 increases rapidly from 190 MPa to 1200 MPa; for 20 m<z< 40 m G_0 varies from about 1200 MPa to about 1400 MPa; below z=40 m the data are more dispersed with an average value of 2000 MPa. Table 2.1 summarises the main mechanical parameters obtained from the geotechnical characterisation above.

Table 2.1. Summary of main mechanical parameters from geotechnical characterization

	depth (m bgl)	K_0	φ'_p (°)	c' (kPa)	K_h (m/s)*	G_0 (MPa)
Coastal dep.	0÷20	0.43÷0.47	41÷42	---	$2.6 \cdot 10^{-3}$	190÷1200
Weath.Pezzo C.	20÷40	0.6÷0.9	40	35÷70	$2.3 \cdot 10^{-2}$	1200÷1400
Pezzo Congl.	>40	0.6÷0.9	40	70	$2.3 \cdot 10^{-2}$	2000

3 Constitutive soil model and soil parameters

In the FE analyses discussed in the following sections, the mechanical behaviour of the soil was described using the constitutive model Hardening Soil available in the model library of the code Plaxis. The model is capable of reproducing soil non-linearity due to the occurrence of plastic strains from the early beginning of a loading process. The computed non linear stress-strain relationship has tangent initial modulus equal to E'_0; upon unloading, the model assumes elastic behaviour with Young's modulus E'_0, thus reproducing a significant change in stiffness. In the model, soil stiffness depends on the effective stress state.

Hardening soil model is an elastic-plastic rate independent model with isotropic hardening. The elastic behaviour is defined by isotropic elasticity through a stress-dependent Young's modulus:

$$E' = E^{ref}\left(\frac{c' \cdot \cot\varphi' + \sigma_3'}{c' \cdot \cot\varphi' + p^{ref}}\right)^m$$

where σ'_3 is the minimum principal effective stress, c′ is the cohesion, φ′ is the angle of shearing resistance, p^{ref} = 100 kPa is a reference pressure; E^{ref} and m are model parameters.

The model has two yield surfaces f_s and f_v with independent isotropic hardening depending on distortional plastic strain $\gamma^p = (2 \cdot \varepsilon^p_1 - \varepsilon^p_v)$ and on volumetric plastic strains ε^p_v, respectively; the two surfaces have the following equations:

$$f_s = \frac{1}{E'_{50}} \frac{q}{(1 - 0.9 \cdot q/q_f)} - \frac{2q}{E'} - \gamma^p = 0$$

$$f_v = \frac{\tilde{q}^2}{\alpha^2} + p'^2 - p_c'^2 = 0$$

Parameter E'_{50} is given by an expression similar to E′, but, in contrast to it, it is not used within a concept of elasticity. Hardening of the f_s surface is isotropic and depends on the plastic distortional strain $\gamma^p = (2 \cdot \varepsilon^p_1 - \varepsilon^p_v)$.

In the equations above, p' is the mean effective stress; $\tilde{q}$ is a generalised deviator stress, that accounts for the dependence of strength on the intermediate principal effective stress σ'_2; α controls the shape of the f_v surface in the $\tilde{q}$ -p' plane and can be related to the coefficient of earth pressure at rest K_0 for normally consolidated states. The hardening parameter p'_c is the size of the current f_v surface and is related to the plastic volumetric strains ε_v^p through the hardening law, written in the incremental form as:

$$d\varepsilon_v^p = \frac{\beta}{p^{ref}}\left(\frac{p'_c}{p^{ref}}\right)^m \cdot dp'_c$$

where β is a parameter that controls the variation of p'_c with the plastic volumetric strains. In the model formulation implemented in Plaxis, the parameter E'_{oed}, which is related to β, has to be specified. This is the constrained modulus for one-dimensional plastic loading, and depends on the maximum principal effective stress σ'_1 through the relationship:

$$E'_{oed} = E'^{ref}_{oed} \cdot \left(\frac{c' \cdot \cot\varphi' + \sigma_1'}{c' \cdot \cot\varphi' + p^{ref}}\right)^m$$

where σ'_1 is the maximum principal effective stress.

The initial value of the hardening parameter p'_c is related to the one-dimensional vertical yield stress, and can therefore be specified by assigning a value for the overconsolidation ratio OCR. OCR has to be regarded as a yield stress ratio (YSR) defined in the framework of strain hardening plasticity, so that values of OCR > 1 can be specified also for geologically normally consolidated soil deposits exhibiting a yield stress larger than the *in-situ* stress.

The flow rule is associated for states lying on the surface f_v, while a non associated flow rule is used for states on the surface f_s. The latter is derived from the theory of stress dilatancy by Rowe (1962): the mobilised dilatancy angle ψ_m depends on the current stress state through the angle of mobilised friction φ'_m and the angle of friction at constant volume φ'_{cv}:

$$\sin\psi_m = \frac{\sin\varphi'_m - \sin\varphi'_{cv}}{1 - \sin\varphi'_m \sin\varphi'_{cv}}$$

In turn, φ'_{cv} can be obtained from the angle of shearing resistance φ' and the angle of dilatancy ψ at failure:

$$\sin\varphi'_{cv} = \frac{\sin\varphi' - \sin\psi}{1 - \sin\varphi' \sin\psi}$$

Figure 3.1 shows the shape of the yield surfaces f_v and f_s and schematically indicates their evolution.

For plastic loading from isotropic stress states, the model predicts a non linear stress-strain relationship with tangent initial modulus equal to E'. Therefore, values of E' were related to the shear modulus at small-strain G_0 obtained from the cross-hole test carried out in the site. In particular, values of E'^{ref} and m were obtained by best fitting the cross-hole test results using the equation given above for E' and assuming $\nu' = 0.2$.

In the FE analyses discussed in the following a simplified soil profile was assumed, characterised by a conservative and constant value of the shear stiffness (G_0 = 1100 MPa). Figure 3.2 shows the profile of G_0 against the depth b.g.l.; the dashed line in the figure represents the assumed profile of G_0, whose value is obtained starting from the values of c', φ', E'^{ref} and m reported in Table 3.1. In the report it is shown that the assumed soil profile results in a conservative estimate of block behaviour in that slightly larger block displacements are computed.

Stiffness decay with shear strain was described using ratios of $E'^{ref} / E'^{ref}_{50} = 2$ and of $E'^{ref}_{50} / E'^{ref}_{oed} = 1.0$ and a value for the angle of dilatancy at failure $\psi = 0$.

Table 3.1. Hardening soil parameters for FE analyses of the anchor block

Soil	γ (kN/m^3)	c' (kPa)	φ' (°)	K_0	YSR	E'^{ref} (kPa)	m	E'^{ref}_{50} (kPa)	E'^{ref}_{oed} (kPa)
Pezzo conglomerate	20.0	70.0	40	0.42	2.0	$2.64 \cdot 10^6$	0.0	$1.32 \cdot 10^6$	$1.32 \cdot 10^6$

4 Anchor Blocks – Safety against sliding

4.1 Static conditions – governing equations

4.1.1 Global safety factor

The global factor of safety against sliding can be written as:

$$F = \frac{[W' \cos\alpha + T\mathrm{sen}(\alpha - i)]\tan\varphi'_s + T_L + R_p \cos(\alpha - \delta)}{T\cos(\alpha - i) - W'\mathrm{sen}\alpha + S_a \cos\alpha} \quad (1)$$

where (Fig. 4.1):

- W' = submerged weight of the anchor block
- T = force transmitted by the cables
- α = inclination of the sliding surface
- *i* = inclination of the forces transmitted by the cables
- φ'_s = angle of shearing resistance on the sliding surface
- T_L = sliding resistance developed on the lateral sides of the block
- R_P = passive earth resistance developed in the front of the block
- S_a = active earth thrust developed behind the block (computed assuming $\delta = 0$)
- δ = friction angle at the soil-concrete interface

The safety factor against sliding becomes $F = \infty$ if $T\cos(\alpha\text{-}i) = W'\mathrm{sen}\alpha - S_a\cos\alpha$. Values of $F < 0$ are meaningless; in these cases only part of the block weight acts on the sliding surfaces and $F = \infty$ can be assumed.

4.1.2 Partial safety factors

In D.M. 14.01.2008 – "Nuove norme tecniche per le costruzioni", partial safety factors are applied to actions, resistances and strength parameters. Once the design values of the actions E_d and the resistance R_d are computed, condition $R_d \geq E_d$ must be satisfied.

For the case at hand the characteristic actions and the characteristic resistance are defined as:

$$\begin{aligned} E_k &= T_k \cos(\alpha - i) - W'_k \mathrm{sen}\alpha + S_{ak} \cos\alpha \\ R_k &= [W'_k \cos\alpha + T_k \mathrm{sen}(\alpha - i)]\tan\varphi'_s + T_{Lk} + R_{Pk} \cos(\alpha - \delta) \end{aligned} \quad (2)$$

In section 2.6.1 of D.M. 14.01.2008 two alternative approaches are defined: the Approach 1 and the Approach 2. In Approach 1, two combinations of partial safety factors are used, in which the design actions are multiplied by factors of group A, the strength parameters are divided by factors of group M and the global resistance of the system is divided by factors of group R. Combination 1 (C1), named

STR, is used for limit state verifications of structural components, while Combination 2 (C2), named GEO, is used to study limit states that involve collapse mechanisms of the soil interacting with the structure. Specifically, the actions are mainly amplified in combination 1, while the soil resistances are mainly reduced in combination 2.

In Approach 2, a single combination of partial safety factors is defined.

Following Approach 1, Combination 2 to study geotechnical (GEO) limit states, it is:

$$E_d = T_d \cos(\alpha - i) - \gamma_{G1} \cdot W'_k \mathrm{sen}\alpha + \gamma_{G1} \cdot S_{ad} \cos\alpha$$
$$R_d = \frac{1}{\gamma_R}\left\{\left[\gamma_{G1} \cdot W'_k \cos\alpha + T_d \mathrm{sen}(\alpha - i)\right]\frac{\tan\varphi'_{sk}}{\gamma_\varphi} + \gamma_{G1} \cdot T_{L_d} + \gamma_{G1} \cdot R_{P_d} \cos(\alpha - \delta)\right\} \tag{3}$$

where γ_φ = 1.25 and γ_R = 1.1

In equation (3):

- the shear resistance on the lateral sides of the block, the passive earth resistance in front of the block and the active earth thrust are computed using reduced values of the angle of shearing resistance acting on the sliding surface φ'_{sd} = atan [(tanφ'_{sk})/γ_φ];
- the cable forces are inclusive of partial load factors, as provided by structural analyses of the tender design for each limit state and therefore are not factored;
- according to D.M. 14.01.2010, the weight of the anchor block (permanent load), present in both the action E_d and the resistance R_d, is multiplied by the same load factor γ_{G1} = 1, irrespective of its effect;
- components of S_a and R_p normal to the sliding surface are neglected.

Safety against sliding under static loading conditions will not be evaluated in the following since the pseudo-static loading conditions are the most critical.

4.2 Seismic conditions – governing equations

Analysis of the anchor blocks under seismic conditions is carried out using the force-based pseudo-static approach and the displacement-based sliding block approach.

4.2.1 Pseudo-static approach

In the pseudo-static approach, the anchor block is assumed to behave as a rigid block and to be in a state of equilibrium under the action of inertial and static forces. The stability of the block is measured either by a global factor of safety F that is the ratio of the total resisting force to the total driving force, or by a comparison of the design action with the design resistance, both including the effect of partial safety factors.

4.2.1.1 Global safety factor

The global factor of safety against sliding can be written as:

$$F = \frac{[W'\cos\alpha + T\text{sen}(\alpha - i) + W(K_h \text{sen}\alpha \pm K_v \cos\alpha)]\tan\varphi'_s + T_L + R_{pE}\cos(\alpha - \delta)}{T\cos(\alpha - i) - W'\text{sen}\alpha + S_{aE}\cos\alpha + W(K_h\cos\alpha \pm K_v \text{sen}\alpha)} \tag{4}$$

where (Fig. 4.2):

- W' = submerged weight of the anchor block
- W = weight of the anchor block
- T = force transmitted by the cables
- α = inclination of the sliding surface
- i = inclination of the forces transmitted by the cables
- φ'_s = angle of shearing resistance on the sliding surface
- T_L = sliding resistance developed on the lateral sides of the block
- R_{PE} = pseudostatic passive earth resistance developed on the front of the block
- S_{aE} = pseudostatic active earth thrust developed behind the block
- δ = friction angle at the soil-concrete interface
- K_h = horizontal seismic coefficient
- K_v = vertical seismic coefficient

4.2.1.2 Partial safety factor

In D.M. 14.01.2008 – "Nuove Norme Tecniche per le Costruzioni", partial safety factors are applied to actions, resistances and strength parameters. However, under seismic condition the load factors of the design actions are set equal to unity: $\gamma_G = \gamma_Q = 1$ (§ 7.11.1 - D.M. 14.01.2008); accordingly these factors are omitted in the following.

Once the design values of the actions E_d and the resistance R_d are computed, condition $R_d \geq E_d$ must be satisfied.

For the case at hand the characteristic actions and the characteristic resistance are defined as:

$$\begin{aligned} E_k &= T_k\cos(\alpha - i) - W'_k\text{sen}\alpha + S_{aE(k)}\cos\alpha + W_k(K_h\cos\alpha \pm K_v\text{sen}\alpha) \\ R_k &= [W'_k\cos\alpha + T_k\text{sen}(\alpha - i) + W_k(K_h\text{sen}\alpha \pm K_v\cos\alpha)]\tan\varphi'_s + T_{L_k} + R_{pE(k)}\cos(\alpha - \delta) \end{aligned} \tag{5}$$

Following, as above, the Approach 1, Combination 2, it can be written:

$$E_d = T_d \cos(\alpha - i) - W'_k \text{sen}\alpha + S_{aE(d)} \cos\alpha + W_k (K_h \cos\alpha \pm K_v \text{sen}\alpha)$$
$$R_d = \frac{1}{\gamma_R}\left\{[W'_k \cos\alpha + T_d \text{sen}(\alpha - i) + W_k (K_h \text{sen}\alpha \pm K_v \cos\alpha)]\frac{\tan\varphi'_s}{\gamma_\varphi} + T_{Ld} + R_{pE(d)} \cos(\alpha - \delta)\right\} \quad (6)$$

with γ_φ = 1.25 and γ_R = 1.1

In equation (6):

- the shear resistance on the lateral sides of the block, the passive earth resistance in front of the block and the active earth thrust behind the block are computed using reduced values of the angle of shearing resistance acting on the sliding surface $\varphi'_{sd} = \text{atan}\,[(\tan\varphi'_{sk})/\gamma_\varphi]$;
- the cable forces are inclusive of partial load factors, as provided by structural analyses of the tender design for each limit state;
- components of S_a and R_p normal to the sliding surface are neglected.

4.2.2 Displacement-based approach

In the displacement-based approach, the safety of the anchor block is evaluated by comparing the permanent displacement developed during the earthquake with a threshold value. The earthquake–induced displacement of the potential sliding mass is determined following a two step procedure: first, the critical acceleration is determined by the pseudo-static approach; then, the cumulative displacement of the potentially sliding mass is evaluated using the sliding block analysis.

In the analysis, the potential sliding mass is treated as a rigid body and permanent displacements take place whenever the ground acceleration exceeds the critical acceleration. For a given earthquake, the permanent displacement is calculated by integrating twice the acceleration time history with the critical acceleration used as the reference datum; more specifically, numerical integration is extended to the time intervals in which the velocity of the sliding mass relative to the ground is positive.

According to section C.7.11 of Circolare No.617 dated 02.02.09 (Istruzioni per l'applicazione delle "Nuove norme tecniche per le costruzioni" di cui al D.M. 14.01.08), the critical acceleration must be evaluated using the characteristic values of the strength parameters c'_k and φ'_k. Recalling that under seismic conditions the load factors are equal to unity, in the following suffix k and coefficients γ_G and γ_Q are omitted for simplicity.

4.2.2.1 Critical seismic coefficient

The pseudo-static seismic action is assumed to act with an angle (α-θ) with respect to the sliding surface (Fig. 3.3). Assuming conditions of limit equilibrium (F = 1) and neglecting at this stage the contributions of passive and active earth thrusts, the following expression for K is obtained:

$$F = \frac{[W'\cos\alpha + T\text{sen}(\alpha - i) + KW\text{sen}(\alpha - \theta)]\tan\varphi'_s + T_L}{T\cos(\alpha - i) - W'\text{sen}\alpha + KW\cos(\alpha - \theta)} = 1 \qquad (7)$$

$$K = \frac{[W'\cos\alpha + T\text{sen}(\alpha - i)]\tan\varphi'_s - T\cos(\alpha - i) + W'\text{sen}\alpha + T_L}{W[\cos(\alpha - \theta) - \text{sen}(\alpha - \theta)\tan\varphi'_s]} \qquad (8)$$

The minimum value of K, that is the critical seismic coefficient K_c, is obtained for $\theta = \alpha + \varphi_s' \Rightarrow \alpha - \theta = -\varphi'_s$ (Fig. 4.3):

$$K_{c(red)} = \frac{[W'\cos\alpha + T\text{sen}(\alpha - i)]\tan\varphi'_s - T\cos(\alpha - i) + W'\text{sen}\alpha + T_L}{W[\cos(-\varphi'_s) - \text{sen}(-\varphi'_s)\tan\varphi'_s]} \qquad (9)$$

During sliding ($K > K_c$), it can be assumed that a net earth thrust ΔR, obtained as the difference between the normal stresses acting in front and behind the anchor block increases gradually with increasing block displacements. Therefore, the effect of ΔR is explicitly included in the equation of relative motion used for computing the earthquake-induced displacement of the anchor block.

ΔR is a function of the relative displacement cumulated during the earthquake loading:

$$\Delta R(u) = k_d(u) \cdot u(t) \qquad (10)$$

where k_d is a non linear spring stiffness, depending on relative displacement u (Fig. 4.4).

4.2.2.2 Equation of relative motion under seismic conditions

The equation of relative motion of the anchor block can be written in its simplest form as:

$$m\ddot{u}(t) = [E_d(K) - E_d(K_{c(red)})] - [R_d(K) - R_d(K_{c(red)})] \qquad (11)$$

where

$[E_d(K) - E_d(K_{c(red)})]$ = net driving action relative to limit equilibrium conditions

$[R_d(K) - R_d(K_{c(red)})]$ = net resisting force relative to limit equilibrium conditions

Since it is:

$$\begin{aligned} E_d(K) &= [T\cos(\alpha - i) - W'\text{sen}\alpha + K(t)W\cos(\alpha - \theta)] \\ E_d(K_{c(red)}) &= [T\cos(\alpha - i) - W'\text{sen}\alpha + K_{c(red)}W\cos(a - \theta)] \end{aligned} \qquad (12)$$

and

$$\begin{aligned} [R_d(K)] &= [W'\cos\alpha + T\text{sen}(\alpha - i) + K(t)W\text{sen}(\alpha - \theta)]\tan\varphi'_s + T_L \\ [R_d(K_{c(red)})] &= [W'\cos\alpha + T\text{sen}(\alpha - i) + K_{c(red)}W\text{sen}(\alpha - \theta)]\tan\varphi'_s + T_L + \Delta R(u) \end{aligned} \qquad (13)$$

it can be obtained:

$$\begin{aligned}\left[E_d(K)-E_d\left(K_{c(red)}\right)\right]&=\left[K(t)-K_{c(red)}\right]\cdot W\cos(\alpha-\theta)\\ \left[R_d(K)-R_d\left(K_{c(red)}\right)\right]&=\left[K(t)-K_{c(red)}\right]\cdot W\mathrm{sen}(\alpha-\theta)\tan\varphi'_s+\Delta R(u)\end{aligned} \quad (14)$$

and

$$\frac{W}{g}\ddot{u}(t)=\left[K(t)-K_{c(red)}\right]\cdot W\frac{\cos(\alpha-\theta+\varphi'_s)}{\cos\varphi'_s}-k_d(u)\cdot u(t) \quad (15)$$

that, for $\theta = \alpha + \varphi_s' \Rightarrow \alpha - \theta = -\varphi'_s$, provides:

$$\ddot{u}(t)+g\frac{k_d(u)}{W}\cdot u(t)=g\left[K(t)-K_{c(red)}\right]\frac{1}{\cos\varphi'_s} \quad (16)$$

Finally, separating the horizontal and vertical components of the acceleration time histories, it can be written:

$$\begin{aligned}E_d(K)&=\left[T\cos(\alpha-i)-W'\mathrm{sen}\alpha+W\left(K_h\cos\alpha+K_v\mathrm{sen}\alpha\right)\right]\\ E_d\left(K_{c(red)}\right)&=\left[T\cos(\alpha-i)-W'\mathrm{sen}\alpha+K_{c(red)}W\cos(a-\theta)\right]\end{aligned} \quad (17)$$

$$\begin{aligned}\left[R_d(K)\right]&=\left[W'\cos\alpha+T\mathrm{sen}(\alpha-i)+W\left(K_h\mathrm{sen}\alpha-K_v\cos\alpha\right)\right]\tan\varphi'_s+T_L\\ \left[R_d\left(K_{c(red)}\right)\right]&=\left[W'\cos\alpha+T\mathrm{sen}(\alpha-i)+K_{c(red)}W\mathrm{sen}(\alpha-\theta)\right]\tan\varphi'_s+T_L+\Delta R(u)\end{aligned} \quad (18)$$

the net driving action and resisting force being:

$$\begin{aligned}\left[E_d(K)-E_d\left(K_{c(red)}\right)\right]&=W\left[K_h\cos\alpha+K_v\mathrm{sen}\alpha-K_{c(red)}\cos(\alpha-\theta)\right]\\ \left[R_d(K)-R_d\left(K_{c(red)}\right)\right]&=W\left[K_h\mathrm{sen}\alpha-K_v\cos\alpha-K_{c(red)}\mathrm{sen}(\alpha-\theta)\right]\tan\varphi'_s+\Delta R(u)\end{aligned} \quad (19)$$

so that the equation of relative motion is:

$$\frac{W}{g}\ddot{u}(t)=W\left\{K_h\left(\cos\alpha-\mathrm{sen}\alpha\tan\varphi'_s\right)+K_v\left(\mathrm{sen}\alpha+\cos\alpha\tan\varphi'_s\right)-K_c\left[\cos(\alpha-\theta)-\mathrm{sen}(\alpha-\theta)\tan\varphi'_s\right]\right\}+k_d\cdot u(t) \quad (20)$$

that, for $\theta = \alpha + \varphi_s' \Rightarrow \alpha - \theta = -\varphi'_s$, provides:

$$\ddot{u}(t)+g\frac{k_d(u)}{W}u(t)=g\left\{\left[K_h(t)+K_v(t)\tan(\alpha+\varphi'_s)\right]\cos(\alpha+\varphi'_s)-K_{c(red)}\right\}\frac{1}{\cos\varphi'_s} \quad (21)$$

5 Calabria Anchor Block – safety against sliding

5.1 Self weight of the anchor block

Figure 5.1 shows a plan view and a section of the Calabria anchor block. The weight of the anchor block was calculated using a Cad scheme based on drawings from the tender design (Fig. 5.2). The original design includes the presence of two chambers filled with granular material. At the location of Calabria anchor block the hydraulic head is H_w = 94.5 m a.s.l.. In order to reduce pore water pressure, the tender design requires the construction of a drainage tunnel, lowering the water head to H_w = 88.0 m a.s.l. In the following analyses both the presence and the absence of the drainage tunnel are considered. Relevant data are listed in Tables 5.1 and 5.2.

Table 5.1. Weight of Calabria anchor block – presence of the drainage tunnel (H_w = 88.0 m a.s.l.)

	volume (m^3)	γ (kN/m^3)	weight (MN)
concrete	230433	24	5530
fill chambers (x2)	36321	20	726
pore water pressure resulting force	37932	10	-379
Total			5877

Table 5.2. Weight of Calabria anchor block – absence of the drainage tunnel (H_w = 94.5 m a.s.l.)

	volume (m^3)	γ (kN/m^3)	weight (MN)
concrete	230433	24	5530
fill chambers (x2)	36321	20	726
pore water pressure resulting force	75323	10	-753
Total			5503

5.2 Sliding mechanisms

Three possible sliding mechanisms have been considered in the analyses (Fig. 5.3), characterised by angles of inclination α = 33.7°, 25.3° and 0°, as reported in Table 5.3 and Table 5.4; all the mechanisms develop within the soil. In the first mechanism it is assumed that the diaphragm wall in front of the block collapses and the sliding surface trespass it; in the second one, the sliding plane is assumed to develop under the diaphragm tip; in the third mechanism, sliding is assumed to occur at the lowest inclination of the block base. The contribution of soil between the sliding surface and the anchor is considered as an added weight, as it is assumed to move together with the anchor block.

Table 5.3: sliding mechanisms of Calabria anchor block – presence of the drainage tunnel

	inclination (°)	anchor block weight (MN)	soil weight (MN)	total weight (MN)
mechanism 1	33.7	5877	86	5963
mechanism 2	25.3	5877	301	6178
mechanism 3	0	5877	645	6522

Table 5.4: sliding mechanisms of Calabria anchor block – absence of the drainage tunnel

	inclination (°)	anchor block weight (MN)	soil weight (MN)	total weight (MN)
mechanism 1	33.7	5503	70	5573
mechanism 2	25.3	5503	228	5731
mechanism 3	0	5503	534	6037

It can be anticipated that companion FE analyses carried under plane strain conditions indicate that, under ULS loading conditions, the prevailing inclination of the displacement vectors is in the range 0°-25.3° so that the second and the third mechanisms are the most likely to occur. Moreover, the results show that the sliding mechanism is only slightly dependent on pore water pressure distribution. Hence the slopes of the sliding surfaces are kept constant in the analyses irrespective of the presence of the drainage system.

5.3 Evaluation of the sliding surface

In order to estimate the most likely sliding mechanism, plane strain FE analyses were carried out using the code Plaxis 8. Figure 5.4 show the adopted mesh, made of 1759 15-node triangular elements with fourth order interpolation for displacements and third order interpolation for pore water pressure. The mesh is 686.9 m wide, its height ranging from 269.4 m to 310 m. At the lower boundary displacements are restrained both in vertical and horizontal direction, while at the side boundaries only horizontal displacements are restrained.

The geometry of the anchor block is based on the drawings provided in the tender design.

Soil-anchor block contact is modelled through interface elements with reduced shear strength and stiffness.

As illustrated in section 3, soil behaviour was described using the constitutive model Hardening Soil available in the model library of the code Plaxis. This is an elastic-plastic rate independent model with isotropic hardening and Mohr-Coulomb failure criterion.

The cross-hole test carried out at the site in 1992 was used to evaluate the shear modulus at small strains G_0. Stiffness decay with shear strain was described using ratios of $E''^{ref} / E'_{50}{}^{ref} = 2$ and of $E'_{50}{}^{ref} / E'_{oed}{}^{ref} = 1.0$ and a value for the angle of dilatancy at failure $\psi = 0$. Soil parameters adopted in the analyses are those listed in Table 3.2 (see section 3).

An elastic-plastic model was used to describe the mechanical behaviour of interface elements. The strength and stiffness parameters were reduced by applying the following rules:

$$\begin{aligned} \tan\varphi'_{int} &= R_{int} \tan\varphi'_{soil} \\ c'_{int} &= R_{int} c'_{soil} \\ \psi'_{int} &= 0° \\ G_{int} &= R_{int}^2 G_{soil} \end{aligned} \tag{22}$$

where R_{int} is a reduction factor; in the analyses a value of $R_{int} = 0.67$ was adopted.

The anchor block is assumed to behave as an elastic non-porous material with Poisson's ratio $\nu = 0.15$ and Young's modulus $E = 3{\cdot}10^7$ MPa

The analyses were carried out in terms of effective stresses, assuming drained conditions.

In order to carry out plane strain analyses, the equivalent unit weight of both the cable chambers and the filled chambers are to be estimated. This was obtained by making the self-weight of the anchor block equal to that of the equivalent 2D scheme. For each item (cable chamber or filled chamber), the equivalent unit weight γ_{eq} is given by the equation

$$\gamma_{eq} V_{eq} = \gamma_{conc} \left(V_{eq} - V\right) + \gamma V \tag{23}$$

where

- V_{eq} is the volume of either the cable chambers or the filled chambers in the equivalent 2D configuration (i.e. distributed along the whole width of the anchor block, equal to 100 m);
- $\gamma_{conc} = 25$ kN/m^3 is the unit weight of the reinforced concrete;
- γ is the unit weight of the material;
- V is the real volume of either the cable chambers or the filled chambers.

From the previous equation it follows that

$$\gamma_{eq} = \gamma_{conc} + \left(\gamma - \gamma_{conc}\right) \frac{V}{V_{eq}} \tag{24}$$

Table 5.5 summarises the values of γ_{eq} used in the plane strain FE analyses.

Table 5.5. Equivalent unit weights assumed in the 2D F.E. analyses

	V (m^3)	V_{eq} (m^3)	γ (kN/m^3)	γ_{conc} (kN/m^3)	γ_{eq} (kN/m^3)
Cable chambers (x2)	13935	39704	0	25	15.58
Filled chambers (x2)	36321	51888	20	25	21.20

The aim of the 2D FE analyses is to estimate the behaviour of the anchor block in a condition of ultimate limit state. To this purpose, ULS loading conditions were considered in the analyses, spreading the cable load *T* over the width B = 100 m of the anchor block, to account for plane strain conditions.
The following sequence of steps was applied in the analyses: computation of the initial stress state; activation of the anchor block; application of the cable load *T* (Table 5.6).

Table 5.6. Sequence of steps for calculations

step	description
0	initial stress state assuming K_0 stress conditions
1	application of gravity loading (to account for non horizontal ground surface)
2	displacement reset and activation of the anchor block
3	displacement reset and activation of cable load *T*

The cable load *T* is applied with an inclination *i* = 15° to the horizontal; the value corresponding to limit state ULS, *T* = 3934 MN, was provided by structural analyses of the tender design. The presence of diaphragm walls in front and behind the anchor block were not accounted for in the analyses.
Figures 5.5 and 5.6 show the contours of mobilized shear strength, expressed in terms of the ratio t/t_{max} where $t = (\sigma_1'-\sigma_3')/2$ and σ_1' and σ_3' are the maximum and minimum principal effective stresses; as values of t/t_{max} approach unity, the full shear strength of the soil is attained. At step 3, when ULS conditions are applied, part of the shear strength is mobilized at both the base and in front of the anchor block, and a wedge of plastic soil can be recognised as the anchor block is pulled by the cable force. Figures 5.7 and 5.8 show the deformed mesh obtained at this stage, with and without the drainage system.
In order to estimate the most likely sliding surface, the block displacement and its direction were evaluated as the average between the displacements of the centre of gravity and of four nodes of the block at the contact with the soil (Figures 5.9 -5.10).
Table 5.7 and Table 5.8 show the results obtained in the hypothesis of presence or absence of the drainage system.

Table 5.7: displacements of the anchor block at the end of step 4, with drainage system

	X	Y	u_x	u_y	u	Direction
Points	m	m	m	m	m	°
A	79.500	102.800	0.030	0.005	0.030	9.705
B	46.000	77.000	0.029	0.005	0.030	10.633
C	26.000	77.000	0.029	0.005	0.029	10.320
D	-10.000	101.000	0.029	0.001	0.029	1.077
G (centre of gr.)	34.463	101.175	0.030	0.006	0.031	10.505
average					0.030	8.448

Table 5.8: displacements of the anchor block at the end of step 4, without drainage system

Points	x	y	u_x	u_y	u	Direction
	m	m	m	m	m	°
A	79.500	102.800	0.031	0.003	0.031	4.841
B	46.000	77.000	0.031	0.004	0.031	7.436
C	26.000	77.000	0.030	0.004	0.030	8.291
D	-10.000	101.000	0.030	0.001	0.030	1.517
G (centre of gr.)	34.529	102.084	0.031	0.004	0.031	8.275
average					0.031	6.072

Under ULS loading condition, the average displacement is of 30 – 31 mm (with or without drainage system, respectively) and the average direction is in the range of 6.1° to 8.4° on the horizontal. Hence the most likely sliding mechanism is in between the second and the third mechanism, being only slightly affected by the drainage system.

The inclination of the displacement vector of the block computed in the 2D analyses (6°-8°) are in a good agreement with the value of about 8° obtained in the three-dimensional analyses, as shown in the companion report "*Calabria anchor block: evaluation of block behaviour via 3D FE analyses and of bearing capacity*".

Also, maximum block displacement computed in the 2D analyses (u = 3 cm) is in a fair agreement with that computed in the 3D analyses (u = 1 cm) if account is taken for the influence of different geometrical conditions. In fact using the equivalence of 2D versus 3D analyses, it results $u^{3D} \cong 0.5 \cdot u^{2D} \cong 1.5$ cm, that is in a fair agreement with the value of about 1.0 cm computed in the 3D analyses (see appendix A.7 of report "*Evaluation of equivalent stiffness matrices for the soil-foundation systems*").

5.4 Sliding resistance on the sides of the anchor block

The sliding resistance T_L developed on the sides of the anchor block was computed under the conservative hypothesis that active limit equilibrium is achieved behind the diaphragm walls during the excavation stages. The shear stress at the contact of the side walls with the soil can be written as:

$$\tau_s = \sigma'_n \cdot \tan\varphi'_s = K_a \sigma'_v \cdot \tan\varphi'_s$$

where the active earth pressure coefficient K_a is conservatively calculated using the characteristic angle of the shearing resistance of the soil φ'_k = 40°, while a friction angle φ'_s = atan[(3/4)tanφ′] is assumed at the block – soil interface; the corresponding characteristic values were φ'_k = 40° and φ'_{sk} = 32°.
The sliding resistance was computed reducing the tanφ′ and $\tan\varphi'_s$ by the factor γ_φ = 1.25 prescribed by D.M. 14.01.2008 – “Nuove norme tecniche per le costruzioni” (Table 5.9).

Table 5.9. Sliding resistance on the sides of the anchor block T_L

	φ_k' (°)	φ_d' (°)	c_k' (kPa)	c_d' (kPa)
active earth pressure coefficient K_a	40	-	-	-
friction angle at block sides φ'_s = atan[(3/4)tanφ_p']	32.2	26.7	-	-

Table 5.10 and 5.11 list the characteristics and design values of lateral resistance T_L assumed in computation to account for the contribution of the block sides to sliding resistance. The former are used to evaluate the critical seismic coefficient $K_{c(red)}$ given by eq. (9), while the latter is used in the pseudostatic approach. The depth of block sides accounted for in calculation of sliding resistance changes according to the sliding mechanism. The Tables in Appendix A give computation details.

Table 5.10. Sliding resistance on the block sides with the drainage system

mechanism	φ'_{sk} (°)	T_{Lk} (MN)	φ'_{sd} (°)	T_{Ld} (MN)
(1)	32	196.7	26.7	157.4
(2)	32	212.3	26.7	169.9
(3)	32	261.5	26.7	209.2

Table 5.11. Sliding resistance on the block sides without the drainage system

mechanism	φ'_{sk} (°)	T_{Lk} (MN)	φ'_{sd} (°)	T_{Ld} (MN)
(1)	32	186.3	26.7	149.1
(2)	32	200.8	26.7	160.6
(3)	32	244.6	26.7	195.7

5.5 Passive resistance in front of the block

5.5.1 Pseudo static approach

The passive resistance developed in front of the block on sliding was computed using the solution obtained by Chen and Liu (1990) via the kinematic theorem of limit analysis. For a value of φ'_K=40° it was assumed $\delta_K = \varphi'_K/2 = 20°$ and $\delta_d = \varphi'_d/2 = 17°$. Again, according to D.M. 14.01.2008, passive resistance was calculated reducing the tanφ′ by the factor $\gamma_\varphi = 1.25$ (Table 5.12).

Table 5.12. Passive resistance in front of the block R_P

	φ_k' (°)	φ_d' (°)	c_k' (kPa)	c_d' (kPa)
passive earth pressure coefficient K_p	40	33.9	-	-
friction angle at the soil block interfaces $\delta_k = \varphi'_k/2$	20	17	-	-

Table 5.13 reports the values of passive earth pressure coefficients, K_{Pk} and K_{Pd}, evaluated using the characteristic ($\varphi'_k = 40°$) and the design ($\varphi'_d = 33.9°$) values of the angle of shearing resistance, respectively.

Values of K_h and K_v used in computation are also listed in Table 5.13. These were obtained assuming the values of a_g specified in document GCG.F.04.01 “Fondamenti progettuali e prestazioni attese per l’Opera di attraversamento”. Site effects were accounted for by assuming a topographic amplification factor $S_T = 1.2$ and a subsoil amplification factor $S_S = 1.0$. According to D.M. 14.01.2008, coefficient $\beta_m = 0.31$ was used for computing K_h.

Table 5.13. Pseudo-static seismic coefficients and passive earth pressure coefficients

Limit state	a_g (g)	K_h	K_v	K_{Pk} ($\varphi'_k = 40°$)	K_{Pd} ($\varphi'_d = 33.9°$)
SLS2	0.26	0.097	0.049	9.005	5.481
ULS	0.58	0.216	0.108	7.655	4.577
SILS	0.64	0.238	0.119	7.395	4.401

The passive resistance was computed from the head of diaphragm walls (114 m a.s.l.) down to different depths according to the sliding mechanism considered in the analyses; a length L = 100 m was assumed in the calculation. Table 5.14 and Table 5.15 summarise the computed design values of passive resistance R_{Pd} developed in front of the block; for comparison the characteristic values of R_p are also given in the Tables. Appendix B gives computation details.

Table 5.14. Passive earth resistance in front of the block – presence of the drainage system

sliding mechanism	SLS2		ULS		SILS	
	R_{Pk} (MN)	R_{Pd} (MN)	R_{Pk} (MN)	R_{Pd} (MN)	R_{Pk} (MN)	R_{Pd} (MN)
(1) z = 13.1 m	1545.3	940.6	1313.7	785.5	1269.1	755.3
(2) z = 20.0 m	3602.0	2192.4	3062.0	1830.8	2958.0	1760.4
(3) z = 37.3 m	11953.6	7275.7	10161.6	6075.7	9816.5	5842.1

Table 5.15. Passive earth resistance in front of the block – absence of the drainage system

sliding mechanism	SLS2		ULS		SILS	
	R_{Pk} (MN)	R_{Pd} (MN)	R_{Pk} (MN)	R_{Pd} (MN)	R_{Pk} (MN)	R_{Pd} (MN)
(1) z = 13.1 m	1545.3	940.6	1313.7	785.5	1269.1	755.3
(2) z = 20.0 m	3600.9	2191.7	3061.0	1830.2	2957.1	1759.8
(3) z = 37.3 m	11102.0	6757.4	9437.6	5642.8	9117.1	5425.9

5.5.2 Displacement based approach

In the displacement based approach, the passive earth resistance R_P in front of the block is assumed to progressively increase with the relative displacement u induced by the earthquake loading. For computations, an analytical relationship between R_P and u is needed. To this aim, plane strain FE analyses were carried out with reference to mechanism 2 (α = 25.3°) and mechanism 3 (α = 0°) that were seen to be an upper and a lower bound for the inclination of the sliding surface. Figures 5.11 and 5.12 show the FE meshes used for calculations. The same soil profile was assumed in the analyses as discussed in § 2 and 3. In the analyses, an ideal wall characterised by perfectly smooth contact with the soil is located in the position corresponding to the front of the anchor block; the wall length extends to the depth of the sliding mechanism modelled in the analysis (z = 20 m and z = 37.3 m).
An uniform displacement is applied to the wall that progressively increases from 1 mm to about 1 m. For each value of the applied displacement, the earth resistance ΔR for unit length is given by:

$$\Delta R = \int_L \left(\sigma_h - \sigma_{h_0}\right) dl \qquad (25)$$

where σ_h and σ_{h0} are the horizontal stresses acting on the wall for a given displacement u and under geostatic conditions, respectively, and *L* is the height of the ideal wall. The relationship between earth resistance in front of the wall ΔR and wall displacement *u* was obtained by best-fitting the *u* – Δ*R* data through the equation

$$\Delta R(u) = \frac{u}{b + m \cdot u} \tag{26}$$

where *b* and *m* are constants. In such condition, the ultimate value of Δ*R* is given by

$$\Delta R_{max} = \lim_{u \to \infty} \frac{u}{b + m \cdot u} = \frac{1}{m} \tag{27}$$

The assumption of smooth soil-wall interface yield a conservative estimate of passive resistance. Also, the hypothesis of plane strain conditions is conservative in that greater displacements are induced by a given pressure under 2D conditions; as a consequence a more deformable non linear spring is obtained.

In the analyses, the mechanical behaviour of the soil was described using the constitutive model Hardening Soil, that is capable of describing the non linear soil behaviour from the early beginning of the loading process; the same parameters listed in Table 3.2 were used to this purpose.

A comparative analysis has been performed modelling three different soil layers, as derived by the in situ investigations, and accounted for in the 3D analyses of the companion report "*Calabria Anchor Block – evaluation of block behaviour via 3D FE analyses and of bearing capacity*". The comparison, reported in Appendix E, shows that the relationships between wall earth resistance ΔR and wall displacement *u* estimated in this report is conservative and can be used safely.

The sequence of steps adopted in the analyses is summarised in Table 5.16.

Both the presence and the absence of the drainage system were considered in the analyses.

Table 5.16. Sequence of steps for calculations

step	description
0	initial stress state assuming K_0 stress conditions
1	application of gravity loading
2	displacement reset and application of constant displacement along the wall
3	application of the first displacement increment
⋮	⋮
n	application of the last displacement increment

The results obtained if the effect of the drainage system is considered are reported in Table 5.17 and are shown in Figure 5.13 in terms of *u* – Δ*R* relationships. The value of earth resistance for unit length was multiplied for the anchor block width (equal to 100 m) to obtain a ΔR value expressed in term of force (MN). Figure 5.15, Figure 5.16 and Figure 5.17 show the plastic points, the contours of horizontal displacement and the contours of mobilised shear strength (t/t_{lim}) obtained for mechanism 2. Figure 5.18, Figure 5.19 and Figure 5.20 show the plastic points, the contours of horizontal displacement and the contours of mobilised shear strength (t/t_{lim}) obtained for mechanism 3.

Table 5.17. F.E. analysis of passive earth resistance – presence of the drainage system

	Mechanism 2	*Mechanism 3*
m (1/MN)	$3.952 \cdot 10^{-4}$	$1.613 \cdot 10^{-4}$
b (m/MN)	$8.339 \cdot 10^{-6}$	$6.822 \cdot 10^{-6}$
ΔR_{max}(MN)	2530	6200

The results obtained assuming the absence of the drainage system are summarized in Table 5.18 and are shown in Figure 5.14 in terms of u – ΔR relationships. Figures 5.21 – 5.23 show the results obtained for mechanism 2 in terms of plastic points, contours of horizontal displacements and mobilised shear strength. The same results are shown in Figures 5.24 – 5.26 for mechanism 3.

Table 5.18. F.E. analysis of passive earth resistance – absence of the drainage system

	Mechanism 2	*Mechanism 3*
m (1/MN)	$4.109 \cdot 10^{-4}$	$1.712 \cdot 10^{-4}$
b (m/MN)	$8.188 \cdot 10^{-6}$	$6.836 \cdot 10^{-6}$
ΔR_{max} (MN)	2433	5840

5.6 Evaluation of safety against sliding – pseudostatic approach

In evaluating the safety against sliding through the pseudo-static approach, equation 6 was used and the prescriptions of D.M. 14.01.2008 were followed.

The design resistances are computed considering the contributions of sliding resistance at the base and at the block sides and the passive resistance in front of the block. The active earth trust behind the block was accounted for down to a depth of 12 m (the vertical portion of the back wall). Both design actions and design resistances were computed using the pseudo-static seismic coefficients reported in Table 5.13.

The cable force T is inclined on the horizontal of an angle i = 15°. Table 5.19 reports the values of T provided by structural analyses of the tender design for each limit state. In the following, computations are carried out for each limit state although safety against sliding should be verified for ULS loading condition only. For this condition, cable forces provided by the tender design are higher than the corresponding values provided by the global IBDAS model (5% for the version 3.3b and 7% for the version 3.3f), this resulting in a conservative estimate of safety against sliding of Calabria Anchor Block.

Table 5.19. Cable force T

Limit state	SLS	ULS	SLIS
T (MN)	3232	3934	3142

The characteristic value of φ'_s mobilised on the sliding surface was assumed to be φ'_{sk} = atan[(3/4)tanφ_k']=32° (Table 5.20).

Table 5.20. Sliding surface

	φ_k' (°)	φ_d' (°)	c_k' (kPa)	c_d' (kPa)
mobilized shear resistance φ'_{sk} = atan[(3/4)tanφ_p']	32	26.6	-	-

Table 5.21 reports the pseudostatic seismic coefficients, the active earth pressure coefficients and the active earth thrust used for computations.

Table 5.21. Pseudo-static seismic coefficients, active earth pressure coefficients and active earth thrust

Limit state	a_g (g)	K_h	K_v	K_{ak} (φ'_k=40°)	K_{ad} (φ'_k=33.9°)	$S_{aE(k)}$ (MN, φ'_k=40°)	$S_{aE(d)}$ (MN, φ'_k=33.9°)
SLS2	0.26	0.097	0.048	0.269	0.343	38.8	49.4
ULS	0.58	0.216	0.108	0.357	0.445	51.4	64.1
SLIS	0.64	0.238	0.119	0.378	0.470	54.4	67.6

Table 5.22 a-d report the comparison between design resistances and design actions for the three sliding mechanisms assumed in the analyses, for each hydraulic condition. The Tables in Appendix C give computation details.

Table 5.22 a. Safety against sliding, presence of the drainage system; active earth pressure neglected

	SLS2			ULS			SILS		
	ΣR_d	ΣE_d	$\Sigma R_d / \Sigma E_d$	ΣR_d	ΣE_d	$\Sigma R_d / \Sigma E_d$	ΣR_d	ΣE_d	$\Sigma R_d / \Sigma E_d$
Mechanism 1	3726.0	434.5	8.6	3740.9	1938.2	1.9	3608.2	1345.3	2.7
Mechanism 2	4919.9	1253.9	3.9	4642.9	2823.3	1.6	4513.6	2208.8	2.0
Mechanism 3	8942.7	3819.8	2.3	7621.3	5356.9	1.4	7474.7	4752.9	1.6

Table 5.22 b. Safety against sliding, presence of the drainage system; active earth pressure included

	SLS2			ULS			SILS		
	ΣR_d	ΣE_d	$\Sigma R_d / \Sigma E_d$	ΣR_d	ΣE_d	$\Sigma R_d / \Sigma E_d$	ΣR_d	ΣE_d	$\Sigma R_d / \Sigma E_d$
Mechanism 1	3726.0	475.6	7.8	3740.9	1991.6	1.9	3608.2	1401.6	2.6
Mechanism 2	4919.9	1298.5	3.8	4642.9	2881.2	1.6	4513.6	2269.9	2.0
Mechanism 3	8942.7	3869.2	2.3	7621.3	5421.0	1.4	7474.7	4820.5	1.6

Table 5.22 c. Safety against sliding; absence of the drainage system; active earth pressure neglected

	SLS2			ULS			SILS		
	ΣR_d	ΣE_d	$\Sigma R_d / \Sigma E_d$	ΣR_d	ΣE_d	$\Sigma R_d / \Sigma E_d$	ΣR_d	ΣE_d	$\Sigma R_d / \Sigma E_d$
Mechanism 1	3571.2	650.5	5.5	3586.1	2154.3	1.7	3453.4	1561.4	2.2
Mechanism 2	4727.5	1444.6	3.3	4450.6	3014.0	1.5	4321.3	2399.5	1.8
Mechanism 3	8259.4	3819.8	2.2	7012.4	5356.9	1.3	6880.2	4752.9	1.4

Table 5.22. d. Safety against sliding; absence of the drainage system; active earth pressure included

	SLS2			ULS			SILS		
	ΣR_d	ΣE_d	$\Sigma R_d / \Sigma E_d$	ΣR_d	ΣE_d	$\Sigma R_d / \Sigma E_d$	ΣR_d	ΣE_d	$\Sigma R_d / \Sigma E_d$
Mechanism 1	3571.2	691.6	5.2	3586.1	2207.6	1.6	3453.4	1617.7	2.1
Mechanism 2	4727.5	1489.3	3.2	4450.6	3072.0	1.4	4321.3	2460.7	1.8
Mechanism 3	8259.4	3869.2	2.1	7012.4	5421.0	1.3	6880.2	4820.5	1.4

Comparison of Tables 5.22 a-b and Tables 5.22 c-d shows that the contribution of active earth thrust is negligible.

In all the cases examined the ratio ΣR_d / ΣE_d is greater than 1 and safety against sliding is satisfied.

5.7 Evaluation of sliding performance – displacement based approach

5.7.1 Seismic action

In the displacement based approach, a number of input accelerograms have to be selected. To this purpose, 22 acceleration time histories were selected from the PEER strong-motion database specifying a range of magnitude M = 6.5–7.28, and hypocentral distances in the range of 12 to 82 km. The peak acceleration of the input accelerograms ranges from 0.29 g, that is half of the design peak acceleration (0.58 g), to 1.16 g, that is twice the design peak acceleration. In addition to the real acceleration time histories, 8 artificial strong motion accelerograms, fully compatible with the response spectrum of the preliminary design, were also used as input motion to the sliding block analyses.

Table 5.23 reports the main parameters of the horizontal components of the selected accelerograms:

the peak acceleration a_{max}, the peak velocity v_{max}, the Arias intensity I_a, the predominant period of Fourier spectrum T_P, and the duration between the first and the last exceedance of 0.05g ($D_{0.05g}$). In Table 5.24, the same parameters are listed for the vertical component of the accelerograms .

Each horizontal component was scaled to the design peak acceleration a_{max} = 0.58g and the corresponding vertical component was scaled by the same factor. Table 5.25 and Table 5.26 show the parameters of the scaled accelerograms.

The horizontal components of each seismic event were independently considered and combined with the vertical component. The analyses were also repeated using the scaled horizontal component combined with the vertical component scaled to 0.58g as well (Table 5.27).

Figures 5.27–5.31 show the elastic response spectra of the selected accelerograms, compared to the design response spectrum.

Table 5.23. Parameters of the selected accelerograms, horizontal components

Time history	a_{MAX} (g)	v_{MAX} (m/s)	I_a (m/s)	T_P (s)	$D_{0.05g}$ (s)
Friuli 76 TOLXC	0.357	0.210	0.799	0.494	7.48
Friuli 76 TOLYC	0.316	0.326	1.169	0.661	6.09
Imperial Valley 1979 DLT352	0.351	0.330	3.289	1.672	70.53
Kobe 1995 TAZ000	0.693	0.683	3.070	1.638	14.92
Kobe 1995 TAZ090	0.694	0.853	3.935	0.488	12.15
Landers 1992 CLWTR	0.417	0.423	2.172	0.706	18.50
Landers 1992 LCN260	0.727	1.465	6.977	0.106	33.26
Landers 1992 LCN345	0.789	0.324	6.585	0.088	33.33
Loma Prieta 1989 CYC285	0.484	0.397	1.503	0.650	16.92
Loma Prieta 1989 G03000	0.555	0.357	2.087	0.569	9.99
Loma Prieta 1989 G03090	0.367	0.447	1.348	1.862	16.59
Loma Prieta 1989 G04000	0.417	0.388	1.241	0.394	14.73
Manjil 90 ABBL	0.515	0.425	4.656	0.340	49.16
Manjil 90 ABBT	0.496	0.521	7.589	0.218	45.24
Northridge 94 CEN245	0.322	0.229	0.994	0.853	14.16
Northridge 94 LAC180	0.316	0.140	1.051	0.339	16.21
Umbria Marche 97 NCRXC	0.524	0.320	3.304	0.159	12.38
Umbria Marche 97 NCRYC	0.463	0.291	2.822	0.378	10.84
Imperial Valley 79 BC230	0.775	0.460	5.987	0.621	19.09
Irpinia 80 STUYC	0.323	0.546	1.506	2.341	43.48
Montenegro 79 ULCXC	0.294	0.386	1.851	1.092	30.90
Montenegro 79 PETXC	0.454	0.389	4.527	0.458	18.67
Art. 1 comp. 1	0.642	0.757	7.457	0.803	36.58
Art. 1 comp. 2	0.633	0.805	7.667	0.819	27.98
Art. 2 comp. 1	0.656	0.667	6.239	0.910	26.93
Art. 2 comp. 2	0.640	0.742	5.835	0.694	24.92
Art. 3 comp. 1	0.675	0.709	9.664	0.759	37.31
Art. 3 comp. 2	0.611	0.722	8.733	0.890	33.92
Art. 4 comp. 1	0.608	0.782	9.588	0.881	59.59
Art. 4 comp. 2	0.534	1.178	6.276	0.433	51.41

Table 5.24. Parameters of the selected accelerograms, vertical components

Time history	a_{MAX} (g)	v_{MAX} (m/s)	I_a (m/s)	T_P (s)	$D_{0.05g}$ (s)
Friuli 76 TOLZC	0.267	0.103	0.336	0.174	6.09
Imperial Valley 1979 DLTDW	0.145	0.148	0.538	4.312	20.45
Kobe 1995 TAZUP	0.433	0.348	1.051	0.466	4.12
Landers 1992 CLWUP	0.174	0.099	0.617	0.146	21.35
Landers 1992 LCNUP	0.818	0.460	8.226	0.075	33.54
Loma Prieta 1989 CYCUP	0.082	0.095	0.122	1.107	8.92
Loma Prieta 1989 G03UP	0.338	0.155	0.807	1.280	12.93
Loma Prieta 1989 G04UP	0.159	0.146	0.315	1.781	12.97
Manjil 90 ABBV	0.538	0.440	4.676	0.134	47.58
Northridge 94 CENUP	0.109	0.106	0.254	1.517	12.66
Northridge 94 LACUP	0.135	0.076	0.215	0.410	11.67
Umbria Marche 97 NCRZC	0.419	0.284	0.711	0.158	5.27
Imperial Valley 79 BCUP	0.425	0.122	1.123	0.146	17.91
Irpinia 80 STUZC	0.235	0.204	0.561	1.707	12.40
Montenegro 79 ULCZC	0.458	0.163	2.512	0.079	16.23
Montenegro 79 PETZC	0.213	0.132	0.577	0.410	15.79
Art. 1 comp. V	0.515	0.463	6.922	0.494	33.86
Art. 2 comp. V	0.656	0.566	4.249	0.706	22.46
Art. 3 comp. V	0.630	0.656	6.408	0.445	27.06
Art. 4 comp. V	0.699	0.576	7.344	0.394	56.42

Table 5.25. Parameters of the selected accelerograms scaled to 0.58g. Horizontal components

Time history	a_{MAX} (g)	v_{MAX} (m/s)	I_a (m/s)	T_P (s)	$D_{0.05g}$ (s)
Friuli 76 TOLXC	0.580	0.341	2.112	0.494	8.88
Friuli 76 TOLYC	0.580	0.599	3.948	0.661	12.66
Imperial Valley 1979 DLT352	0.580	0.545	8.974	1.672	77.41
Kobe 1995 TAZ000	0.580	0.571	2.148	1.638	9.53
Kobe 1995 TAZ090	0.580	0.713	2.752	0.488	12.01
Landers 1992 CLWTR	0.580	0.589	4.204	0.706	20.40
Landers 1992 LCN260	0.580	1.169	4.442	0.106	33.26
Landers 1992 LCN345	0.580	0.238	3.557	0.088	33.30
Loma Prieta 1989 CYC285	0.580	0.476	2.159	0.650	17.44
Loma Prieta 1989 G03000	0.580	0.373	2.279	0.569	11.80
Loma Prieta 1989 G03090	0.580	0.705	3.360	1.862	22.84
Loma Prieta 1989 G04000	0.580	0.540	2.408	0.394	21.55
Manjil 90 ABBL	0.580	0.479	5.916	0.340	49.30
Manjil 90 ABBT	0.580	0.609	10.363	0.218	45.24
Northridge 94 CEN245	0.580	0.412	3.232	0.853	21.26
Northridge 94 LAC180	0.580	0.257	3.535	0.339	24.64
Umbria Marche 97 NCRXC	0.580	0.354	4.052	0.159	12.38
Umbria Marche 97 NCRYC	0.580	0.365	4.435	0.378	11.95
Imperial Valley 79 BC230	0.580	0.344	3.355	0.621	16.11
Irpinia 80 STUYC	0.580	0.982	4.797	2.341	46.29
Montenegro 79 ULCXC	0.580	0.761	7.225	1.092	35.88
Montenegro 79 PETXC	0.580	0.497	7.392	0.458	31.58
Art. 1 comp. 1	0.580	0.683	6.080	0.803	36.56
Art. 1 comp. 2	0.580	0.738	6.444	0.819	27.96
Art. 2 comp. 1	0.580	0.590	4.879	0.910	24.75
Art. 2 comp. 2	0.580	0.672	4.791	0.694	24.91
Art. 3 comp. 1	0.580	0.609	7.138	0.759	32.85
Art. 3 comp. 2	0.580	0.685	7.876	0.890	30.57
Art. 4 comp. 1	0.580	0.746	8.724	0.881	59.59
Art. 4 comp. 2	0.580	1.279	7.395	0.433	51.42

Table 5.26. Parameters of the vertical components scaled by the same factor of the corresponding horizontal components

Time history	scale factor	a_{MAX} (g)	v_{MAX} (m/s)	I_a (m/s)	T_P (s)	$D_{0.05g}$ (s)
Friuli 76 TOLZC	1.6246	0.434	0.167	0.886	0.174	7.05
Friuli 76 TOLZC	1.8354	0.490	0.188	1.130	0.174	8.62
Imperial Valley 1979 DLTDW	1.6524	0.240	0.244	1.469	4.120	57.14
Kobe 1995 TAZUP	0.8369	0.362	0.292	0.736	0.466	3.12
Kobe 1995 TAZUP	0.8357	0.362	0.291	0.734	0.466	3.12
Landers 1992 CLWUP	1.3909	0.242	0.138	1.193	0.146	23.19
Landers 1992 LCNUP	0.7978	0.653	0.367	5.236	0.075	33.52
Landers 1992 LCNUP	0.7351	0.601	0.338	4.445	0.075	25.08
Loma Prieta 1989 CYCUP	1.1983	0.098	0.114	0.175	1.107	8.99
Loma Prieta 1989 G03UP	1.0450	0.353	0.162	0.881	1.280	12.94
Loma Prieta 1989 G03UP	1.5804	0.534	0.244	2.016	1.280	20.44
Loma Prieta 1989 G04UP	1.3909	0.221	0.203	0.610	1.781	14.12
Manjil 90 ABBV	1.1262	0.606	0.495	5.931	0.134	47.60
Manjil 90 ABBV	1.1694	0.629	0.514	6.395	0.134	47.60
Northridge 94 CENUP	1.8012	0.196	0.191	0.824	1.517	21.90
Northridge 94 LACUP	1.8354	0.248	0.139	0.724	0.410	17.60
Umbria Marche 97 NCRZC	1.1069	0.464	0.314	0.871	0.158	6.18
Umbria Marche 97 NCRZC	1.2527	0.525	0.356	1.157	0.158	7.49
Imperial Valley 79 BCUP	0.7484	0.318	0.091	0.629	0.146	11.59
Irpinia 80 STUZC	1.7957	0.422	0.367	1.809	1.707	44.99
Montenegro 79 ULCZC	1.9728	0.904	0.321	9.776	0.079	30.24
Montenegro 79 PETZC	1.2775	0.272	0.169	0.941	0.410	17.61
Art. 1 comp. V	0.9034	0.465	0.418	5.649	0.494	30.44
Art. 1 comp. V	0.9163	0.472	0.424	5.812	0.494	30.44
Art. 2 comp. V	0.8841	0.580	0.500	3.321	0.706	21.79
Art. 2 comp. V	0.9063	0.595	0.513	3.490	0.706	21.79
Art.3 comp. V	0.8593	0.541	0.564	4.732	0.445	27.03
Art. 3 comp. V	0.9493	0.598	0.623	5.775	0.445	27.05
Art. 4 comp. V	0.9539	0.667	0.549	6.682	0.394	56.40
Art. 4 comp. V	1.0861	0.759	0.625	8.663	0.394	56.42

Table 5.27. Parameters of the selected accelerograms scaled to 0.58g. Vertical components

Time history	a_{MAX} (g)	v_{MAX} (m/s)	I_a (m/s)	T_P (s)	$D_{0.05g}$ (s)
Friuli 76 TOLZC	0.580	0.223	1.579	0.174	4.12
Imperial Valley 1979 DLTDW	0.580	0.592	8.612	4.120	30.57
Kobe 1995 TAZUP	0.580	0.467	1.882	0.466	2.79
Landers 1992 CLWUP	0.580	0.332	6.885	0.146	16.52
Landers 1992 LCNUP	0.580	0.323	4.131	0.075	25.08
Loma Prieta 1989 CYCUP	0.580	0.678	6.160	1.107	31.40
Loma Prieta 1989 G03UP	0.580	0.265	2.373	1.280	20.44
Loma Prieta 1989 G04UP	0.580	0.534	4.211	1.781	23.16
Manjil 90 ABBV	0.580	0.474	5.438	0.134	47.60
Northridge 94 CENUP	0.580	0.566	7.216	1.517	27.44
Northridge 94 LACUP	0.580	0.326	3.992	0.410	30.29
Umbria Marche 97 NCRZC	0.580	0.393	1.362	0.158	7.49
Imperial Valley 79 BCUP	0.580	0.166	2.093	0.146	17.93
Irpinia 80 STUZC	0.580	0.503	3.409	1.707	46.03
Montenegro 79 ULCZC	0.580	0.206	4.034	0.079	28.45
Montenegro 79 PETZC	0.580	0.361	4.292	0.410	32.63
Art. 1 comp. V	0.580	0.521	8.776	0.494	34.18
Art. 2 comp. V	0.580	0.500	3.320	0.706	21.79
Art. 3 comp. V	0.580	0.604	5.433	0.445	27.05
Art. 4 comp. V	0.580	0.478	5.062	0.394	52.24

5.7.2 Critical seismic coefficient

The values of critical seismic coefficients were evaluated for each limit state, considering the contribution of the base and the lateral sides of the block, while the passive earth resistance in front of the block is assumed to gradually increase as the block displacement relative to the ground develops.
The values of K_c, computed using equation (9), with φ'_{sk} = 32°, are listed in Table 5.28 and Table 5.29 for both the presence and the absence of the drainage system.

Table 5.28. Critical seismic coefficients K_c, presence of drainage system

	SLS2	ULS	SILS
Mechanism 1	0.56	0.49	0.57
Mechanism 2	0.45	0.37	0.46
Mechanism 3	0.08	0.00	0.09

Table 5.29. Critical seismic coefficients K_c, absence of drainage system

	SLS2	ULS	SILS
Mechanism 1	0.50	0.43	0.51
Mechanism 2	0.39	0.32	0.40
Mechanism 3	0.04	0.00	0.06

The lowest values of K_c are obtained for the ULS condition. For this reason the earthquake-induced displacement computed for the Calabria anchor block are in the following referred to the ULS condition only.

5.7.3 Earthquake-induced displacements

The pseudo-static analyses show that mechanism 1 is the less critical among the three assumed mechanisms, in terms of both safety against sliding and critical seismic coefficient K_c. In addition, the FE analyses showed that the inclination of the most likely sliding surface is in between the ones of mechanisms 2 and 3. For these reasons the earthquake-induced displacements were evaluated for mechanisms 2 and 3.
Both the presence (H_w = 88 m a.s.l.) and the absence (H_w = 94.5 m a.s.l.) of the drainage systems were considered in computations.
Calculations were carried out combining each scaled horizontal component with the corresponding vertical component first scaled by the same factor and then scaled to 0.58g as well. The analyses were also repeated considering the opposite accelerograms, i.e. $a_{opposite}(t) = - a(t)$.

Earthquake induced displacements were computed through numerical integration of equation (21), with φ'_{sk} = 32°. Maximum computed displacements are summarised in Table 5.30 and Table 5.31.

For mechanism 2, the maximum computed displacement of the anchor block is u_{max} = 14 mm in the presence of the drainage system (H_w = 88 m a.s.l.), while it is u_{max} = 21 mm assuming the original water head (H_w = 94.5 m a.s.l.).

For mechanism 3, the maximum earthquake-induced displacement is u_{max} = 69 mm for H_w = 88 m a.s.l., and u_{max} = 72 mm for H_w = 94.5 m a.s.l..

The highest displacements induced by the selected seismic events are obtained for mechanism 3, characterised by the lower inclination of the sliding plane (α = 0), in absence of the drainage system and when the vertical components are scaled by the same factor of the corresponding horizontal component. In fact, for events having $a_{v,max} > a_{h,max}$, the scaled $a_{v,max}$ is higher than 0.58g (see Tables 5.23 - Table 5.27).

The results obtained for each accelerogram are summarised in Table 5.32 and Table 5.33, while Appendix D reports time histories of acceleration, velocity and displacement obtained for each seismic input considering sliding mechanism 3, that was recognised to be the most critical.

Table 5.30. Earthquake-induced displacements (mm); scaled horizontal component and corresponding vertical component scaled by the same factor

	H_w = 88 m a.s.l.	H_w = 94.5 m a.s.l.
Mechanism 2	14	21
Mechanism 3	70	72

Table 5.31. Earthquake-induced displacements (mm); horizontal component and corresponding vertical component scaled to 0.58g

	H_w = 88 m a.s.l.	H_w = 94.5 m a.s.l.
Mechanism 2	14	20
Mechanism 3	69	71

Finally, a comparative analysis was carried out in which the sliding surface inclination is α = 8°, as obtained from 2D and 3D FE analyses. In this analysis, the following assumptions were made: values of T_L corresponding to mechanism 1 were considered; the net earth trust ΔR was computed down to the depth of the diaphragm wall (mechanism 2); the weight of the anchor block only was considered in computation. The results reported in Table 5.34 show that, under these conservative hypotheses, the permanent displacement of the anchor block induced by earthquake loading is equal to 152 mm.

Table 5.32. Earthquake-induced displacements (mm); scaled horizontal component and corresponding vertical component scaled by the same factor

Time history	Mechanism 2		Mechanism 3	
	H_w=88.0 m a.s.l.	H_w =94.5 m a.s.l.	H_w =88.0 m a.s.l.	H_w =94.5 m a.s.l.
Friuli 76 TOLXC	1	2	31	31
Friuli 76 TOLYC	3	5	67	69
Imperial Valley 1979 DLT352	0	0	28	29
Kobe 1995 TAZ000	0	1	42	43
Kobe 1995 TAZ090	5	9	58	60
Landers 1992 CLWTR	0	0	51	53
Landers 1992 LCN260	3	6	32	33
Landers 1992 LCN345	1	2	23	23
Loma Prieta 1989 CYC285	0	0	27	28
Loma Prieta 1989 G03000	0	0	36	36
Loma Prieta 1989 G03090	2	4	39	40
Loma Prieta 1989 G04000	0	0	55	57
Manjil 90 ABBL	4	7	33	34
Manjil 90 ABBT	5	10	46	48
Northridge 94 CEN245	0	1	45	46
Northridge 94 LAC180	0	1	32	33
Umbria Marche 97 NCRXC	1	4	38	39
Umbria Marche 97 NCRYC	1	3	38	39
Imperial Valley 79 BC230	0	0	36	37
Irpinia 80 STUYC	0	0	39	39
Montenegro 79 ULCXC	6	11	44	46
Montenegro 79 PETXC	0	2	45	48
Art. 1 comp. 1	2	6	36	38
Art. 1 comp. 2	4	8	43	45
Art. 2 comp. 1	9	13	38	39
Art. 2 comp. 2	14	21	55	56
Art. 3 comp. 1	3	7	43	45
Art. 3 comp. 2	1	5	41	43
Art. 4 comp. 1	6	12	70	72
Art. 4 comp. 2	9	14	46	48

Table 5.33. Earthquake-induced displacements (mm); scaled horizontal component and corresponding vertical component scaled to 0.58g

Time history	Mechanism 2		Mechanism 3	
	H_w=88.0 m a.s.l.	H_w=94.5 m a.s.l.	H_w=88.0 m a.s.l.	H_w=94.5 m a.s.l.
Friuli 76 TOLXC	3	5	31	32
Friuli 76 TOLYC	5	8	67	68
Imperial Valley 1979 DLT352	2	5	30	31
Kobe 1995 TAZ000	4	10	35	36
Kobe 1995 TAZ090	13	20	66	68
Landers 1992 CLWTR	3	6	46	48
Landers 1992 LCN260	2	4	31	32
Landers 1992 LCN345	1	2	22	23
Loma Prieta 1989 CYC285	1	3	33	33
Loma Prieta 1989 G03000	0	1	33	34
Loma Prieta 1989 G03090	2	5	40	41
Loma Prieta 1989 G04000	1	3	57	58
Manjil 90 ABBL	3	6	33	33
Manjil 90 ABBT	4	8	45	47
Northridge 94 CEN245	2	5	44	46
Northridge 94 LAC180	4	9	39	40
Umbria Marche 97 NCRXC	3	6	41	42
Umbria Marche 97 NCRYC	2	5	39	40
Imperial Valley 79 BC230	0	1	35	36
Irpinia 80 STUYC	0	1	38	38
Montenegro 79 ULCXC	1	3	39	40
Montenegro 79 PETXC	8	15	57	60
Art. 1 comp. 1	7	12	39	40
Art. 1 comp. 2	8	14	48	49
Art. 2 comp. 1	9	13	38	39
Art. 2 comp. 2	14	20	55	57
Art. 3 comp. 1	4	8	45	47
Art. 3 comp. 2	1	4	41	43
Art. 4 comp. 1	3	7	69	71
Art. 4 comp. 2	2	5	44	46

Table 5.34. Comparative analysis: earthquake-induced displacements (mm); scaled horizontal component and corresponding vertical component scaled to 0.58g

Time history	α=8°, K_c=0.021	
	a_{vmax}<>0.58g	a_{vmax}=0.58g
Friuli 76 TOLXC	34	36
Friuli 76 TOLYC	75	75
Imperial Valley 1979 DLT352	35	45
Kobe 1995 TAZ000	41	65
Kobe 1995 TAZ090	86	113
Landers 1992 CLWTR	69	74
Landers 1992 LCN260	50	46
Landers 1992 LCN345	30	29
Loma Prieta 1989 CYC285	30	47
Loma Prieta 1989 G03000	38	38
Loma Prieta 1989 G03090	54	55
Loma Prieta 1989 G04000	64	68
Manjil 90 ABBL	54	52
Manjil 90 ABBT	81	76
Northridge 94 CEN245	54	60
Northridge 94 LAC180	39	68
Umbria Marche 97 NCRXC	56	63
Umbria Marche 97 NCRYC	54	55
Imperial Valley 79 BC230	46	46
Irpinia 80 STUYC	42	42
Montenegro 79 ULCXC	87	66
Montenegro 79 PETXC	95	152
Art. 1 comp. 1	65	81
Art. 1 comp. 2	85	106
Art. 2 comp. 1	60	60
Art. 2 comp. 2	82	80
Art. 3 comp. 1	93	100
Art. 3 comp. 2	92	89
Art. 4 comp. 1	104	96
Art. 4 comp. 2	91	82
max	104	152

6 Calabria Anchor Block – Safety against rotation

Safety against rotation ensures that the resultant force transmitted to the foundation acts within the foundation plane; it was evaluated by imposing momentum equilibrium around point O belonging to the plane of motion (Figure 6.1).

According to D.M. 14.01.2008, safety against rotation is treated as an equilibrium limit state of rigid body (EQU) using the partial safety factor of group M2 to evaluate the earth pressures. Moreover, under seismic conditions, the load factors of the design actions are set equal to unity (§ 7.11.1 - D.M. 14.01.2008); accordingly these factors are omitted in the following

A conservative estimate of safety against rotation was obtained through the following assumptions:

- the passive earth resistance R_{Pd} accounted for in the computations was referred to mechanism 3, corresponding to the lower resisting moment;
- the contribution of slide resistance T_{Ld} developed along the sides of the anchor block was neglected.

Safety against rotation is ensured when the resistant moments are equal or larger than driving moments:

$$\frac{\sum M_{R_d}}{\sum M_{D_d}} = \frac{W' \cdot e_W + R_{P_d} \cos\delta \cdot e_{R_P}}{K_h W \cdot e_{K_h} + K_v W \cdot e_{K_v} + T \cos i \cdot e_{T_h} + T \sin i \cdot e_{T_v}} \geq 1 \qquad (28)$$

where e_i is the distance of the line of action of each force from point O. Factored values of the cable force T were introduced in equation (28), as provided by structural analyses of the tender design, for the ULS loading condition.

Calculations were carried out for both the hypothesis of presence or absence of the drainage system.

Table 6.1 reports the shear strength parameters used in the computations.

Table 6.1. Safety against rotation

	φ_k' (°)	φ_d' (°)	c_k' (kPa)	c_d' (kPa)
passive earth resistance R_p	40	33.9	-	-

6.1 Presence of drainage system (H_w = 88.0 m a.s.l.)

Table 6.2 and Table 6.3 report the resistant and the driving actions, respectively.

Table 6.2. Design resistance – H_w = 88.0 m a.s.l.

	resistance (MN)	distance (m)	M_{Rd} (MN·m)
W'	5877	44.7	262702
$R_{Pd}\cos\delta$	5812	12.4	72265
ΣM_{Rd}			334967

Table 6.3. Driving forces – H_w = 88.0 m a.s.l.

	action (MN)	distance (m)	M_{Dd} (MN·m)
K_hW	1350	24.4	32937
K_vW	675	44.7	30170
T_h	3800	41.0	155798
T_v	1018	10.0	10182
ΣM_{Dd}			229083

It follows that

$\frac{\Sigma M_{Rd}}{\Sigma M_{Dd}} = 1.5$. Hence the requirements of D.M. 14.01.2008 are fulfilled.

6.2 Absence of drainage system (H_w = 94.5 m a.s.l.)

Table 6.4 and Table 6.5 report the resisting and the driving actions respectively.

Table 6.4. Resisting actions, H_w = 94.5 m a.s.l.

	resistance (MN)	distance (m)	M_{Rd} (MN·m)
W'	5503	44.7	245984
$R_{Pd}\cos\delta$	5398	12.4	67117
ΣM_{Rd}			313101

Table 6.5. Driving actions, H_w = 94.5 m a.s.l.

	action (MN)	distance (m)	M_{Dd} (MN·m)
K_hW	1350	24.4	32937
K_vW	675	44.7	30170
T_h	3800	41.0	155798
T_v	1018	10.0	10182
Total			229083

Again the requirements of D.M. 14.01.2008 are satisfied in that it is

$$\frac{\sum M_{R_d}}{\sum M_{D_d}} = 1.4$$

7 Calabria Anchor Block – Bearing capacity

Safety against bearing capacity failure was evaluated using Approach 1, Combination 2 of Italian Building Code (D.M. 14.01.2008, "Nuove norme tecniche per le costruzioni).

The loads to be considered for evaluation of bearing capacity are the cable force *T*, the weight of the anchor block *W* and the horizontal and vertical components of the pseudostatic inertial force, K_hW and K_vW.

The conservative assumptions adopted in computation were as follows:

- the sliding resistance developed on the side walls of the anchor block was not taken into account;
- the passive earth resistance was neglected assuming that it was not fully mobilised when bearing capacity is attained.

The bearing capacity is evaluated in terms of effective stress using appropriate correction factors to take into account the inclination of the applied load, the shape of the foundation, and the inclination of the foundation base. To this aim, the geometry of the anchor block considered in the analysis is as shown in Figure 6.1. To account for the eccentricity of the load, the bearing capacity is computed for an equivalent rectangular foundation with reduced width *B′* and length *L′*.

Safety against bearing capacity failure is ensured if the design resistance R_d is equal or larger than design loads E_d:

$$\frac{R_d}{E_d} \geq 1$$

Design values of resistances and forces are obtained from the corresponding characteristic values and are those acting normally to the foundation plane.

The design resistance is:

$$R_{N_d} = \frac{1}{\gamma_R} R_{N_k} = \frac{1}{\gamma_R}\left(Q'_{ult_d} + U_{bd}\right) \qquad (29)$$

with γ_R = 1.8. In equation (29):

- $Q'_{ult_d} = A \cdot q'_{ult_d}$ is the ultimate effective bearing capacity provided by Terzaghi equation;
- *A* is the area of the foundation base of the anchor block;
- q'_{ultd} is the ultimate effective bearing pressure computed using the reduced values of the angle of shearing resistance acting on the failure surface φ'_d = atan [$(\tan\varphi'_k)/\gamma_\varphi$], with γ_φ = 1.25;
- $U_{bd} = U_{bk}$ is the resultant of the pore water pressure acting at the foundation level.

According to Terzaghi's theory, the ultimate effective bearing pressure q'_{ult} is given by the equation

$$q'_{ult} = N_q \cdot q' \cdot \zeta_q \cdot \xi_q \cdot \alpha_q + N_c \cdot c'_d \cdot \zeta_c \cdot \xi_c \cdot \alpha_c + N_\gamma \cdot \gamma_{av} \cdot \frac{B'}{2} \cdot \zeta_\gamma \cdot \xi_\gamma \cdot \alpha_\gamma \qquad (30)$$

where:

- $q' = \gamma z_w + \gamma'(D - z_w)$ is the vertical effective stress acting at the foundation level;
- z_w is the depths of the groundwater table;
- D is the minimum depth of the foundation base below ground level;
- γ_{av} is the average unit weight of the soil below the foundation level.

Soil parameters used in computations are those listed in Table 3.2.

When evaluating the effect of seismic actions, the Italian Building Code (§ 7.11.1 - D.M. 14.01.2008) specifies that the partial safety factors of the design actions are set equal to unity: $\gamma_G = \gamma_Q = 1$. Accordingly, load factors γ_F (γ_G and γ_Q) are omitted in the following.

The design components of the loads acting normally to the foundation plane are:

$$E_{N_d} = \gamma_F E_{N_k} = W'_k \cos\varepsilon + T\,\text{sen}(\varepsilon - i) + K_h W \text{sen}\varepsilon \pm K_v W \cos\varepsilon \qquad (31)$$

The design components of the loads acting tangentially to the foundation plane are:

$$E_{S_d} = \gamma_F E_{S_k} = W'_k \text{sen}\varepsilon - T\cos(\varepsilon - i) - K_h W \cos\varepsilon \mp K_v W \text{sen}\varepsilon \qquad (32)$$

Note, however, that cable forces in equations 31 and 32 are inclusive of partial load factors, as provided by structural analyses of the tender design.

Calculations were carried out both considering and neglecting the effect of the drainage system, with reference to the ULS loading condition.

Table 7.1 reports the shear strength parameters used in the computations.

Table 7.1. Parameters for bearing capacity

	φ_k' (°)	φ_d' (°)	c_k' (kPa)	c_d' (kPa)
shearing resistance	40	33.9	70	56

7.1 Presence of drainage system (H_w = 88.0 m a.s.l.)

Table 7.2 lists the values of the design loads acting normally to the foundation plane, while Table 7.3 summarises the those acting tangentially to the foundation plane:

Table 7.2. normal design loads, H_w = 88 m a.s.l.

	E_{Nd} (MN)
$W'_k\cos\varepsilon$	5409.8
$T\text{sen}(\varepsilon\text{-}i)$	547.5
$k_h W\text{sen}\varepsilon$	527.4
$-K_v W\cos\varepsilon$	-621.3
ΣE_{Nd}	5863.5

Table 7.3. tangent design loads, H_w = 88 m a.s.l.

	E_{Sd} (MN)
$W'_k\text{sen}\varepsilon$	2296.3
$-T\cos(\varepsilon\text{-}i)$	-3895.7
$-k_h W\cos\varepsilon$	-1242.6
$-K_v W\text{sen}\varepsilon$	-263.7
ΣE_{Sd}	-3105.7

To evaluate the design resistance, the reduced width *B′* is first calculated through equation

$$B' = B - 2e$$

where *B* = 60.9 m is the original width and *e* = 3.55 m is the eccentricity of E_{Nd} from the centre of gravity of the foundation plane. The reduced width is then *B′* = 53.8 m.

The length of the foundation surface is *L* = 100 m and no correction is needed as the loads are centred in the longitudinal direction.

According to Approach 1, Combination 2 of D.M. 14.01.2008, the design strength parameter adopted for evaluation of bearing capacity were: $\varphi'_d = \tan^{-1}[(\tan\varphi_k')/1.25]$ = 33.9° and $c'_d = c'_k/1.25$ = 56 kPa.

For the hypotheses mentioned above, the following was obtained:

– bearing capacity coefficients:

N_{qd} = 29.44

N_{cd} = 42.16

$N_{\gamma d}$ = 41.06

– correction factors for load inclination:

$\zeta_q = (1 - E_{Sd}/E_{Nd})^m = 0.332$ $\quad$ $m = (2 + B'/L)/(1 + B'/L) = 1.65$

$$\zeta_c = \zeta_q - \frac{1-\zeta_c}{N_{c_d} \tan\varphi'_d} = 0.308$$

$$\zeta_\gamma = (1 - E_{Sd}/E_{Nd})^{m+1} = 0.170$$

– correction factors for foundation shape:

$\xi_q = 1 + (B'/L)\times\tan\varphi'_d = 1.36$

$\xi_c = 1 - 0.4\times(B'/L\times N_{qd}/N_{cd}) = 1.38$

$\xi_\gamma = 1 - 0.4\times(B'/L) = 0.78$

– correction factors for inclination of foundation plane ($\varepsilon = 23°$):

$\alpha_q = \alpha_\gamma = (1 - \varepsilon \tan \varphi'_d)^2 = 0.534$

$$\alpha_c = \alpha_q - \frac{1-\alpha_c}{N_{c_d} \tan\varphi'_d} = 0.517$$

At the site of Calabria anchor block, the average elevation of ground surface is 114 m a.s.l. The minimum thickness of soil adjacent to the anchor block is D = 13 m. Assuming H_w = 88.0 m a.s.l., it is z_w = 26 m > D; hence no water pressure is to be considered in the calculation of q′.

The average unit weight γ_{av} is obtained by averaging the soil unit weight γ and the submerged unit weight $\gamma = \gamma - \gamma_w$ on a soil thickness B':

$$\gamma_{av} = \gamma\frac{z_w - D}{B'} + (\gamma - \gamma_w)\frac{B' + D - z_w}{B'} = 12.4 \text{ kN/m}^3.$$

The computed ultimate effective bearing pressure is:

q'_{ultd} = 3340 kPa

while the resultant of pore water pressure, acting on B′·L, is

$$U_b = \frac{1}{2}\gamma_w (D + B'\sin\varepsilon - z_w)\frac{D + B'\sin\varepsilon - z_w}{\sin\varepsilon}\cdot L = 82.2 \text{ MN}$$

Then, the design bearing resistance is

$$R_{N_d} = \frac{1}{\gamma_R}\left(q_{ult_d} \cdot B'L + U_{bd}\right) = 10026 \text{ MN}$$

and the ratio $\frac{R_{Nd}}{E_{Nd}} = \frac{10026}{5863.5} = 1.71 \geq 1$, that satisfies the requirements of D.M. 14.01.2008.

7.2 Absence of drainage system (H_w = 94.5 m a.s.l.)

Table 7.4 lists the values of the design loads acting normally to the foundation plane, while Table 7.5 summarises those acting tangentially to the foundation plane:

Table 7.4. normal design loads, H_w = 94.5 m a.s.l.

	E_{Nd} (MN)
$W'_k\cos\varepsilon$	5065.5
$T\text{sen}(\varepsilon\text{-}i)$	547.5
$k_h W\text{sen}\varepsilon$	527.4
$-K_v W\cos\varepsilon$	-621.3
ΣE_{Nd}	5519.2

Table 7.5. tangent design loads, H_w = 94.5 m a.s.l.

	E_{Sd} (MN)
$W'_k\text{sen}\varepsilon$	2150.2
$T\cos(\varepsilon\text{-}i)$	-3895.7
$k_h W\cos\varepsilon$	-1242.5
$K_v W\text{sen}\varepsilon$	-263.7
ΣE_{Sd}	-3251.7

To evaluate the design resistance, the reduced width *B′* is first calculated through equation

$$B' = B - 2e$$

where *B* = 60.9 m is the original width and *e* = 4.9 m is the eccentricity of E_{Nd} from the centre of gravity of the foundation plane. The reduced width is then *B′* = 51.1 m.

The length of the foundation surface is *L* = 100 m and no correction is needed as the loads are centred in the longitudinal direction.

According to Approach 1, Combination 2 of D.M. 14.01.2008, the design strength parameter adopted for evaluation of bearing capacity were: $\varphi'_d = \tan^{-1}[(\tan\varphi')/1.25] = 33.9°$ and $c'_d = c'_k/1.25 = 56$ kPa.

For the hypotheses mentioned above, the following was obtained:

– bearing capacity coefficients:

$N_{qd} = 29.44$

$N_{cd} = 42.16$

$N_{\gamma d} = 41.06$

– correction factors for load inclination:

$\zeta_q = (1 - R_S/R_N)^m = 0.276$ m = (2 + B'/L)/(1 + B'/L) =1.66

$$\zeta_c = \zeta_q - \frac{1-\zeta_c}{N_c \tan\varphi'_d} = 0.250$$

$\zeta_\gamma = (1 - R_S/R_N)^{m+1} = 0.127$

– correction factors for foundation shape:

$\xi_q = 1 + (B'/L)\times\tan\varphi' = 1.34$

$\xi_c = 1 - 0.4\times(B'/L\times N_q/N_c) = 1.36$

$\xi_\gamma = 1 - 0.4\times(B'/L) = 0.80$

– correction factors for inclination of foundation plane (ε = 23°):

$\alpha_q = \alpha_\gamma = (1 - \varepsilon \tan \varphi'_d)^2 = 0.534$

$$\alpha_c = \alpha_q - \frac{1-\alpha_c}{N_c \tan\varphi'_d} = 0.517$$

At the site of Calabria anchor block the average elevation of ground surface is 114 m a.s.l. The minimum thickness of soil adjacent to the anchor block is D = 13 m. Assuming H_w = 94.5 m a.s.l. it is z_w = 19.5 m > D; hence no water pressure is to be considered in calculating q′.

The average unit weight γ_{av} is obtained by averaging the soil unit weight γ and the submerged unit weight $\gamma = \gamma - \gamma_w$ on a soil thickness B':

$$\gamma_{av} = \gamma\frac{z_w - D}{B'} + (\gamma - \gamma_w)\frac{B' + D - z_w}{B'} = 11.3 \text{ kN/m}^3.$$

The computed ultimate effective bearing pressure is:

q'_{ult} = 2563 kPa

while the resultant of pore water pressure, acting on B′·L, is

$$U_b = \frac{1}{2}\gamma_w (D + B'\sin\varepsilon - z_w)\frac{D + B'\sin\varepsilon - z_w}{\sin\varepsilon}\cdot L = 231.6 \text{ MN}.$$

Then, the design bearing resistance is

$$R_{N_d} = \frac{1}{\gamma_R}\left(q_{ult_d}\cdot B'L + U_{bd}\right) = 7400 \text{ MN}$$

and the ratio $\frac{R_{Nd}}{E_{Nd}} = \frac{7400}{5519} = 1.34 \geq 1$, that satisfies the requirements of D.M. 14.01.2008.

8 Conclusions

Seismic performance of the Calabria anchor block was evaluated using two approaches: the pseudo-static approach, in which the anchor block is assumed to be in a state of limit equilibrium under the action of inertial and static forces, and the displacement-based approach, in which the earthquake-induced displacements of the anchor block are evaluated for a number of input seismic motions. Computations were carried out using the cable forces provided by the tender design that for the ULS load combination result slightly higher than the values obtained from the global IBDAS model (5% for the version 3.3b – Table F.3 – and 7% for the version 3.3f – Table G.3), this resulting in a conservative estimate of the behaviour of the Calabria Anchor Block. In the pseudostatic approach, according to the Italian Building Code (D.M. 14.01.2008), safety of the block against eventual failure mechanisms is ensured comparing the design actions with the design resistances, the first increased and the second reduced by partial factors of safety. In the displacement-based approach, the critical acceleration is first determined through the pseudo-static approach and the cumulative displacement of the potential sliding mass is then evaluated using the sliding block analysis, in which the equation of the relative motion is integrated twice with the critical acceleration used as a reference datum.

In order to reduce the pore water pressure acting at the foundation level, construction of a drainage tunnel was planned in the tender design. Safety verifications were carried out both considering and neglecting the effect of the drainage system.

For evaluation of safety against sliding, design resistances were computed considering the contributions of the sliding resistance at the base and at the block sides and that of the passive resistance in front of the block.

In the analyses three possible sliding mechanisms were assumed, characterised by angles of inclination α = 33.7°, 25.3° and 0°. Companion plane strain FE analyses of the anchor block permitted to evaluate that under ULS loading conditions the prevailing inclination of the displacement vectors is in the range 0°-25.3° so that the second and the third mechanisms were recognised to be the most likely to occur. Moreover, it was observed that the sliding mechanism is only slightly affected by the pore water pressure distribution.

As far as the pseudo-static conditions are concerned, both design actions and design resistances were computed using the pseudo-static seismic coefficients given by the Italian building code (D.M. 14.01.2008). The obtained results showed that safety against sliding is adequately satisfied for each of the analysed loading conditions.

In the displacement-based approach, the earth resistance ΔR mobilised in front of the block was assumed to progressively increase with increasing relative displacement *u* induced by earthquake loading. In this conditions, its contribution was neglected in the expression of the critical seismic coefficient and was included in the equation of relative motion. The relationship between ΔR and the relative displacement was evaluated by best fitting the $u - \Delta R$ data as obtained from 2D FE analyses in which a uniform horizontal displacements were applied to an ideal smooth wall.

Earthquake-induced displacements were computed using 30 input accelerograms. The horizontal component of the selected acceleration time histories was scaled to 0.58 g, while the vertical component was scaled either by the same factor used for the corresponding horizontal component, or to 0.58 g as well. Computation were repeated assuming both directions of applications of the horizontal accelerograms.

The results show that the earthquake-induced displacements decrease with decreasing inclination of the sliding mechanism. If the effect of the drainage tunnel is accounted for, the maximum displacement is equal to 14 mm for mechanism 2 (α =25.3°) and equal to 69 mm for mechanism 3 (α =0°), while, if the effect of the drainage system is neglected, the maximum displacement is equal to 21 mm for mechanism 2 and to 72 mm for mechanism 3. A comparative analysis carried out under conservative hypotheses provided a maximum value of the earthquake-induced displacement equal to 152 mm.

Finally, bearing capacity and safety against rotation were estimated following the prescriptions of D.M. 14.01.2008, the results showing that both the requirements are satisfied for the considered loading conditions.

9 Figures

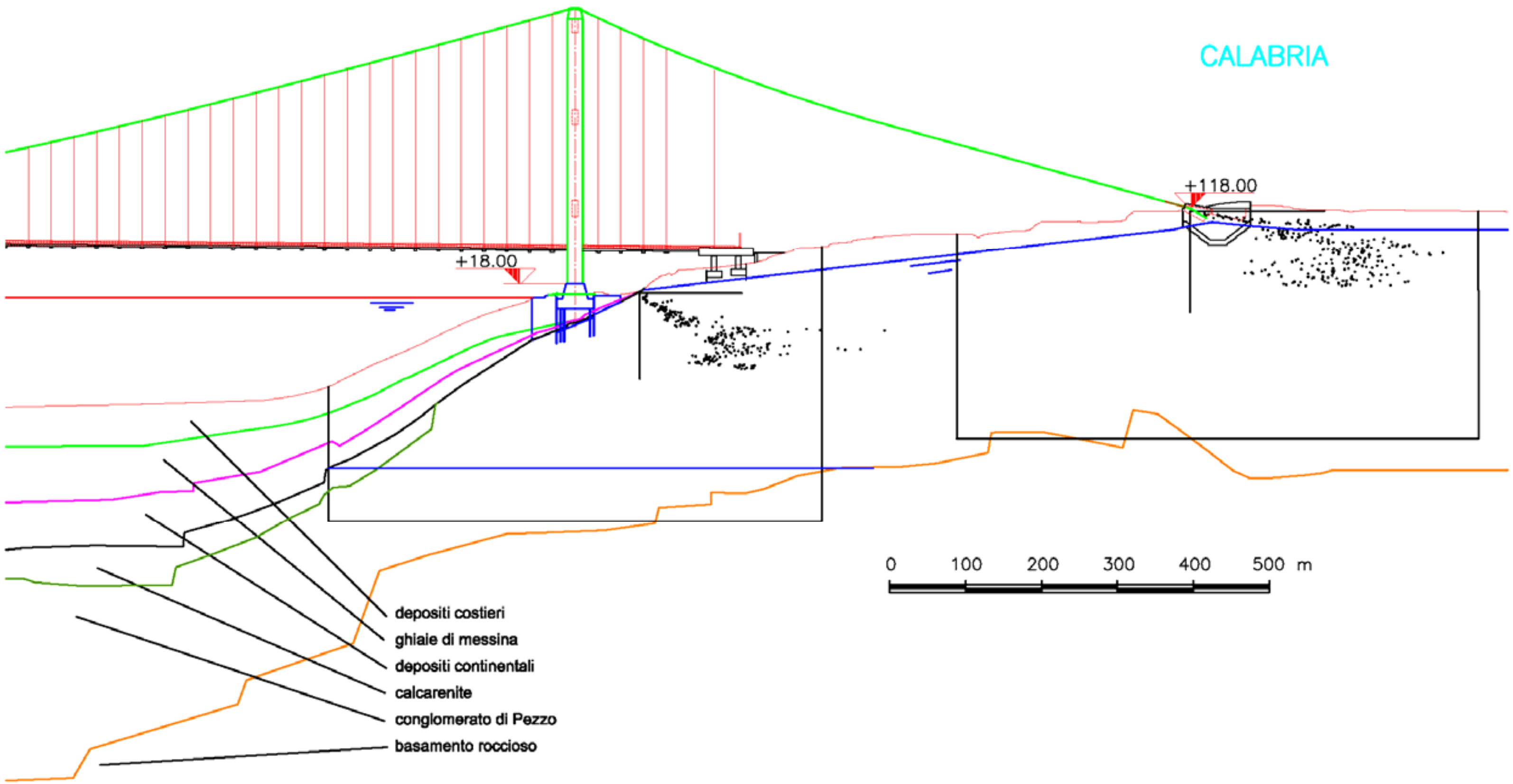

Figure 2.1. Soil profile on Calabria shore of Messina Strait

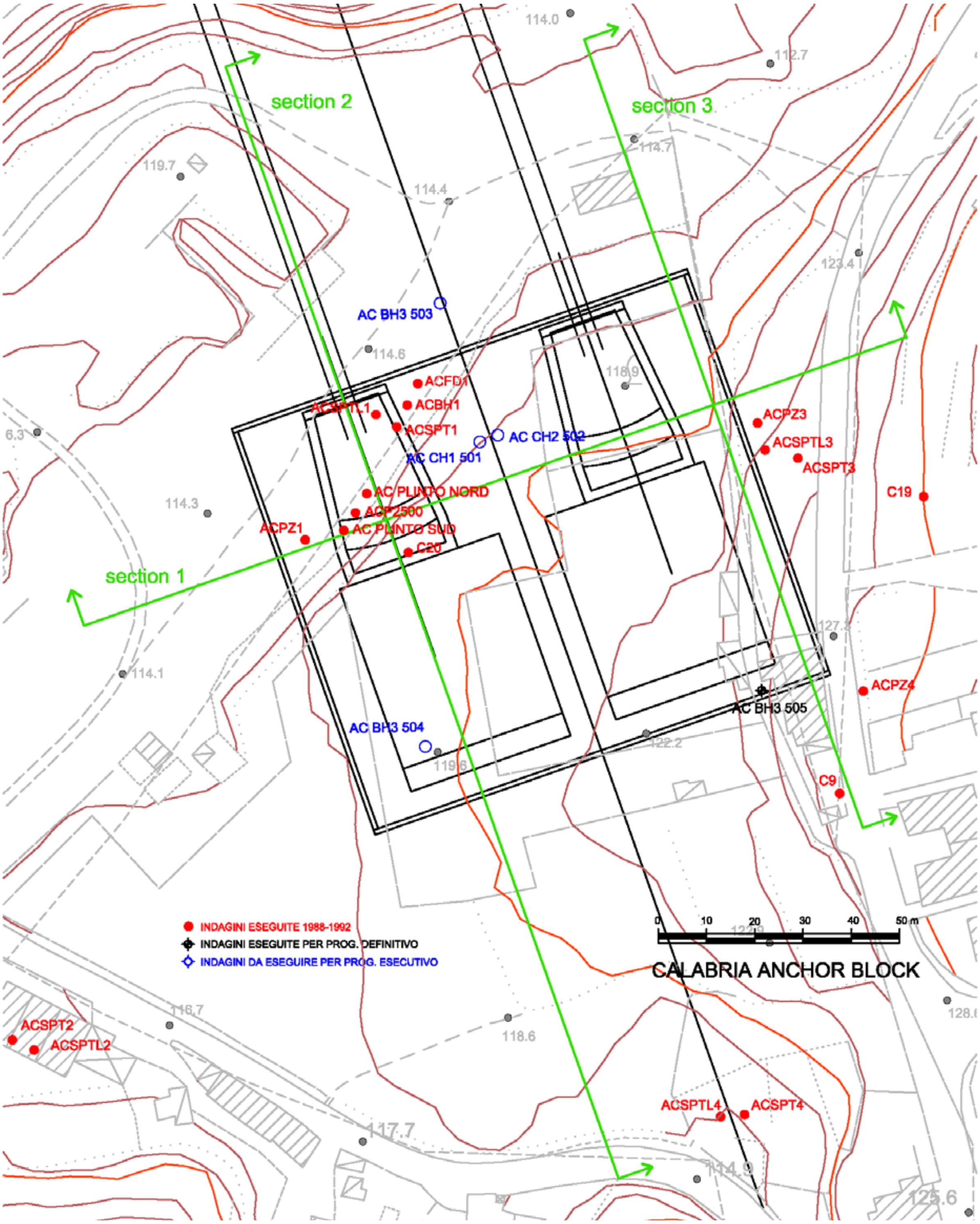

Figure 2.2. Plan view at the location of Calabria Anchor Block

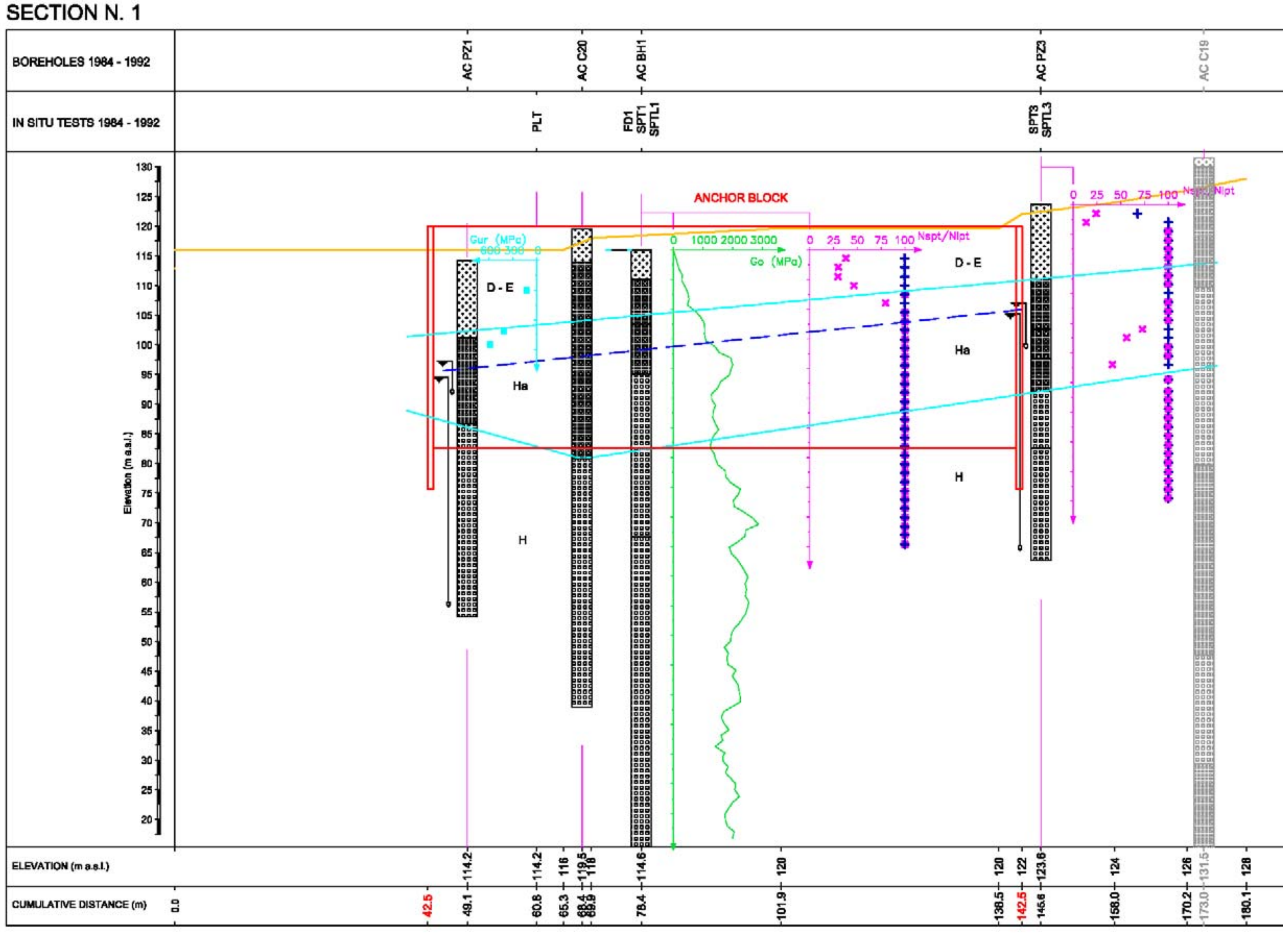

Figure 2.3. Calabria Anchor Block, cross section (section No. 1)

SECTION N. 2

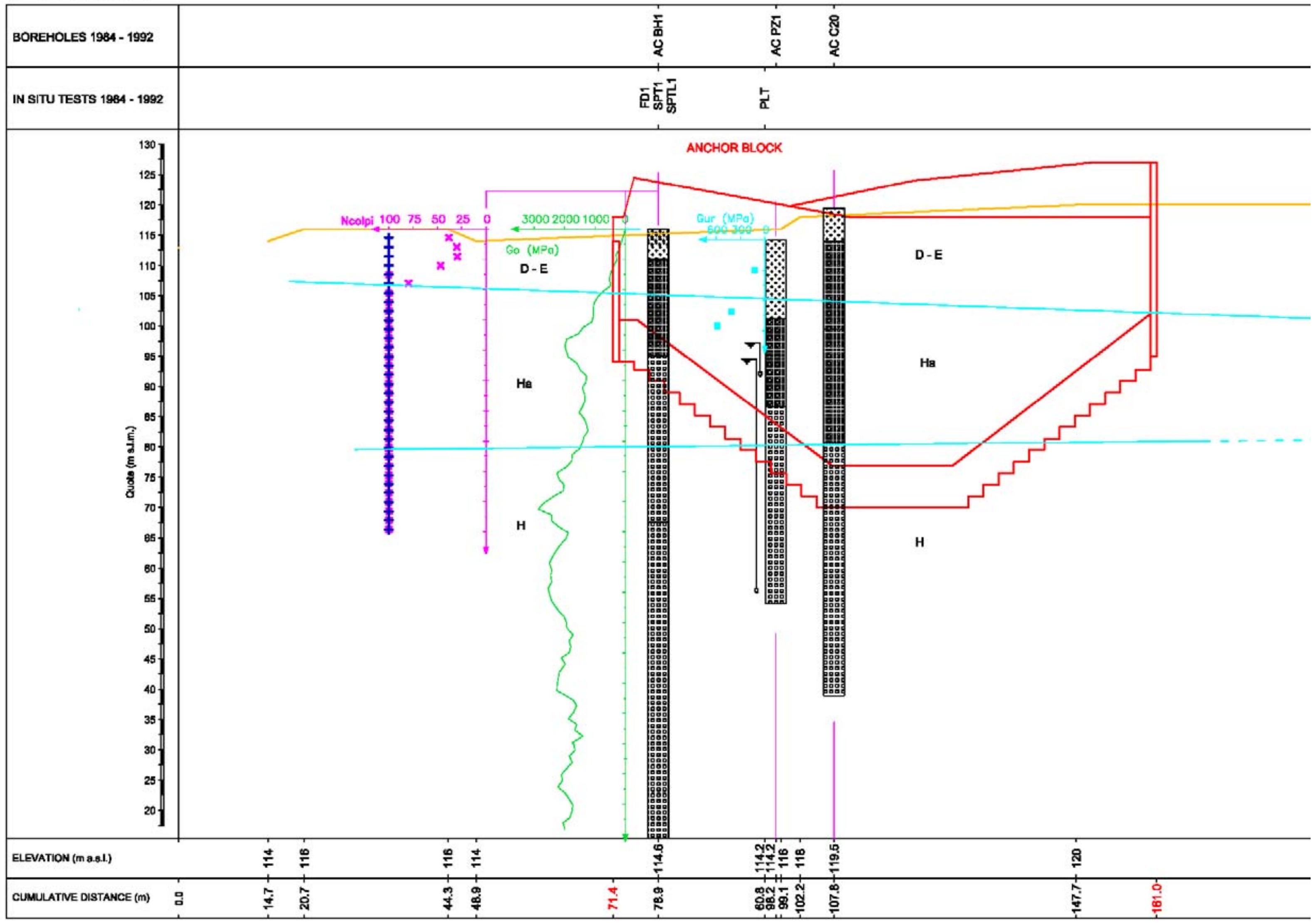

Figure 2.4. Calabria Anchor Block, longitudinal section (Section No. 2)

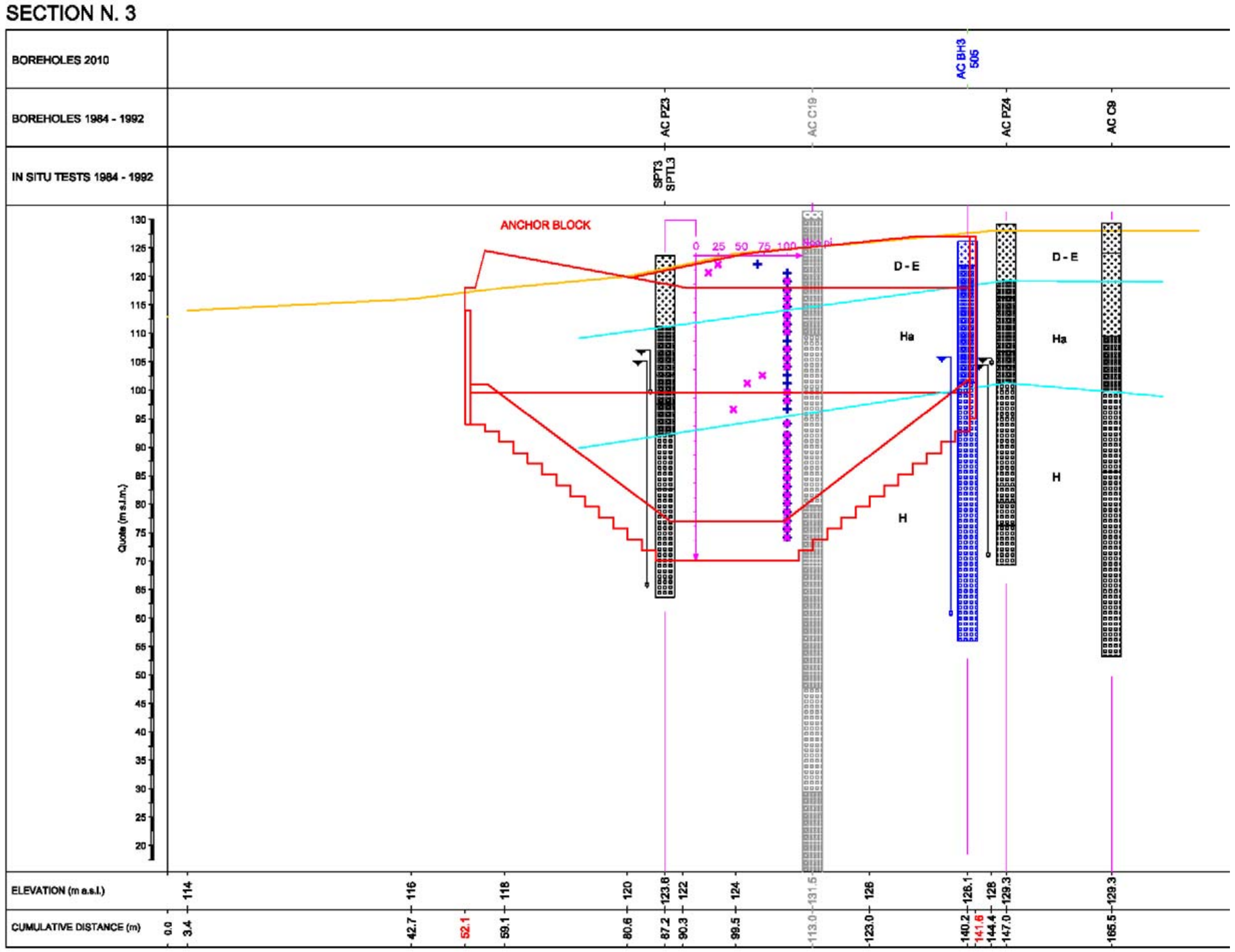

Figure 2.5. Calabria Anchor Block, longitudinal section (Section No. 3)

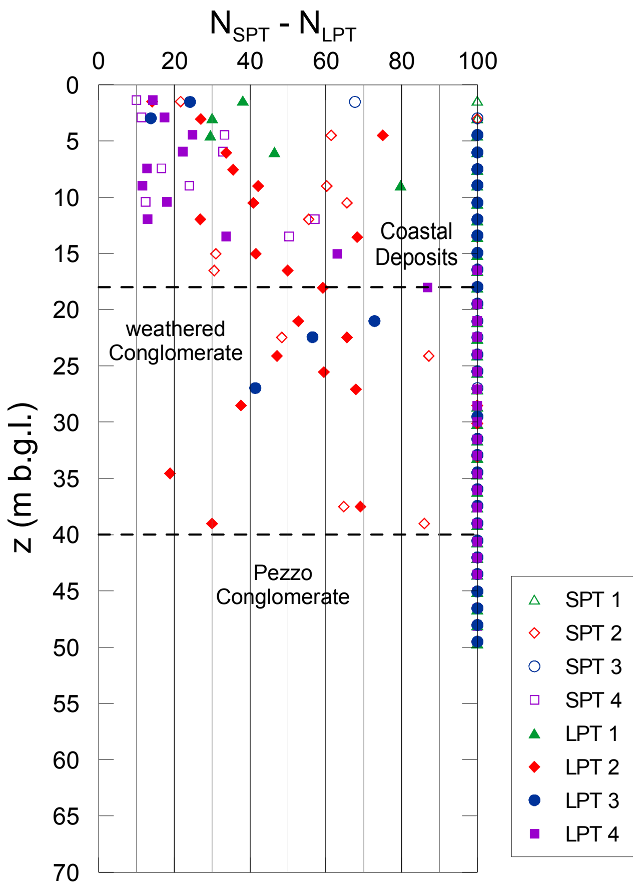

Figure 2.6: Calabria Anchor Block – SPT and LPT test results

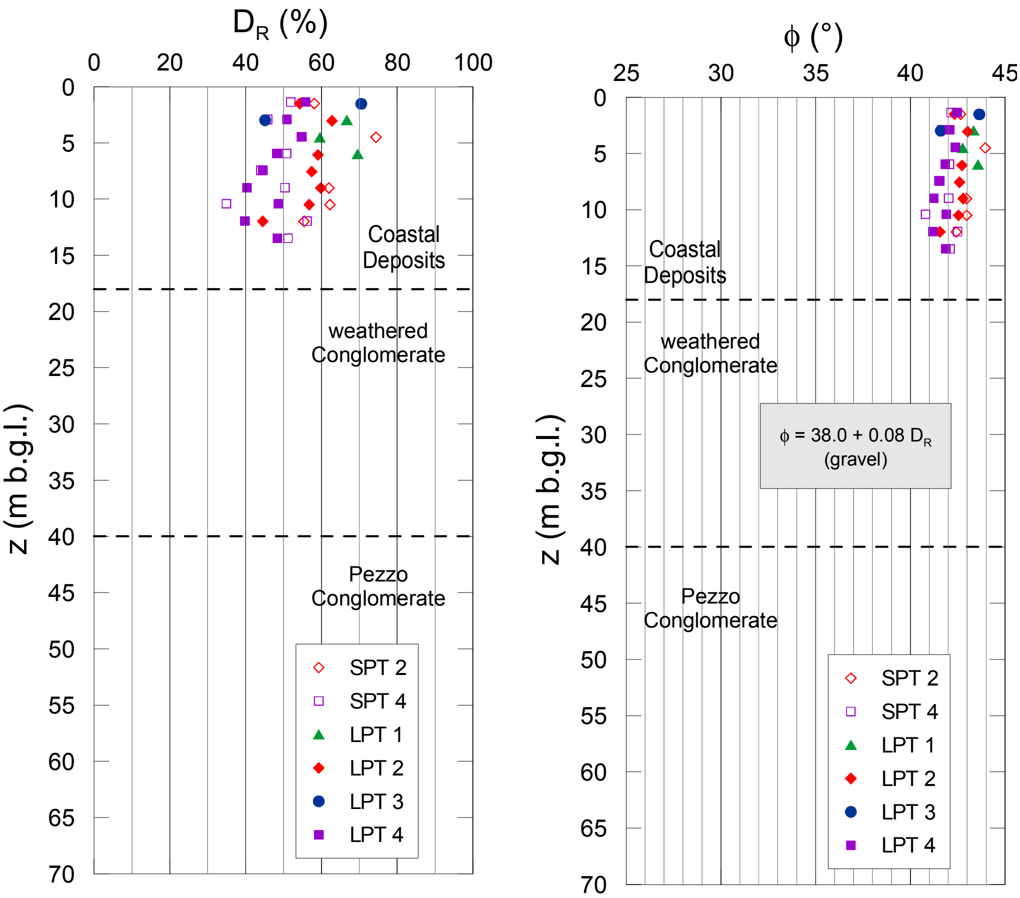

Figure 2.7: Calabria Anchor Block – relative density and angle of shearing resistance

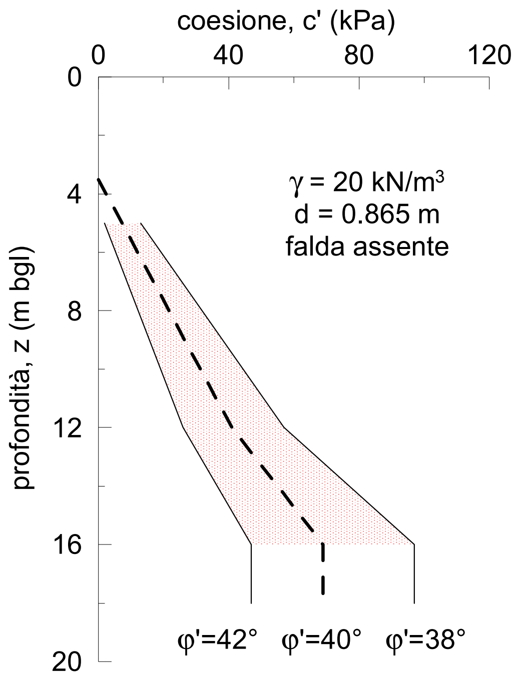

Figure 2.8. Calabria Anchor Block, c' profile from large diameter plate loading test (Report PP-2R-A24 - Figure 4.3.58)

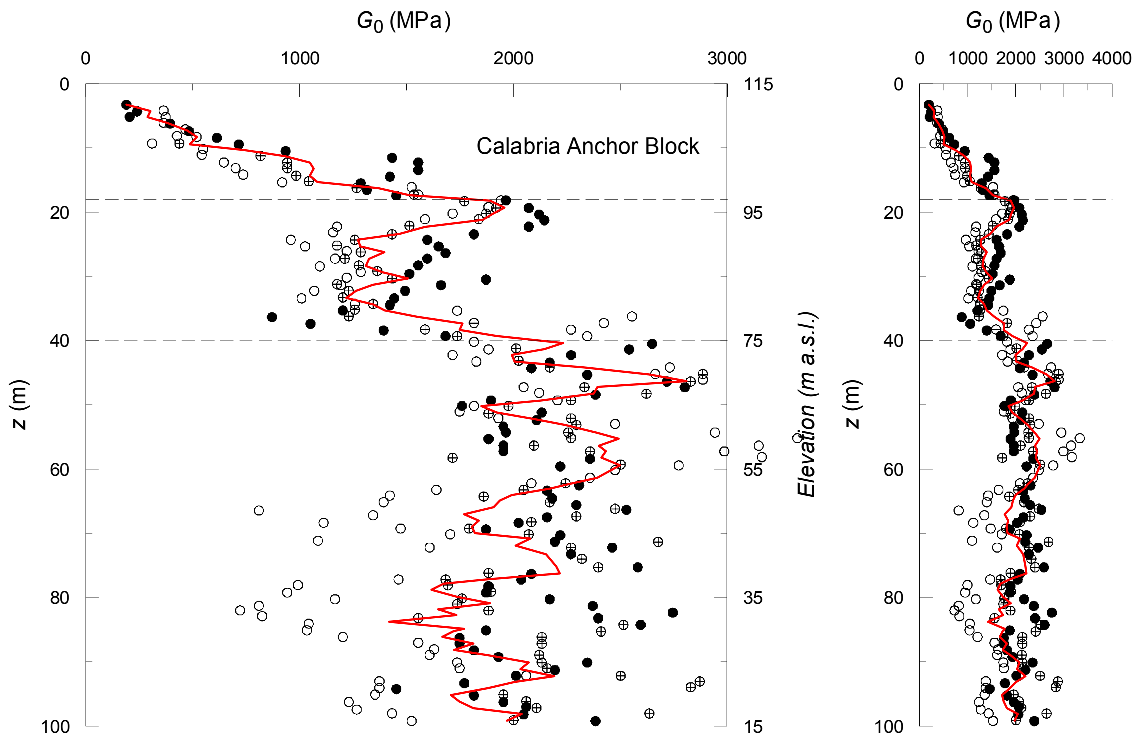

Figure 2.9. Calabria Anchor Block, G_0 profile from cross-hole test

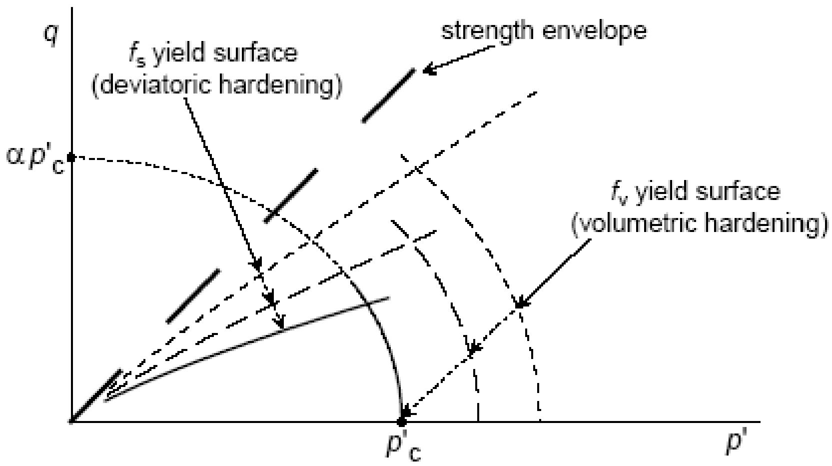

Figure 3.1. Yield surfaces of the Hardening Soil model and their evolution

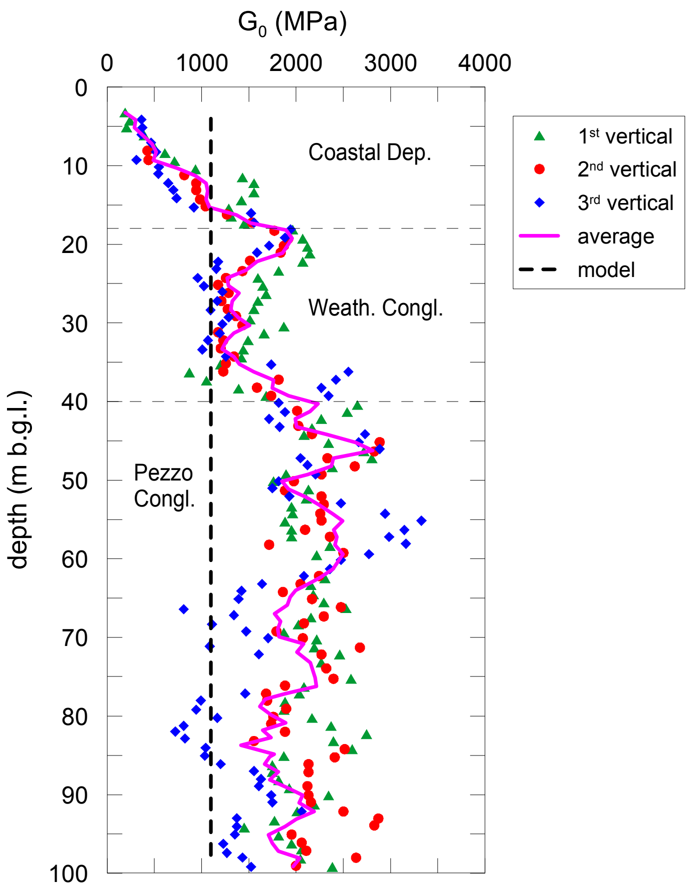

Figure 3.2. Calabria Anchor Block, G_0 profile from cross-hole test and HS model prediction

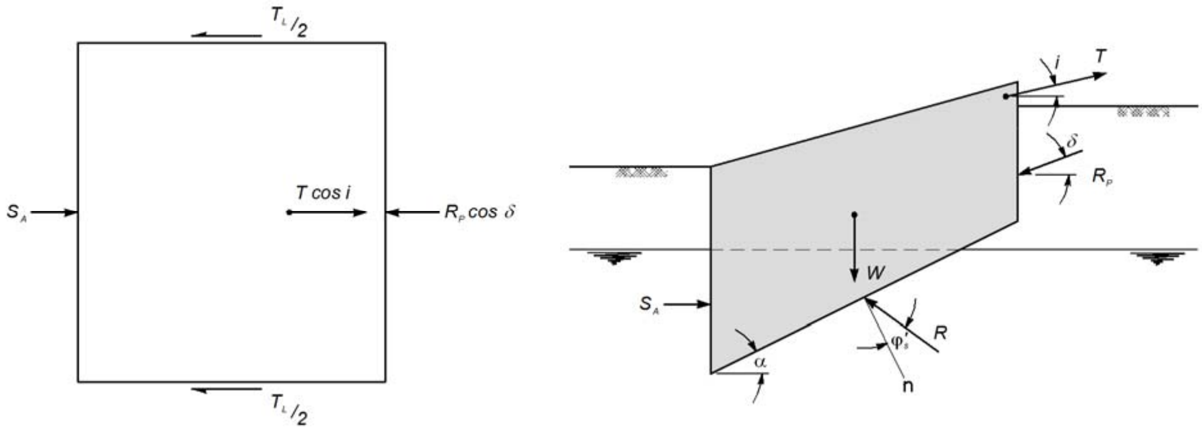

Figure 4.1. Rigid block, static conditions

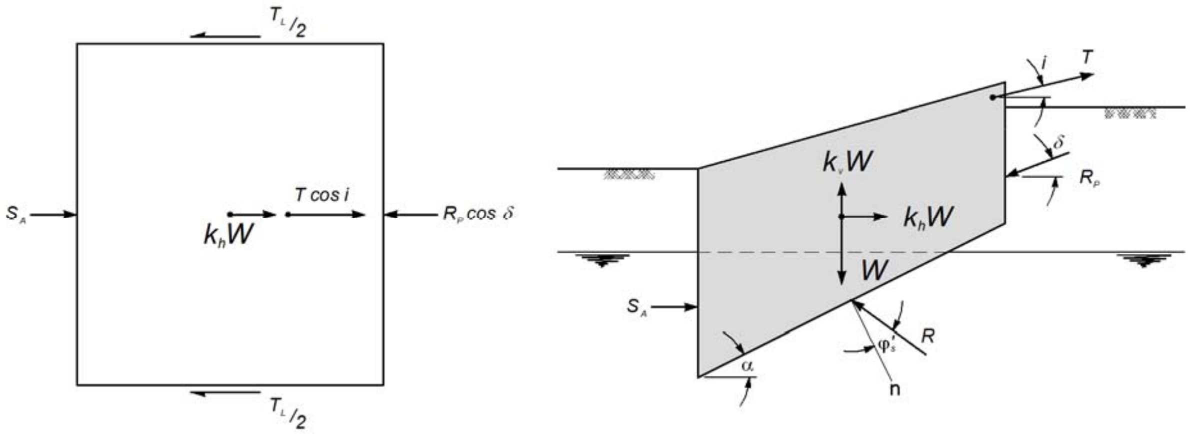

Figure 4.2. Rigid block, pseudo-static conditions

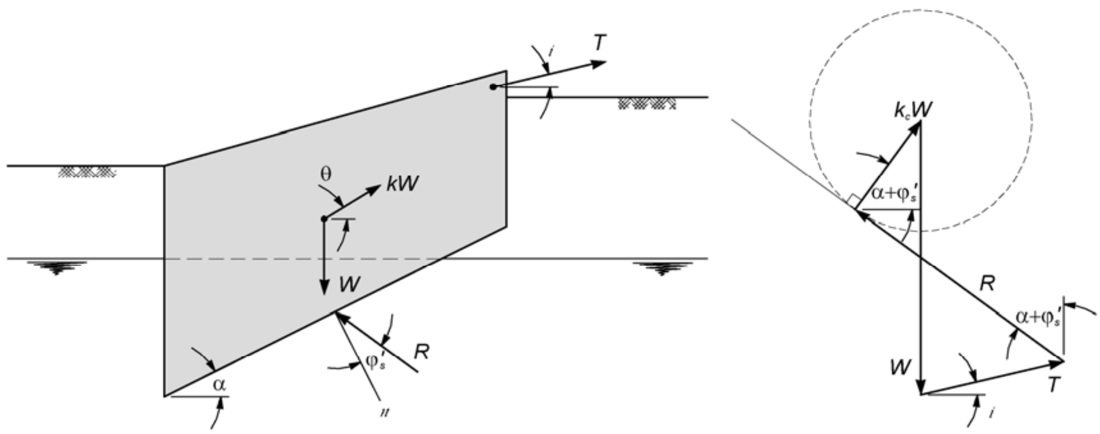

Figure 4.3. Rigid block, critical seismic coefficient

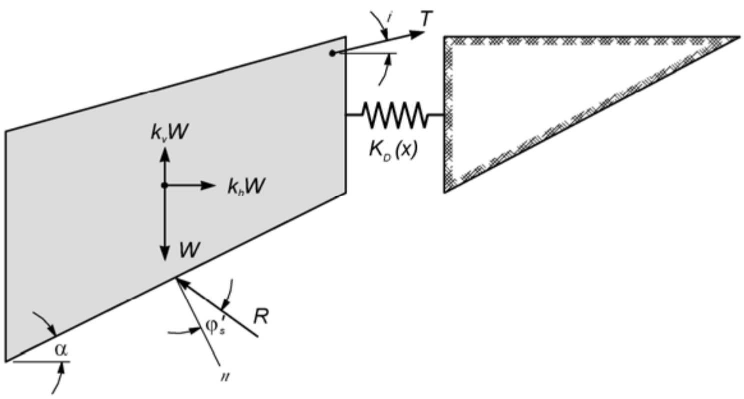

Figure 4.4. Rigid block, displacement dependent passive earth resistance

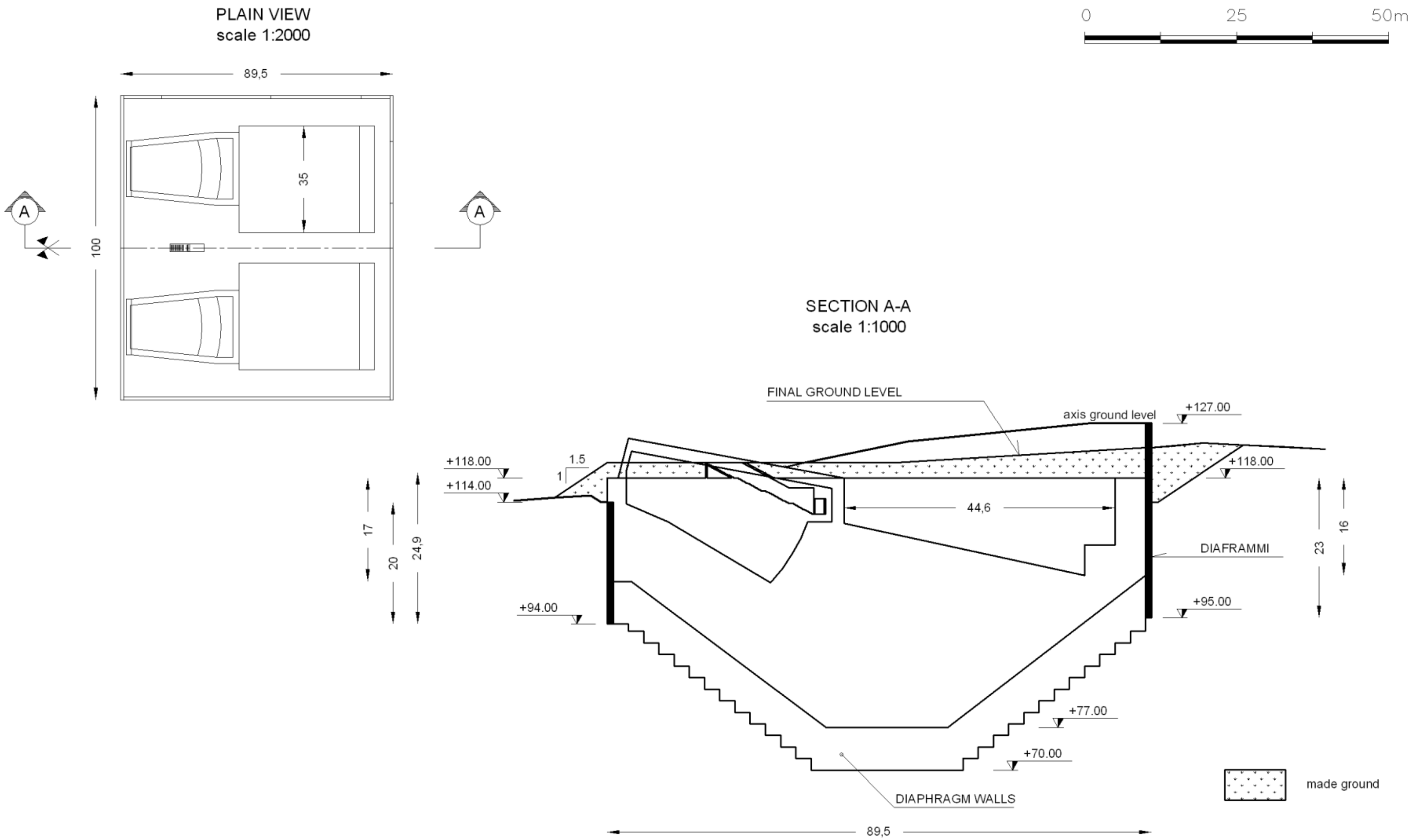

Figure 5.1. Plan view and cross section of Calabria anchor block

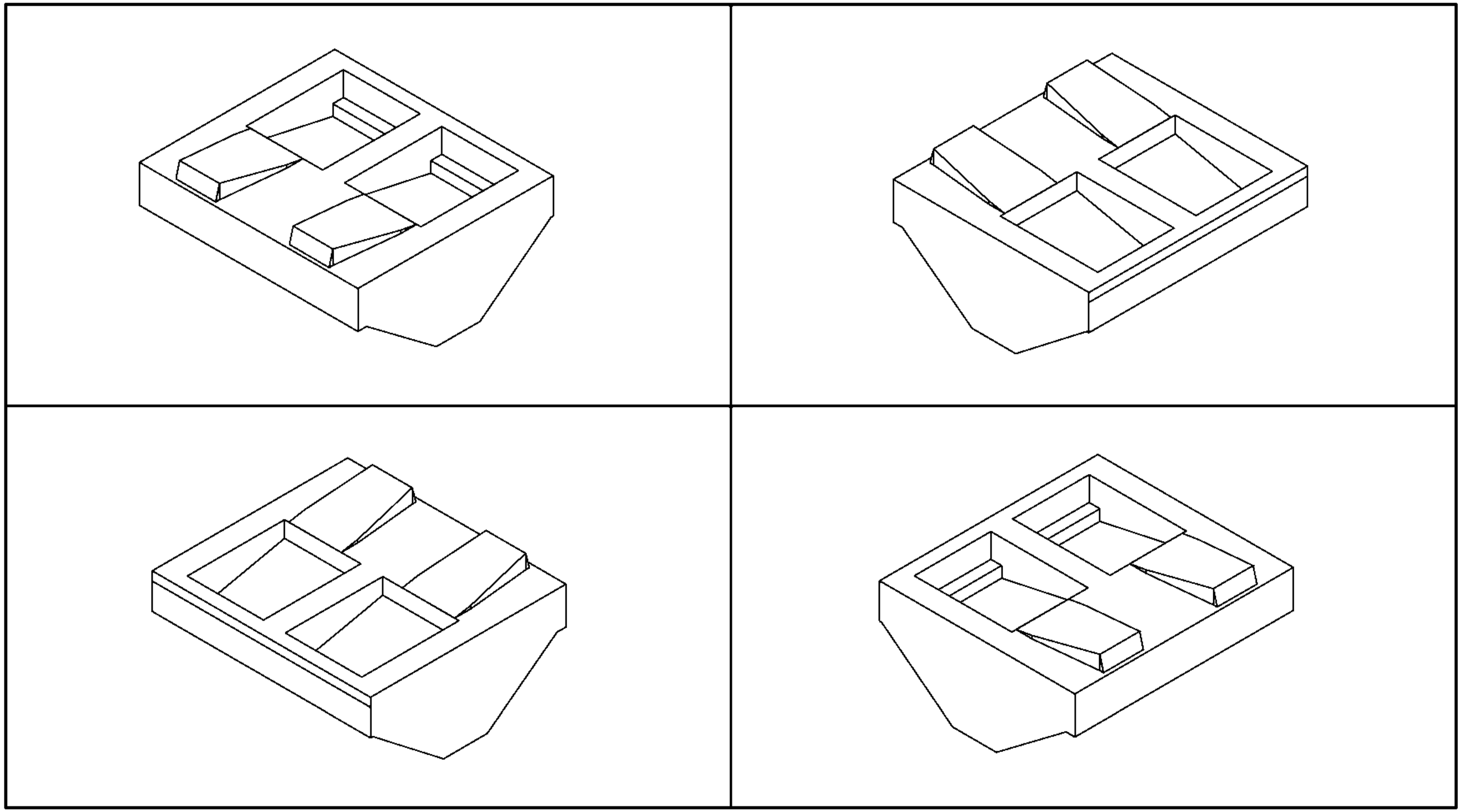

Figure 5.2. Calabria anchor block 3D CAD model

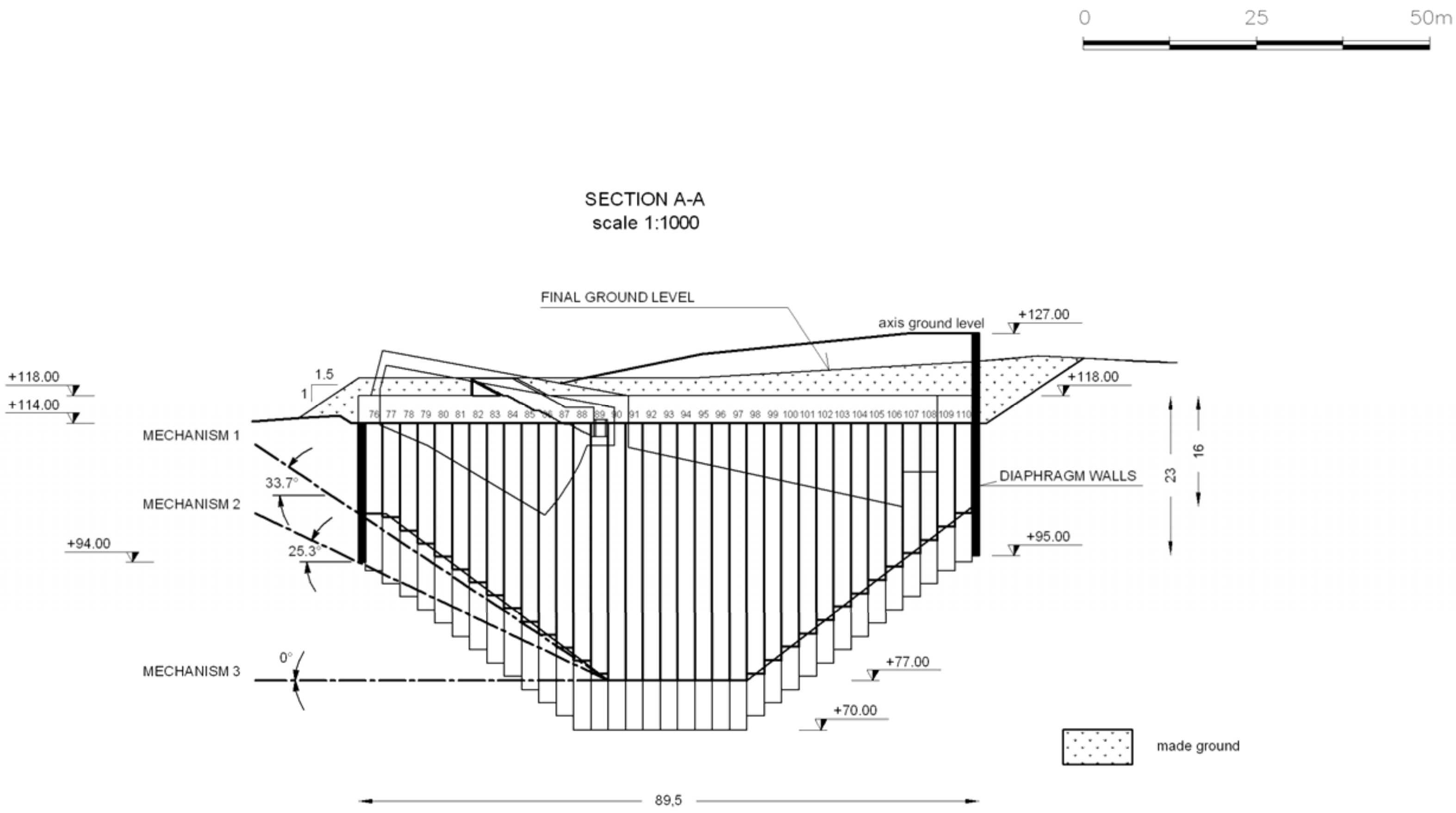

Figure 5.3. Sliding mechanisms

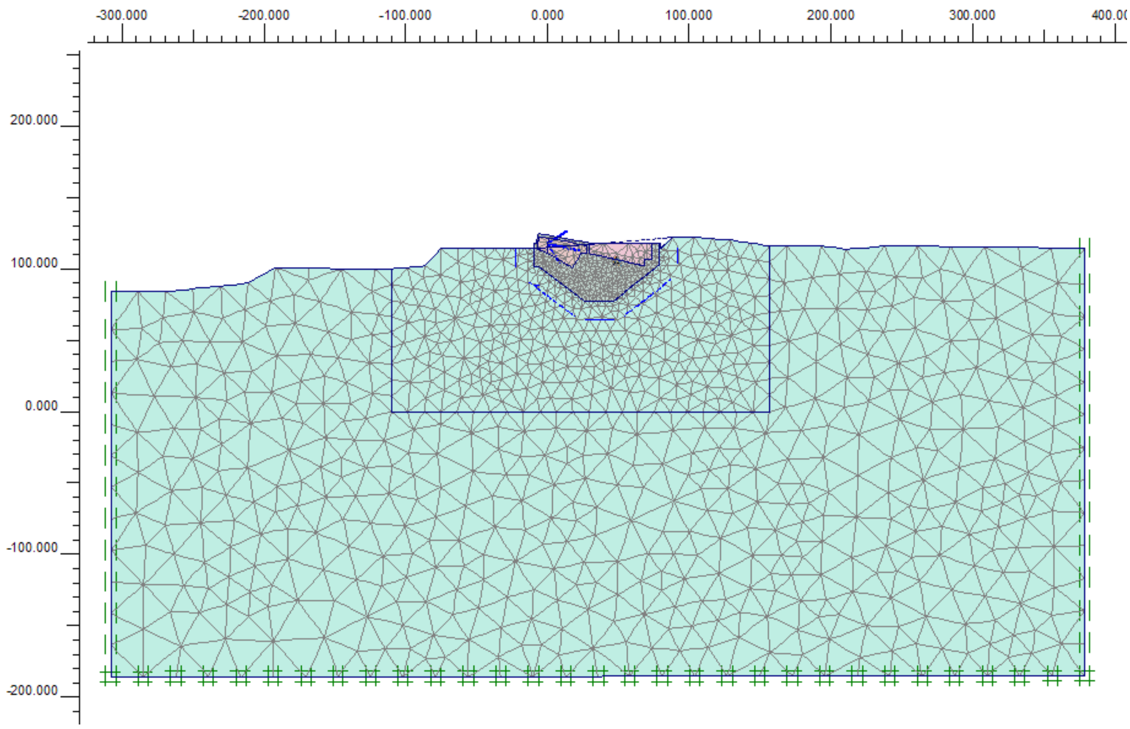

Figure 5.4. Mesh used for plane strain F.E. simulations

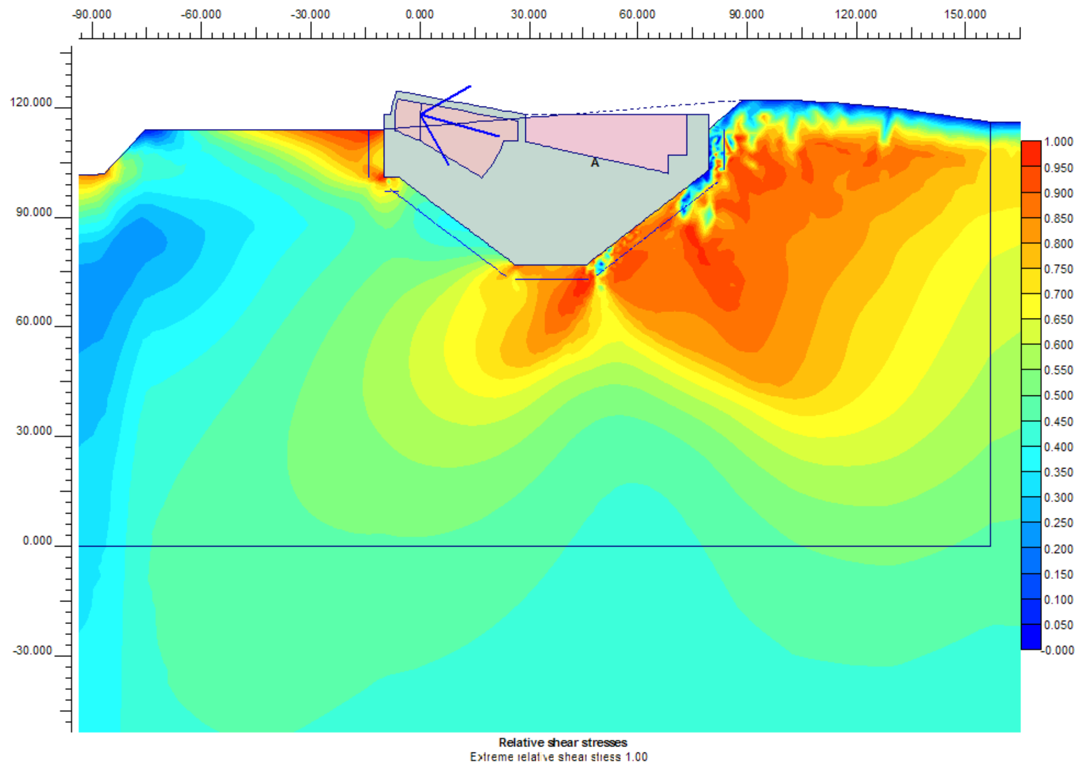

Figure 5.5. Relative shear stress (t/t_{max}) contours, H_w = 88 m a.s.l.

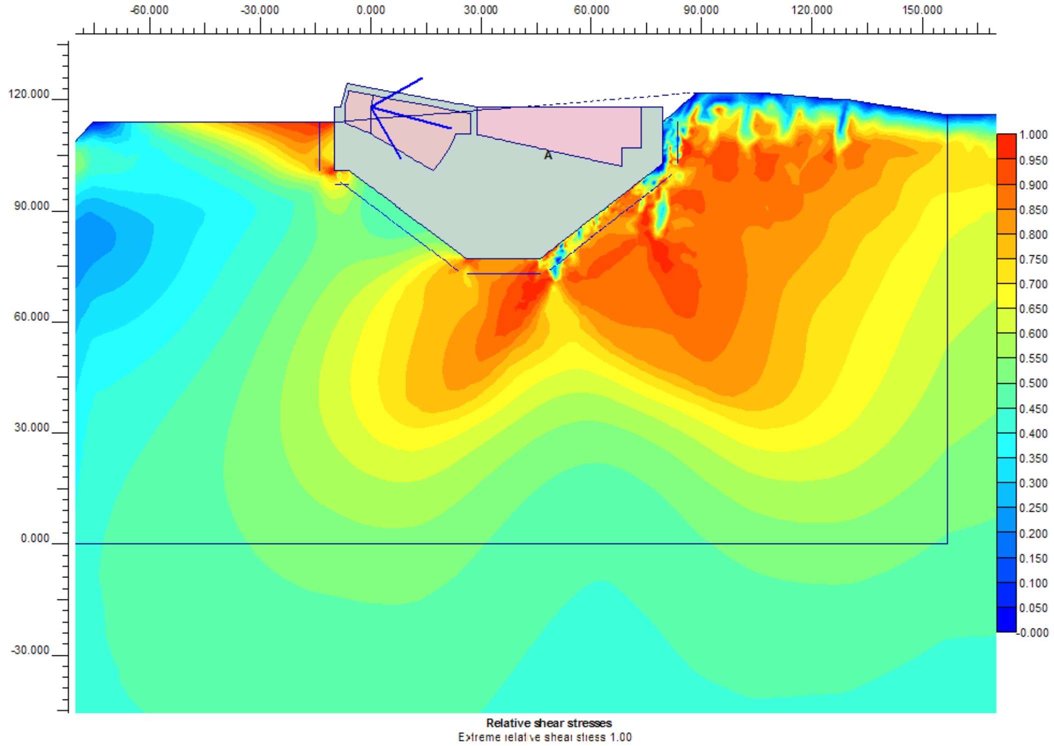

Figure 5.6. Relative shear stress (t/t_{max}) contours, H_w = 94.5 m a.s.l.

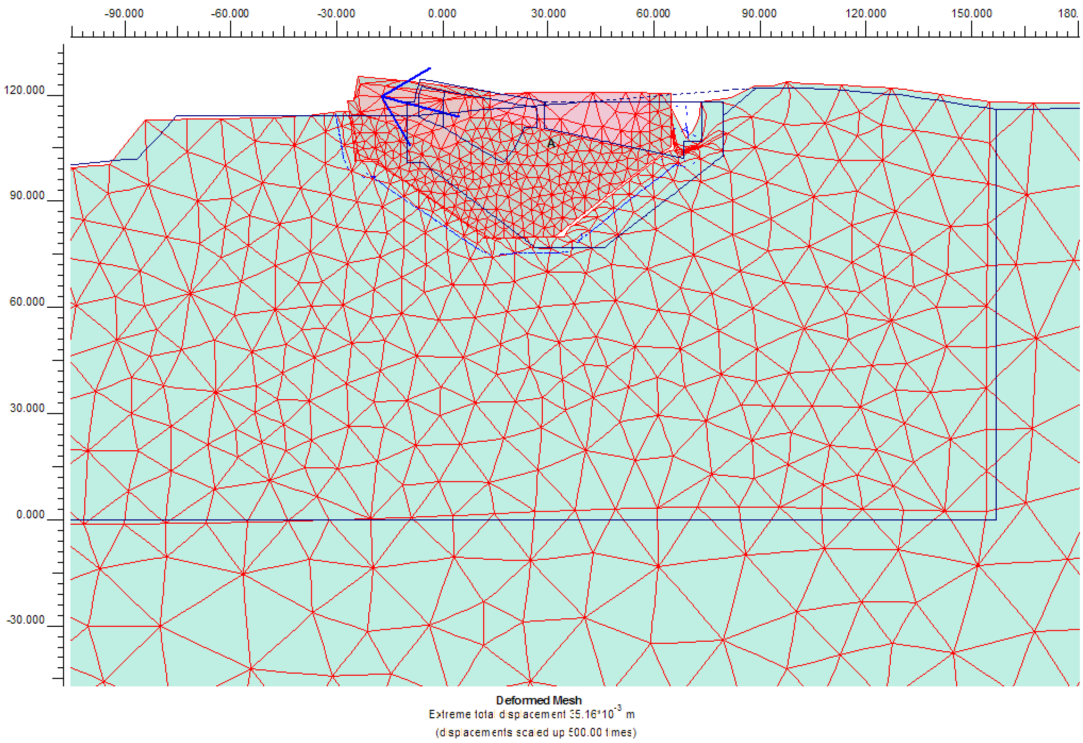

Figure 5.7. Deformed mesh, H_w = 88 m a.s.l.

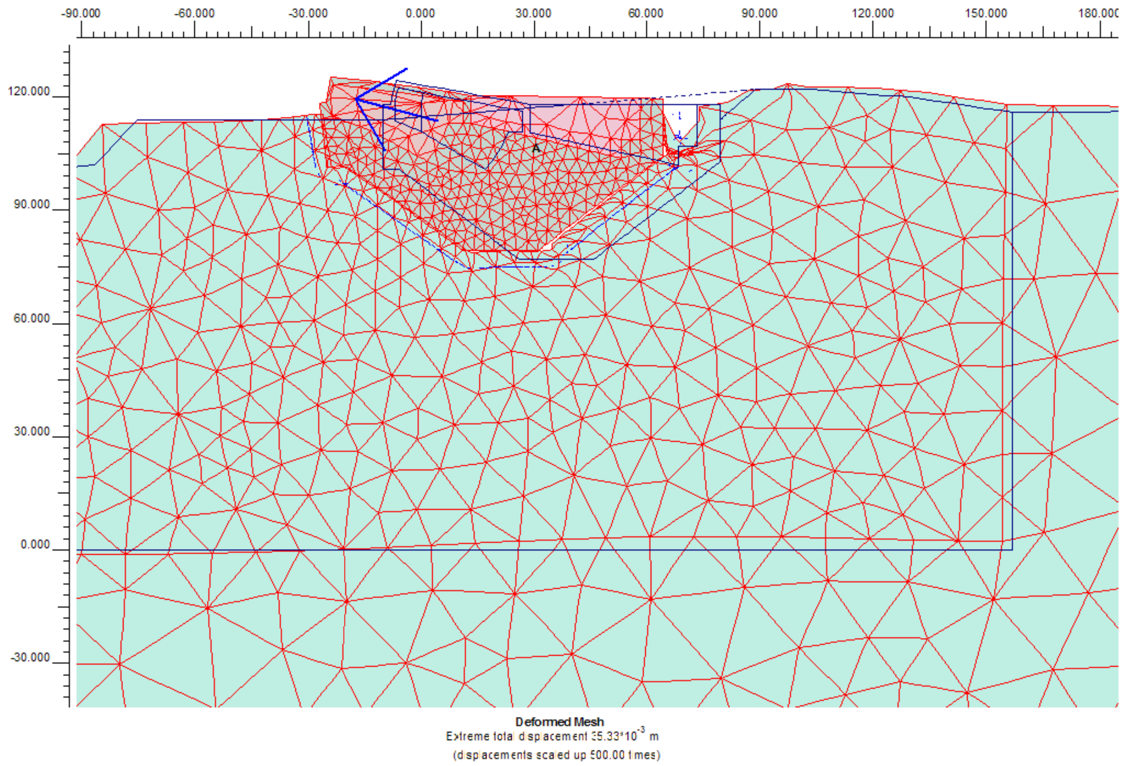

Figure 5.8. Deformed mesh, H_w = 94.5 m a.s.l.

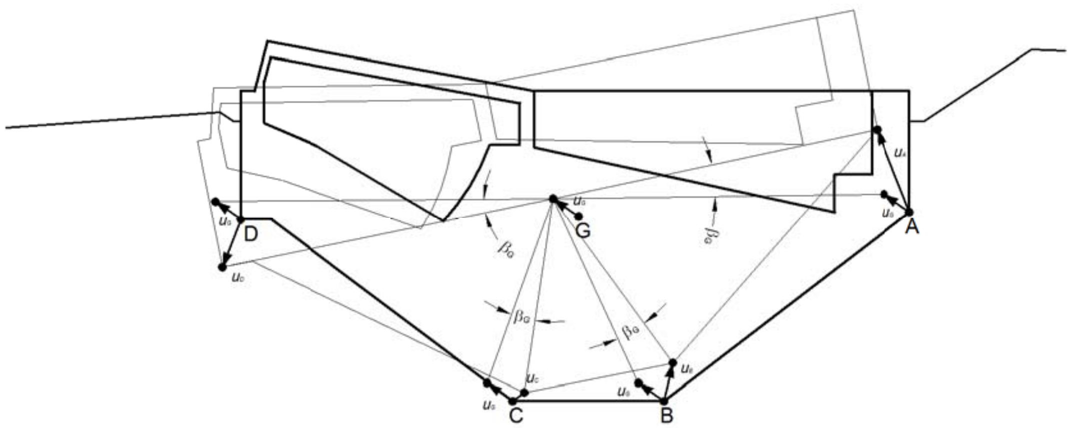

Figure 5.9. Reference displacement points for 2D F.E. simulation results

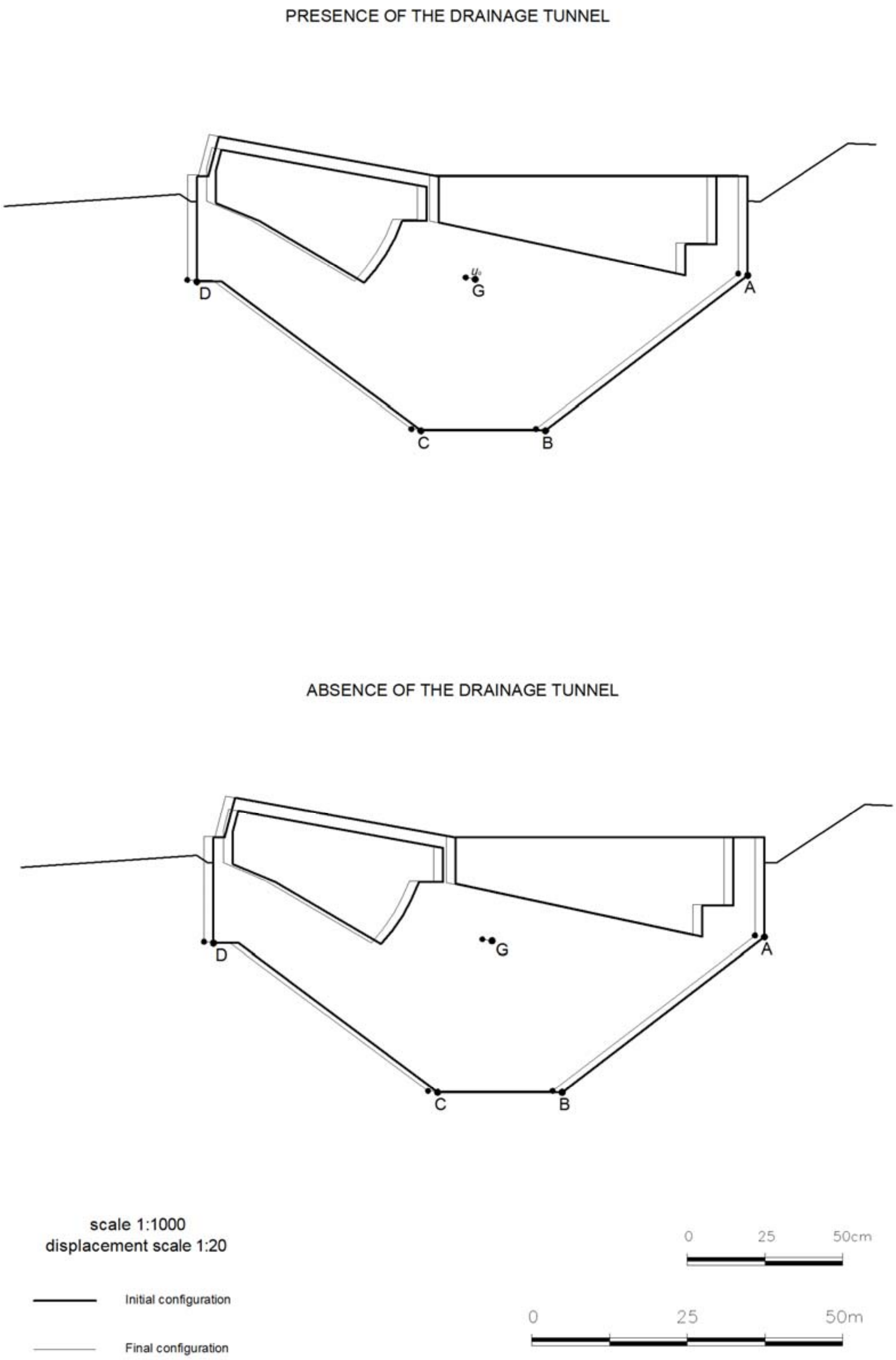

Figure 5.10. 2D F.E. simulations, sliding mechanism; presence (up) and absence (down) of the drainage system

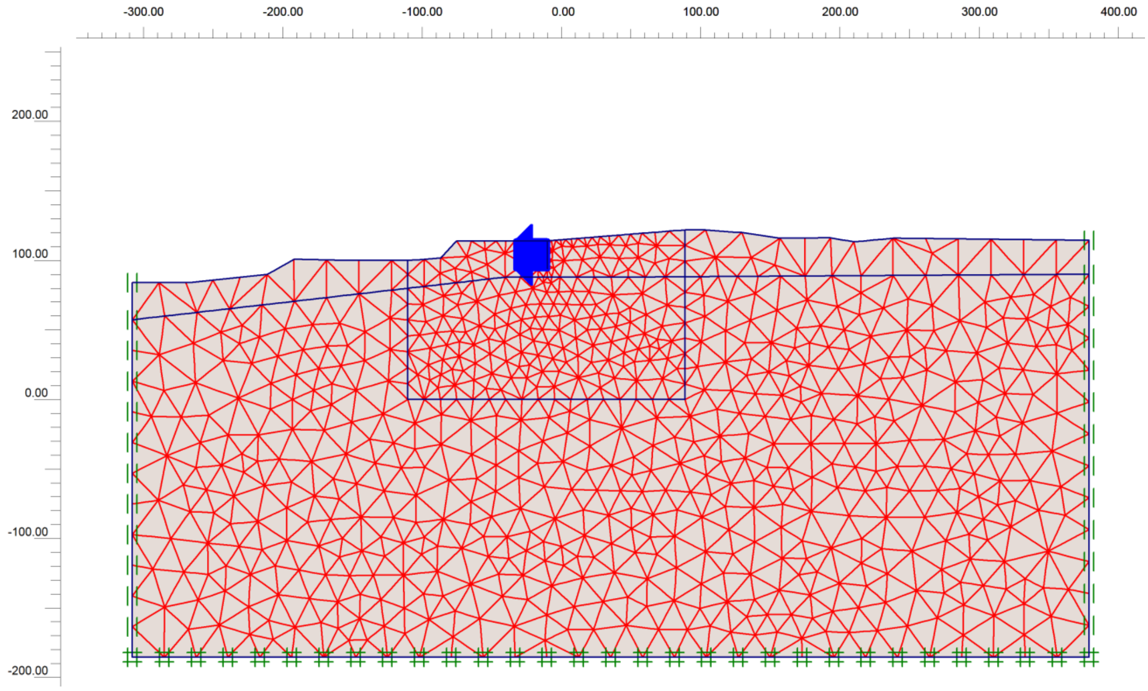

Figure 5.11. Mesh used in plane strain F.E. for simulating the earth resistance in front of the anchor block (mechanism 2)

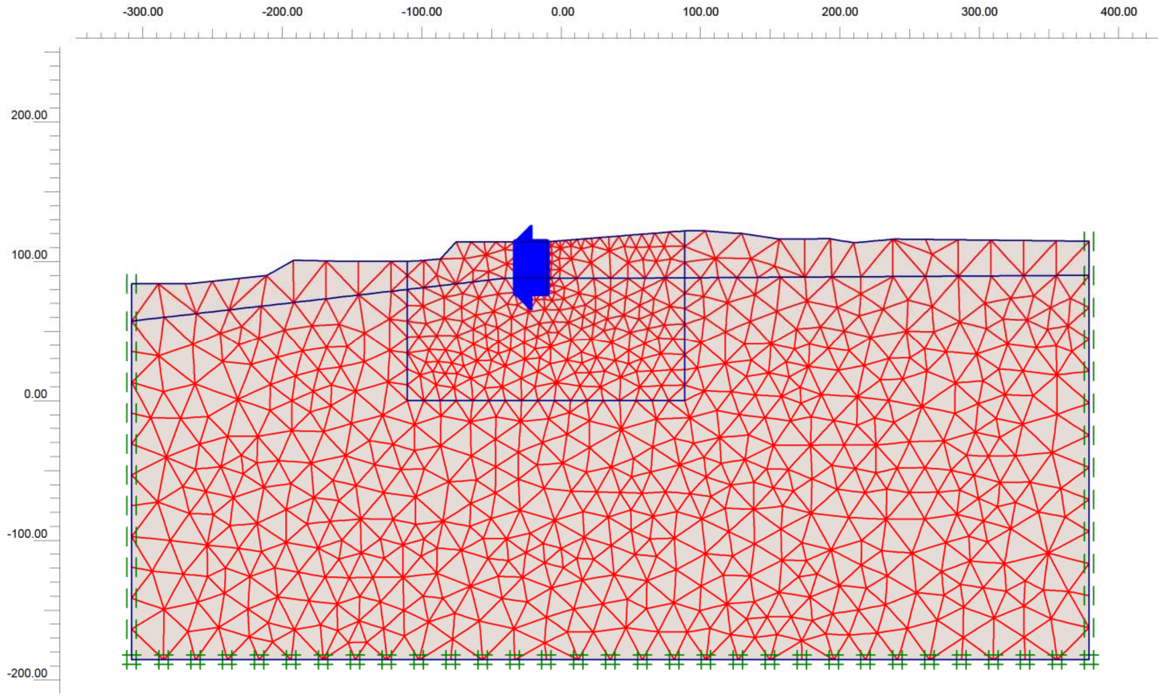

Figure 5.12. Mesh used in plane strain F.E. for simulating the earth resistance in front of the anchor block (mechanism 3)

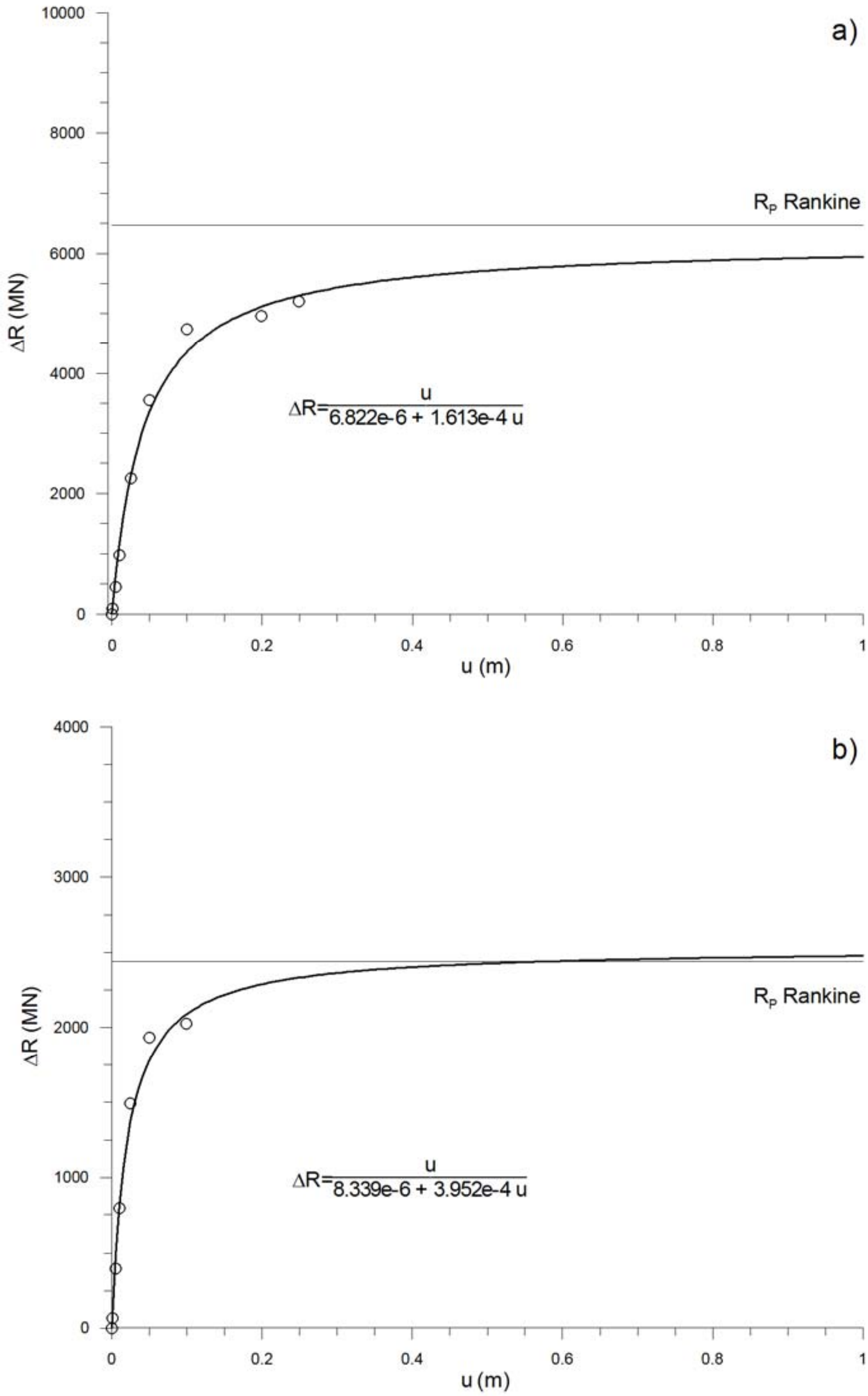

Figure 5.13. ΔR = f(u) equation, presence of the drainage system; a) mechanism 3; b) mechanism 2

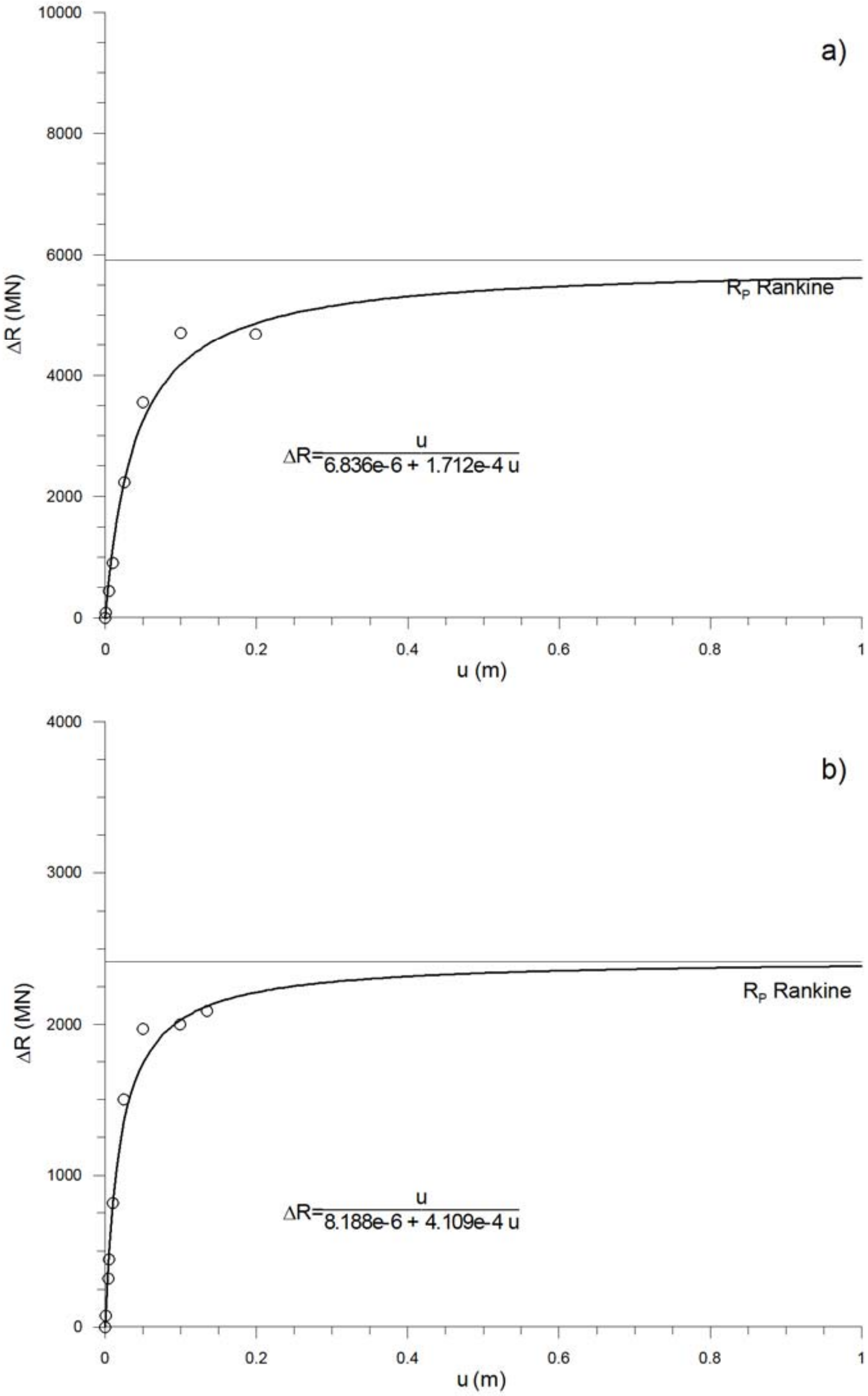

Figure 5.14. ΔR = f(u) equation, absence of the drainage system; a) mechanism 3; b) mechanism 2

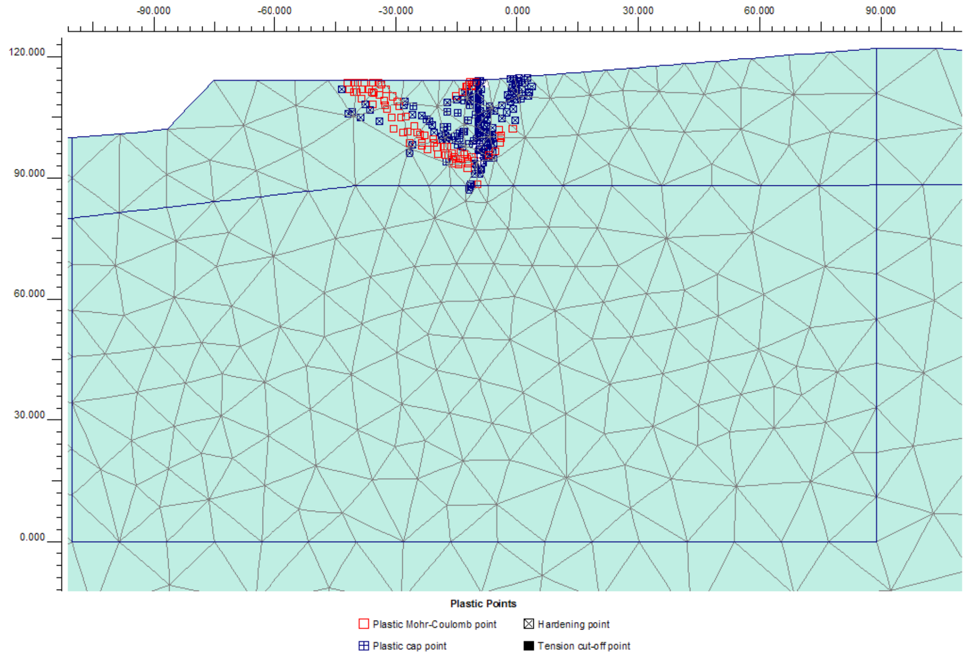

Figure 5.15. 2D F.E. simulation of earth resistance, H_w = 88.0 m a.s.l., mechanism 2, plastic points

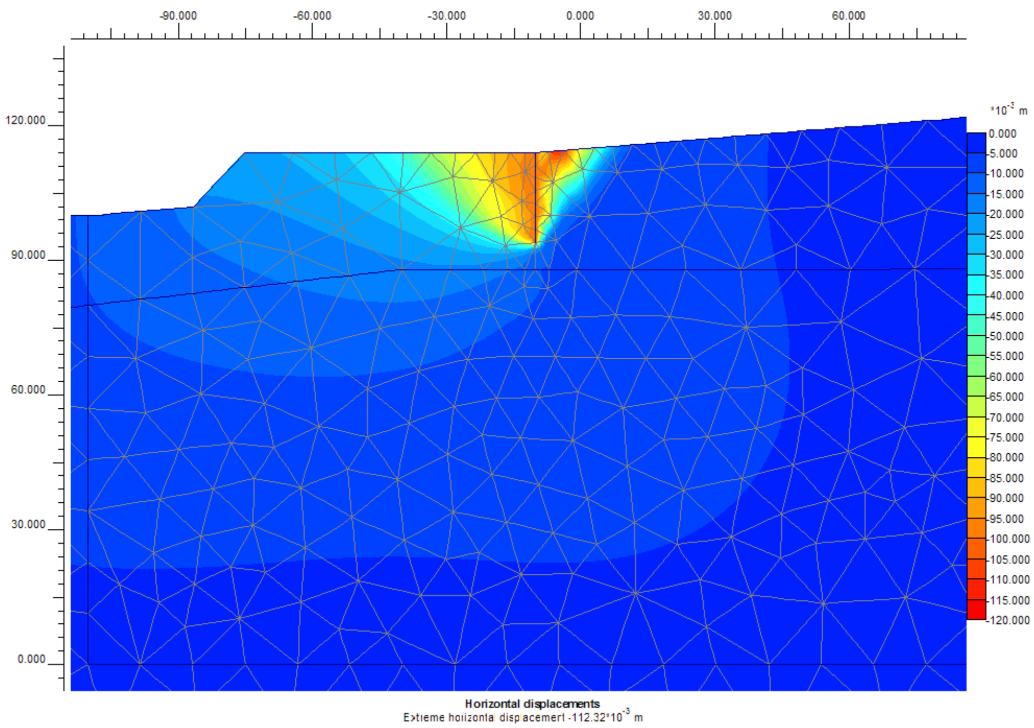

Figure 5.16. 2D F.E. simulation of earth resistance, H_w = 88.0 m a.s.l., mechanism 2, horizontal displacements contours

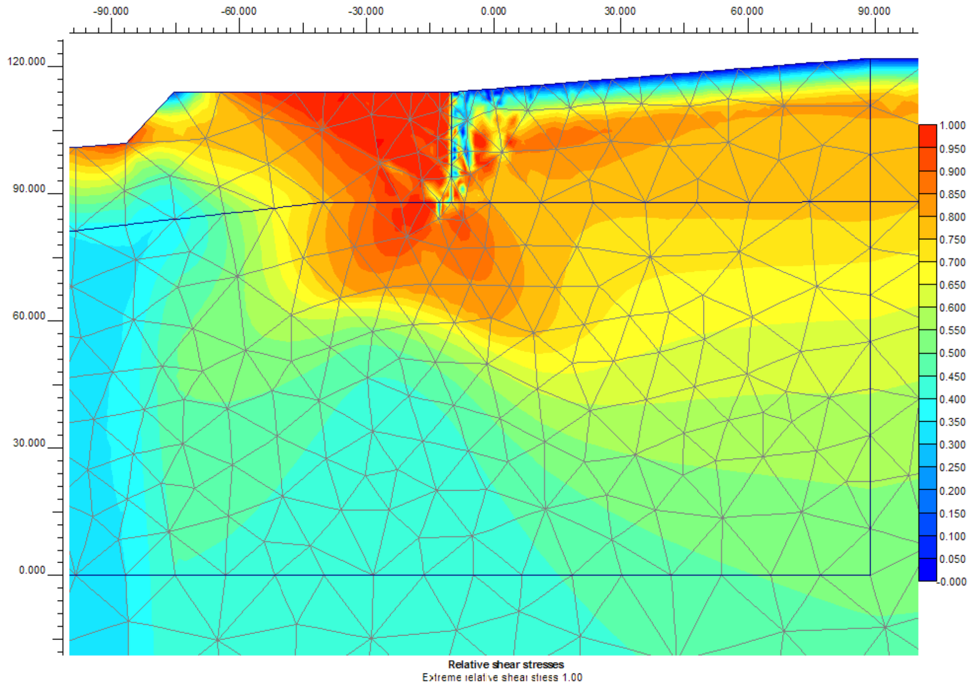

Figure 5.17. 2D F.E. simulation of earth resistance, H_w = 88.0 m a.s.l., mechanism 2, relative shear (t/t_{max}) contours

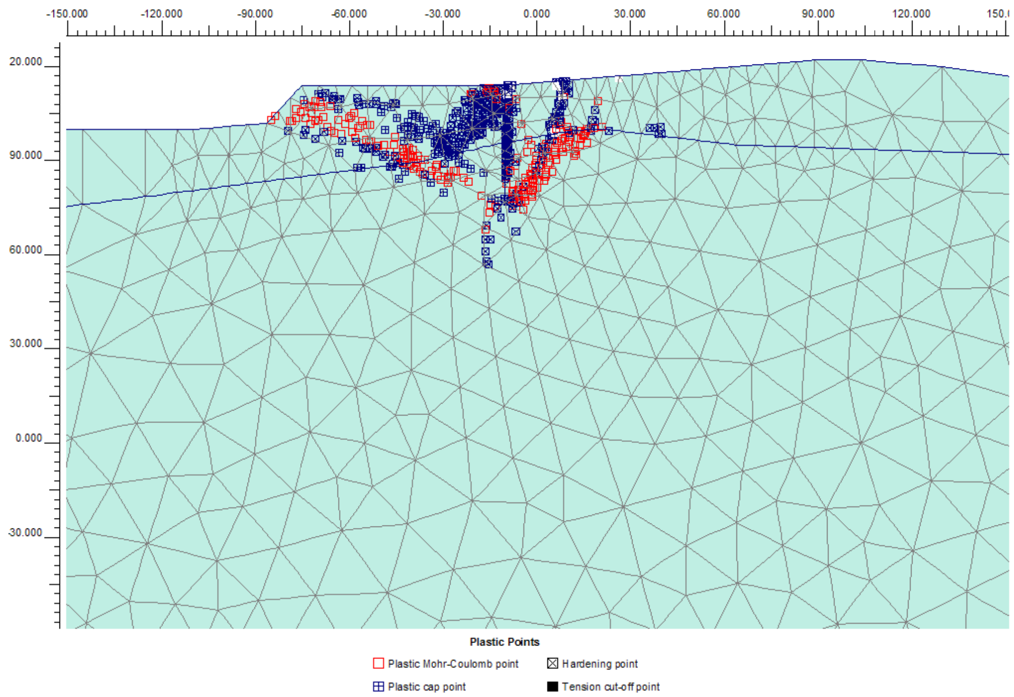

Figure 5.18. 2D F.E. simulation of earth resistance, H_w = 88.0 m a.s.l., mechanism 3, plastic points

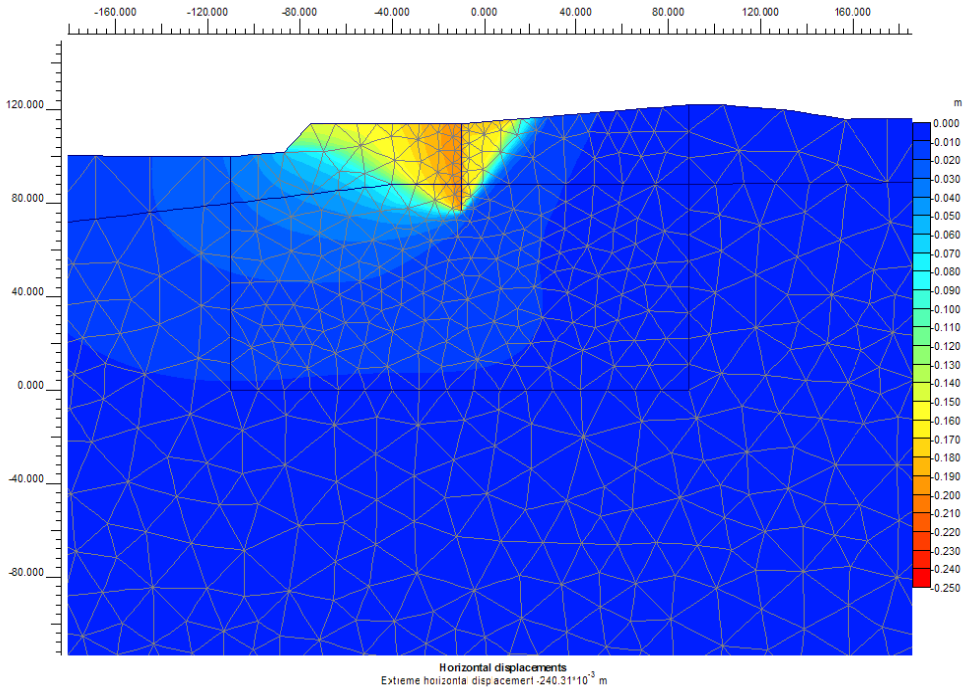

Figure 5.19 2D F.E. simulation of earth resistance, H_w = 88.0 m a.s.l., mechanism 3, horizontal displacements contours

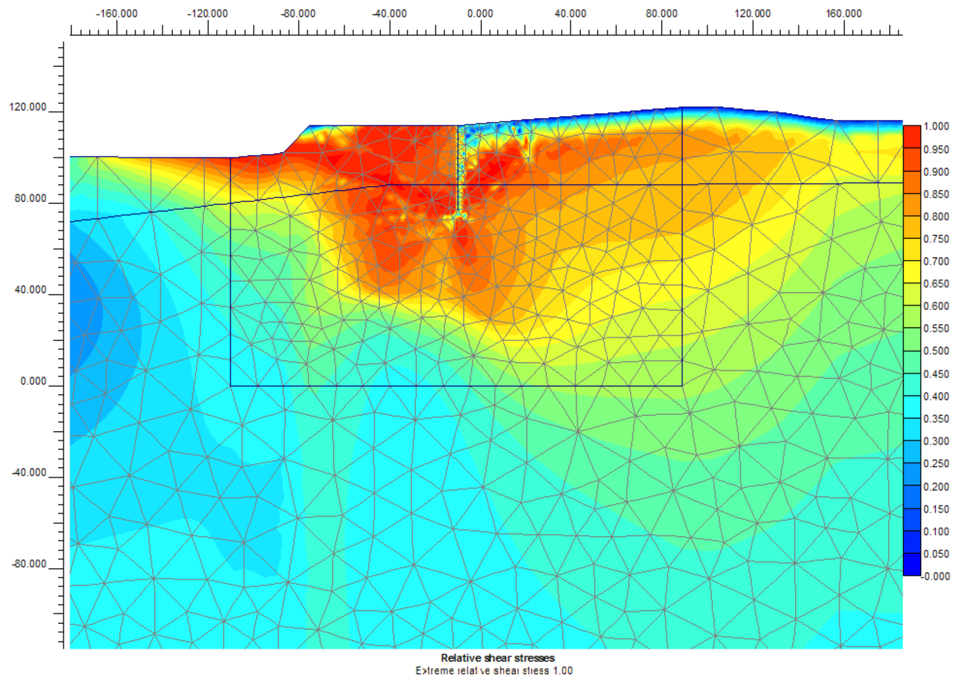

Figure 5.20. 2D F.E. simulation of earth resistance, H_w = 88.0 m a.s.l., mechanism 3, relative shear (t/t_{max}) contours

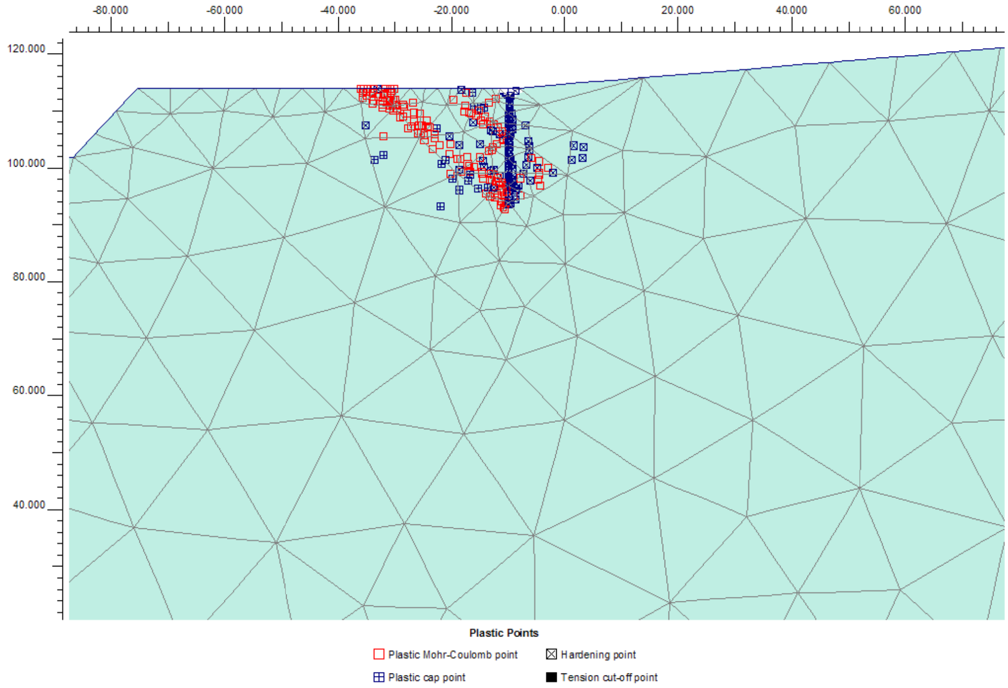

Figure 5.21. 2D F.E. simulation of earth resistance, H_w = 94.5 m a.s.l., mechanism 2, plastic points

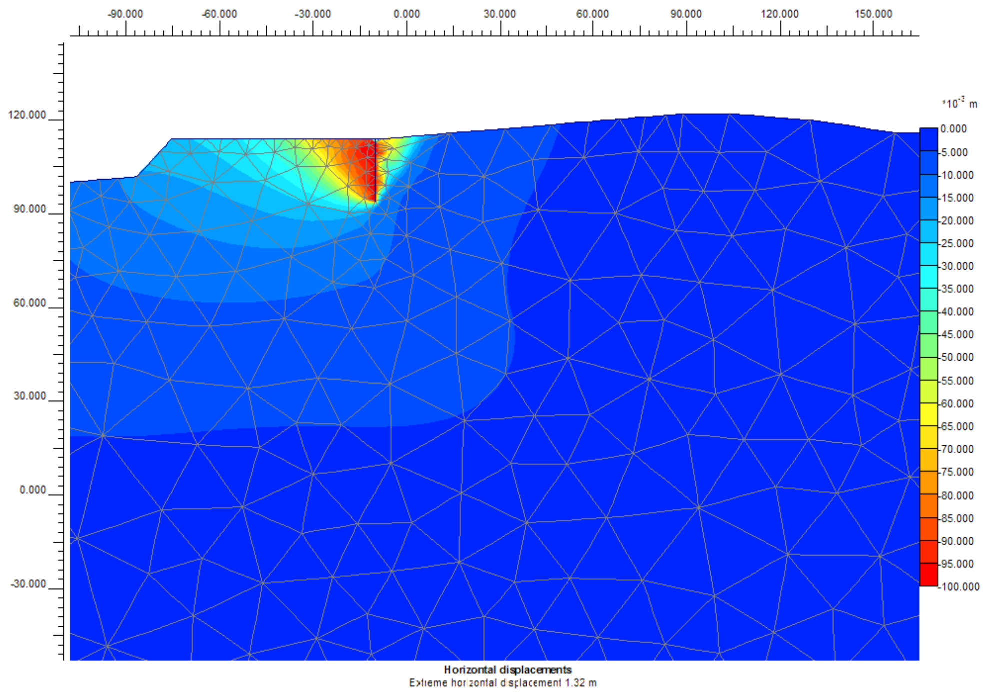

Figure 5.22. F.E. simulation of earth resistance, H_w = 94.5 m a.s.l., mechanism 2, horizontal displacements contours

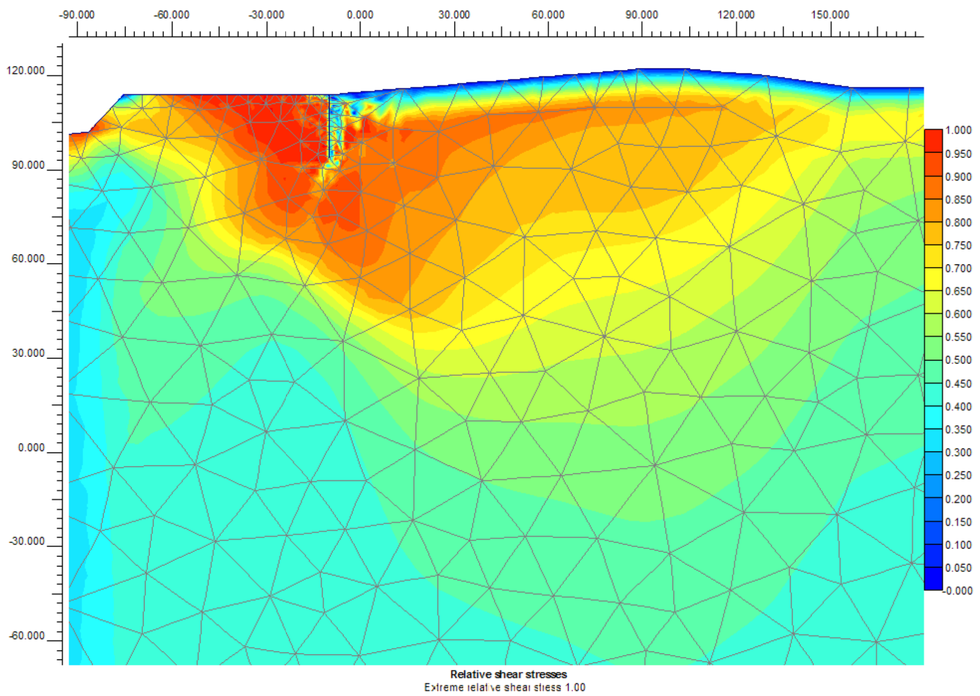

Figure 5.23. 2D F.E. simulation of earth resistance, H_w = 94.5 m a.s.l., mechanism 2, relative shear (t/t_{max}) contours

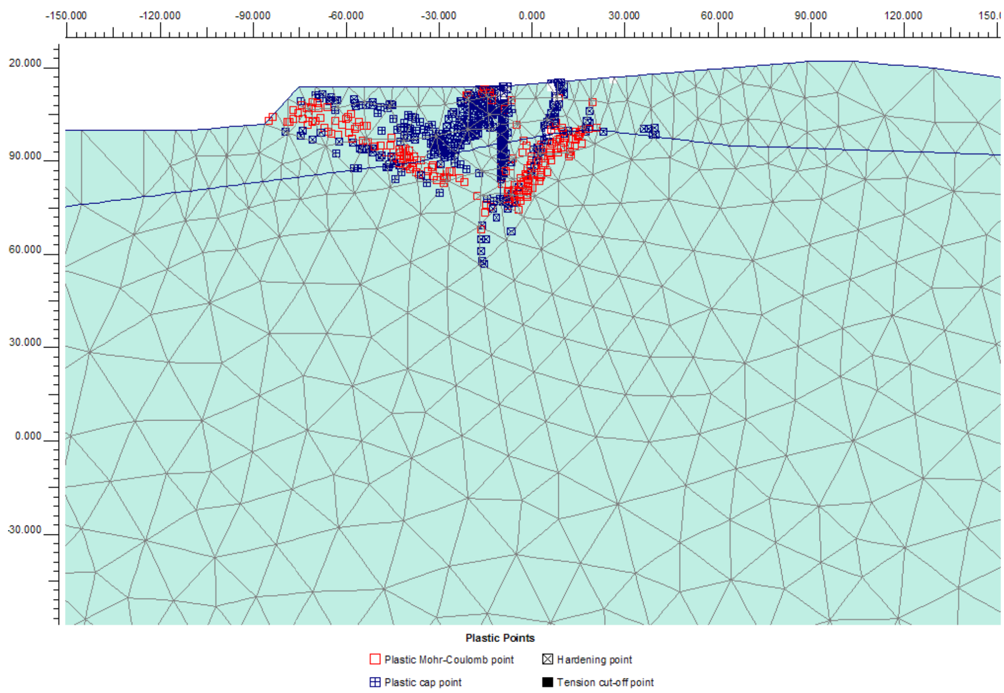

Figure 5.24. 2D F.E. simulation of earth resistance, H_w = 94.5 m a.s.l., mechanism 3, plastic points

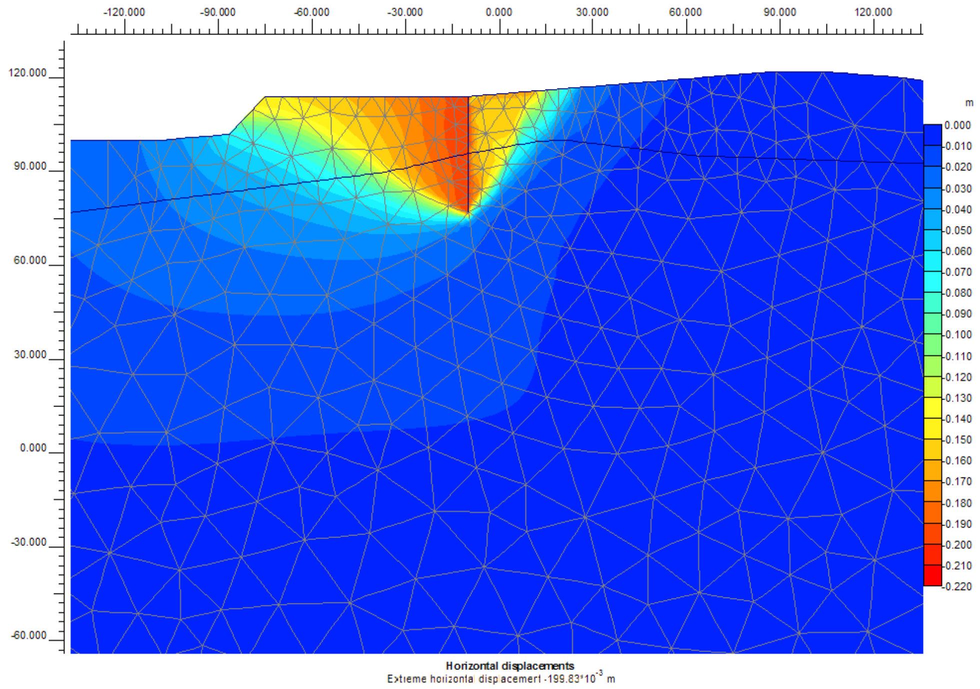

Figure 5.25. F.E. simulation of earth resistance, H_w = 94.5 m a.s.l., mechanism 3, horizontal displacements contours

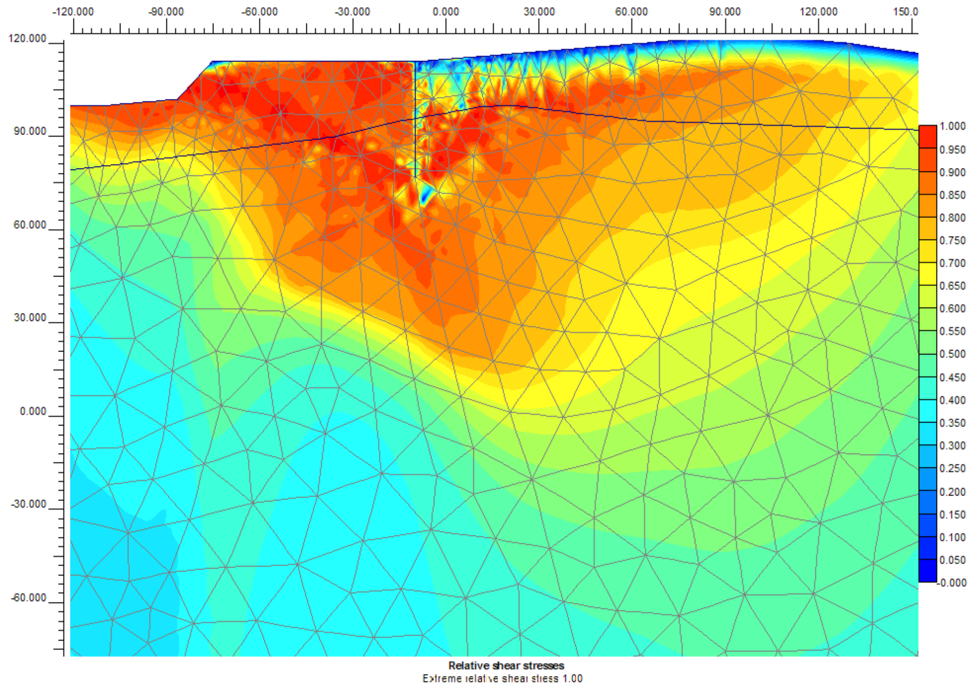

Figure 5.26. 2D F.E. simulation of earth resistance, H_w = 94.5 m a.s.l., mechanism 3, relative shear (t/t_{max}) contours

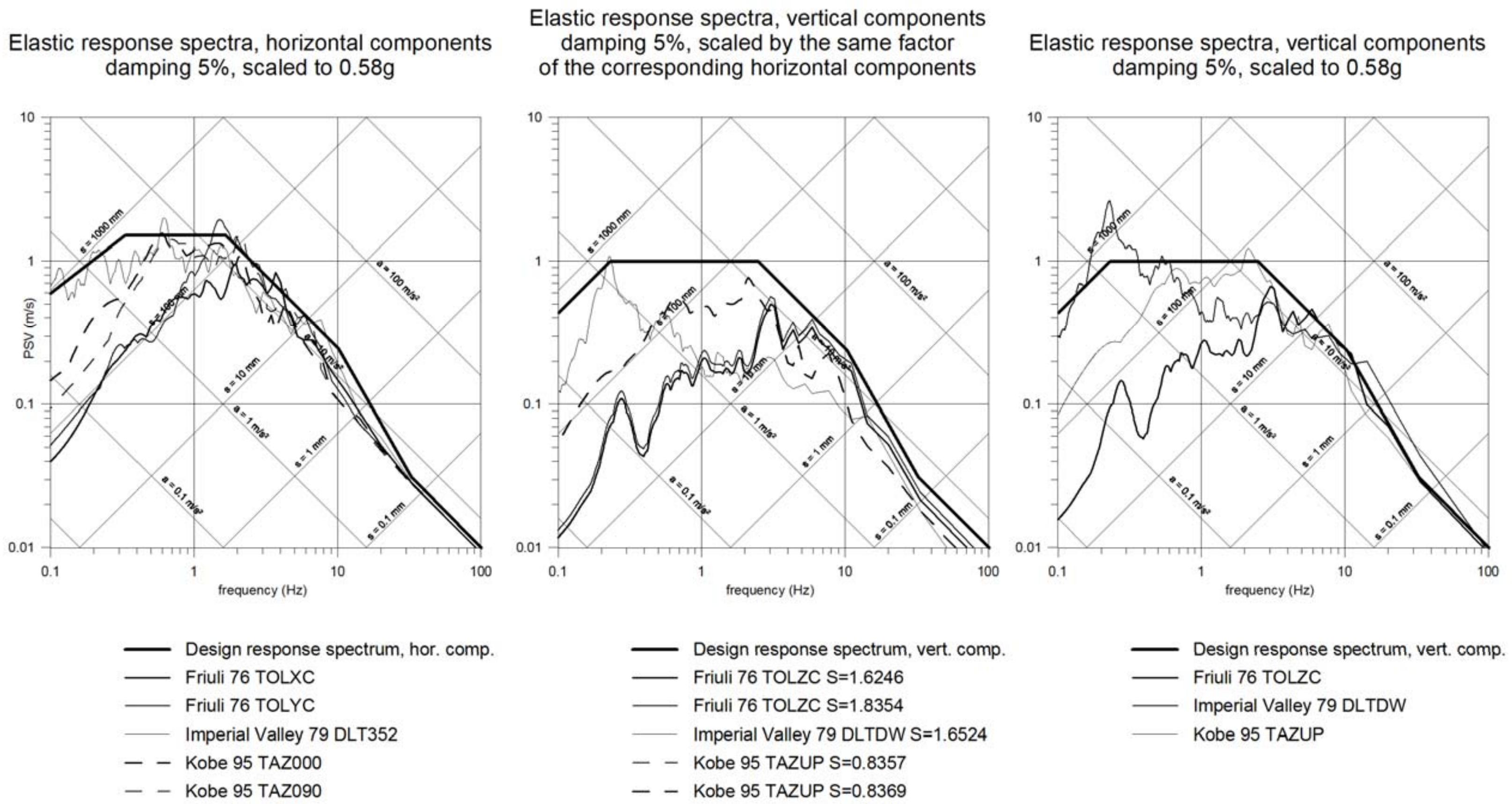

Figure 5.27. Elastic response spectra of the accelerograms used in the analyses

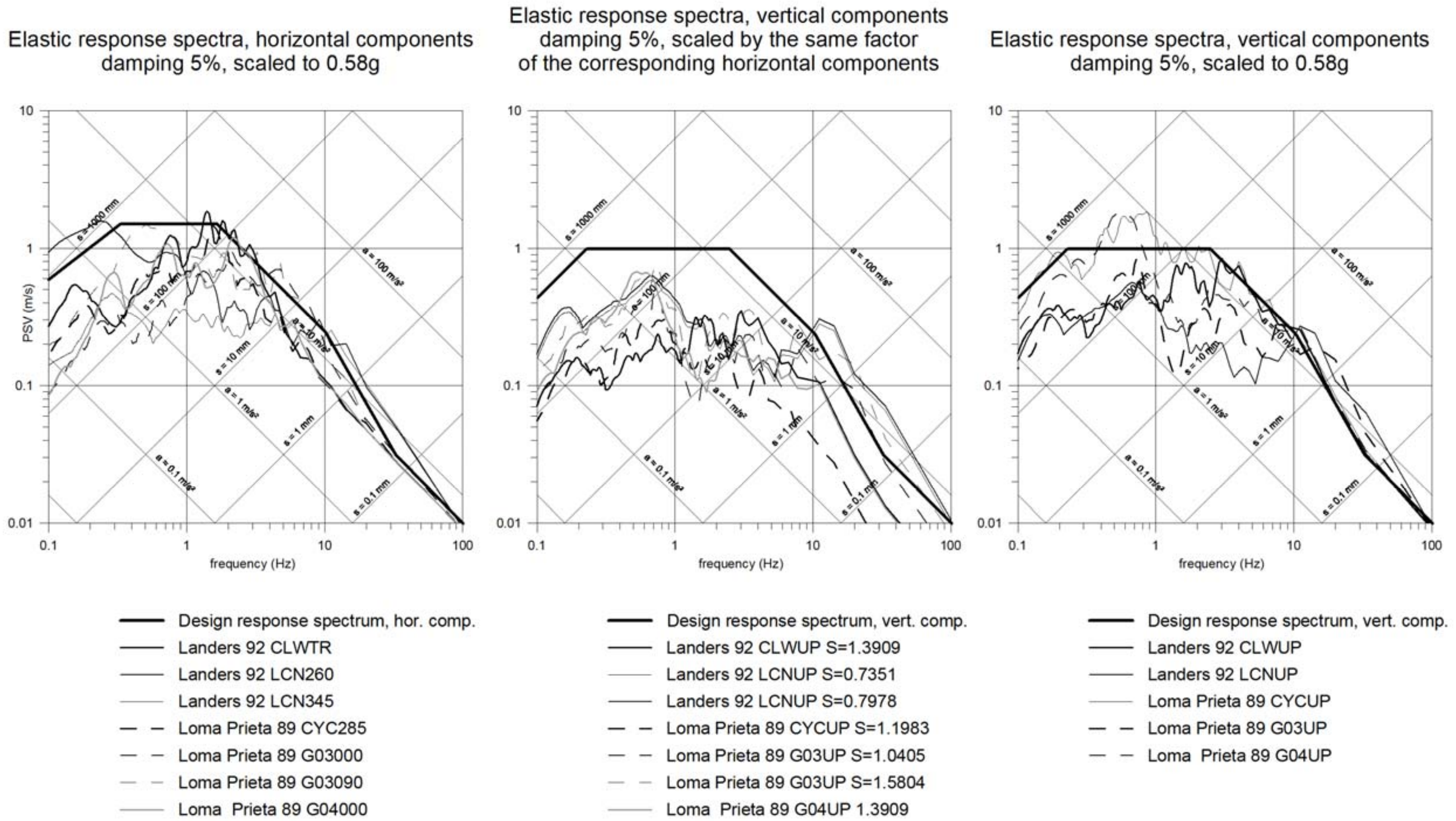

Figure 5.28. Elastic response spectra of the accelerograms used in the analyses

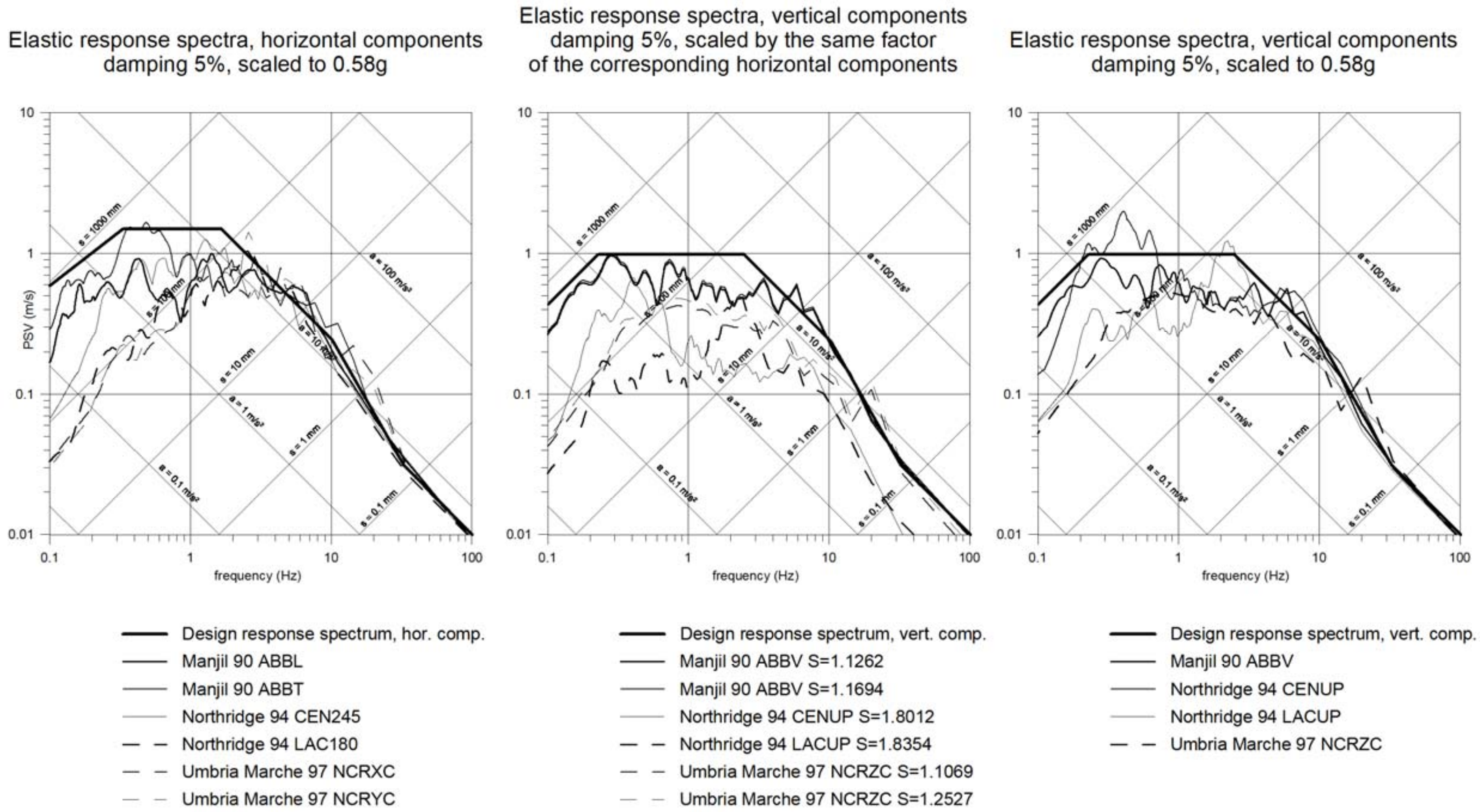

Figure 5.29. Elastic response spectra of the accelerograms used in the analyses

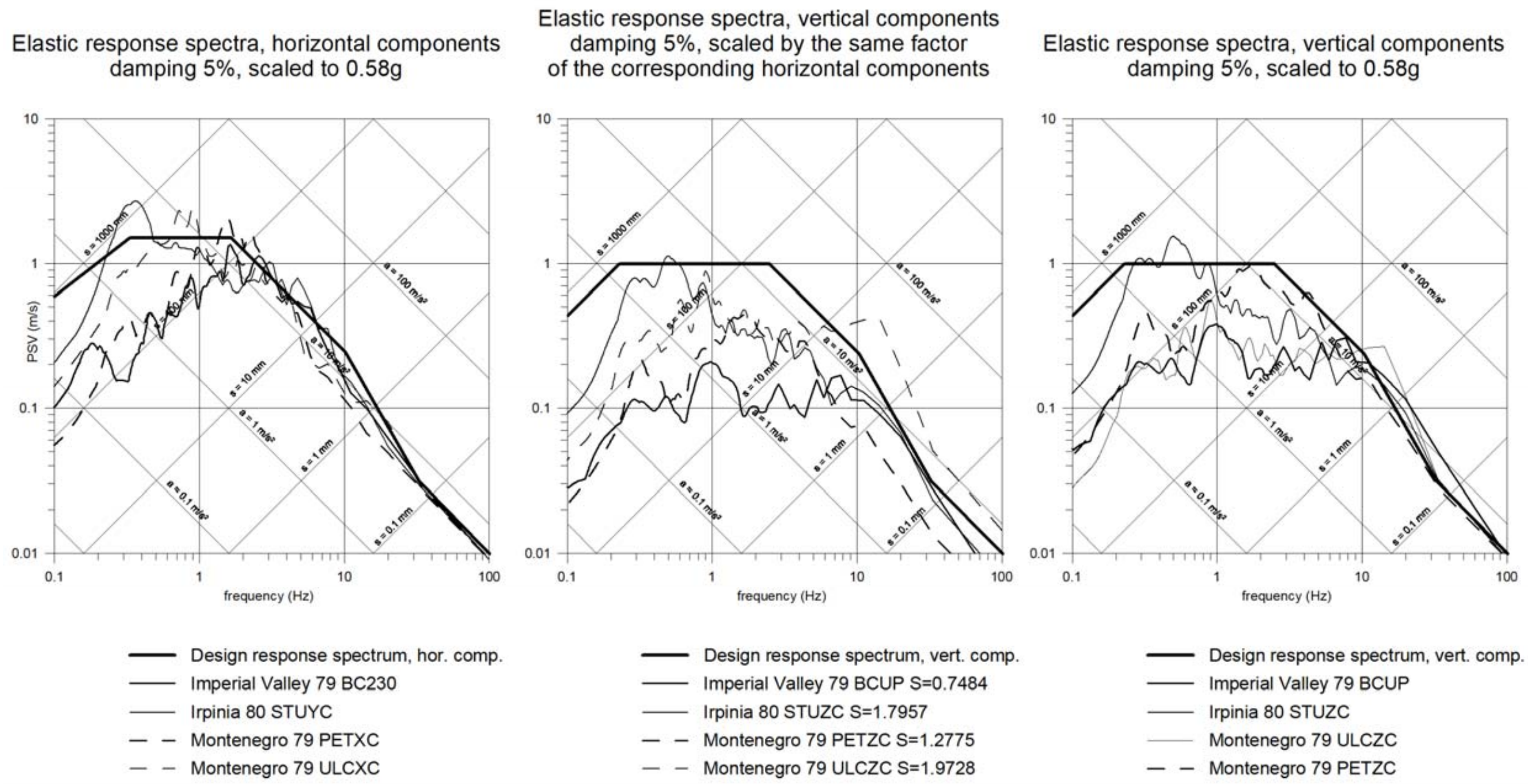

Figure 5.30. Elastic response spectra of the accelerograms used in the analyses

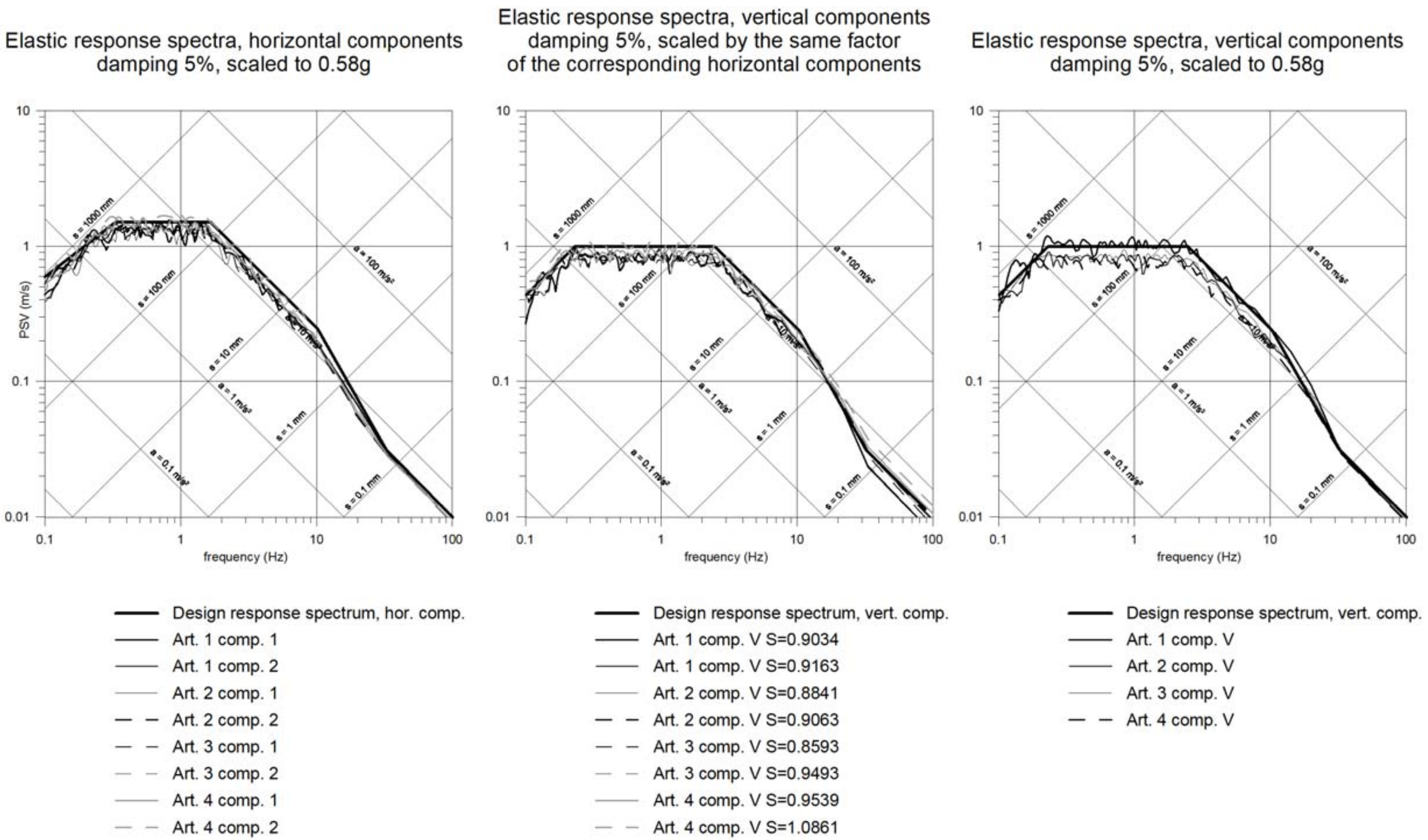

Figure 5.31. Elastic response spectra of the accelerograms used in the analyses

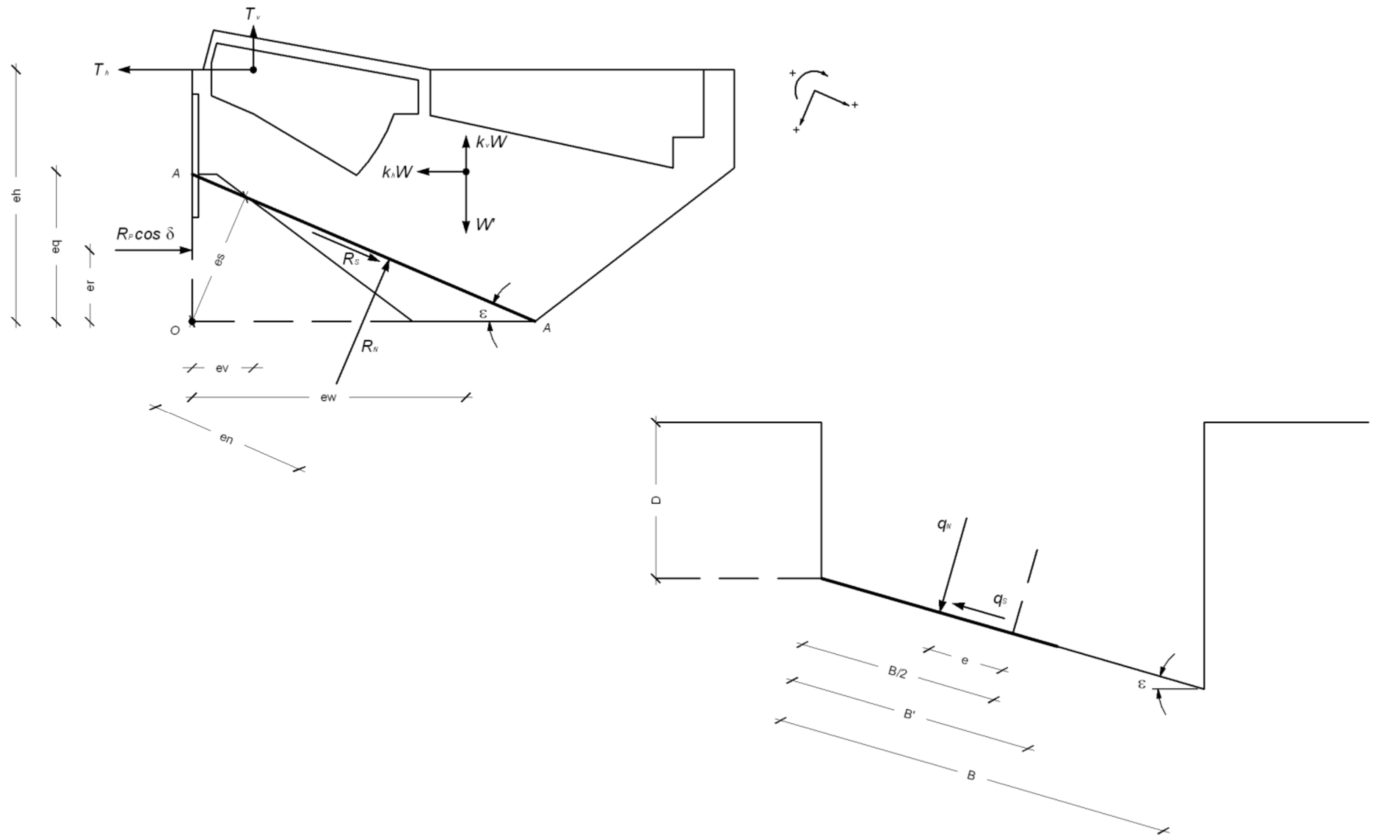

Figure 6.1. Assumptions for evaluating safety against rotation and bearing capacity failure

Appendices

Appendix A – Sliding resistance along the block sides

Mechanism 1
characteristic values of T_L (H_w = 88.0 m a.s.l. – presence of the drainage tunnel)

Diaphragm wall	Head m	Toe m	Length m	τ_{Head} kPa	τ_{TOE} kPa	T_{Lk} kN/m	Width m	T_{Lk}/wall kN
110	0.0	14.3	14.3	0	39.1	279.8	3.5	979.4
109	0.0	16.3	16.3	0	44.6	363.6	2.5	908.9
108	0.0	17.9	17.9	0	49.0	438.5	2.5	1096.1
107	0.0	19.6	19.6	0	53.6	525.7	2.5	1314.2
106	0.0	21.3	21.3	0	58.3	620.8	2.5	1552.1
105	0.0	23.0	23.0	0	62.9	723.9	2.5	1809.7
104	0.0	24.6	24.6	0	67.3	828.1	2.5	2070.3
103	0.0	26.3	26.3	0	71.6	946.5	2.5	2366.2
102	0.0	28.0	28.0	0	73.9	1070.1	2.5	2675.3
101	0.0	29.6	29.6	0	76.1	1190.1	2.5	2975.2
100	0.0	31.3	31.3	0	78.4	1321.4	2.5	3303.5
99	0.0	33.0	33.0	0	80.7	1456.7	2.5	3641.7
98	0.0	34.6	34.6	0	82.9	1587.6	2.5	3969.0
97	0.0	36.3	36.3	0	85.3	1730.6	2.5	4326.4
96	0.0	37.3	37.3	0	86.6	1816.5	2.5	4541.3
95	0.0	37.3	37.3	0	86.6	1816.5	2.5	4541.3
94	0.0	37.3	37.3	0	86.6	1816.5	2.5	4541.3
93	0.0	37.3	37.3	0	86.6	1816.5	2.5	4541.3
92	0.0	37.3	37.3	0	86.6	1816.5	2.5	4541.3
91	0.0	37.3	37.3	0	86.6	1816.5	2.5	4541.3
90	0.0	37.3	37.3	0	86.6	1816.5	2.5	4541.3
89	0.0	37.3	37.3	0	86.6	1816.5	2.5	4541.3
88	0.0	36.2	36.2	0	85.1	1722.0	2.5	4305.1
87	0.0	34.2	34.2	0	82.4	1554.6	2.5	3886.4
86	0.0	32.3	32.3	0	79.8	1400.5	2.5	3501.3
85	0.0	30.4	30.4	0	77.2	1251.4	2.5	3128.5
84	0.0	28.5	28.5	0	74.6	1107.2	2.5	2768.1
83	0.0	26.5	26.5	0	71.8	960.8	2.5	2402.0
82	0.0	24.6	24.6	0	67.3	828.1	2.5	2070.3
81	0.0	22.7	22.7	0	62.1	705.1	2.5	1762.8
80	0.0	20.8	20.8	0	56.9	592.0	2.5	1480.1
79	0.0	18.9	18.9	0	51.7	488.8	2.5	1222.0
78	0.0	16.9	16.9	0	46.3	390.8	2.5	977.1
77	0.0	15.0	15.0	0	41.1	307.9	2.5	769.7
76	0.0	12.7	12.7	0	34.8	220.7	3.5	772.5
total								98364

φ'_k (°)	40.0	K_{ak}	0.217			
φ'_{sk} (°)	32.2	γ (kN/m^3)	20	**T_{Lk} = 2 x total =**	**196.7**	**MN**

Mechanism 1

design values of T_L (H_w = 88.0 m a.s.l. – presence of the drainage tunnel)

Diaphragm wall	Head m	Toe m	Length m	τ_{Head} kPa	τ_{TOE} kPa	T_{Ld} kN/m	Width m	T_{Ld}/wall kN
110	0	14.3	14.3	0	31.3	223.9	3.5	783.5
109	0	16.3	16.3	0	35.7	290.9	2.5	727.2
108	0	17.9	17.9	0	39.2	350.8	2.5	876.9
107	0	19.6	19.6	0	42.9	420.6	2.5	1051.4
106	0	21.3	21.3	0	46.6	496.7	2.5	1241.7
105	0	23.0	23.0	0	50.4	579.1	2.5	1447.8
104	0	24.6	24.6	0	53.9	662.5	2.5	1656.2
103	0	26.3	26.3	0	57.3	757.2	2.5	1892.9
102	0	28.0	28.0	0	59.1	856.1	2.5	2140.2
101	0	29.6	29.6	0	60.9	952.1	2.5	2380.2
100	0	31.3	31.3	0	62.7	1057.1	2.5	2642.8
99	0	33.0	33.0	0	64.6	1165.3	2.5	2913.4
98	0	34.6	34.6	0	66.3	1270.1	2.5	3175.2
97	0	36.3	36.3	0	68.2	1384.5	2.5	3461.1
96	0	37.3	37.3	0	69.3	1453.2	2.5	3633.0
95	0	37.3	37.3	0	69.3	1453.2	2.5	3633.0
94	0	37.3	37.3	0	69.3	1453.2	2.5	3633.0
93	0	37.3	37.3	0	69.3	1453.2	2.5	3633.0
92	0	37.3	37.3	0	69.3	1453.2	2.5	3633.0
91	0	37.3	37.3	0	69.3	1453.2	2.5	3633.0
90	0	37.3	37.3	0	69.3	1453.2	2.5	3633.0
89	0	37.3	37.3	0	69.3	1453.2	2.5	3633.0
88	0	36.2	36.2	0	68.1	1377.6	2.5	3444.1
87	0	34.2	34.2	0	65.9	1243.6	2.5	3109.1
86	0	32.3	32.3	0	63.8	1120.4	2.5	2801.0
85	0	30.4	30.4	0	61.7	1001.1	2.5	2502.8
84	0	28.5	28.5	0	59.7	885.8	2.5	2214.4
83	0	26.5	26.5	0	57.5	768.6	2.5	1921.6
82	0	24.6	24.6	0	53.9	662.5	2.5	1656.2
81	0	22.7	22.7	0	49.7	564.1	2.5	1410.3
80	0	20.8	20.8	0	45.5	473.6	2.5	1184.1
79	0	18.9	18.9	0	41.4	391.1	2.5	977.6
78	0	16.9	16.9	0	37.0	312.7	2.5	781.7
77	0	15.0	15.0	0	32.8	246.3	2.5	615.8
76	0	12.7	12.7	0	27.8	176.6	3.5	618.0
total								78691.3

φ'_k (°)	40.0	K_{ak}	0.217
φ'_{sd} (°)	26.7	γ (kN/m^3)	20

T_{Ld} = 2 x total= 157.4 MN

Mechanism 2

characteristic values of T_L (H_w = 88.0 m a.s.l. – presence of the drainage tunnel)

Diaphragm wall	Head m	Toe m	Length m	τ_{Head} kPa	τ_{TOE} kPa	T_{Lk} kN/m	Width m	T_{Lk}/wall kN
110	0.0	20.8	20.8	0	56.9	592.0	3.5	2072.1
109	0.0	22.3	22.3	0	61.0	680.5	2.5	1701.3
108	0.0	23.5	23.5	0	64.3	755.7	2.5	1889.3
107	0.0	24.7	24.7	0	67.6	834.9	2.5	2087.2
106	0.0	25.8	25.8	0	70.6	910.9	2.5	2277.2
105	0.0	27.0	27.0	0	72.5	996.9	2.5	2492.2
104	0.0	28.2	28.2	0	74.2	1084.9	2.5	2712.3
103	0.0	29.4	29.4	0	75.8	1174.9	2.5	2937.2
102	0.0	30.6	30.6	0	77.5	1266.9	2.5	3167.1
101	0.0	31.8	31.8	0	79.1	1360.8	2.5	3402.0
100	0.0	33.0	33.0	0	80.7	1456.7	2.5	3641.7
99	0.0	34.2	34.2	0	82.4	1554.6	2.5	3886.4
98	0.0	35.4	35.4	0	84.0	1654.4	2.5	4136.0
97	0.0	36.6	36.6	0	85.7	1756.2	2.5	4390.5
96	0.0	37.3	37.3	0	86.6	1816.5	2.5	4541.3
95	0.0	37.3	37.3	0	86.6	1816.5	2.5	4541.3
94	0.0	37.3	37.3	0	86.6	1816.5	2.5	4541.3
93	0.0	37.3	37.3	0	86.6	1816.5	2.5	4541.3
92	0.0	37.3	37.3	0	86.6	1816.5	2.5	4541.3
91	0.0	37.3	37.3	0	86.6	1816.5	2.5	4541.3
90	0.0	37.3	37.3	0	86.6	1816.5	2.5	4541.3
89	0.0	37.3	37.3	0	86.6	1816.5	2.5	4541.3
88	0.0	36.2	36.2	0	85.1	1722.0	2.5	4305.1
87	0.0	34.2	34.2	0	82.4	1554.6	2.5	3886.4
86	0.0	32.3	32.3	0	79.8	1400.5	2.5	3501.3
85	0.0	30.4	30.4	0	77.2	1251.4	2.5	3128.5
84	0.0	28.5	28.5	0	74.6	1107.2	2.5	2768.1
83	0.0	26.5	26.5	0	71.8	960.8	2.5	2402.0
82	0.0	24.6	24.6	0	67.3	828.1	2.5	2070.3
81	0.0	22.7	22.7	0	62.1	705.1	2.5	1762.8
80	0.0	20.8	20.8	0	56.9	592.0	2.5	1480.1
79	0.0	18.9	18.9	0	51.7	488.8	2.5	1222.0
78	0.0	16.9	16.9	0	46.3	390.8	2.5	977.1
77	0.0	15.0	15.0	0	41.1	307.9	2.5	769.7
76	0.0	12.7	12.7	0	34.8	220.7	3.5	772.5
total								106168

φ'_k (°)	40.0	K_{ak}	0.217		
φ'_{sk} (°)	32.2	γ (kN/m^3)	20	**T_{Lk} = 2 x total=**	**212.3 MN**

Mechanism 2

design values of T_L (H_w = 88.0 m a.s.l. – presence of the drainage tunnel)

Diaphragm wall	Head m	Toe m	Length m	τ_{Head} kPa	τ_{TOE} kPa	T_{Ld} kN/m	Width m	T_{Ld}/wall kN
110	0	20.8	20.8	0	45.5	473.6	3.5	1657.7
109	0	22.3	22.3	0	48.8	544.4	2.5	1361.0
108	0	23.5	23.5	0	51.5	604.6	2.5	1511.4
107	0	24.7	24.7	0	54.1	667.9	2.5	1669.7
106	0	25.8	25.8	0	56.5	728.7	2.5	1821.8
105	0	27.0	27.0	0	58.0	797.5	2.5	1993.8
104	0	28.2	28.2	0	59.3	867.9	2.5	2169.8
103	0	29.4	29.4	0	60.6	939.9	2.5	2349.8
102	0	30.6	30.6	0	62.0	1013.5	2.5	2533.7
101	0	31.8	31.8	0	63.3	1088.6	2.5	2721.6
100	0	33.0	33.0	0	64.6	1165.3	2.5	2913.4
99	0	34.2	34.2	0	65.9	1243.6	2.5	3109.1
98	0	35.4	35.4	0	67.2	1323.5	2.5	3308.8
97	0	36.6	36.6	0	68.5	1405.0	2.5	3512.4
96	0	37.3	37.3	0	69.3	1453.2	2.5	3633.0
95	0	37.3	37.3	0	69.3	1453.2	2.5	3633.0
94	0	37.3	37.3	0	69.3	1453.2	2.5	3633.0
93	0	37.3	37.3	0	69.3	1453.2	2.5	3633.0
92	0	37.3	37.3	0	69.3	1453.2	2.5	3633.0
91	0	37.3	37.3	0	69.3	1453.2	2.5	3633.0
90	0	37.3	37.3	0	69.3	1453.2	2.5	3633.0
89	0	37.3	37.3	0	69.3	1453.2	2.5	3633.0
88	0	36.2	36.2	0	68.1	1377.6	2.5	3444.1
87	0	34.2	34.2	0	65.9	1243.6	2.5	3109.1
86	0	32.3	32.3	0	63.8	1120.4	2.5	2801.0
85	0	30.4	30.4	0	61.7	1001.1	2.5	2502.8
84	0	28.5	28.5	0	59.7	885.8	2.5	2214.4
83	0	26.5	26.5	0	57.5	768.6	2.5	1921.6
82	0	24.6	24.6	0	53.9	662.5	2.5	1656.2
81	0	22.7	22.7	0	49.7	564.1	2.5	1410.3
80	0	20.8	20.8	0	45.5	473.6	2.5	1184.1
79	0	18.9	18.9	0	41.4	391.1	2.5	977.6
78	0	16.9	16.9	0	37.0	312.7	2.5	781.7
77	0	15.0	15.0	0	32.8	246.3	2.5	615.8
76	0	12.7	12.7	0	27.8	176.6	3.5	618.0
total								84934.7

φ'_k (°)	40.0	K_{ak}	0.217
φ'_{sd} (°)	26.7	γ (kN/m^3)	20

T_{Ld} = 2 x total= 169.9 MN

Mechanism 3

characteristic values of T_L (H_w = 88.0 m a.s.l. – presence of the drainage tunnel)

Diaphragm wall	Head m	Toe m	Length m	τ_{Head} kPa	τ_{TOE} kPa	T_L kN/m	Width m	T_L/wall kN
110	0.0	37.3	37.3	0	86.6	1816.5	3.5	6357.8
109	0.0	37.3	37.3	0	86.6	1816.5	2.5	4541.3
108	0.0	37.3	37.3	0	86.6	1816.5	2.5	4541.3
107	0.0	37.3	37.3	0	86.6	1816.5	2.5	4541.3
106	0.0	37.3	37.3	0	86.6	1816.5	2.5	4541.3
105	0.0	37.3	37.3	0	86.6	1816.5	2.5	4541.3
104	0.0	37.3	37.3	0	86.6	1816.5	2.5	4541.3
103	0.0	37.3	37.3	0	86.6	1816.5	2.5	4541.3
102	0.0	37.3	37.3	0	86.6	1816.5	2.5	4541.3
101	0.0	37.3	37.3	0	86.6	1816.5	2.5	4541.3
100	0.0	37.3	37.3	0	86.6	1816.5	2.5	4541.3
99	0.0	37.3	37.3	0	86.6	1816.5	2.5	4541.3
98	0.0	37.3	37.3	0	86.6	1816.5	2.5	4541.3
97	0.0	37.3	37.3	0	86.6	1816.5	2.5	4541.3
96	0.0	37.3	37.3	0	86.6	1816.5	2.5	4541.3
95	0.0	37.3	37.3	0	86.6	1816.5	2.5	4541.3
94	0.0	37.3	37.3	0	86.6	1816.5	2.5	4541.3
93	0.0	37.3	37.3	0	86.6	1816.5	2.5	4541.3
92	0.0	37.3	37.3	0	86.6	1816.5	2.5	4541.3
91	0.0	37.3	37.3	0	86.6	1816.5	2.5	4541.3
90	0.0	37.3	37.3	0	86.6	1816.5	2.5	4541.3
89	0.0	37.3	37.3	0	86.6	1816.5	2.5	4541.3
88	0.0	36.2	36.2	0	85.1	1722.0	2.5	4305.1
87	0.0	34.2	34.2	0	82.4	1554.6	2.5	3886.4
86	0.0	32.3	32.3	0	79.8	1400.5	2.5	3501.3
85	0.0	30.4	30.4	0	77.2	1251.4	2.5	3128.5
84	0.0	28.5	28.5	0	74.6	1107.2	2.5	2768.1
83	0.0	26.5	26.5	0	71.8	960.8	2.5	2402.0
82	0.0	24.6	24.6	0	67.3	828.1	2.5	2070.3
81	0.0	22.7	22.7	0	62.1	705.1	2.5	1762.8
80	0.0	20.8	20.8	0	56.9	592.0	2.5	1480.1
79	0.0	18.9	18.9	0	51.7	488.8	2.5	1222.0
78	0.0	16.9	16.9	0	46.3	390.8	2.5	977.1
77	0.0	15.0	15.0	0	41.1	307.9	2.5	769.7
76	0.0	12.7	12.7	0	34.8	220.7	3.5	772.5
total								130770

φ'_k (°)	40.0	K_{ak}	0.217			
φ'_{sk} (°)	32.2	γ (kN/m^3)	20	**T_{Lk} =**	**2 x total=**	**261.5 MN**

Mechanism 3

design values of T_L (H_w = 88.0 m a.s.l. – presence of the drainage tunnel)

Diaphragm wall	Head m	Toe m	Length m	τ_{Head} kPa	τ_{TOE} kPa	T_L kN/m	Width m	T_L/wall kN
110	0	37.3	37.3	0	69.3	1453.2	3.5	5086.2
109	0	37.3	37.3	0	69.3	1453.2	2.5	3633.0
108	0	37.3	37.3	0	69.3	1453.2	2.5	3633.0
107	0	37.3	37.3	0	69.3	1453.2	2.5	3633.0
106	0	37.3	37.3	0	69.3	1453.2	2.5	3633.0
105	0	37.3	37.3	0	69.3	1453.2	2.5	3633.0
104	0	37.3	37.3	0	69.3	1453.2	2.5	3633.0
103	0	37.3	37.3	0	69.3	1453.2	2.5	3633.0
102	0	37.3	37.3	0	69.3	1453.2	2.5	3633.0
101	0	37.3	37.3	0	69.3	1453.2	2.5	3633.0
100	0	37.3	37.3	0	69.3	1453.2	2.5	3633.0
99	0	37.3	37.3	0	69.3	1453.2	2.5	3633.0
98	0	37.3	37.3	0	69.3	1453.2	2.5	3633.0
97	0	37.3	37.3	0	69.3	1453.2	2.5	3633.0
96	0	37.3	37.3	0	69.3	1453.2	2.5	3633.0
95	0	37.3	37.3	0	69.3	1453.2	2.5	3633.0
94	0	37.3	37.3	0	69.3	1453.2	2.5	3633.0
93	0	37.3	37.3	0	69.3	1453.2	2.5	3633.0
92	0	37.3	37.3	0	69.3	1453.2	2.5	3633.0
91	0	37.3	37.3	0	69.3	1453.2	2.5	3633.0
90	0	37.3	37.3	0	69.3	1453.2	2.5	3633.0
89	0	37.3	37.3	0	69.3	1453.2	2.5	3633.0
88	0	36.2	36.2	0	68.1	1377.6	2.5	3444.1
87	0	34.2	34.2	0	65.9	1243.6	2.5	3109.1
86	0	32.3	32.3	0	63.8	1120.4	2.5	2801.0
85	0	30.4	30.4	0	61.7	1001.1	2.5	2502.8
84	0	28.5	28.5	0	59.7	885.8	2.5	2214.4
83	0	26.5	26.5	0	57.5	768.6	2.5	1921.6
82	0	24.6	24.6	0	53.9	662.5	2.5	1656.2
81	0	22.7	22.7	0	49.7	564.1	2.5	1410.3
80	0	20.8	20.8	0	45.5	473.6	2.5	1184.1
79	0	18.9	18.9	0	41.4	391.1	2.5	977.6
78	0	16.9	16.9	0	37.0	312.7	2.5	781.7
77	0	15.0	15.0	0	32.8	246.3	2.5	615.8
76	0	12.7	12.7	0	27.8	176.6	3.5	618.0
total								104616.1

φ'_k (°)	40.0	K_{ak}	0.217				
φ'_{sd} (°)	26.7	γ (kN/m^3)	20	**T_{Ld} =**	**2 x total=**	**209.2**	**MN**

Mechanism 1

characteristic values of T_L (H_w = 94.5 m a.s.l. – absence of the drainage tunnel)

Diaphragm wall	Head m	Toe m	Length m	τ_{Head} kPa	τ_{TOE} kPa	T_{Lk} kN/m	Width m	T_{Lk}/wall kN
110	0.0	14.3	14.3	0	39.1	279.8	3.5	979.4
109	0.0	16.3	16.3	0	44.6	363.6	2.5	908.9
108	0.0	17.9	17.9	0	49.0	438.5	2.5	1096.1
107	0.0	19.6	19.6	0	53.5	525.7	2.5	1314.2
106	0.0	21.3	21.3	0	55.8	618.6	2.5	1546.6
105	0.0	23.0	23.0	0	58.2	715.5	2.5	1788.8
104	0.0	24.6	24.6	0	60.3	810.3	2.5	2025.8
103	0.0	26.3	26.3	0	62.7	914.9	2.5	2287.2
102	0.0	28.0	28.0	0	65.0	1023.4	2.5	2558.5
101	0.0	29.6	29.6	0	67.2	1129.2	2.5	2822.9
100	0.0	31.3	31.3	0	69.5	1245.4	2.5	3113.4
99	0.0	33.0	33.0	0	71.8	1365.5	2.5	3413.8
98	0.0	34.6	34.6	0	74.0	1482.2	2.5	3705.5
97	0.0	36.3	36.3	0	76.4	1610.0	2.5	4025.1
96	0.0	37.3	37.3	0	77.7	1687.1	2.5	4217.7
95	0.0	37.3	37.3	0	77.7	1687.1	2.5	4217.7
94	0.0	37.3	37.3	0	77.7	1687.1	2.5	4217.7
93	0.0	37.3	37.3	0	77.7	1687.1	2.5	4217.7
92	0.0	37.3	37.3	0	77.7	1687.1	2.5	4217.7
91	0.0	37.3	37.3	0	77.7	1687.1	2.5	4217.7
90	0.0	37.3	37.3	0	77.7	1687.1	2.5	4217.7
89	0.0	37.3	37.3	0	77.7	1687.1	2.5	4217.7
88	0.0	36.2	36.2	0	76.2	1602.4	2.5	4006.0
87	0.0	34.2	34.2	0	73.5	1452.7	2.5	3631.8
86	0.0	32.3	32.3	0	70.9	1315.6	2.5	3288.9
85	0.0	30.4	30.4	0	68.3	1183.3	2.5	2958.4
84	0.0	28.5	28.5	0	65.7	1056.1	2.5	2640.2
83	0.0	26.5	26.5	0	62.9	927.4	2.5	2318.6
82	0.0	24.6	24.6	0	60.3	810.3	2.5	2025.8
81	0.0	22.7	22.7	0	57.7	698.1	2.5	1745.3
80	0.0	20.8	20.8	0	55.1	590.9	2.5	1477.2
79	0.0	18.9	18.9	0	51.7	488.8	2.5	1222.0
78	0.0	16.9	16.9	0	46.3	390.8	2.5	977.1
77	0.0	15.0	15.0	0	41.1	307.9	2.5	769.7
76	0.0	12.7	12.7	0	34.8	220.7	3.5	772.5
total								93162

φ'_k (°)	40.0	K_{ak}	0.217		
φ'_{sk} (°)	32.2	γ (kN/m^3)	20	**T_{Lk} = 2 x total=**	**186.3 MN**

Mechanism 1

design values of T_L (H_w = 94.5 m a.s.l. – absence of the drainage tunnel)

Diaphragm wall	Head m	Toe m	Length m	τ_{Head} kPa	τ_{TOE} kPa	T_{Ld} kN/m	Width m	T_{Ld}/wall kN
110	0	14.3	14.3	0	31.3	223.9	3.5	783.5
109	0	16.3	16.3	0	35.7	290.9	2.5	727.2
108	0	17.9	17.9	0	39.2	350.8	2.5	876.9
107	0	19.6	19.6	0	42.8	420.5	2.5	1051.4
106	0	21.3	21.3	0	44.7	494.9	2.5	1237.2
105	0	23.0	23.0	0	46.5	572.4	2.5	1431.0
104	0	24.6	24.6	0	48.3	648.3	2.5	1620.6
103	0	26.3	26.3	0	50.1	731.9	2.5	1829.8
102	0	28.0	28.0	0	52.0	818.7	2.5	2046.8
101	0	29.6	29.6	0	53.8	903.3	2.5	2258.3
100	0	31.3	31.3	0	55.6	996.3	2.5	2490.7
99	0	33.0	33.0	0	57.5	1092.4	2.5	2731.0
98	0	34.6	34.6	0	59.2	1185.8	2.5	2964.4
97	0	36.3	36.3	0	61.1	1288.0	2.5	3220.1
96	0	37.3	37.3	0	62.2	1349.7	2.5	3374.2
95	0	37.3	37.3	0	62.2	1349.7	2.5	3374.2
94	0	37.3	37.3	0	62.2	1349.7	2.5	3374.2
93	0	37.3	37.3	0	62.2	1349.7	2.5	3374.2
92	0	37.3	37.3	0	62.2	1349.7	2.5	3374.2
91	0	37.3	37.3	0	62.2	1349.7	2.5	3374.2
90	0	37.3	37.3	0	62.2	1349.7	2.5	3374.2
89	0	37.3	37.3	0	62.2	1349.7	2.5	3374.2
88	0	36.2	36.2	0	61.0	1281.9	2.5	3204.8
87	0	34.2	34.2	0	58.8	1162.2	2.5	2905.4
86	0	32.3	32.3	0	56.7	1052.4	2.5	2631.1
85	0	30.4	30.4	0	54.6	946.7	2.5	2366.7
84	0	28.5	28.5	0	52.5	844.9	2.5	2112.2
83	0	26.5	26.5	0	50.4	742.0	2.5	1854.9
82	0	24.6	24.6	0	48.3	648.3	2.5	1620.6
81	0	22.7	22.7	0	46.2	558.5	2.5	1396.3
80	0	20.8	20.8	0	44.1	472.7	2.5	1181.8
79	0	18.9	18.9	0	41.4	391.1	2.5	977.6
78	0	16.9	16.9	0	37.0	312.7	2.5	781.7
77	0	15.0	15.0	0	32.8	246.3	2.5	615.8
76	0	12.7	12.7	0	27.8	176.6	3.5	618.0
total								74529.2

φ'_k (°)	40.0	K_{ad}	0.217
φ'_{sd} (°)	26.7	γ (kN/m^3)	20

T_{Ld} = 2 x total= 149.1 MN

Mechanism 2

characteristic values of T_L (H_w = 94.5 m a.s.l. – absence of the drainage tunnel)

Diaphragm wall	Head m	Toe m	Length m	τ_{Head} kPa	τ_{TOE} kPa	T_{Lk} kN/m	Width m	T_{Lk}/wall kN
110	0.0	20.8	20.8	0	55.1	590.9	3.5	2068.1
109	0.0	22.3	22.3	0	57.2	675.1	2.5	1687.8
108	0.0	23.5	23.5	0	58.8	744.8	2.5	1861.9
107	0.0	24.7	24.7	0	60.5	816.4	2.5	2040.9
106	0.0	25.8	25.8	0	62.0	883.7	2.5	2209.3
105	0.0	27.0	27.0	0	63.6	959.1	2.5	2397.7
104	0.0	28.2	28.2	0	65.3	1036.4	2.5	2591.1
103	0.0	29.4	29.4	0	66.9	1115.7	2.5	2789.4
102	0.0	30.6	30.6	0	68.6	1197.0	2.5	2992.6
101	0.0	31.8	31.8	0	70.2	1280.3	2.5	3200.7
100	0.0	33.0	33.0	0	71.8	1365.5	2.5	3413.8
99	0.0	34.2	34.2	0	73.5	1452.7	2.5	3631.8
98	0.0	35.4	35.4	0	75.1	1541.9	2.5	3854.7
97	0.0	36.6	36.6	0	76.8	1633.0	2.5	4082.5
96	0.0	37.3	37.3	0	77.7	1687.1	2.5	4217.7
95	0.0	37.3	37.3	0	77.7	1687.1	2.5	4217.7
94	0.0	37.3	37.3	0	77.7	1687.1	2.5	4217.7
93	0.0	37.3	37.3	0	77.7	1687.1	2.5	4217.7
92	0.0	37.3	37.3	0	77.7	1687.1	2.5	4217.7
91	0.0	37.3	37.3	0	77.7	1687.1	2.5	4217.7
90	0.0	37.3	37.3	0	77.7	1687.1	2.5	4217.7
89	0.0	37.3	37.3	0	77.7	1687.1	2.5	4217.7
88	0.0	36.2	36.2	0	76.2	1602.4	2.5	4006.0
87	0.0	34.2	34.2	0	73.5	1452.7	2.5	3631.8
86	0.0	32.3	32.3	0	70.9	1315.6	2.5	3288.9
85	0.0	30.4	30.4	0	68.3	1183.3	2.5	2958.4
84	0.0	28.5	28.5	0	65.7	1056.1	2.5	2640.2
83	0.0	26.5	26.5	0	62.9	927.4	2.5	2318.6
82	0.0	24.6	24.6	0	60.3	810.3	2.5	2025.8
81	0.0	22.7	22.7	0	57.7	698.1	2.5	1745.3
80	0.0	20.8	20.8	0	55.1	590.9	2.5	1477.2
79	0.0	18.9	18.9	0	51.7	488.8	2.5	1222.0
78	0.0	16.9	16.9	0	46.3	390.8	2.5	977.1
77	0.0	15.0	15.0	0	41.1	307.9	2.5	769.7
76	0.0	12.7	12.7	0	34.8	220.7	3.5	772.5
total								100398

φ'_k (°)	40.0	K_{ak}	0.217		
φ'_{sk} (°)	32.2	γ (kN/m^3)	20	**T_{Lk} = 2 x total=**	**200.8 MN**

Mechanism 2

design values of T_L (H_w = 94.5 m a.s.l. – absence of the drainage tunnel)

Diaphragm wall	Head m	Toe m	Length m	τ_{Head} kPa	τ_{TOE} kPa	T_{Ld} kN/m	Width m	T_{Ld}/wall kN
110	0	20.8	20.8	0	44.1	472.7	3.5	1654.5
109	0	22.3	22.3	0	45.8	540.1	2.5	1350.3
108	0	23.5	23.5	0	47.1	595.8	2.5	1489.5
107	0	24.7	24.7	0	48.4	653.1	2.5	1632.7
106	0	25.8	25.8	0	49.6	707.0	2.5	1767.4
105	0	27.0	27.0	0	50.9	767.3	2.5	1918.2
104	0	28.2	28.2	0	52.2	829.1	2.5	2072.9
103	0	29.4	29.4	0	53.5	892.6	2.5	2231.5
102	0	30.6	30.6	0	54.8	957.6	2.5	2394.1
101	0	31.8	31.8	0	56.2	1024.2	2.5	2560.6
100	0	33.0	33.0	0	57.5	1092.4	2.5	2731.0
99	0	34.2	34.2	0	58.8	1162.2	2.5	2905.4
98	0	35.4	35.4	0	60.1	1233.5	2.5	3083.8
97	0	36.6	36.6	0	61.4	1306.4	2.5	3266.0
96	0	37.3	37.3	0	62.2	1349.7	2.5	3374.2
95	0	37.3	37.3	0	62.2	1349.7	2.5	3374.2
94	0	37.3	37.3	0	62.2	1349.7	2.5	3374.2
93	0	37.3	37.3	0	62.2	1349.7	2.5	3374.2
92	0	37.3	37.3	0	62.2	1349.7	2.5	3374.2
91	0	37.3	37.3	0	62.2	1349.7	2.5	3374.2
90	0	37.3	37.3	0	62.2	1349.7	2.5	3374.2
89	0	37.3	37.3	0	62.2	1349.7	2.5	3374.2
88	0	36.2	36.2	0	61.0	1281.9	2.5	3204.8
87	0	34.2	34.2	0	58.8	1162.2	2.5	2905.4
86	0	32.3	32.3	0	56.7	1052.4	2.5	2631.1
85	0	30.4	30.4	0	54.6	946.7	2.5	2366.7
84	0	28.5	28.5	0	52.5	844.9	2.5	2112.2
83	0	26.5	26.5	0	50.4	742.0	2.5	1854.9
82	0	24.6	24.6	0	48.3	648.3	2.5	1620.6
81	0	22.7	22.7	0	46.2	558.5	2.5	1396.3
80	0	20.8	20.8	0	44.1	472.7	2.5	1181.8
79	0	18.9	18.9	0	41.4	391.1	2.5	977.6
78	0	16.9	16.9	0	37.0	312.7	2.5	781.7
77	0	15.0	15.0	0	32.8	246.3	2.5	615.8
76	0	12.7	12.7	0	27.8	176.6	3.5	618.0
total								80318.1

φ'_k (°)	40.0	K_{ad}	0.217		
φ'_{sd} (°)	26.7	γ (kN/m^3)	20	**T_{Ld} = 2 x total=**	**160.6 MN**

Mechanism 3

characteristic values of T_L (H_w = 94.5 m a.s.l. – absence of the drainage tunnel)

Diaphragm wall	Head m	Toe m	Length m	τ_{Head} kPa	τ_{TOE} kPa	T_L kN/m	Width m	T_L/wall kN
110	0.0	37.3	37.3	0	77.7	1687.1	3.5	5904.8
109	0.0	37.3	37.3	0	77.7	1687.1	2.5	4217.7
108	0.0	37.3	37.3	0	77.7	1687.1	2.5	4217.7
107	0.0	37.3	37.3	0	77.7	1687.1	2.5	4217.7
106	0.0	37.3	37.3	0	77.7	1687.1	2.5	4217.7
105	0.0	37.3	37.3	0	77.7	1687.1	2.5	4217.7
104	0.0	37.3	37.3	0	77.7	1687.1	2.5	4217.7
103	0.0	37.3	37.3	0	77.7	1687.1	2.5	4217.7
102	0.0	37.3	37.3	0	77.7	1687.1	2.5	4217.7
101	0.0	37.3	37.3	0	77.7	1687.1	2.5	4217.7
100	0.0	37.3	37.3	0	77.7	1687.1	2.5	4217.7
99	0.0	37.3	37.3	0	77.7	1687.1	2.5	4217.7
98	0.0	37.3	37.3	0	77.7	1687.1	2.5	4217.7
97	0.0	37.3	37.3	0	77.7	1687.1	2.5	4217.7
96	0.0	37.3	37.3	0	77.7	1687.1	2.5	4217.7
95	0.0	37.3	37.3	0	77.7	1687.1	2.5	4217.7
94	0.0	37.3	37.3	0	77.7	1687.1	2.5	4217.7
93	0.0	37.3	37.3	0	77.7	1687.1	2.5	4217.7
92	0.0	37.3	37.3	0	77.7	1687.1	2.5	4217.7
91	0.0	37.3	37.3	0	77.7	1687.1	2.5	4217.7
90	0.0	37.3	37.3	0	77.7	1687.1	2.5	4217.7
89	0.0	37.3	37.3	0	77.7	1687.1	2.5	4217.7
88	0.0	36.2	36.2	0	76.2	1602.4	2.5	4006.0
87	0.0	34.2	34.2	0	73.5	1452.7	2.5	3631.8
86	0.0	32.3	32.3	0	70.9	1315.6	2.5	3288.9
85	0.0	30.4	30.4	0	68.3	1183.3	2.5	2958.4
84	0.0	28.5	28.5	0	65.7	1056.1	2.5	2640.2
83	0.0	26.5	26.5	0	62.9	927.4	2.5	2318.6
82	0.0	24.6	24.6	0	60.3	810.3	2.5	2025.8
81	0.0	22.7	22.7	0	57.7	698.1	2.5	1745.3
80	0.0	20.8	20.8	0	55.1	590.9	2.5	1477.2
79	0.0	18.9	18.9	0	51.7	488.8	2.5	1222.0
78	0.0	16.9	16.9	0	46.3	390.8	2.5	977.1
77	0.0	15.0	15.0	0	41.1	307.9	2.5	769.7
76	0.0	12.7	12.7	0	34.8	220.7	3.5	772.5
total								122310

φ'_k (°)	40.0	K_{ak}	0.217		
φ'_{sk} (°)	32.2	γ (kN/m^3)	20	**T_{Lk} = 2 x total=**	**244.6 MN**

Mechanism 3

design values of T_L (H_w = 94.5 m a.s.l. – absence of the drainage tunnel)

Diaphragm wall	Head m	Toe m	Length m	τ_{Head} kPa	τ_{TOE} kPa	T_L kN/m	Width m	T_L/wall kN
110	0	37.3	37.3	0	62.2	1349.7	3.5	4723.8
109	0	37.3	37.3	0	62.2	1349.7	2.5	3374.2
108	0	37.3	37.3	0	62.2	1349.7	2.5	3374.2
107	0	37.3	37.3	0	62.2	1349.7	2.5	3374.2
106	0	37.3	37.3	0	62.2	1349.7	2.5	3374.2
105	0	37.3	37.3	0	62.2	1349.7	2.5	3374.2
104	0	37.3	37.3	0	62.2	1349.7	2.5	3374.2
103	0	37.3	37.3	0	62.2	1349.7	2.5	3374.2
102	0	37.3	37.3	0	62.2	1349.7	2.5	3374.2
101	0	37.3	37.3	0	62.2	1349.7	2.5	3374.2
100	0	37.3	37.3	0	62.2	1349.7	2.5	3374.2
99	0	37.3	37.3	0	62.2	1349.7	2.5	3374.2
98	0	37.3	37.3	0	62.2	1349.7	2.5	3374.2
97	0	37.3	37.3	0	62.2	1349.7	2.5	3374.2
96	0	37.3	37.3	0	62.2	1349.7	2.5	3374.2
95	0	37.3	37.3	0	62.2	1349.7	2.5	3374.2
94	0	37.3	37.3	0	62.2	1349.7	2.5	3374.2
93	0	37.3	37.3	0	62.2	1349.7	2.5	3374.2
92	0	37.3	37.3	0	62.2	1349.7	2.5	3374.2
91	0	37.3	37.3	0	62.2	1349.7	2.5	3374.2
90	0	37.3	37.3	0	62.2	1349.7	2.5	3374.2
89	0	37.3	37.3	0	62.2	1349.7	2.5	3374.2
88	0	36.2	36.2	0	61.0	1281.9	2.5	3204.8
87	0	34.2	34.2	0	58.8	1162.2	2.5	2905.4
86	0	32.3	32.3	0	56.7	1052.4	2.5	2631.1
85	0	30.4	30.4	0	54.6	946.7	2.5	2366.7
84	0	28.5	28.5	0	52.5	844.9	2.5	2112.2
83	0	26.5	26.5	0	50.4	742.0	2.5	1854.9
82	0	24.6	24.6	0	48.3	648.3	2.5	1620.6
81	0	22.7	22.7	0	46.2	558.5	2.5	1396.3
80	0	20.8	20.8	0	44.1	472.7	2.5	1181.8
79	0	18.9	18.9	0	41.4	391.1	2.5	977.6
78	0	16.9	16.9	0	37.0	312.7	2.5	781.7
77	0	15.0	15.0	0	32.8	246.3	2.5	615.8
76	0	12.7	12.7	0	27.8	176.6	3.5	618.0
total								97848.3

φ'_k (°)	40.0	K_{ad}	0.217
φ'_{sd} (°)	26.7	γ (kN/m^3)	20

T_{Ld} = 2 x total= 195.7 MN

Appendix B – Passive earth resistance in front of the anchor block

H_w = 88.0 m a.s.l. (presence of the drainage tunnel)

Mechanism 1 (z = 13.1 m)

	SLS2	ULS	SLIS
K_h	0.097	0.216	0.238
K_v	0.048	0.108	0.119
K_{Pk}	9.005	7.655	7.395
diaphragm wall head (m)	0	0	0
diaphragm wall toe (m)	13.1	13.1	13.1
$\sigma'_{hp(k)}$ head (kPa)	0	0	0
$\sigma'_{hp(k)}$ toe (kPa)	2359.3	2005.6	1937.5
R'_{Pk} (kN/m)	15453.5	13136.7	12690.6
pore pressure resultant (kN/m)	0	0	0
R_{Pk} (MN)	1545.3	1313.7	1269.1

	SLS2	ULS	SLIS
K_h	0.097	0.216	0.238
K_v	0.048	0.108	0.119
K_{Pd}	5.481	4.577	4.401
diaphragm wall head (m)	0	0	0
diaphragm wall toe (m)	13.1	13.1	13.1
$\sigma'_{hp(d)}$ head (kPa)	0.0	0.0	0.0
$\sigma'_{hp(d)}$ toe (kPa)	1436.0	1199.2	1153.1
R'_{Pd} (kN/m)	9405.9	7854.6	7552.6
pore pressure resultant (kN/m)	0	0	0
R_{Pd} (MN)	940.6	785.5	755.3

H_w = 88.0 m a.s.l. (presence of the drainage tunnel)

Mechanism 2 (z = 20.0 m)

	SLS2	ULS	SLIS
K_h	0.097	0.216	0.238
K_v	0.048	0.108	0.119
K_{Pk}	9.005	7.655	7.395
diaphragm wall head (m)	0	0	0
diaphragm wall toe (m)	20	20	20
$\sigma'_{hp(k)}$ head (kPa)	0	0	0
$\sigma'_{hp(k)}$ toe (kPa)	3602.0	3062.0	2958.0
R'_{Pk} (kN/m)	36020.0	30620.0	29580.0
pore pressure resultant (kN/m)	0	0	0
R_{Pk} (MN)	3602.0	3062.0	2958.0

	SLS2	ULS	SLIS
K_h	0.097	0.216	0.238
K_v	0.048	0.108	0.119
K_{Pd}	5.481	4.577	4.401
diaphragm wall head (m)	0	0	0
diaphragm wall toe (m)	20	20	20
$\sigma'_{hp(d)}$ head (kPa)	0.0	0.0	0.0
$\sigma'_{hp(d)}$ toe (kPa)	2192.4	1830.8	1760.4
R'_{Pd} (kN/m)	21924.0	18308.0	17604.0
pore pressure resultant (kN/m)	0	0	0
R_{Pd} (MN)	2192.4	1830.8	1760.4

H_w = 88.0 m a.s.l. (presence of the drainage tunnel)

Mechanism 3 (z = 37.3 m)

	SLS2	ULS	SLIS
K_h	0.097	0.216	0.238
K_v	0.048	0.108	0.119
K_{Pk}	9.005	7.655	7.395
diaphragm wall head (m)	0	0	0
diaphragm wall toe (m)	37.3	37.3	37.3
$\sigma'_{hp(k)}$ head (kPa)	0	0	0
$\sigma'_{hp(k)}$ toe (kPa)	5700.2	4845.6	4681.0
R'_{Pk} (kN/m)	119536.4	101615.9	98164.6
pore pressure resultant (kN/m)	638.45	638.45	638.45
R_{Pk} (MN)	11953.6	10161.6	9816.5

	SLS2	ULS	SLIS
K_h	0.097	0.216	0.238
K_v	0.048	0.108	0.119
K_{Pd}	5.481	4.577	4.401
diaphragm wall head (m)	0	0	0
diaphragm wall toe (m)	37.3	37.3	37.3
$\sigma'_{hp(d)}$ head (kPa)	0.0	0.0	0.0
$\sigma'_{hp(d)}$ toe (kPa)	3469.5	2897.2	2785.8
$R'_{P(d)}$ (kN/m)	72757.3	60757.2	58420.9
pore pressure resultant (kN/m)	638.45	638.45	638.45
$R_{P(d)}$ (MN)	7275.7	6075.7	5842.1

H_w = 94.5 m a.s.l. (absence of the drainage tunnel)

Mechanism 1 (z = 13.1 m)

	SLS2	ULS	SLIS
K_h	0.097	0.216	0.238
K_v	0.048	0.108	0.119
K_{Pk}	9.005	7.655	7.395
diaphragm wall head (m)	0	0	0
diaphragm wall toe (m)	13.1	13.1	13.1
$\sigma'_{hp(k)}$ head (kPa)	0	0	0
$\sigma'_{hp(k)}$ toe (kPa)	2359.3	2005.6	1937.5
R'_{Pk} (kN/m)	15453.5	13136.7	12690.6
pore pressure resultant (kN/m)	0	0	0
R_{Pk} (MN)	1545.3	1313.7	1269.1

	SLS2	ULS	SLIS
K_h	0.097	0.216	0.238
K_v	0.048	0.108	0.119
K_{Pd}	5.481	4.577	4.401
diaphragm wall head (m)	0	0	0
diaphragm wall toe (m)	13.1	13.1	13.1
$\sigma'_{hp(d)}$ head (kPa)	0.0	0.0	0.0
$\sigma'_{hp(d)}$ toe (kPa)	1436.0	1199.2	1153.1
R'_{Pd} (kN/m)	9405.9	7854.6	7552.6
pore pressure resultant (kN/m)	0	0	0
R_{Pd} (MN)	940.6	785.5	755.3

H_w = 94.5 m a.s.l. (absence of the drainage tunnel)

Mechanism 2 (z = 20.0 m)

	SLS2	ULS	SLIS
K_h	0.097	0.216	0.238
K_v	0.048	0.108	0.119
K_{Pk}	9.005	7.655	7.395
diaphragm wall head (m)	0	0	0
diaphragm wall toe (m)	20	20	20
$\sigma'_{hp(k)}$ head (kPa)	0	0	0
$\sigma'_{hp(k)}$ toe (kPa)	3557.0	3023.7	2921.0
R'_{Pk} (kN/m)	36008.7	30610.4	29570.8
pore pressure resultant (kN/m)	1.25	1.25	1.25
R_{Pk} (MN)	3600.9	3061.0	2957.1

	SLS2	ULS	SLIS
K_h	0.097	0.216	0.238
K_v	0.048	0.108	0.119
K_{Pd}	5.481	4.577	4.401
diaphragm wall head (m)	0	0	0
diaphragm wall toe (m)	20	20	20
$\sigma'_{hp(d)}$ head (kPa)	0.0	0.0	0.0
$\sigma'_{hp(d)}$ toe (kPa)	2165.0	1807.9	1738.4
R'_{Pd} (kN/m)	21917.1	18302.3	17598.5
pore pressure resultant (kN/m)	1.25	1.25	1.25
R_{Pd} (MN)	2191.7	1830.2	1759.8

H_w = 94.5 m a.s.l. (absence of the drainage tunnel)

Mechanism 3 (z = 37.3 m)

	SLS2	ULS	SLIS
K_h	0.097	0.216	0.238
K_v	0.048	0.108	0.119
K_{Pk}	9.005	7.655	7.395
diaphragm wall head (m)	0	0	0
diaphragm wall toe (m)	37.3	37.3	37.3
$\sigma'_{hp(k)}$ head (kPa)	0	0	0
$\sigma'_{hp(k)}$ toe (kPa)	5114.8	4348.0	4200.4
R'_{Pk} (kN/m)	111019.9	94376.2	91170.7
pore pressure resultant (kN/m)	1584.2	1584.2	1584.2
R_{Pk} (MN)	11102.0	9437.6	9117.1

	SLS2	ULS	SLIS
K_h	0.097	0.216	0.238
K_v	0.048	0.108	0.119
K_{Pd}	5.481	4.577	4.401
diaphragm wall head (m)	0	0	0
diaphragm wall toe (m)	37.3	37.3	37.3
$\sigma'_{hp(d)}$ head (kPa)	0.0	0.0	0.0
σ'_{hp} toe (kPa)	3113.2	2599.7	2499.8
R'_{Pd} (kN/m)	67573.6	56428.5	54258.6
pore pressure resultant (kN/m)	1584.2	1584.2	1584.2
R_{Pd} (MN)	6757.4	5642.8	5425.9

Appendix C – Safety against sliding, pseudo-static approach

H_w = 88.0 m a.s.l. (presence of the drainage tunnel)

General input parameters

Anchor block weight W_b	6256	MN
Anchor block width	100	m
Pore pressure resultant force U	379	MN
Anchor block submerged weight W_b'	5877	MN
Cable force angle i	15	°
Ground water depth	26	m b.g.l.
Unit weight of soil	20	kN/m^3
Characteristic angle of shear resistance of soil φ'_k	40	°
Design angle of shear resistance of soil φ'_d	33.9	°
Characteristic angle of shear resistence on the sliding surface φ'_{sk}	32	°
Design angle of shear resistence on the sliding surface φ'_{sd}	26.6	°
Characteristic friction angle at soil-concrete interface δ_k	20	°
Design friction angle at soil-concrete interface δ_d	16.9	°

CABLE FORCE (MN)

SLS2	ULS	SLIS
3232	3934	3142

SEISMIC COEFFICIENT

	SLS2	ULS	SLIS
K_h	0.097	0.216	0.238
K_v	0.048	0.108	0.119
a_h/g	0.26	0.58	0.64

$S_T \times S_s \times \beta_m$ 0.372

PASSIVE EARTH PRESSURE COEFFICIENT

	SLS2	ULS	SLIS
K_{Pk}	9.005	7.655	7.395
K_{Pd}	5.481	4.577	4.401

Mechanism 1 (H_w = 88.0 m a.s.l. – presence of the drainage tunnel)

Input parameters

sliding surface inclination	33.7	°
Soil volume above the sliding surface	4800.0	m^3
Submerged soil volume aboce the sliding surface	1008.3	m^3
Soil weight above the sliding surface	96	MN
Submerged soil weight aboce the sliding surface	86	MN
Total weight *W*	6352	MN
Total submerged *W'*	5963	MN
θ critical ($\alpha+\varphi'_s$)	69.7	°
Design sliding resistance along the block side T_{Ld}	157.4	MN

Passive earth resistance

	SLS2	ULS	SILS
R_{Pk} (MN)	1545.3	1313.7	1269.1
R_{Pd} (MN)	940.6	785.5	755.3

R_d (MN)	***SLS2***	***ULS***	***SLIS***
W' cosα tanφ'$_k$	3099.9	3099.9	3099.9
W (K_h senα - $K_v$cosα) tanφ'$_k$	53.3	118.9	131.2
T sen(α-i) tanφ'$_k$	647.5	788.1	629.5
E_d (MN)	***SLS2***	***ULS***	***SLIS***
W' senα	3308.5	3308.5	3308.5
W (K_h cosα + K_v senα)	681.6	1520.4	1677.7
T cos(α-i)	3061.4	3726.3	2976.1
$\Sigma R_d/\Sigma E_d$ (MN)	8.6	1.9	2.7

Mechanism 2 (H_w = 88.0 m a.s.l. – presence of the drainage tunnel)

Input parameters

sliding surface inclination	25.3	°
Soil volume above the sliding surface	17400.0	m^3
Submerged soil volume aboce the sliding surface	4745.1	m^3
Soil weight above the sliding surface	348	MN
Submerged soil weight aboce the sliding surface	301	MN
Total weight *W*	6604	MN
Total submerged *W'*	6178	MN
θ critical ($\alpha+\varphi'_s$)	61.3	°
Design sliding resistance along the block side T_{Ld}	169.9	MN

Passive earth resistance

	SLS2	ULS	SILS
R_{Pk} (MN)	3602.0	3062.0	2958.0
R_{Pd} (MN)	2192.4	1830.8	1760.4

R_d (MN)	***SLS2***	***ULS***	***SLIS***
W' cosα tanφ_k'	3489.9	3489.9	3489.9
W (K_h senα - $K_v$cosα) tanφ_k'	-9.9	-22.0	-24.3
T sen(α-i) tanφ_k'	361.1	439.5	351.0
E_d (MN)	***SLS2***	***ULS***	***SLIS***
W' senα	2640.0	2640.0	2640.0
W (Kh cosα + Kv senα)	714.0	1592.7	1757.4
T cos(α-i)	3179.9	3870.6	3091.4
$\Sigma R_d/\Sigma E_d$ (MN)	3.9	1.6	2.0

Mechanism 3 (H_w = 88.0 m a.s.l. – presence of the drainage tunnel)

Input parameters

sliding surface inclination	0	°
Soil volume above the sliding surface	48000	m^3
Submerged soil volume aboce the sliding surface	31533	m^3
Soil weight above the sliding surface	960.0	MN
Submerged soil weight aboce the sliding surface	644.7	MN
Total weight *W*	7216	MN
Total submerged *W'*	6522	MN
θ critical ($\alpha+\varphi'_s$)	36	°
Design sliding resistance along the block side T_{Ld}	209.2	MN

Passive earth resistance

	SLS2	ULS	SILS
R_{Pk} (MN)	11953.6	10161.6	9816.5
R_{Pd} (MN)	7275.7	6075.7	5842.1

R_d (MN)	SLS2	ULS	SLIS
W' cosα tanφ$_k$'	4075.2	4075.2	4075.2
W (K_h senα - $K_v$cosα) tanφ$_k$'	-218.1	-486.4	-536.8
T sen(α-i) tanφ$_k$'	-522.7	-636.2	-508.1

E_d (MN)	SLS2	ULS	SLIS
W' senα	0.0	0.0	0.0
W (Kh cosα + Kv senα)	697.9	1556.9	1718.0
T cos(α-i)	3121.9	3800.0	3034.9

$\Sigma R_d/\Sigma E_d$ (MN)	2.3	1.4	1.6

H_w = 94.5 m a.s.l. (absence of the drainage tunnel)

General input parameters

Anchor block weight W_b	6256	MN
Anchor block width	100	m
Pore pressure resultant force U	753	MN
Anchor block submerged weight W_b'	5503	MN
Cable force angle i	15	°
Ground water depth	19.5	m b.g.l.
Unit weight of soil	20	kN/m^3
Characteristic angle of shear resistance of soil φ'_k	40	°
Design angle of shear resistance of soil φ'_d	33.9	°
Characteristic angle of shear resistence on the sliding surface φ'_{sk}	32	°
Design angle of shear resistence on the sliding surface φ'_{sd}	26.6	°
Characteristic friction angle at soil-concrete interface δ_k	20	°
Design friction angle at soil-concrete interface δ_d	16.9	°

CABLE FORCE (MN)

SLS2	ULS	SLIS
3232	3934	3142

SEISMIC COEFFICIENT

	SLS2	ULS	SLIS
K_h	0.097	0.216	0.238
K_v	0.048	0.108	0.119
a_h/g	0.26	0.58	0.64

$S_T \times S_s \times \beta_m$ 0.372

PASSIVE EARTH PRESSURE COEFFICIENT

	SLS2	ULS	SLIS
K_{Pk}	9.005	7.655	7.395
K_{Pd}	5.481	4.577	4.401

Mechanism 1 (H_w = 94.5 m a.s.l. – absence of the drainage tunnel)

Input parameters

sliding surface inclination	33.7	°
Soil volume above the sliding surface	4800.0	m^3
Submerged soil volume aboce the sliding surface	2552.1	m^3
Soil weight above the sliding surface	96	MN
Submerged soil weight aboce the sliding surface	70	MN
Total weight *W*	6352	MN
Total submerged *W'*	5573	MN
θ critical ($\alpha+\varphi'_s$)	69.7	°
Design sliding resistance along the block side T_{Ld}	149.1	MN

Passive earth resistance

	SLS2	ULS	SILS
R_{Pk} (MN)	1545.3	1313.7	1269.1
R_{Pd} (MN)	940.6	785.5	755.3

R_d (MN)	SLS2	ULS	SLIS
W' cosα tanφ'$_k$	2897.4	2897.4	2897.4
W (K_h senα - $K_v$cosα) tanφ'$_k$	53.3	118.9	131.2
T sen(α-i) tanφ'$_k$	647.5	788.1	629.5
E_d (MN)	**SLS2**	**ULS**	**SLIS**
W' senα	3092.4	3092.4	3092.4
W (K_h cosα + K_v senα)	681.6	1520.4	1677.7
T cos(α-i)	3061.4	3726.3	2976.1
$\Sigma R_d/\Sigma E_d$ (MN)	5.5	1.7	2.2

Mechanism 2 (H_w = 94.5 m a.s.l. – absence of the drainage tunnel)

Input parameters

sliding surface inclination	25.3	°
Soil volume above the sliding surface	17400.0	m^3
Submerged soil volume aboce the sliding surface	11983.3	m^3
Soil weight above the sliding surface	348	MN
Submerged soil weight aboce the sliding surface	228	MN
Total weight *W*	6604	MN
Total submerged *W'*	5731	MN
θ critical (α+φ'_s)	61.3	°
Design sliding resistance along the block side T_{Ld}	160.6	MN

Passive earth resistance

	SLS2	ULS	SILS
R_{Pk} (MN)	3600.9	3061.0	2957.1
R_{Pd} (MN)	2191.7	1830.2	1759.8

R_d (MN)	***SLS2***	***ULS***	***SLIS***
W' cosα tanφ_k'	3237.7	3237.7	3237.7
W (K_h senα - $K_v$cosα) tanφ_k'	-9.9	-22.0	-24.3
T sen(α-i) tanφ_k'	361.1	439.5	351.0
E_d (MN)	***SLS2***	***ULS***	***SLIS***
W' senα	2449.3	2449.3	2449.3
W (K_h cosα + K_v senα)	714.0	1592.7	1757.4
T cos(α-i)	3179.9	3870.6	3091.4
$\Sigma R_d/\Sigma E_d$ (MN)	3.3	1.5	1.8

Mechanism 3 (H_w = 94.5 m a.s.l. – absence of the drainage tunnel)

Input parameters

sliding surface inclination	0	°
Soil volume above the sliding surface	48000	m^3
Submerged soil volume aboce the sliding surface	42583	m^3
Soil weight above the sliding surface	960.0	MN
Submerged soil weight aboce the sliding surface	534.2	MN
Total weight *W*	7216	MN
Total submerged *W'*	6037	MN
θ critical ($\alpha+\varphi'_s$)	36	°
Design sliding resistance along the block side T_{Ld}	195.7	MN

Passive earth resistance

	SLS2	ULS	SILS
R_{Pk} *(MN)*	11102.0	9437.6	9117.1
R_{Pd} *(MN)*	6757.4	5642.8	5425.9

R_d (MN)	SLS2	ULS	SLIS
W' cosα tanφ'$_k$	3772.4	3772.4	3772.4
W (K_h senα - $K_v$cosα) tanφ'$_k$	-218.1	-486.4	-536.8
T sen(α-i) tanφ'$_k$	-522.7	-636.2	-508.1

E_d (MN)	SLS2	ULS	SLIS
W' senα	0.0	0.0	0.0
W (K_h cosα + K_v senα)	697.9	1556.9	1718.0
T cos(α-i)	3121.9	3800.0	3034.9

$\Sigma R_d/\Sigma E_d$ (MN)	2.2	1.3	1.4

Appendix D – Time histories

No drainage tunnel

Friuli 76 TOLXC

Mechanism 3

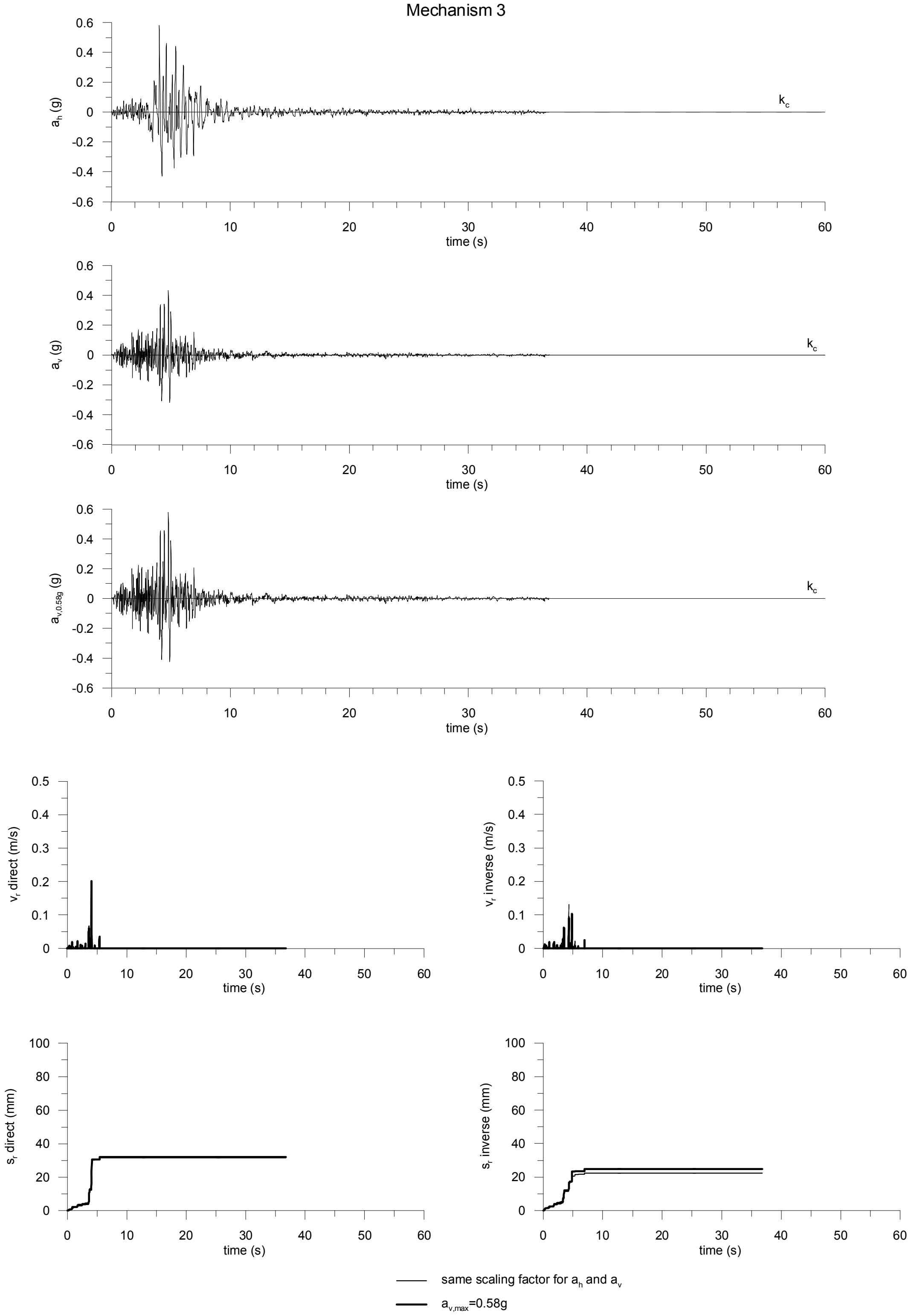

No drainage tunnel

Friuli 76 TOLYC

Mechanism 3

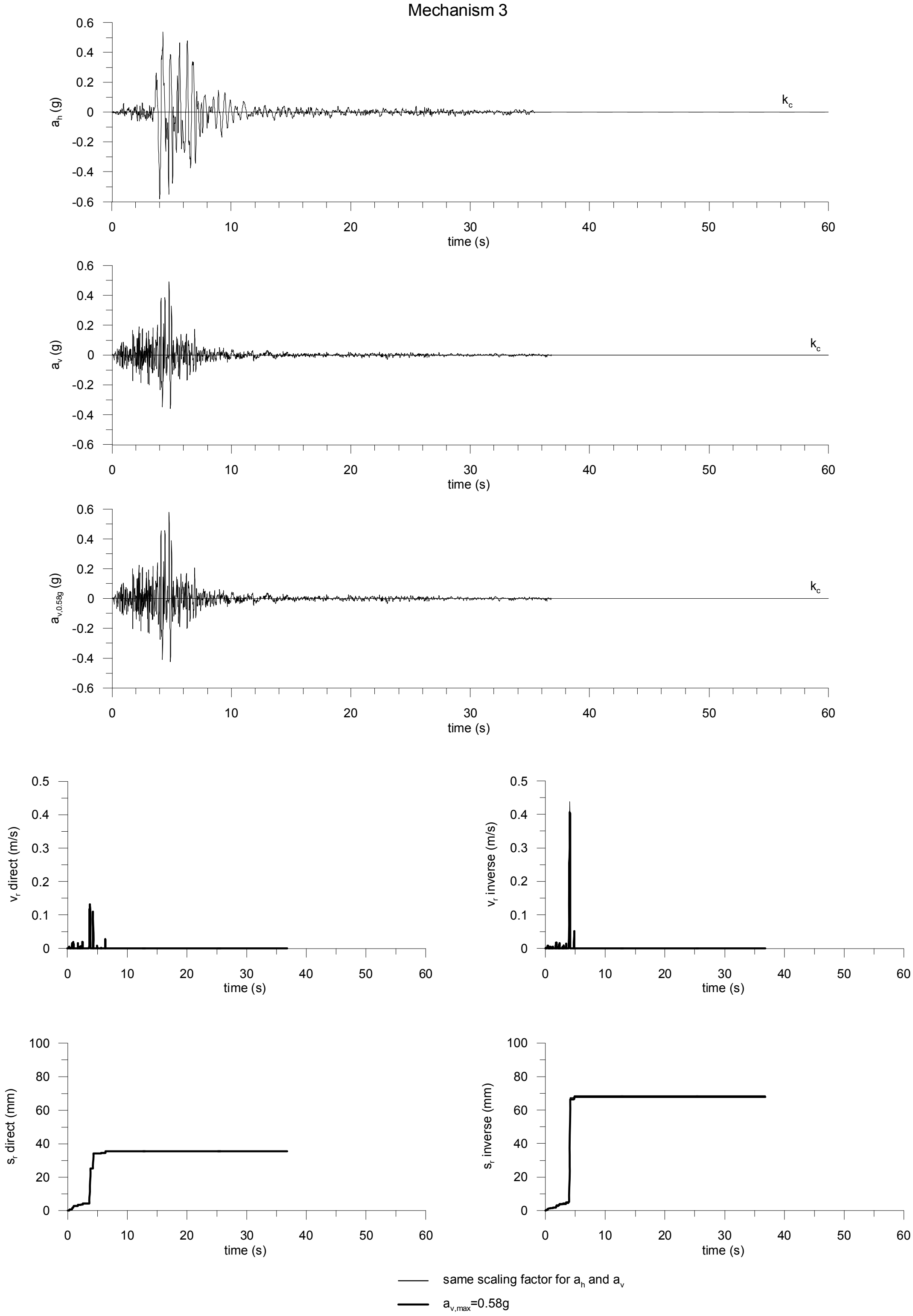

No drainage tunnel

Imperial Valley 79 DLT352

Mechanism 3

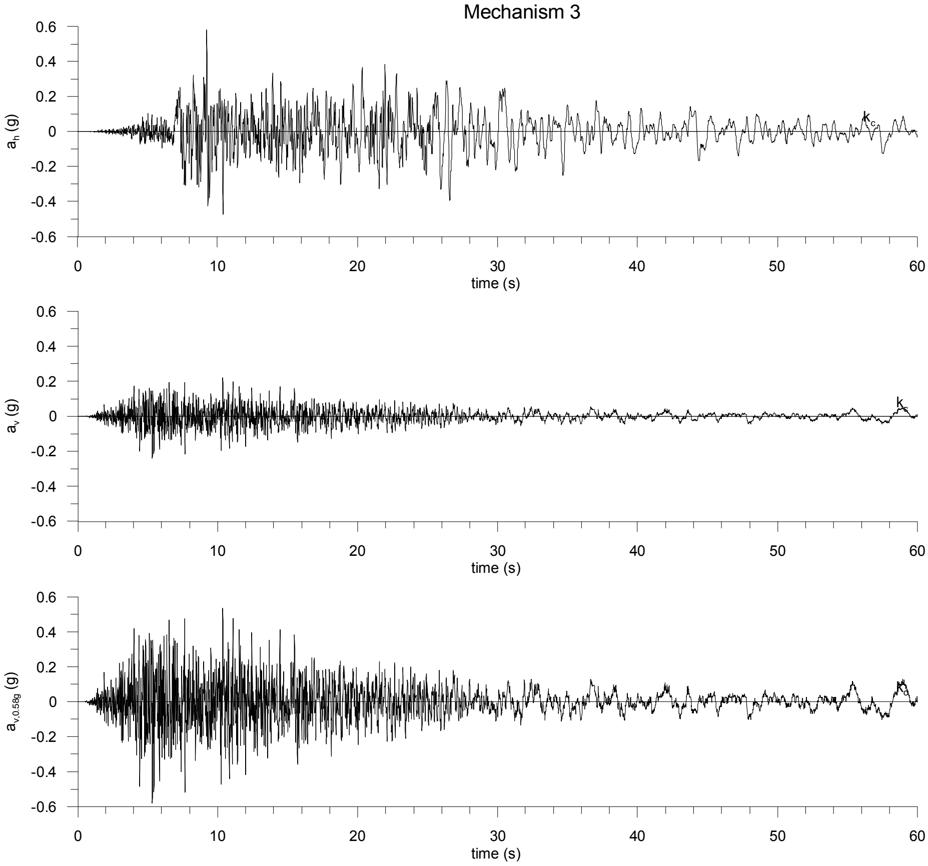

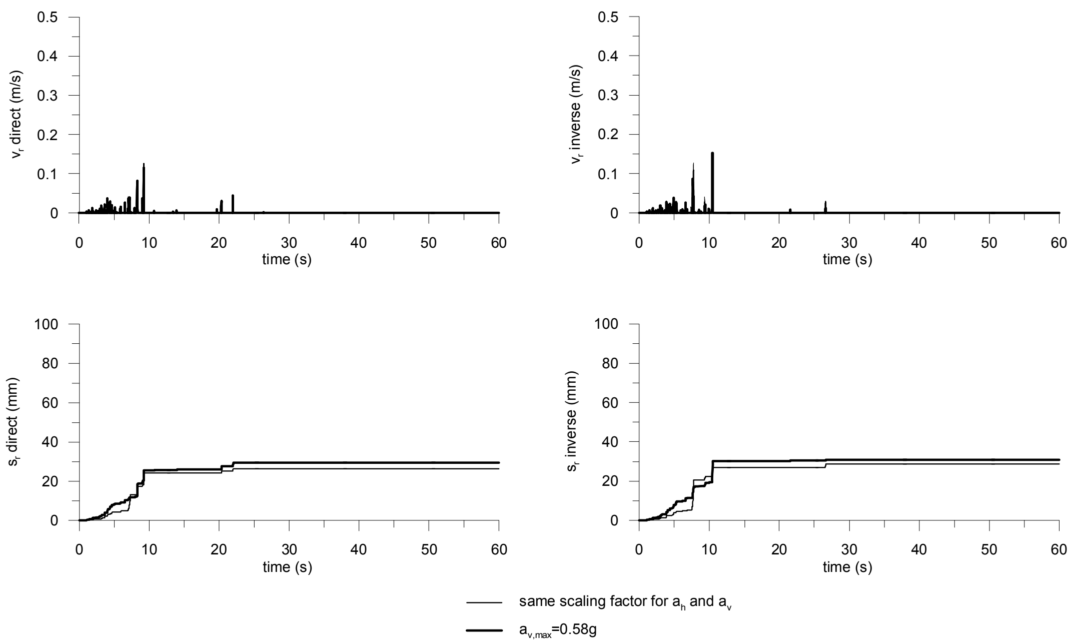

No drainage tunnel

Kobe 95 TAZ000

Mechanism 3

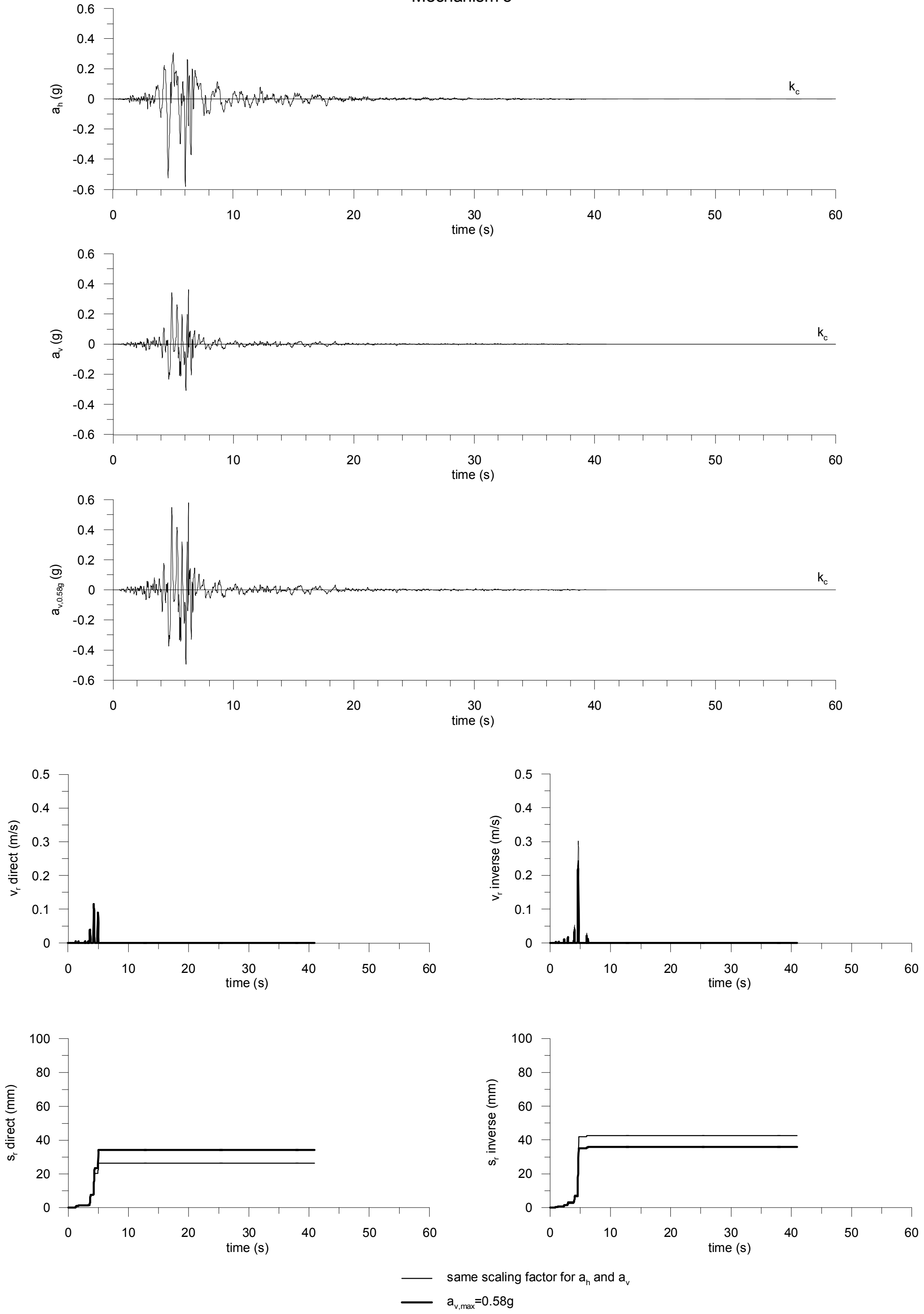

No drainage tunnel
Kobe 95 TAZ090
Mechanism 3

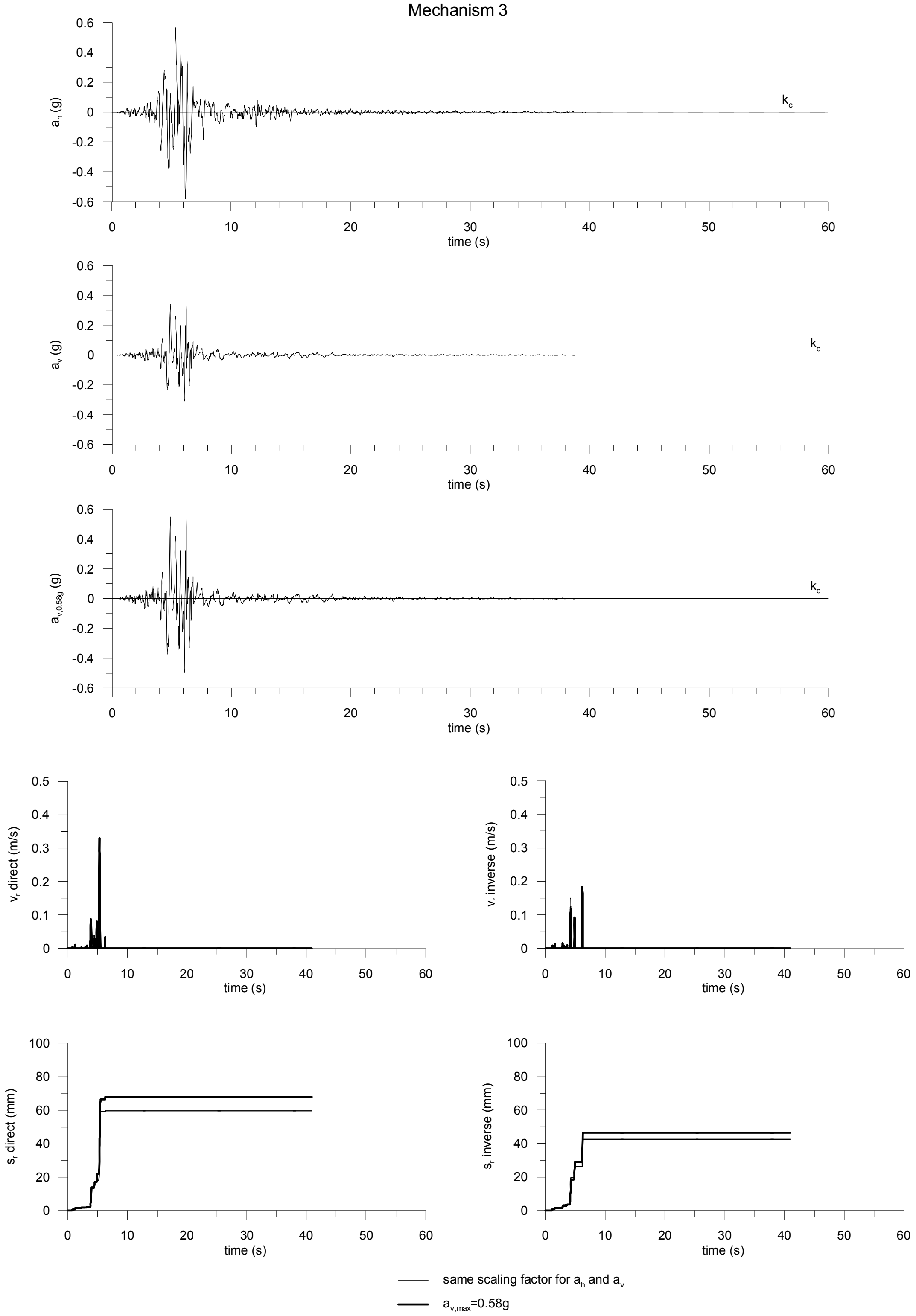

No drainage tunnel

Landers 92 CLWTR

Mechanism 3

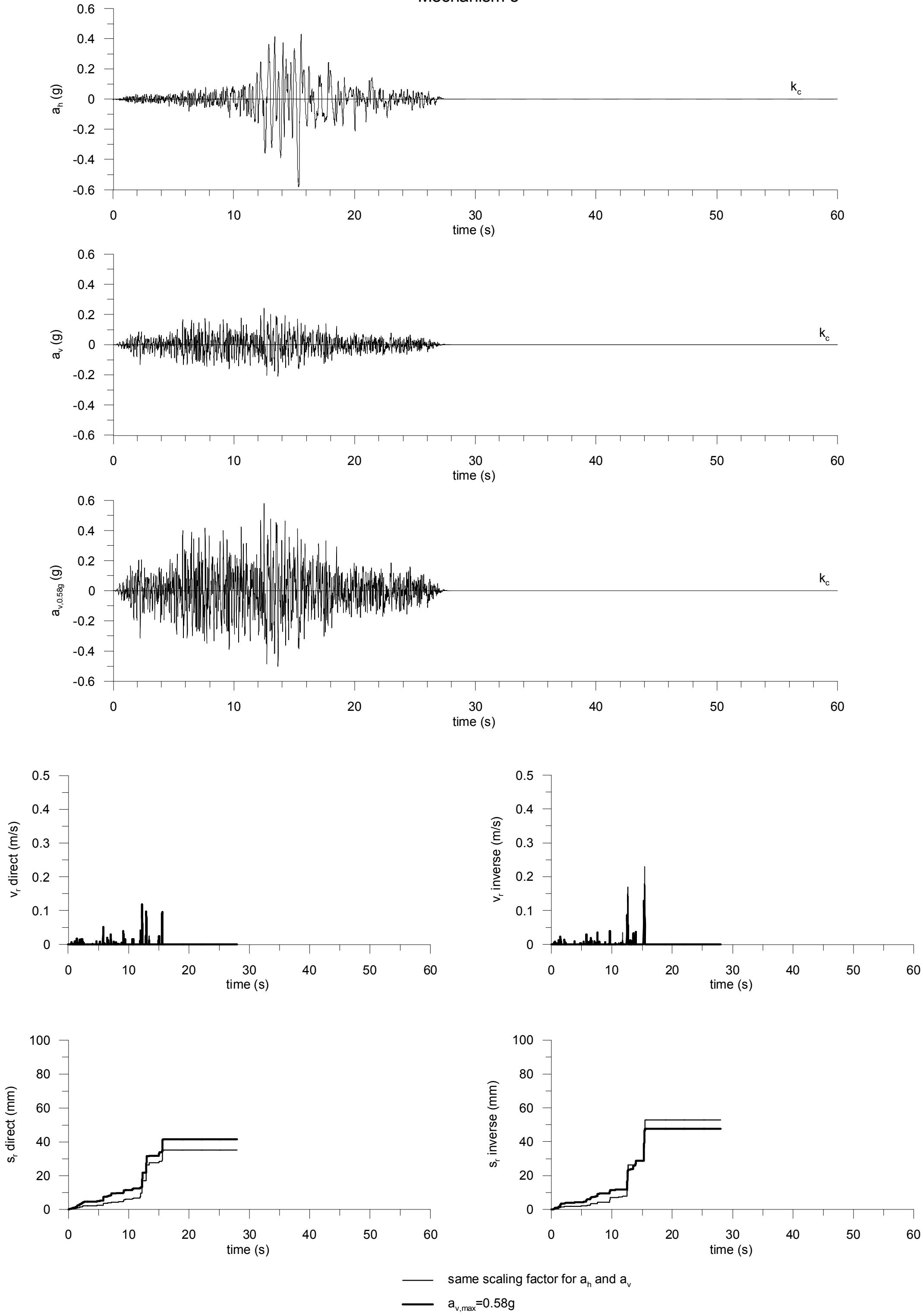

No drainage tunnel

Landers 92 LCN260

Mechanism 3

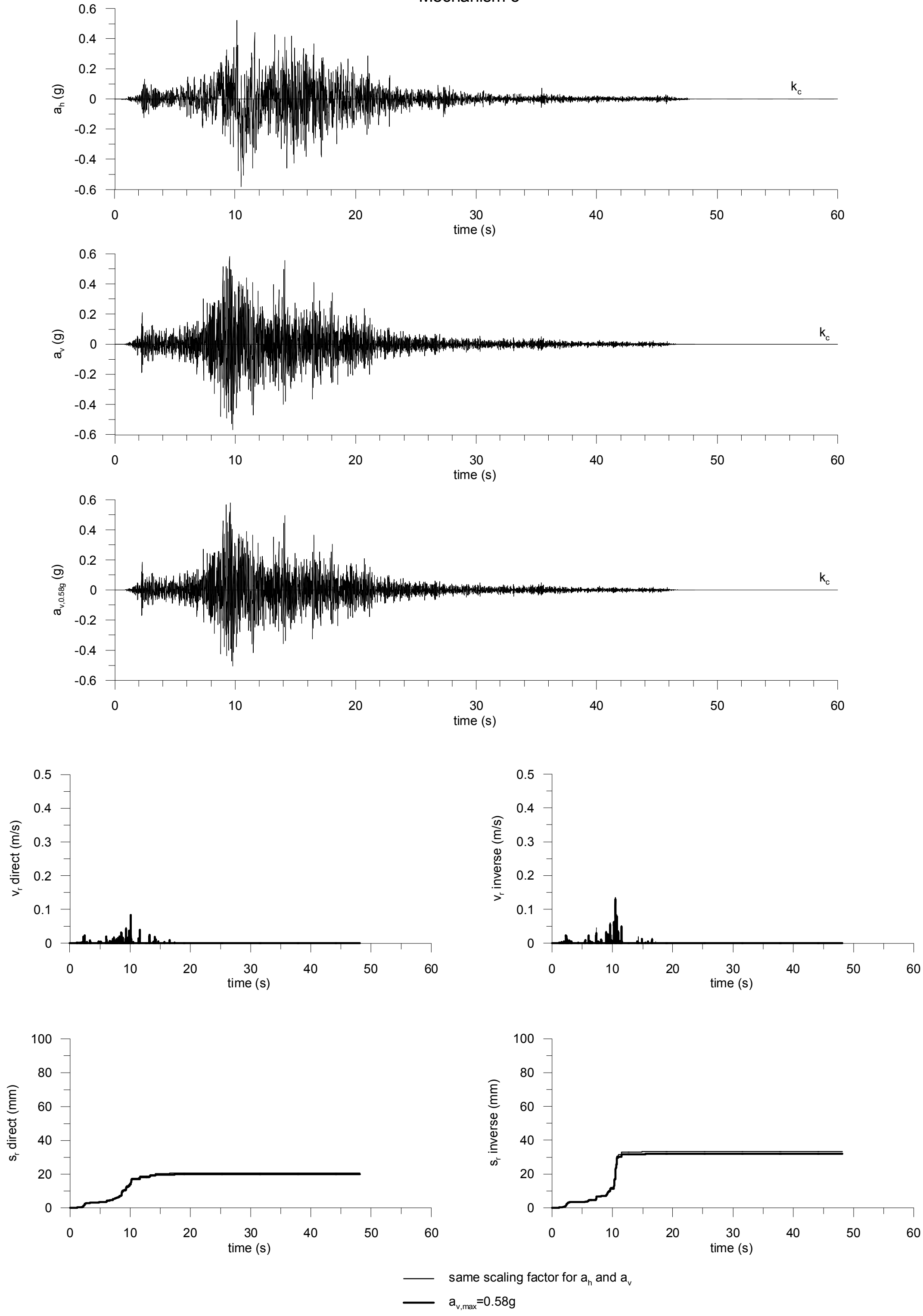

No drainage tunnel

Landers 92 LCN345

Mechanism 3

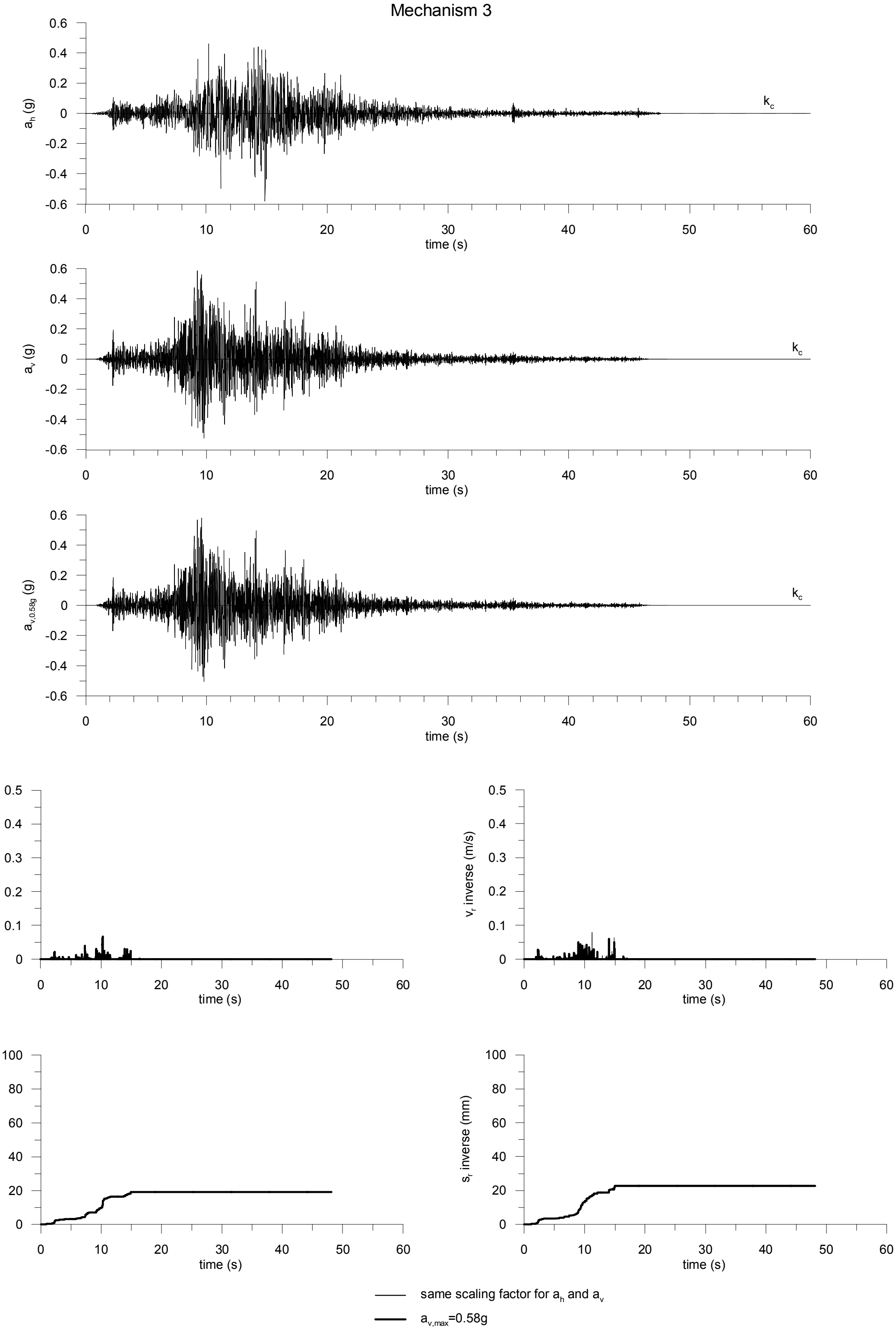

No drainage tunnel

Loma Prieta 89 CYC285

Mechanism 3

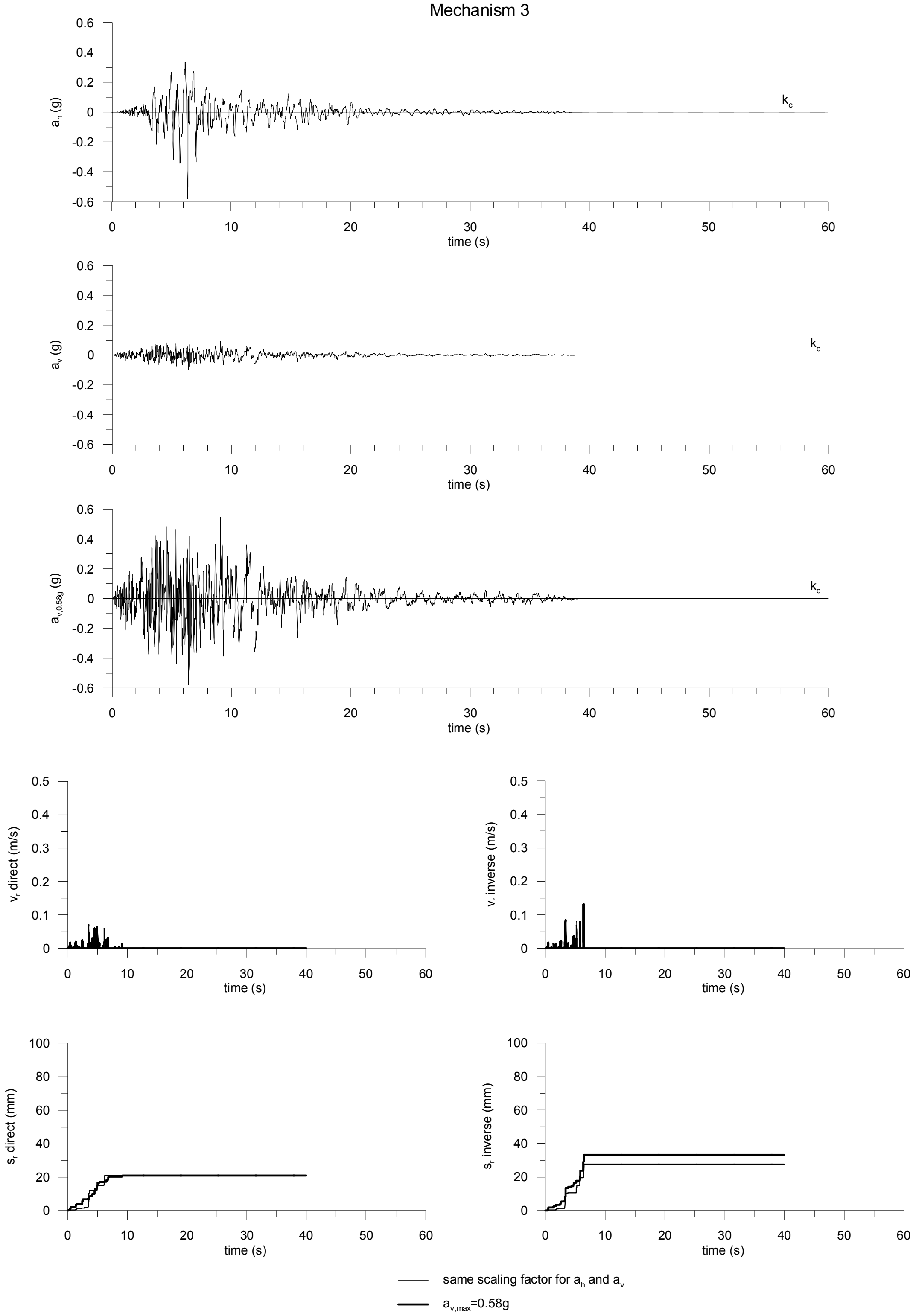

No drainage tunnel

Loma Prieta 89 G03000

Mechanism 3

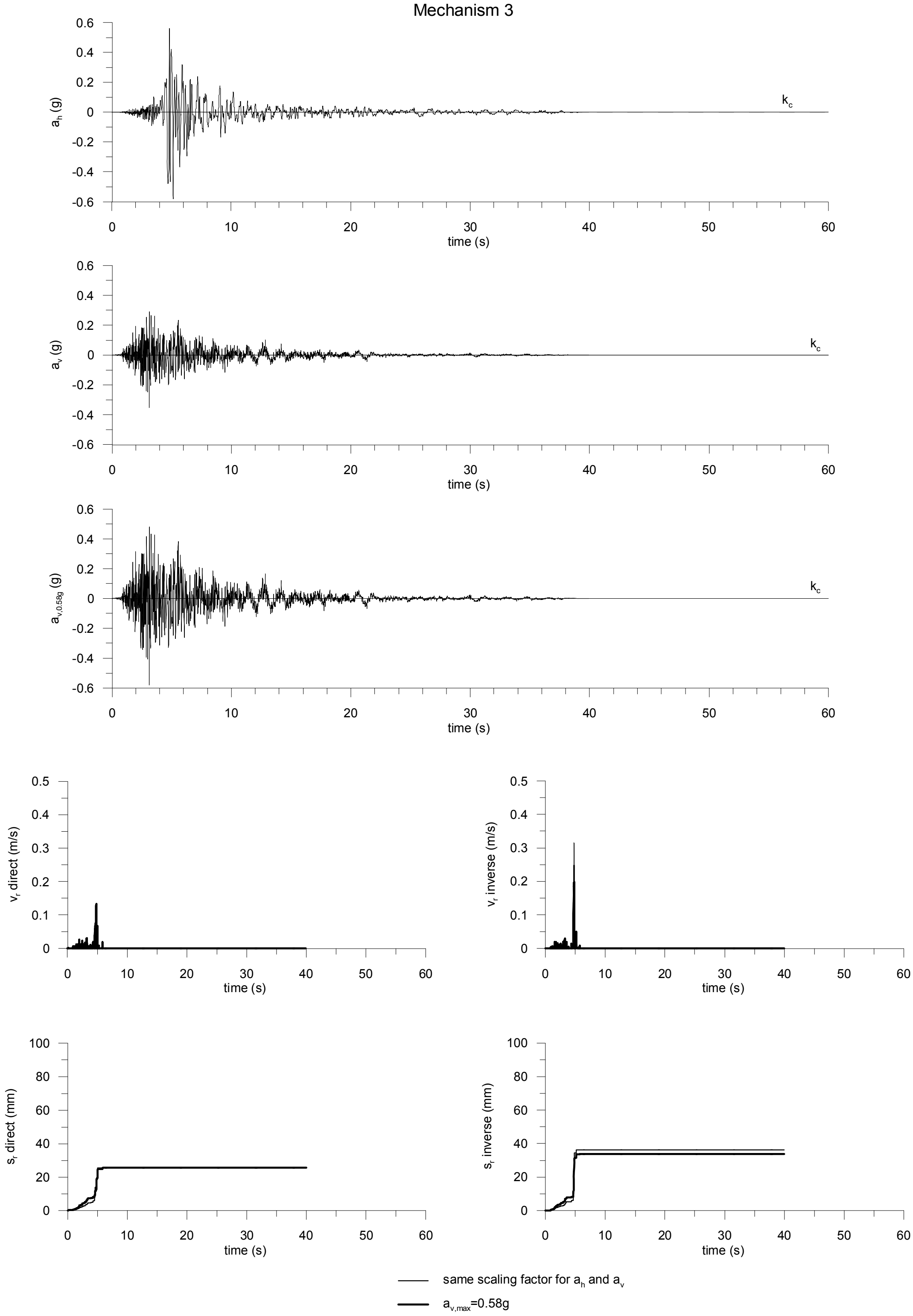

No drainage tunnel

Loma Prieta 89 G03090

Mechanism 3

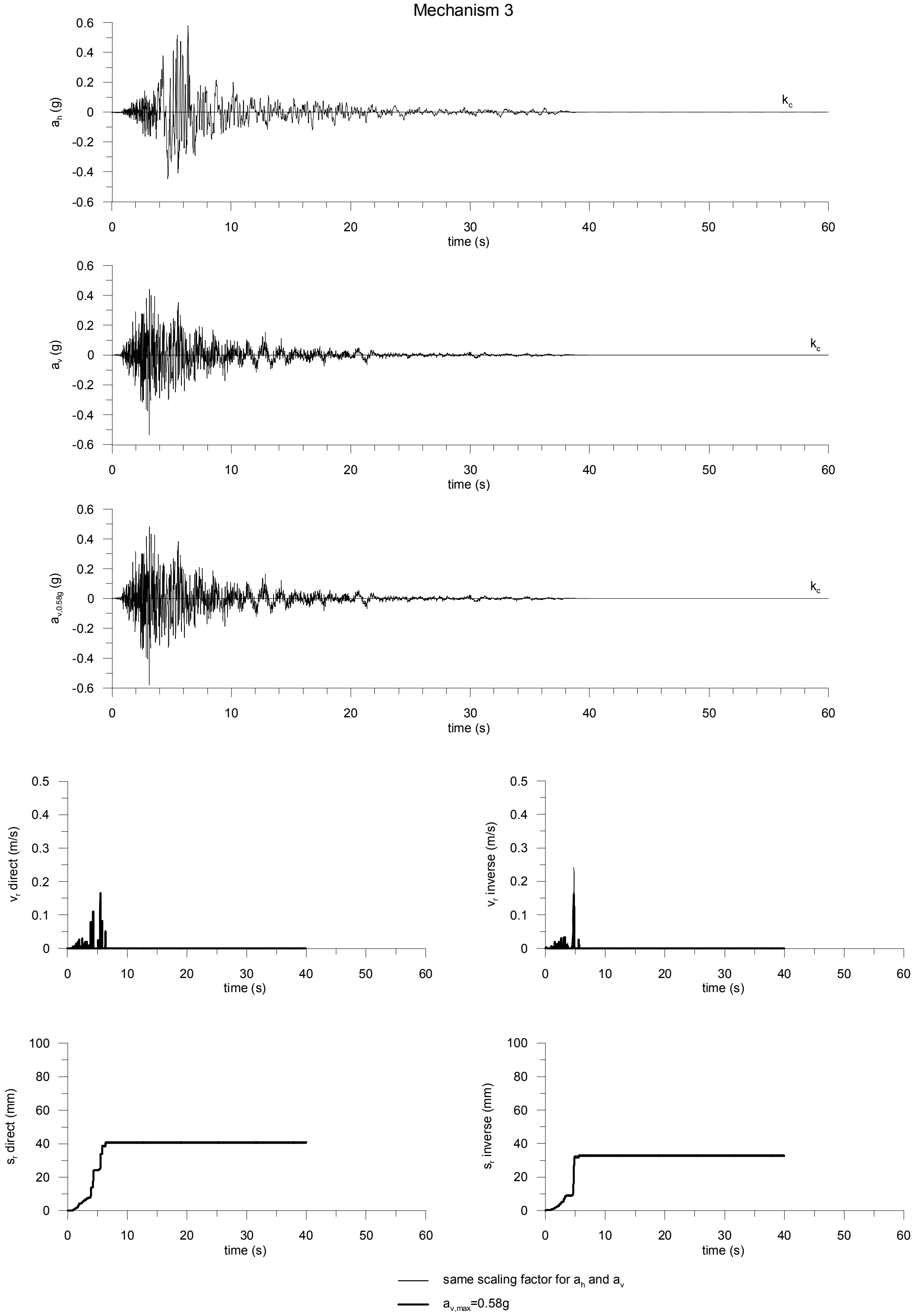

No drainage tunnel
Loma Prieta 89 G04000
Mechanism 3

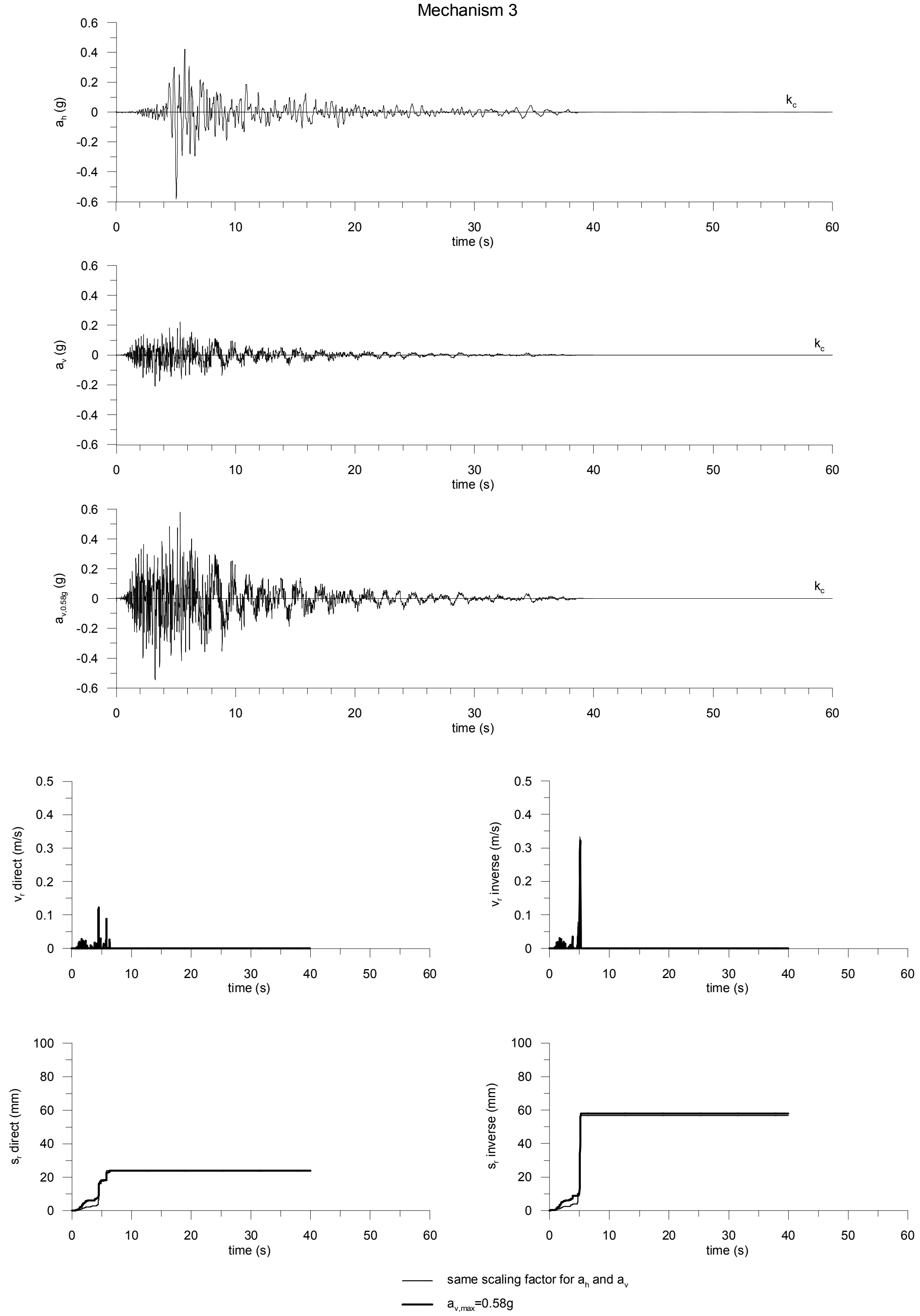

No drainage tunnel
Manjil 90 ABBL
Mechanism 3

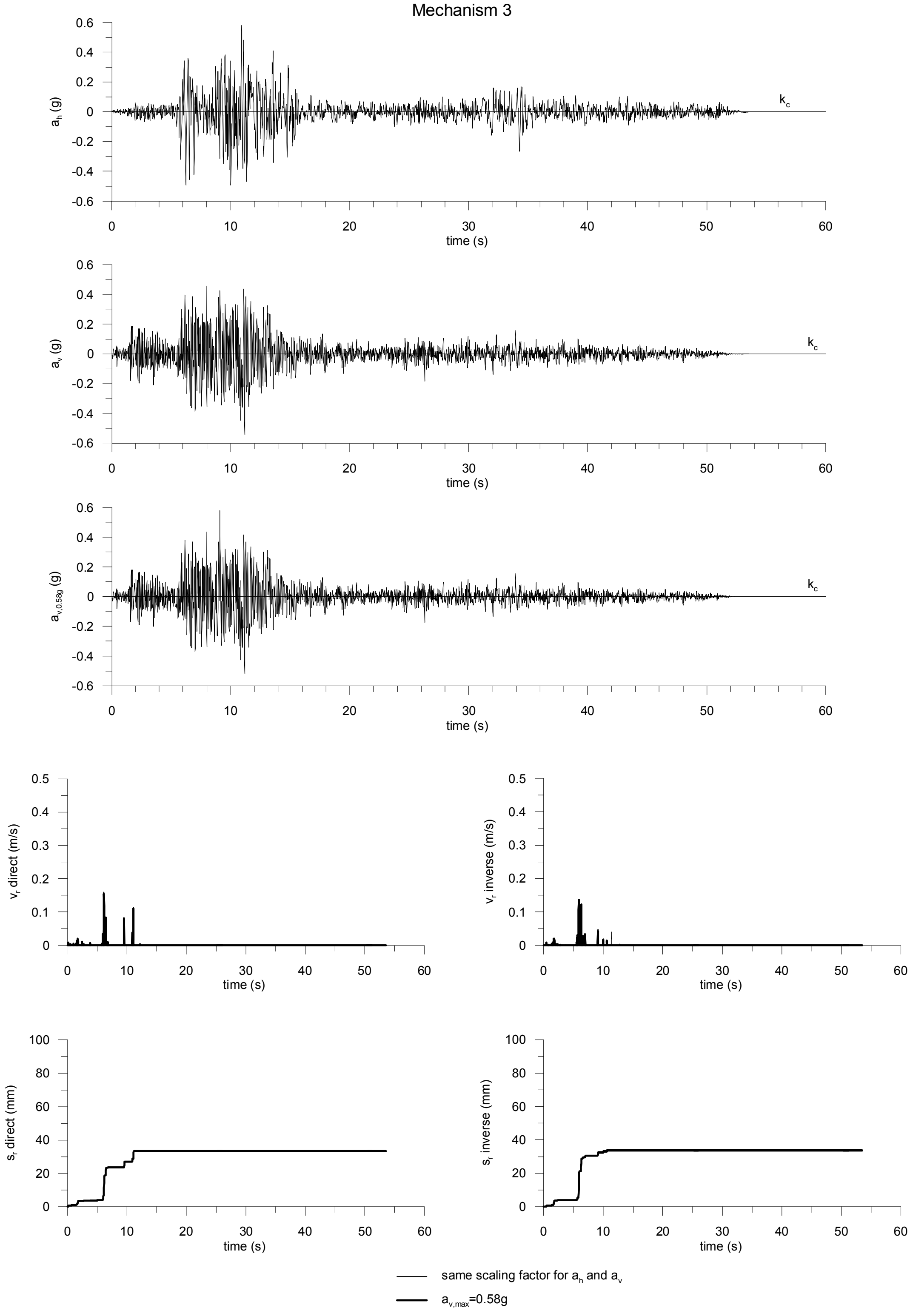

No drainage tunnel

Manjil 90 ABBT

Mechanism 3

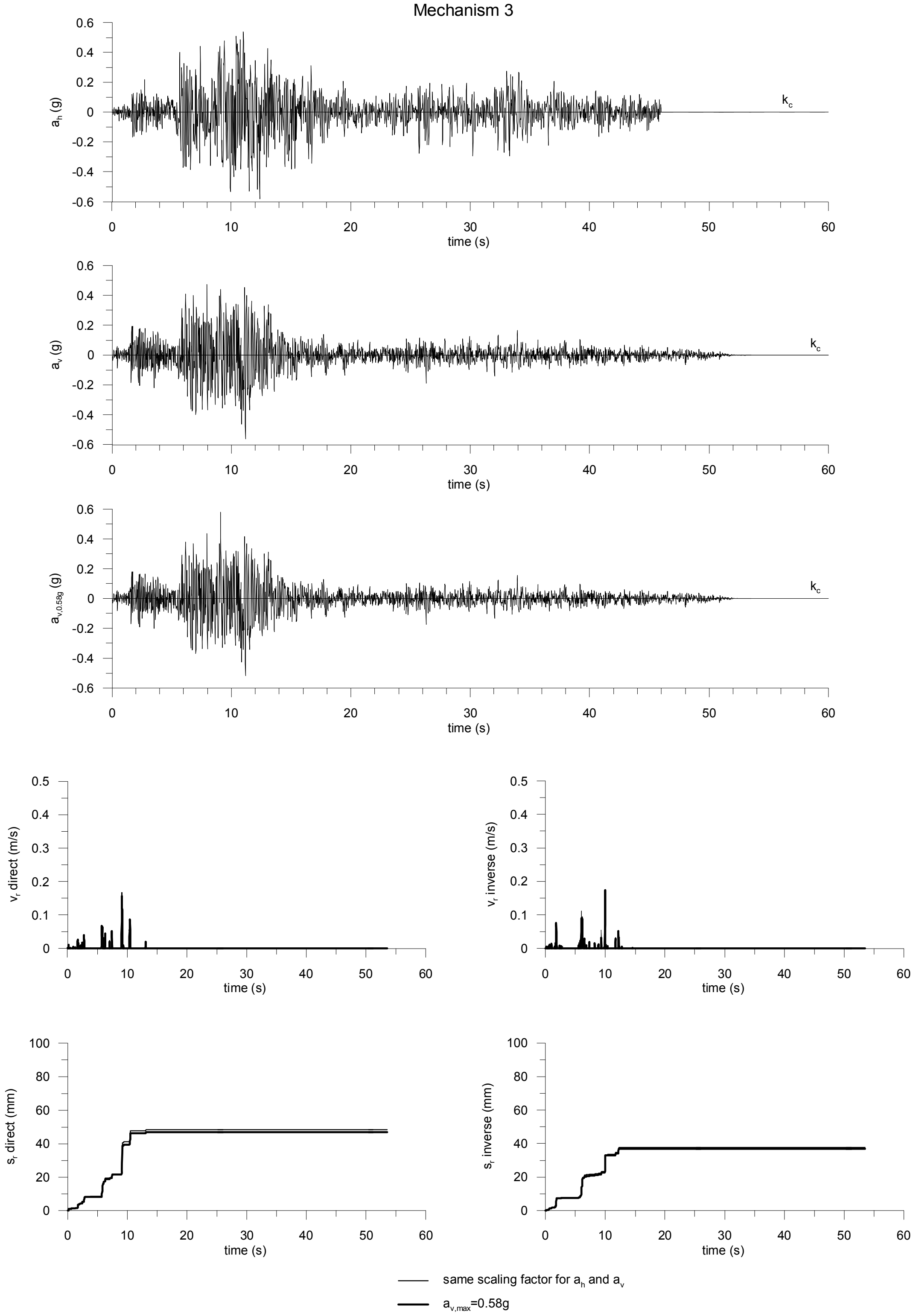

No drainage tunnel

Northridge 94 CEN245

Mechanism 3

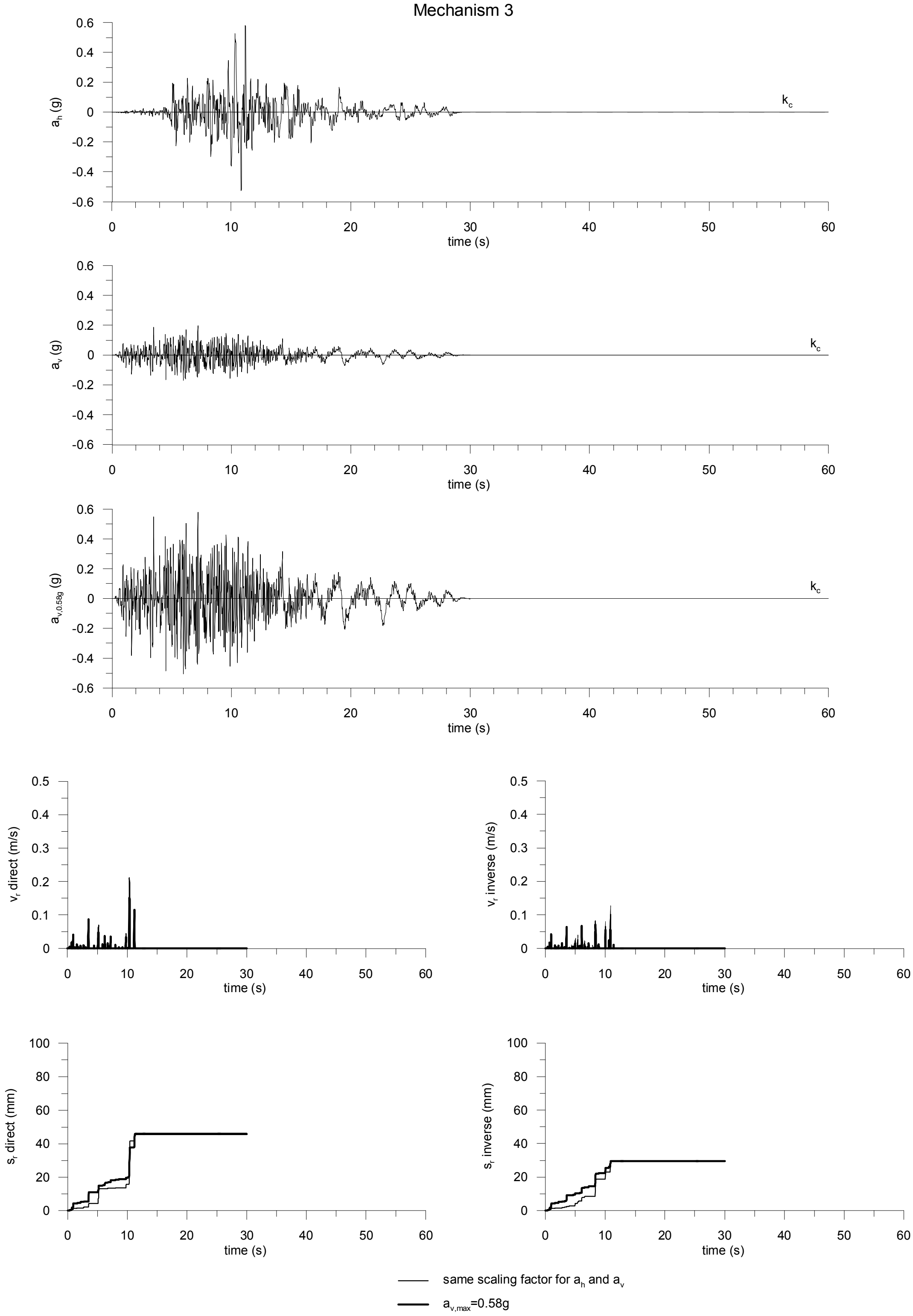

No drainage tunnel

Northridge 94 LAC180

Mechanism 3

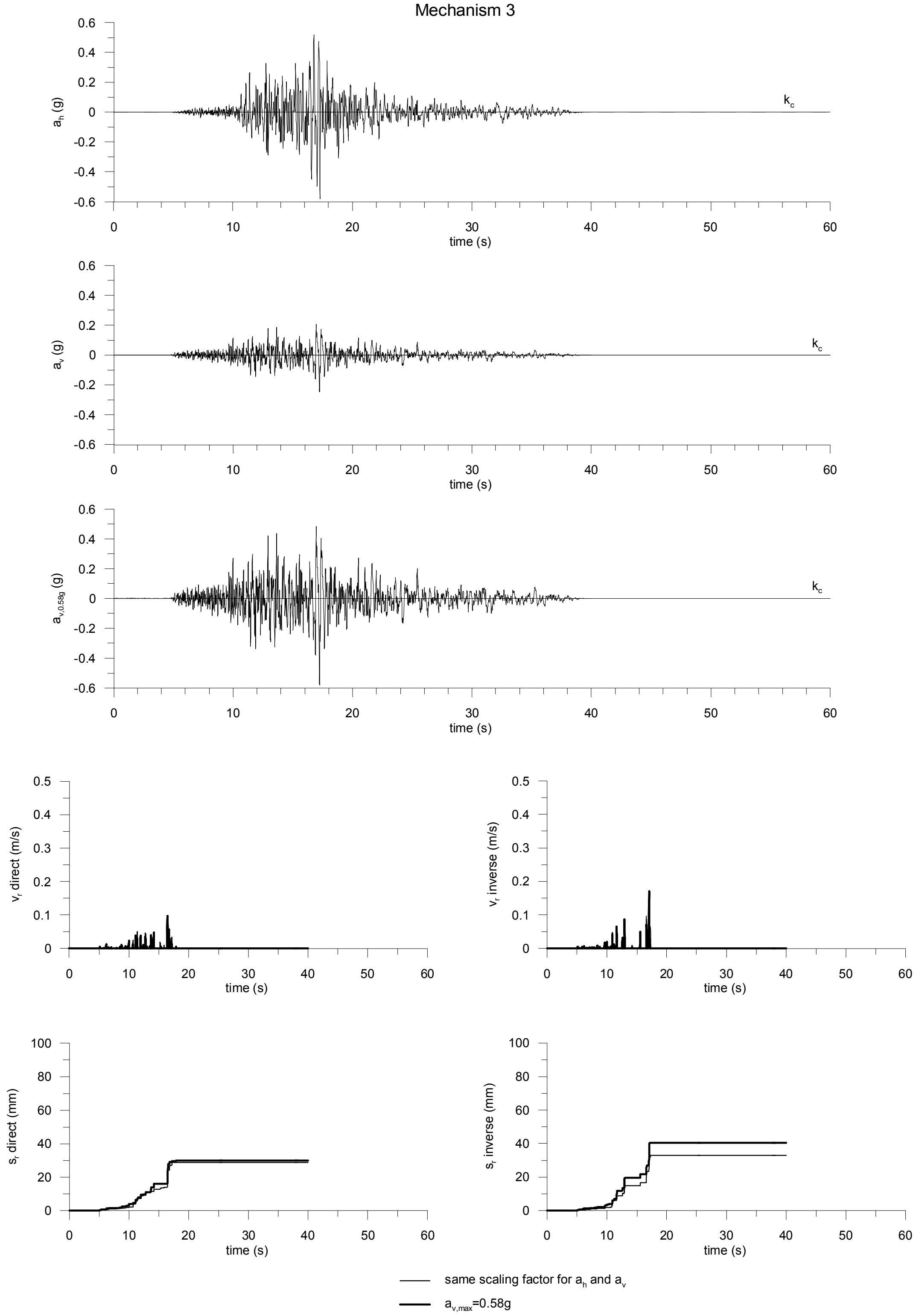

No drainage tunnel

Umbria Marche 97 NCRXC

Mechanism 3

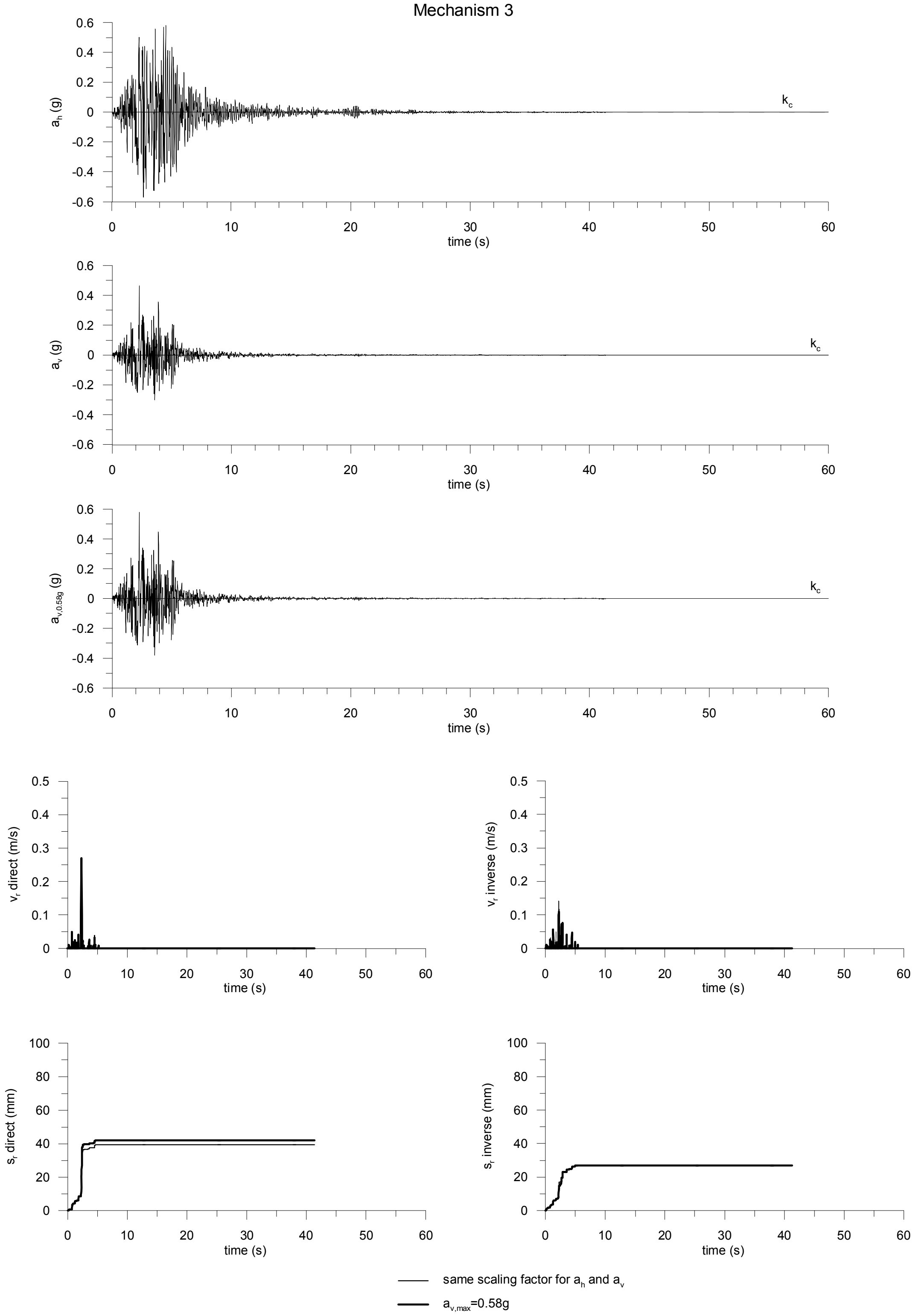

No drainage tunnel

Umbria Marche 97 NCRYC

Mechanism 3

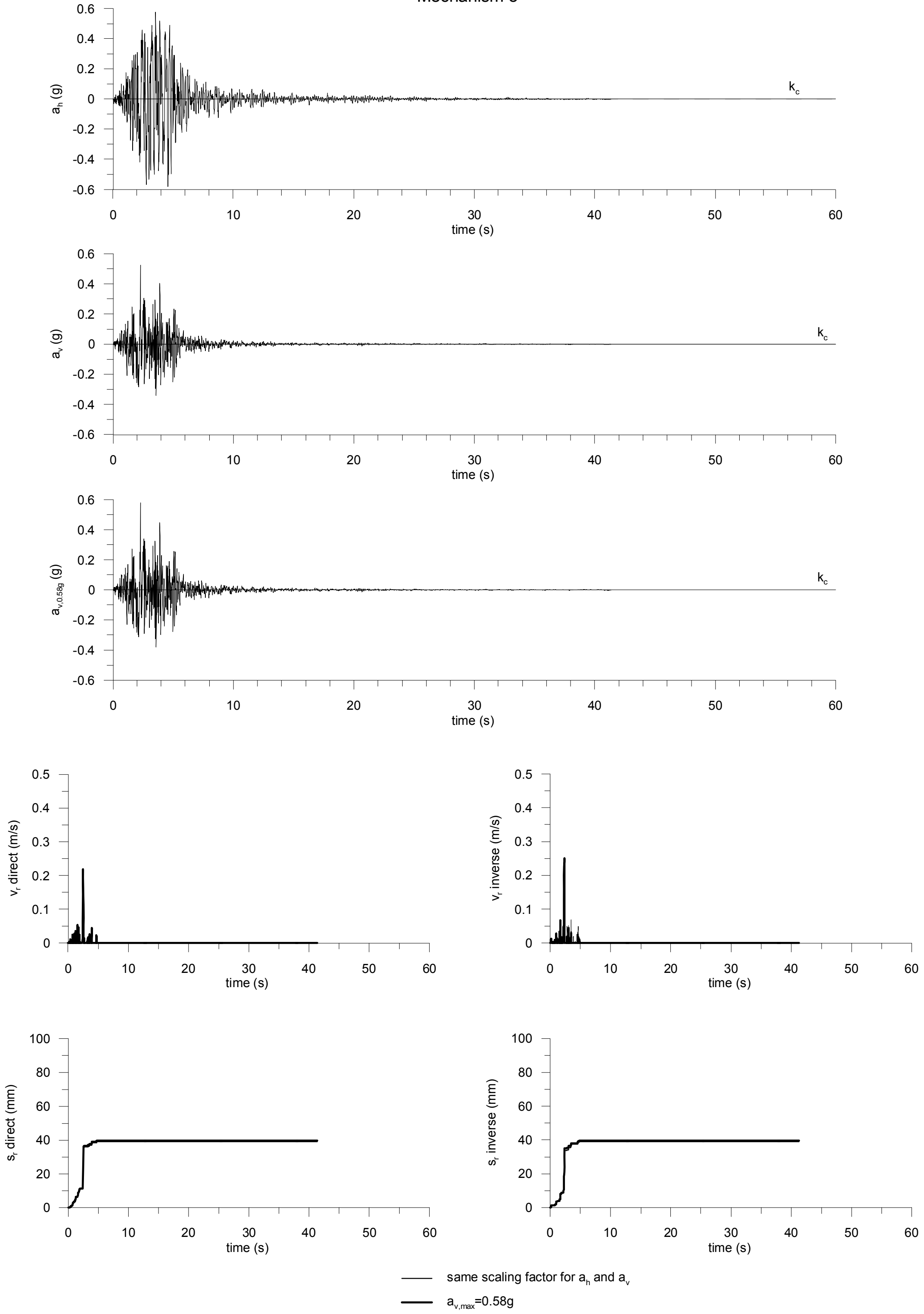

No drainage tunnel
Imperial Valley 79 BC230
Mechanism 3

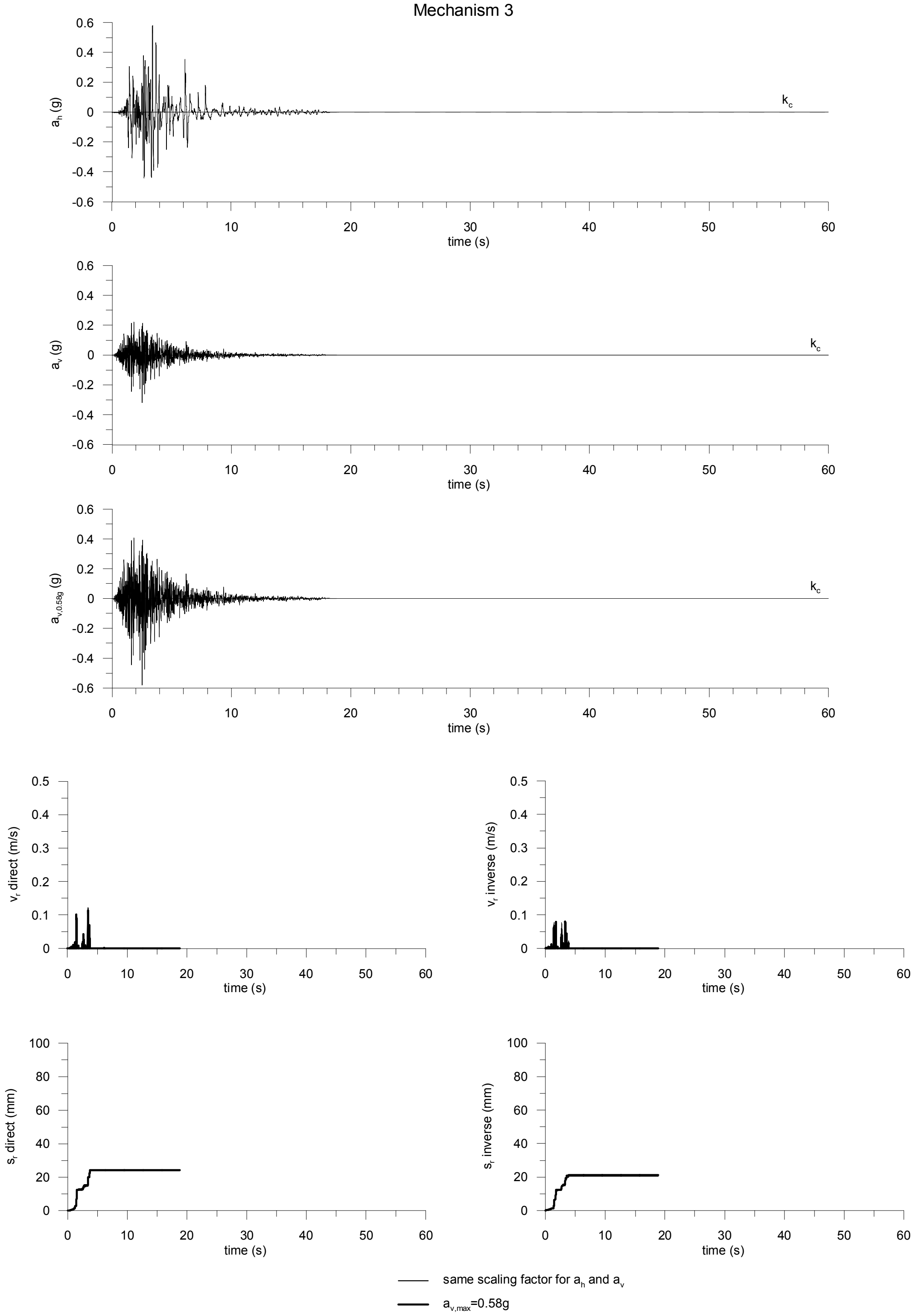

No drainage tunnel

Irpinia 80 STUYC

Mechanism 3

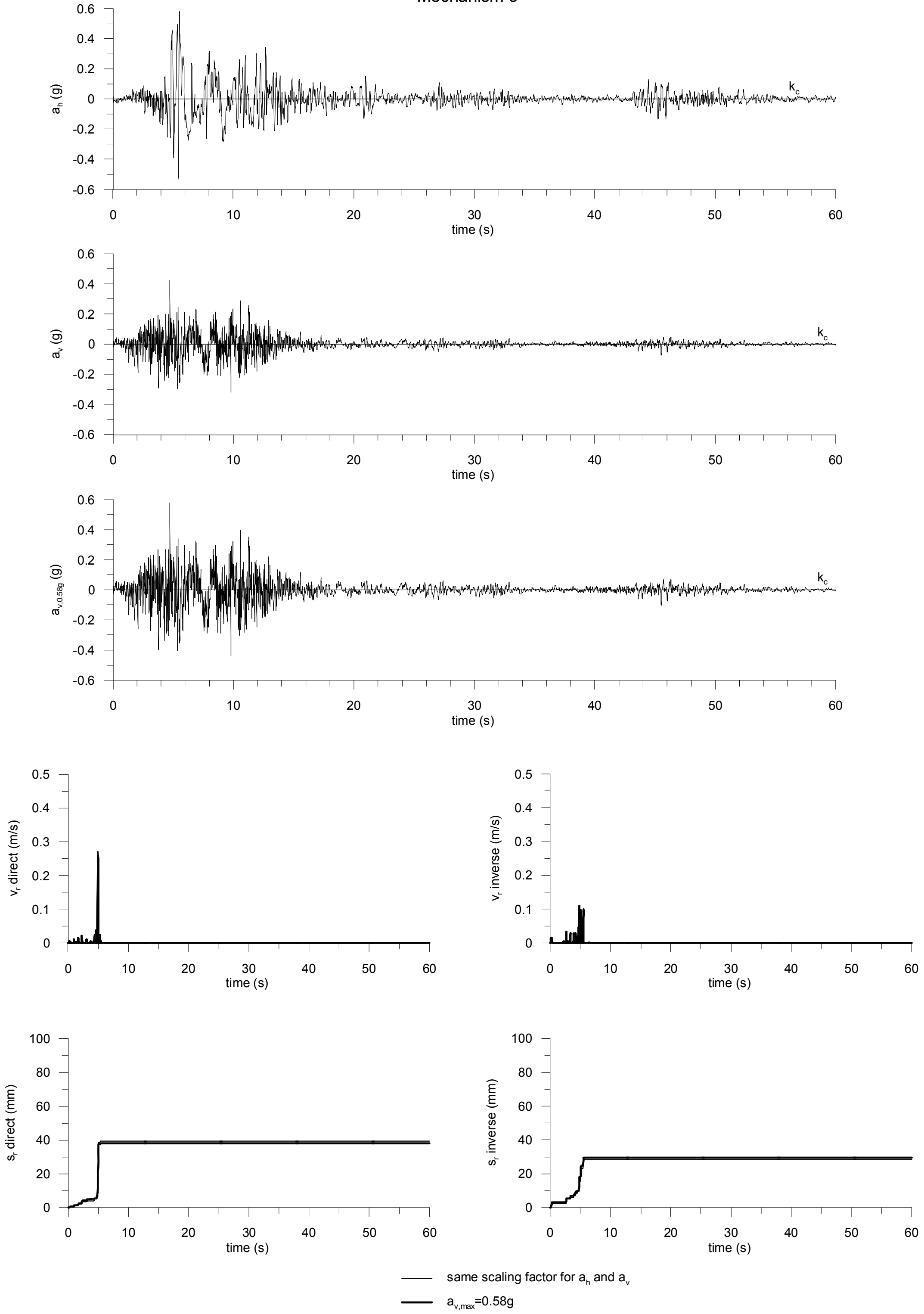

No drainage tunnel

Montenegro 79 ULCXC

Mechanism 3

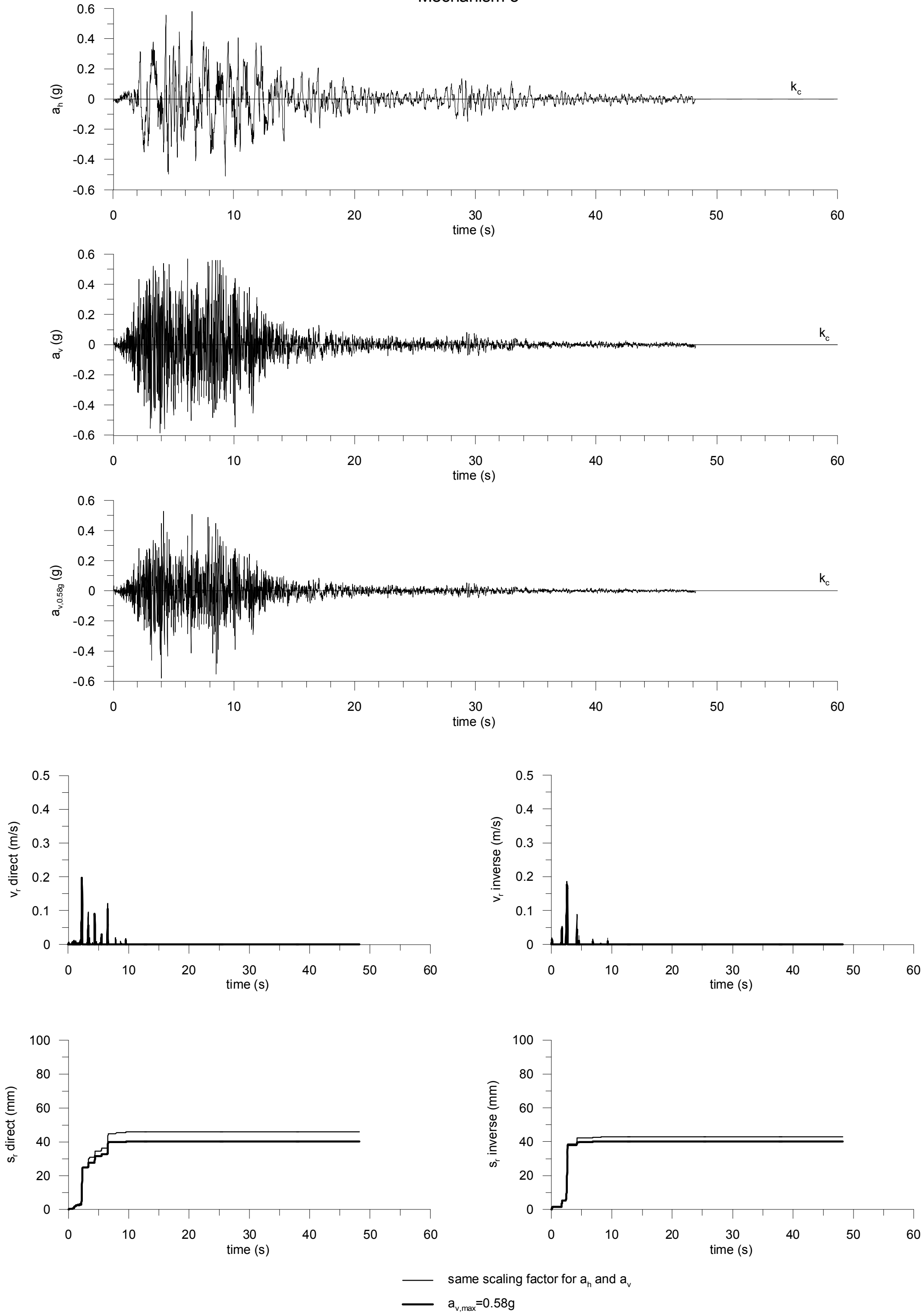

No drainage tunnel

Montenegro 79 PETXC

Mechanism 3

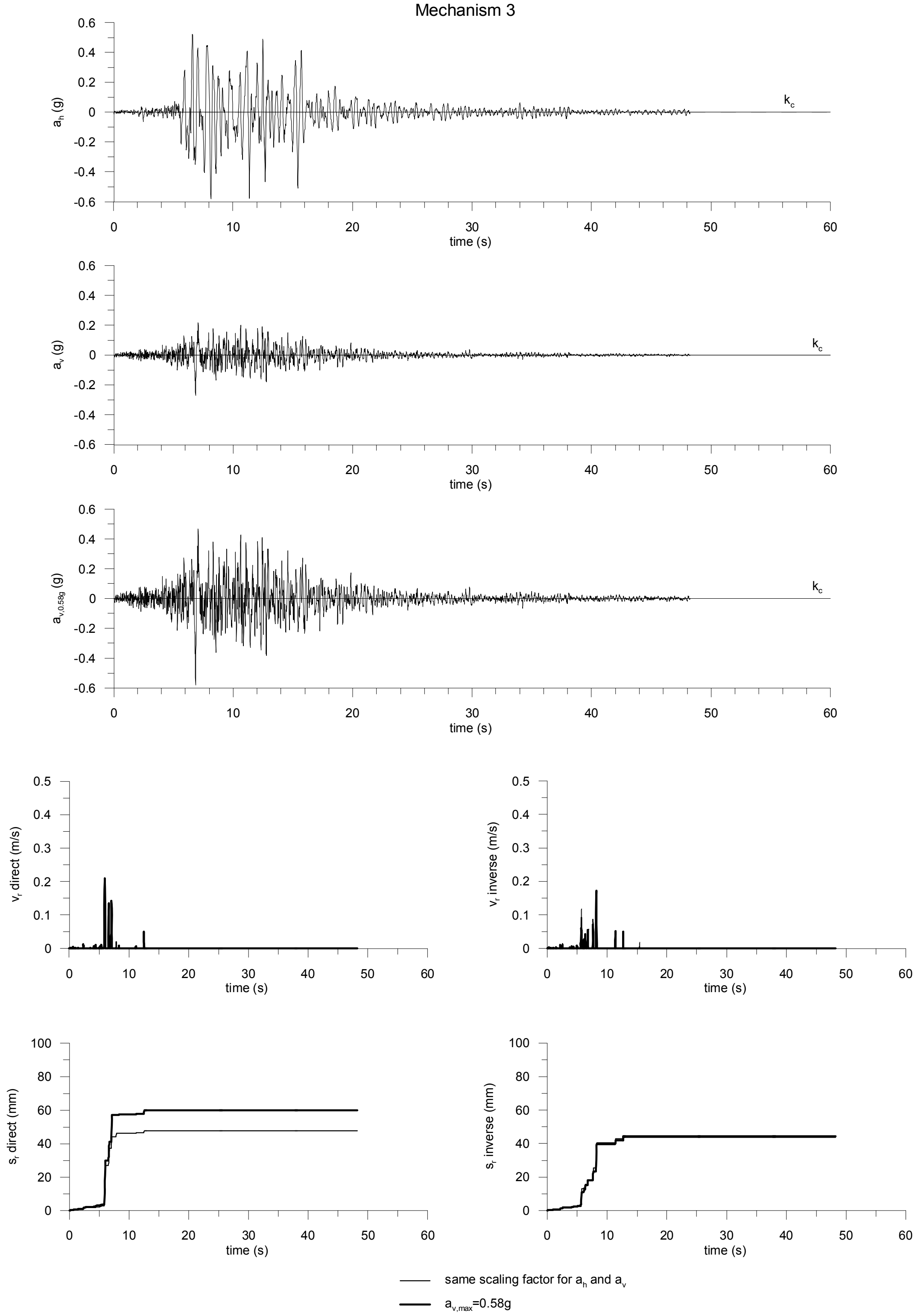

No drainage tunnel

Artificial 1 component 1

Mechanism 3

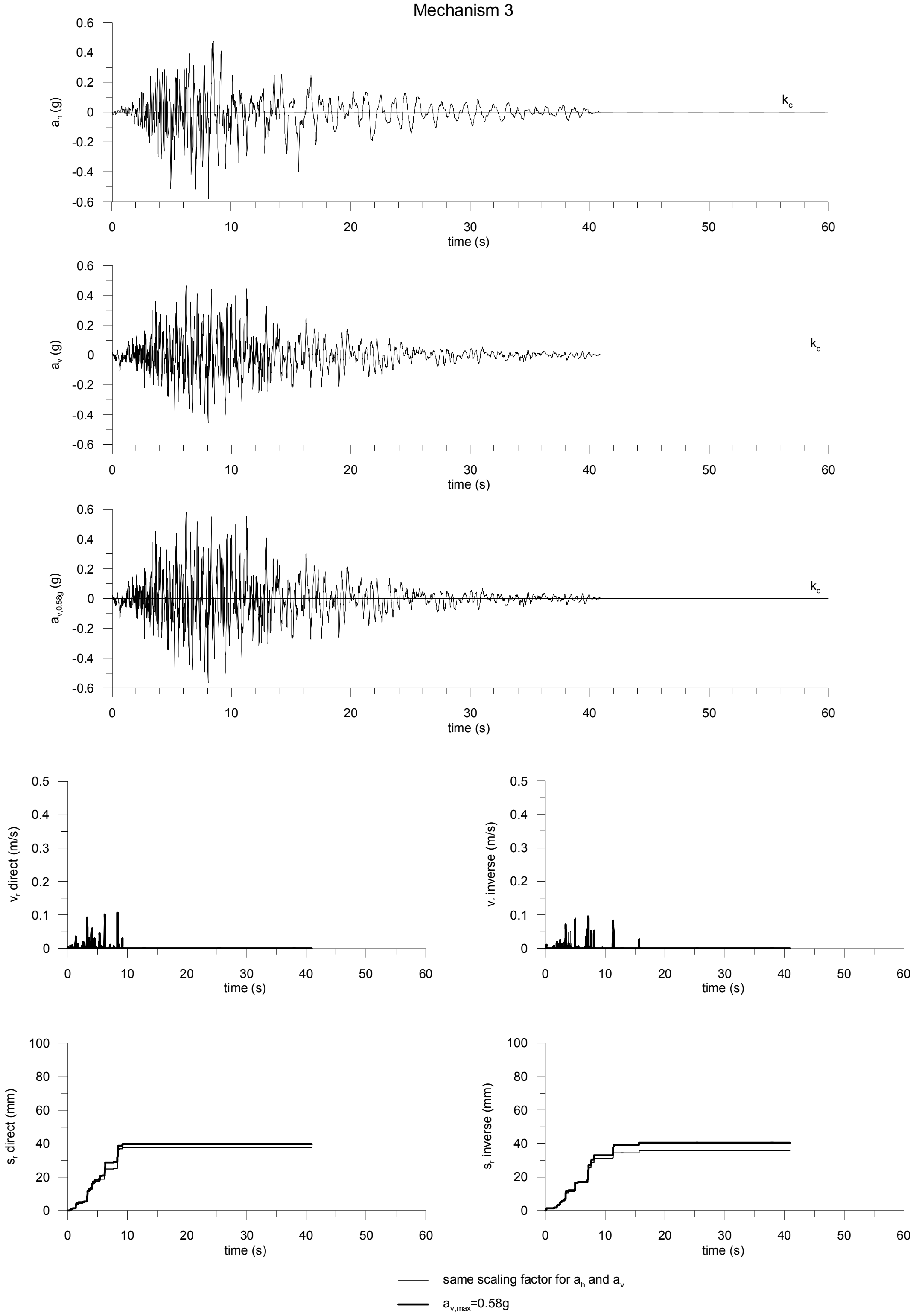

No drainage tunnel

Artificial 1 component 2

Mechanism 3

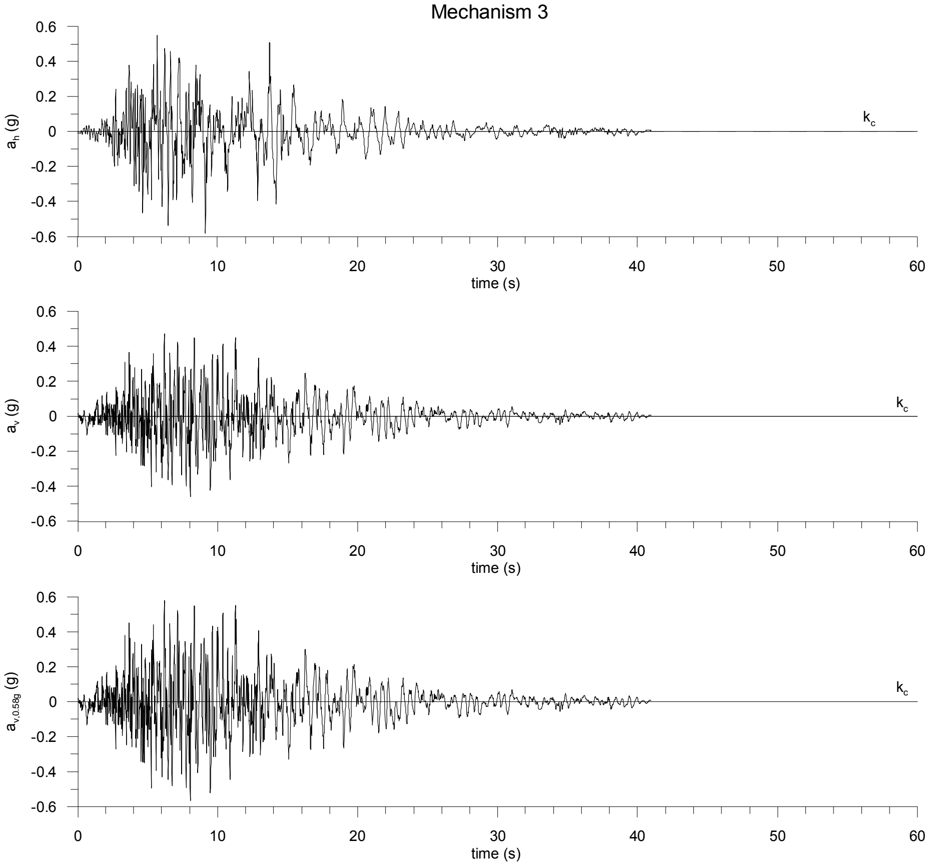

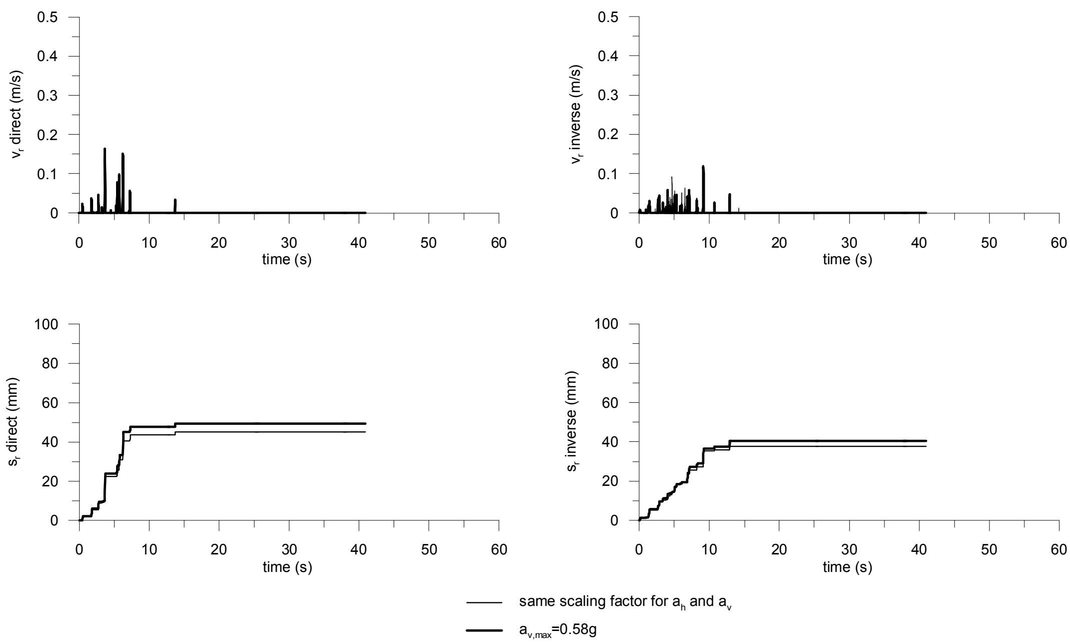

No drainage tunnel

Artificial 2 component 1

Mechanism 3

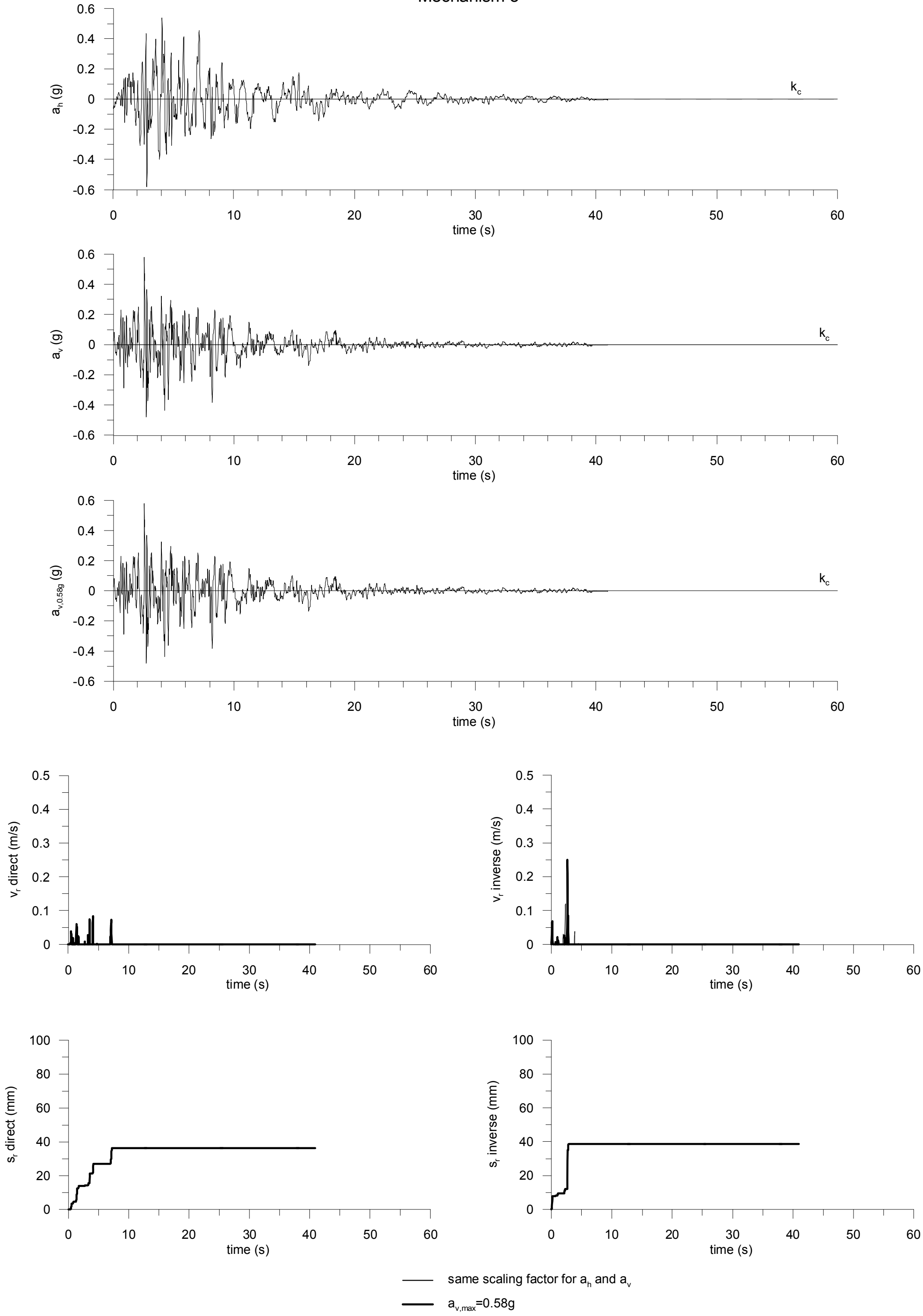

No drainage tunnel

Artificial 2 component 2

Mechanism 3

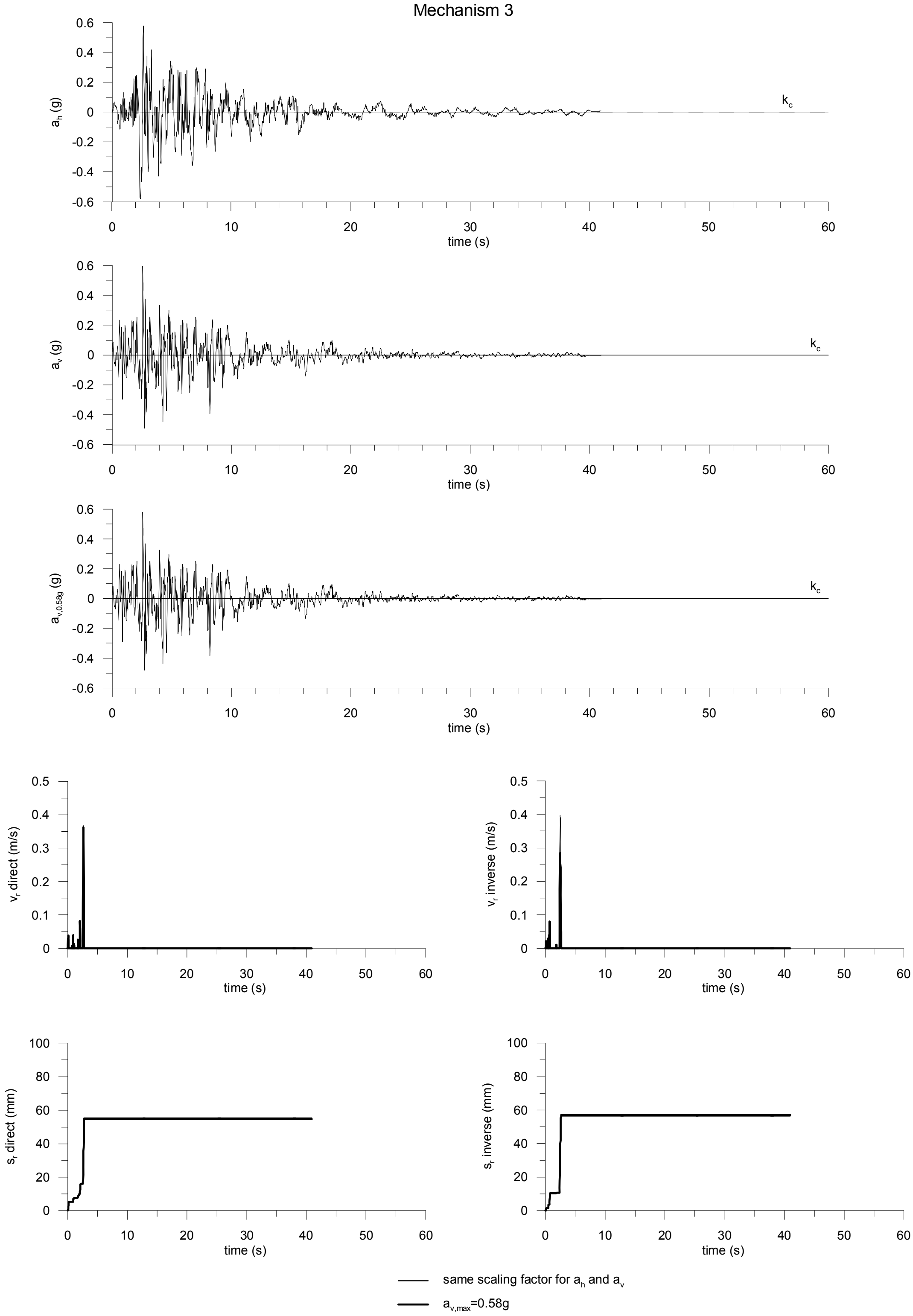

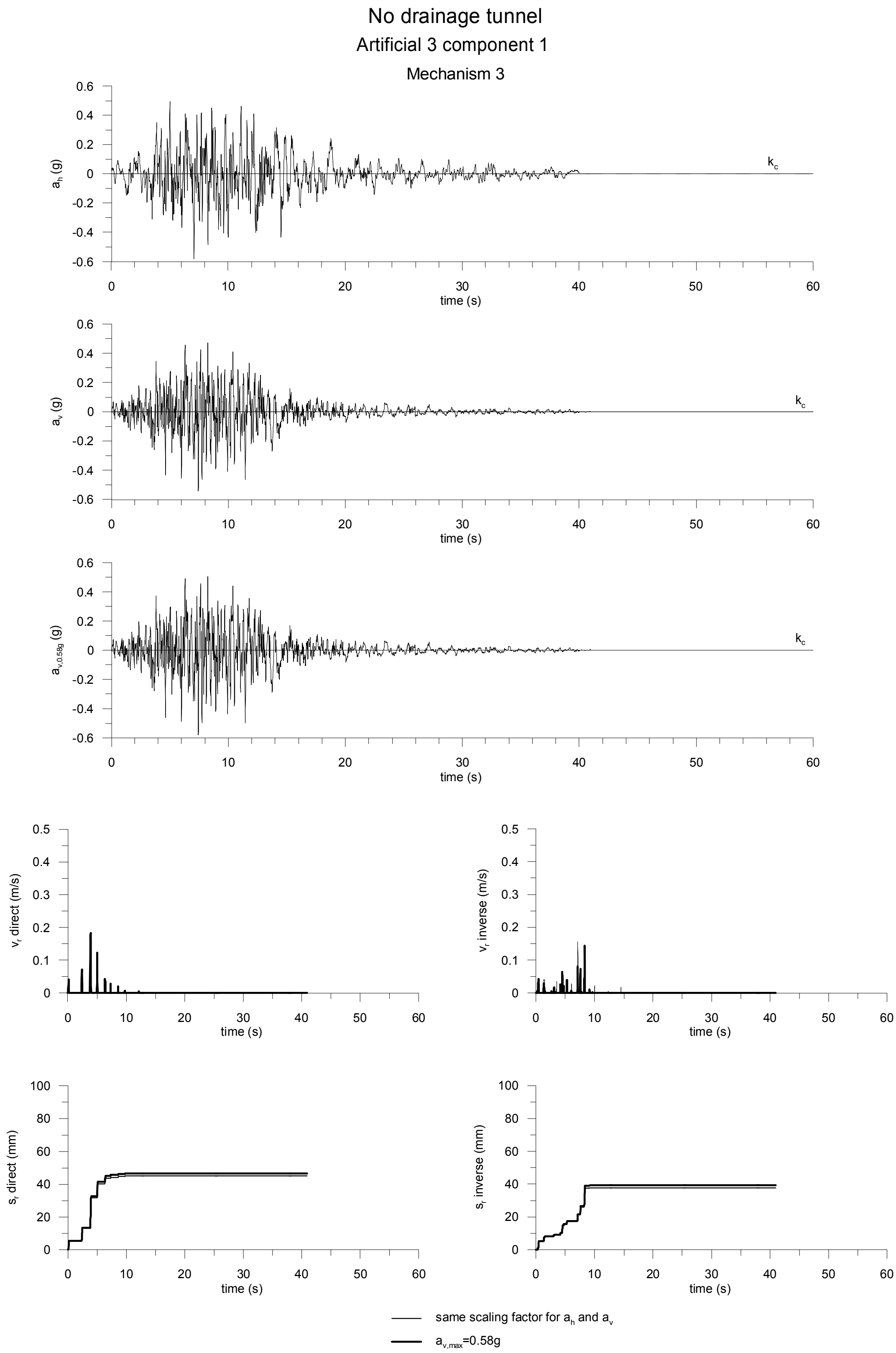
No drainage tunnel
Artificial 3 component 1
Mechanism 3
a_h (g)
a_v (g)
a_v,0.58g (g)
k_c
time (s)
v_r direct (m/s)
v_r inverse (m/s)
s_r direct (mm)
s_r inverse (mm)
same scaling factor for a_h and a_v
a_v,max=0.58g

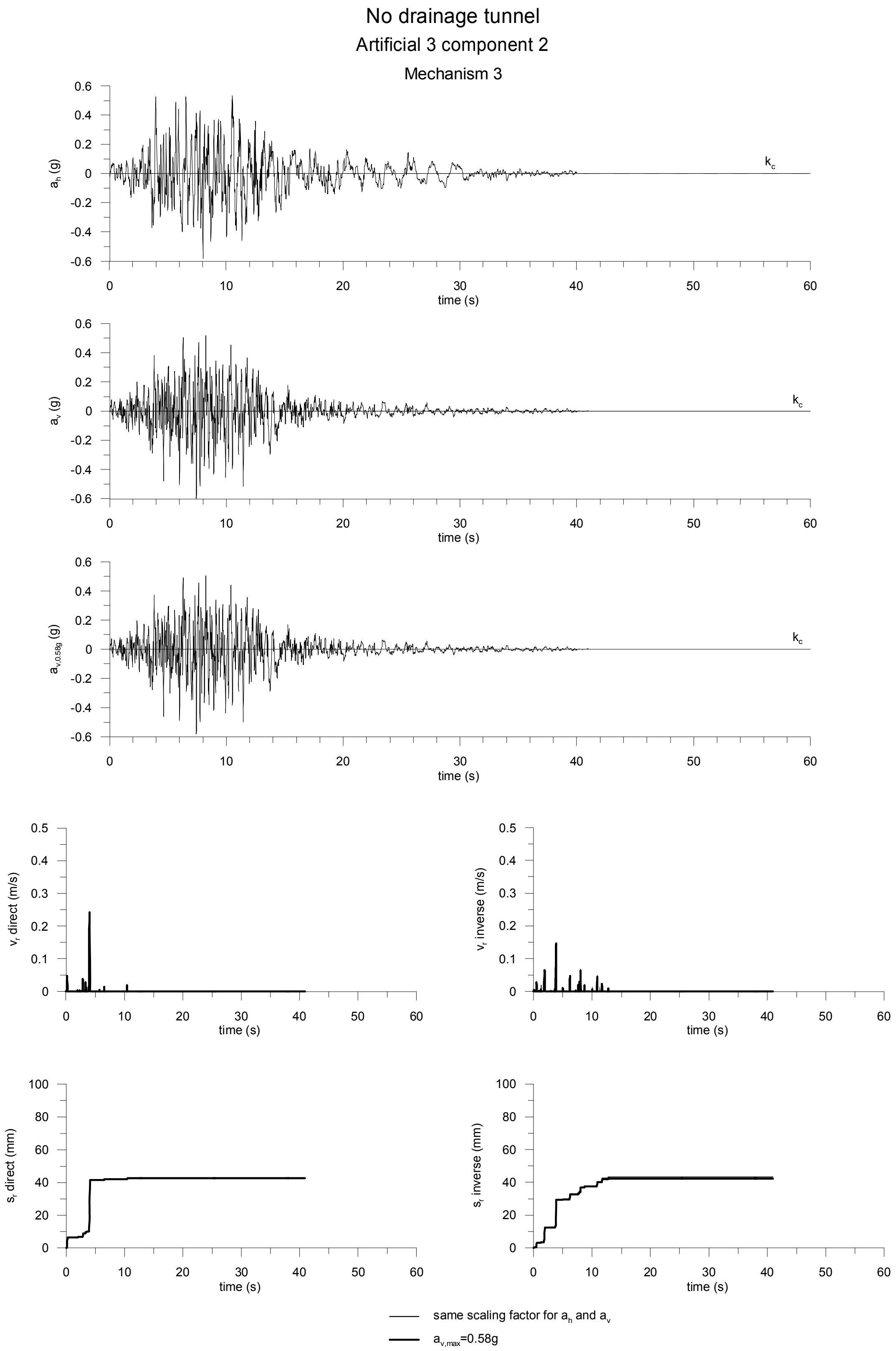
No drainage tunnel
Artificial 3 component 2
Mechanism 3
a_h (g)
a_v (g)
a_v,0.58g (g)
k_c
time (s)
v_r direct (m/s)
v_r inverse (m/s)
s_r direct (mm)
s_r inverse (mm)
same scaling factor for a_h and a_v
a_v,max=0.58g

No drainage tunnel

Artificial 4 component 1

Mechanism 3

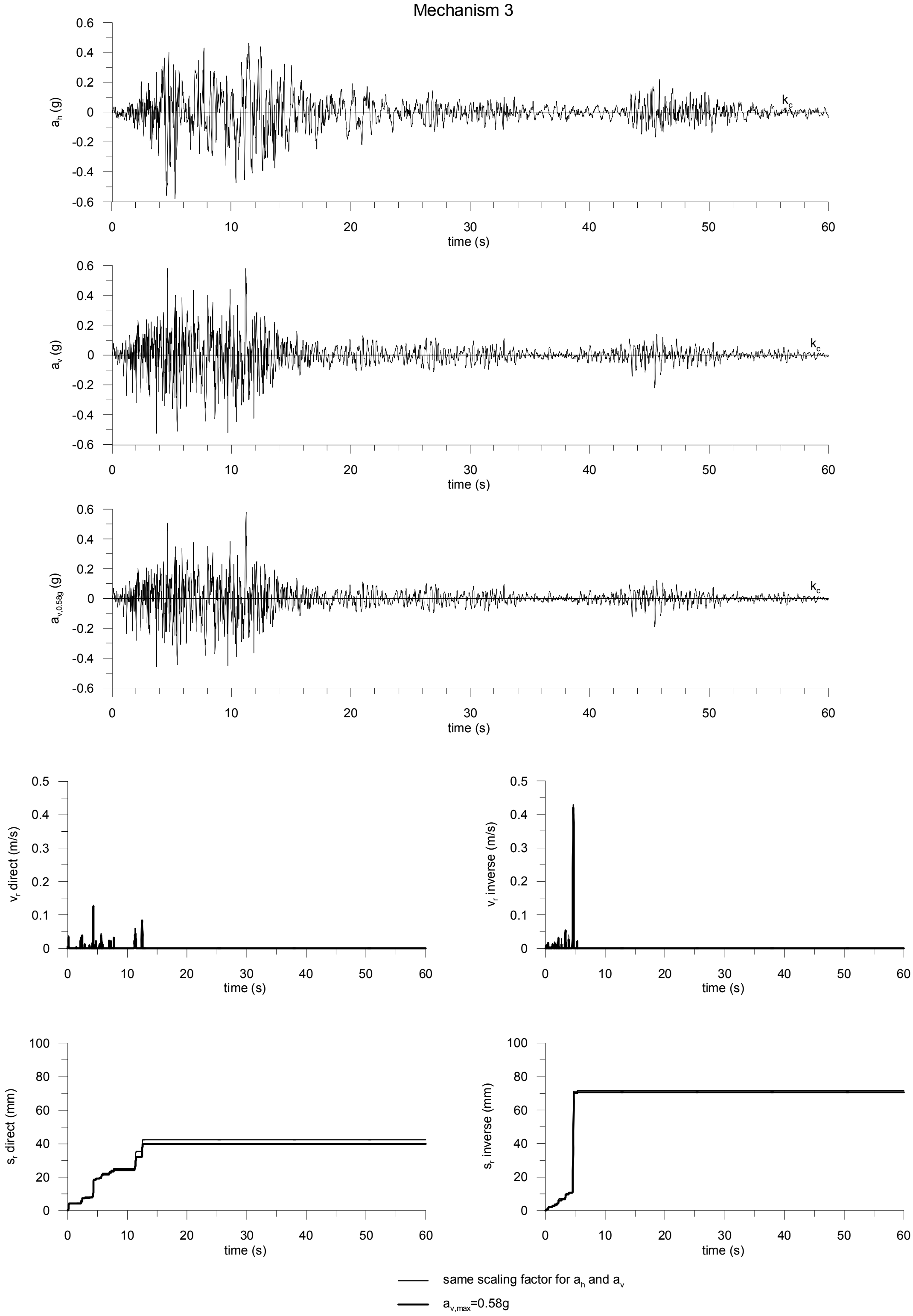

No drainage tunnel

Artificial 4 component 2

Mechanism 3

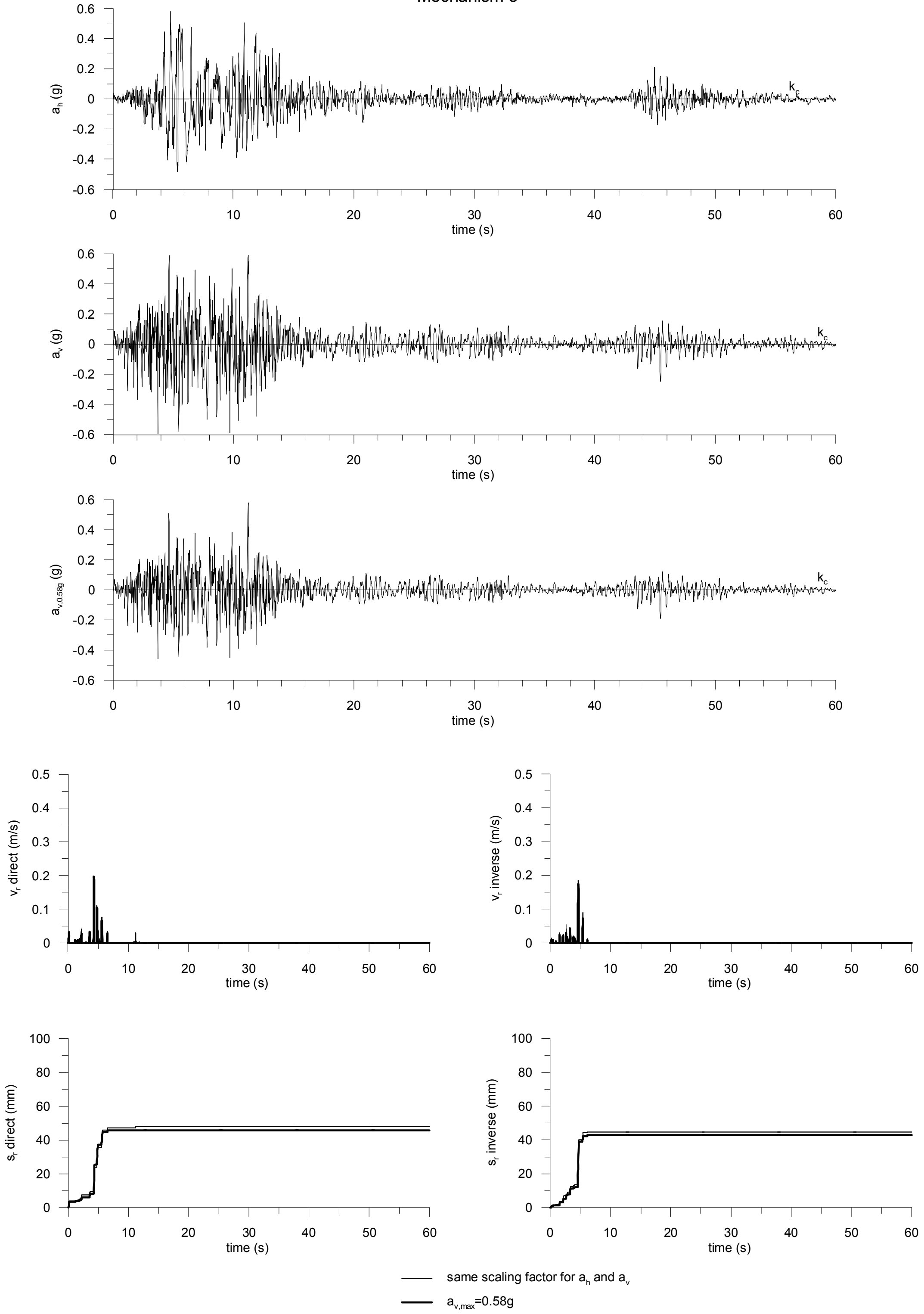

Appendix E – Passive earth resistance

In § 5.5.2 an analytical relationship between the net earth trust ΔR in front of the block and the relative displacement u has been determined referring to 2D F.E. analyses. The geometrical model, the calculation steps, the applied equations and the results obtained are described in that section.

In this Appendix the analytical relationship between ΔR and the relative displacement u has been determined considering the presence of three soil layers instead of a single simplified soil profile, consistently with results from new site investigations and as modelled in the 3D analyses of the companion report “Calabria Anchor Block – evaluation of block behaviour via 3D FE analyses and of bearing capacity”.

The plane strain FE analysis has been carried out with reference to mechanism 3 (α = 0°) and in absence of the drainage system (H_w = 94.5 m a.s.l.). Further analyses have been carried out considering the hydraulic head H_w at 102 m a.s.l., as in the 3D analyses.

The sequence of the three layers is: a) Coastal Deposits, from g.l. to 106 m a.s.l.; b) Weathered Pezzo Conglomerate, up to 87.5 m a.s.l.; c) Pezzo Conglomerate, with an indefinite depth. Mechanical parameters assigned to each layer are reported in Table E.1 and Table E.2, as determined in the 3D FE analyses. Figure E.1 shows the FE mesh adopted for calculations.

Figure E.2 shows the results of four different analyses, obtained considering one or three soil layers in the model and two different positions of the phreatic level (H_w = 94.5 m a.s.l. and 102 m a.s.l.). The interpolation curve shown in the figure is defined by the parameters reported in Table 5.18 (mechanism 3: b = 6.84 10^{-6} m/MN and m = 1.71 10^{-4} MN^{-1}) and is referred to the one-layer analysis, assuming H_w = 94.5 m a.s.l.

The comparison between the one-layer and the three-layers analyses shows that, referring to the 0 – 50 mm interval, the adopted one-layer interpolation curve is conservative. For greater values of displacement, instead, the limit value of the net earth resistance is strongly influenced by the position of the phreatic level.

Table E.1: numerical simulation: physical and mechanic properties of soil layers

layer	Model	γ (kN/m3)	c' (kPa)	φ' (°)	YSR	$K_{0,NC}$	K_0	ν
Coastal Deposit	Hardening soil	20	4.2	40	2.0	0.357	0.470	0.2
Weathered Conglomerate	Hardening soil	20	35	40	2.0	0.357	0.470	0.2
Pezzo Conglomerate	Hardening soil	20	70	40	2.0	0.357	0.600	0.2

Table E.2: numerical simulation: stiffness parameters of soil layers

layer	E'^{ref} (MPa)	m	$E'^{ref}/E'_{50}{}^{ref}$	$E'^{ref}/E'_{oed}{}^{ref}$	$E'_{50}{}^{ref}$ (MPa)	$E'_{oed}{}^{ref}$(MPa)
Coastal Deposit	1920	1.0	7	7	274	274
Weathered Conglomerate	2520	0.2	3	3	840	840
Pezzo Conglomerate	4800	0.0	2	2	2400	2400

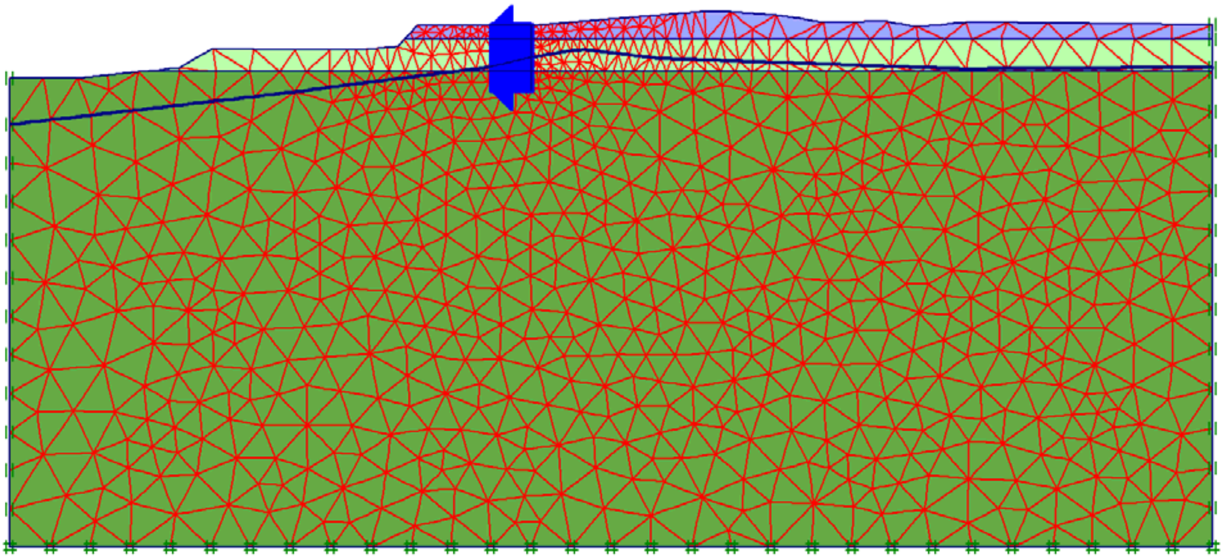

Figure E.1. Three layers F.E. analysis mesh for simulating the earth resistance in front of the anchor block (mechanism 3, H_w = 94.5 m a.s.l)

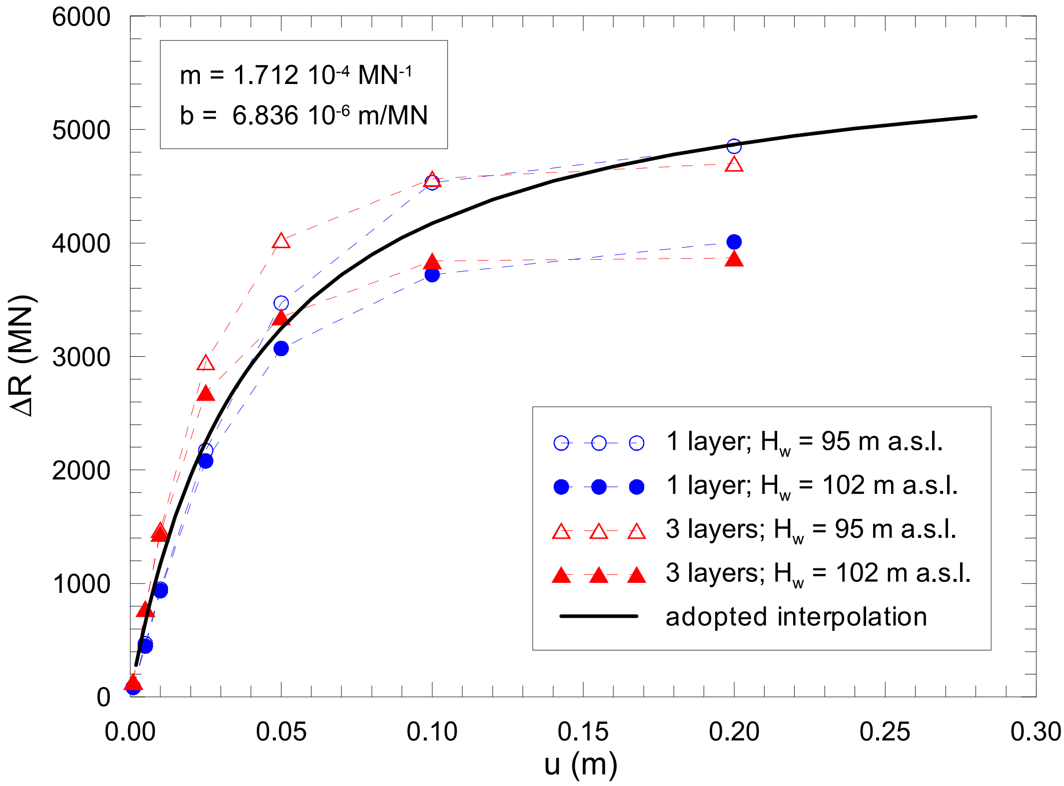

Figure E.2. $\Delta R = f(u)$ equation: comparison between FE analyses (mechanism 3)

Appendix F – Updated cable forces obtained from global IBDAS model version 3.3b

The forces transmitted by the main cables to the Calabria Anchor Block have been re-evaluated using the global IBDAS model version 3.3b. The worst load combinations were selected for each limit state (SILS, SLS2 and ULS) for both static and seismic conditions, using 6 different criteria. Table F.1 resumes the values obtained for static loading conditions, while Table F.2 refers to seismic loading conditions.

Low differences are observed between values of the cable forces computed in the Tender Design and those recently provided by the global IBDAS model version 3.3b. Considering the maximum values of cable forces given by the different criteria for each load case, the ratio of the Tender Design cable forces to those provided by IBDAS model are in the range 1.05 to 0.96 (Table F.3); the higher ratio refers to the ULS load combination, while the lower is obtained for the SILS load combination.

For the Ultimate Limit State (ULS) cable forces provided by the Tender Design are 5% higher than the corresponding IBDAS values, this resulting in a conservative estimate of the behaviour of the Calabria Anchor Block.

Table F.1 – Static Loading Conditions – updated global IBDAS model version 3.3b

Criteria	Load case	F_{long} (MN)	F_{vert} (MN)	F (MN)
min u_{vert}	ULS	-2183	593	2262
max u_{vert}		-3578	1059	**3731**
min u_{hor}		-3578	1058	3731
max u_{hor}		-2183	594	2262
min R_{transv}		-3578	1058	3731
max R_{transv}		-2183	594	2262
min u_{vert}	SILS	-2479	692	2574
max u_{vert}		-3246	946	**3381**
min u_{hor}		-3246	946	3381
max u_{hor}		-2479	693	2574
min R_{transv}		-3246	946	3381
max R_{transv}		-2479	693	2574
min u_{vert}	SLS2	-2187	595	2267
max u_{vert}		-3217	938	**3351**
min u_{hor}		-3217	938	3351
max u_{hor}		-2187	595	2267
min R_{transv}		-3217	938	3351
max R_{transv}		-2187	595	2267

Table F.2 – Seismic Loading Conditions – updated global IBDAS model version 3.3b

Criteria	Load case	F_{long} (MN)	F_{vert} (MN)	F (MN)
min u_{vert}	ULS	-2093	533	2160
max u_{vert}		-3467	1052	**3623**
min u_{hor}		-3434	989	3574
max u_{hor}		-2125	596	2207
min R_{transv}		-3439	989	3578
max R_{transv}		-2121	596	2203
min u_{vert}	SILS	-2383	627	2464
max u_{vert}		-3316	1002	**3464**
min u_{hor}		-3281	934	3411
max u_{hor}		-2418	696	2516
min R_{transv}		-3285	933	3415
max R_{transv}		-2413	697	2512
min u_{vert}	SLS2	-2152	570	2227
max u_{vert}		-3235	958	**3374**
min u_{hor}		-3220	929	3351
max u_{hor}		-2167	598	2248
min R_{transv}		-3222	929	3353
max R_{transv}		-2165	598	2246

Table F.3: Cable forces in the Calabria Anchor Block: Tender Design and IBDAS values (version 3.3b)

	Tender Design	Static IBDAS	Seismic IBDAS	
Load case	F (MN)	F (MN)	F (MN)	F_{TD}/F_{IBDAS}
ULS	3933	3731	3623	1.05
SILS	3142	3381	3464	0.91
SLS2	3232	3351	3374	0.96

Appendix G – Updated cable forces obtained from global IBDAS model version 3.3f

The forces transmitted by the main cables to the Calabria Anchor Block have been further re-evaluated using the global IBDAS model version 3.3f. The worst load combinations were selected for each limit state (SILS, SLS2 and ULS) for both static and seismic conditions, using 6 different criteria. Table G.1 resumes the values obtained for static loading conditions, while Table G.2 refers to seismic loading conditions.

Low differences are observed between values of the cable forces computed in the Tender Design and those recently provided by the global IBDAS model version 3.3f. Considering the maximum values of cable forces given by the different criteria for each load case, the ratio of the Tender Design cable forces to those provided by IBDAS model are in the range 1.07 to 0.93 (Table G.3); the higher ratio refers to the ULS load combination, while the lower is obtained for the SILS load combination.

For the Ultimate Limit State (ULS) cable forces provided by the Tender Design are 7% higher than the corresponding IBDAS values, this resulting in a conservative estimate of the behaviour of the Calabria Anchor Block.

Table G.1 – Static Loading Conditions – updated global IBDAS model version 3.3f

Criteria	Load case	F_{long} (MN)	F_{vert} (MN)	F (MN)
min u_{vert}	ULS	-2176	590	2254
max u_{vert}		-3528	1041	**3678**
min u_{hor}		-3528	1041	3678
max u_{hor}		-2175	591	2254
min R_{transv}		-3528	1041	3678
max R_{transv}		-2175	591	2254
min u_{vert}	SILS	-2440	679	2532
max u_{vert}		-3206	932	**3338**
min u_{hor}		-3206	932	3338
max u_{hor}		-2439	679	2532
min R_{transv}		-3206	932	3338
max R_{transv}		-2439	679	2532
min u_{vert}	SLS2	-2180	592	2259
max u_{vert}		-3177	924	**3308**
min u_{hor}		-3177	924	3308
max u_{hor}		-2180	592	2259
min R_{transv}		-3177	924	3308
max R_{transv}		-2180	592	2259

Table G.2 – Seismic Loading Conditions – updated global IBDAS model version 3.3f

Criteria	Load case	F_{long} (MN)	F_{vert} (MN)	F (MN)
min u_{vert}	ULS	-2114	540	2182
max u_{vert}		-3390	1024	**3541**
min u_{hor}		-3371	983	3512
max u_{hor}		-2132	581	2210
min R_{transv}		-3319	957	3454
max R_{transv}		-2185	608	2268
min u_{vert}	SILS	-2374	624	2454
max u_{vert}		-3245	977	**3389**
min u_{hor}		-3225	932	3357
max u_{hor}		-2394	670	2486
min R_{transv}		-3166	903	3292
max R_{transv}		-2452	699	2550
min u_{vert}	SLS2	-2158	571	2232
max u_{vert}		-3182	939	**3318**
min u_{hor}		-3174	920	3304
max u_{hor}		-2166	590	2245
min R_{transv}		-3150	908	3278
max R_{transv}		-2190	602	2272

Table G.3: Cable forces in the Calabria Anchor Block: Tender Design and IBDAS values (model version 3.3f)

	Tender Design	Static IBDAS	Seismic IBDAS	
Load case	F (MN)	F (MN)	F (MN)	F_{TD}/F_{IBDAS}
ULS	3933	3678	3541	1.07
SILS	3142	3338	3389	0.93
SLS2	3232	3308	3318	0.97

References

Berezantzev W.G. (1964). *Calculation of foundation basis*. Construction Literature, Leningrad, U.S.S.R.

Cubrinovski M. and Ishihara K. (1999). *Empirical correlation between SPT N-value and relative density for sandy soils*. Soils and Foundations, 39 n. 5, 61 – 71.

Jamiolkowski M., Leroueil S., and Lo Presti D. C. F. (1991). "*Theme lecture: Design parameters from theory to practice*.'' Proc., Geo-Coast'91, 1–41.

Newmark N.M. (1965). Effect of earthquakes on dam and embankment. Geotèchnique, 15 (2), 139-160.

Rowe P.W. (1962). *The stress – dilatancy relation for static equilibrium of an assembly of particles in contact*. Proceedings Royal Society, London, Ser. A 269, 500 – 527.

Schmertmann J.H. (1975). *Measurement of in situ shear strength. State – of – the – art report*. ASCE Speciality Conference on in Situ Measurements of Soil Properties, 2, 57 – 138

Tanaka Y., Kudo Y., Yoshida Y. & Ikemi M. (1987). *A study on the mechanical properties of sandy gravel – dynamic properties of reconstituted samples*. Central Research Institute of Electric Power Industry, Report U87019.